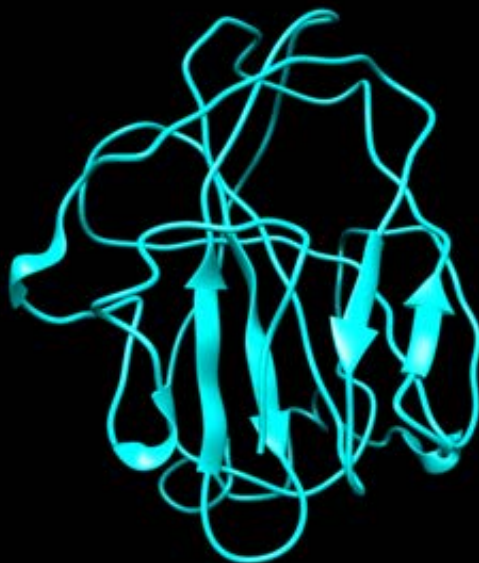


Universidad de Málaga  
Facultad de Ciencias. Departamento de Microbiología  
Programa de Doctorado en Biología Celular y Molecular

**TESIS DOCTORAL**

**Deciphering the molecular basis of *Podosphaera  
xanthii* – cucurbits interaction**



**Álvaro A. Polonio Escalona  
2019**

**Director: Alejandro Pérez García**



UNIVERSIDAD DE MÁLAGA

*Departamento de Microbiología*

*Facultad de Ciencias*

---

**Deciphering the molecular basis of  
*Podosphaera xanthii* – cucurbits interaction**

---

**TESIS DOCTORAL**


**Álvaro Acisclo Polonio Escalona**

**Málaga, 2019**



UNIVERSIDAD  
DE MÁLAGA

AUTOR: Álvaro Acisclo Polonio Escalona

 <http://orcid.org/0000-0002-4977-9305>

EDITA: Publicaciones y Divulgación Científica. Universidad de Málaga



Esta obra está bajo una licencia de Creative Commons Reconocimiento-NoComercial-SinObraDerivada 4.0 Internacional:

<http://creativecommons.org/licenses/by-nc-nd/4.0/legalcode>

Cualquier parte de esta obra se puede reproducir sin autorización pero con el reconocimiento y atribución de los autores.

No se puede hacer uso comercial de la obra y no se puede alterar, transformar o hacer obras derivadas.

Esta Tesis Doctoral está depositada en el Repositorio Institucional de la Universidad de Málaga (RIUMA): [riuma.uma.es](http://riuma.uma.es)



UNIVERSIDAD DE MÁLAGA

*Departamento de Microbiología*

*Facultad de Ciencias*

---

**Deciphering the molecular basis of  
*Podosphaera xanthii* – cucurbits interaction**

---

Memoria presentada por **Álvaro Aciselo Polonio Escalona** para optar  
al grado de Doctor por la Universidad de Málaga





UNIVERSIDAD DE MÁLAGA

*Departamento de Microbiología*

*Facultad de Ciencias*

**D. JUAN JOSÉ BORREGO GARCÍA**, Director del Departamento de Microbiología de la Universidad de Málaga.

**INFORMA:**

Que **ÁLVARO ACISCLO POLONIO ESCALONA** ha realizado en los laboratorios de este departamento el trabajo experimental conducente a la elaboración de la presente Memoria de Tesis Doctoral.

Y para que así conste, y tenga los efectos que correspondan, en cumplimiento de la legislación vigente, expido el presente informe.

En Málaga, 24 de junio de 2019

Fdo. D. Juan José Borrego García





UNIVERSIDAD DE MÁLAGA

*Departamento de Microbiología*

*Facultad de Ciencias*

**D. ALEJANDRO PÉREZ GARCÍA**, Catedrático del Departamento de Microbiología de la Universidad de Málaga.

**INFORMA:**

Que **ÁLVARO ACISCLO POLONIO ESCALONA** ha realizado bajo mi dirección el trabajo experimental conducente a la elaboración de la presente Memoria de Tesis Doctoral.

Y para que así conste, y tenga los efectos que correspondan, en cumplimiento de la legislación vigente, expido el presente informe.

En Málaga, 24 de junio de 2019

Fdo. D. Alejandro Pérez García







UNIVERSIDAD DE MÁLAGA

*Departamento de Microbiología*

*Facultad de Ciencias*

**Este trabajo ha sido subvencionado por los proyectos:**

EXPLOTACIÓN DE LA GENÓMICA PARA EL CONTROL DEL OÍDIO DE LAS CUCURBITÁCEAS. Ministerio de Economía y Competitividad, Programa Estatal de I+D+i orientada a los Retos de la Sociedad (AGL-2013-41939-R). Investigador principal: Dr. Alejandro Pérez García.

DESARROLLO DE NUEVAS HERRAMIENTAS PARA EL CONTROL DE OÍDIOS. Ministerio de Economía y Competitividad, Programa Estatal de I+D+i orientada a los Retos de la Sociedad (AGL-2016-76216-C2-1-R). Investigador principal: Dr. Alejandro Pérez García.

Álvaro Acisclo Polonio Escalona disfrutó de un contrato predoctoral para la formación de doctores del Ministerio de Economía y Competitividad de referencia BES- 2014-068602 asociada al proyecto de investigación AGL-2013-41939-R



## Artículos derivados de esta Tesis Doctoral

Seaone, P. Espigares, M. Carmona, R. **Polonio**, Á. Quintana, J. Cretazzo, E. Bota, J. Pérez-García, A. Alché, J. Gómez, L. & Claros, MG. (2018). TransFlow: a modular framework for assembling and assessing accurate *de novo* transcriptomes in non-model organism. BMC Bioinformatics 19 (Supple 14):416. (*Apéndice I – Necesario para la realización del Capítulo III*).

**Polonio**, Á. Pineda, M. Bautista, R. Martínez-Cruz, J. Pérez-Bueno, ML. Barón, & Pérez-García A. (2019). RNA-seq analysis and fluorescence imaging of melon powdery mildew disease reveal an orchestrated reprogramming of host physiology. Scientific Reports, 9:7978. (*Capítulo II*).

**Polonio**, Á. Seaone, P. Claros, MG. & Pérez-García A. (2019). The haustorial transcriptome of the cucurbit pathogen *Podosphaera xanthii* reveals new insights into the biotrophy and pathogenesis of powdery mildew fungi. BMC Genomic, 20:543. (*Capítulo III*).

**Polonio**, Á. & Pérez-García A. The haustorium or how biotrophic fungi parasitize plants without being seen. Progress in Botany, Volume 82. Under review. (Sección “*The haustorium*” del *Capítulo I*).

**Polonio**, Á. & Pérez-García, A. Two secreted haustorial acid phosphatases are key factors for *Podosphaera xanthii* development and promising targets for fungicide design. Paper draft (*Capítulo IV*).

**Polonio, Á.** El-Azaz, J. & Pérez-García, A. Contribution of a secreted haustorial lytic polysaccharide monooxygenase of *Podosphaera xanthii* to the manipulation of chitin-triggered immunity of its host. Paper draft (*Capítulo V*).

**Polonio, Á.** Bautista, R. & Pérez-García, A. Simultaneous transcriptomic analysis of *Podosphaera xanthii* - *Cucumis melo* compatible interaction. Scientific Data. Manuscript in preparation (*Conjunto de datos del Capítulo II. Discutido en la sección “Transcriptomic approaches to unravel the plant-pathogen molecular dialogue” del Capítulo VI*).

### **Comunicaciones a congreso derivadas de esta Tesis Doctoral**

**Polonio, Á.** Seoane, P. Martínez-Cruz, J. de Vicente, A. Pérez-García, A. Transcriptoma haustorial de *Podosphaera xanthii*. Retos en muestras de difícil aislamiento y ARN degradado. XVIII Congreso de la Sociedad Española de Fitopatología. Palencia, España (2016). *Póster*.

Espigares, M. Seoane, P. **Polonio, Á.** Bautista, R. Quintana, J. Pérez-García, A. Gómez, L. Claros, MG. Seeking the best *de novo* transcriptome assembling in non-model organisms. 5th Plant Genomics and Gene Editing Congress. Amsterdam, Holanda (2017). *Póster*.

García-Sánchez, J. **Polonio, Á.** de Vicente, A. Pérez-García, A. El modelado proteico como herramienta para el análisis funcional de efectores haustoriales de *Podospaera xanthii*. VII Reunión del Grupo Especializado de Microbiología de Plantas. Salamanca. España (2017). *Comunicación oral*.

**Polonio, Á.** Bautista, R. de Vicente, A. Pérez-García, A. El análisis RNA-seq dual como herramienta para el estudio de la interacción melón-*Podospaera xanthii*. VII Reunión del Grupo Especializado de Microbiología de Plantas. Salamanca. España (2017). *Comunicación oral*.

**Polonio, Á.** Seoane, P. de Vicente, A. Pérez-García, A. The *de novo* haustorial transcriptome of *Podospaera xanthii* reveals new candidate secreted effector proteins. FEMS 7th Congress of European Microbiologists. Valencia, España (2017). *Póster*.

**Polonio, Á.** Seoane, P. de Vicente, A. Pérez-García, A. El análisis mediante RNA-seq y técnicas de captura de imagen de la interacción melón-*Podospaera xanthii* revela modulación de la fotosíntesis y del metabolismo secundario de la planta por el patógeno. XIX Congreso de la Sociedad Española de Fitopatología. Palencia, España (2018). *Comunicación oral*.

**Polonio, Á.** El-Azaz, J. Fernández-Ortuño, D. de Vicente, A. Pérez-García, A. Proteínas secretadas por el haustorio y su importancia en el desarrollo de *Podospaera xanthii*. VIII Reunión del Grupo Especializado de Microbiología de Plantas. Osuna. España (2019). *Comunicación oral*.



## AGRADECIMIENTOS

Han pasado bastantes años desde que aquel Álvaro de tercero de carrera iba al laboratorio durante el verano. En todo este tiempo he visto defender muchas Tesis Doctorales, pero nunca pensé que llegaría el momento de la mía. Han sido unos años inolvidables en los que se me ha permitido cumplir un sueño, en los que he aprendido muchísimo, pero en los que también he sufrido muchísimo. Gracias, en parte, a ese sufrimiento he podido comprobar lo importante que es tener a grandes personas a tu lado durante el incierto y, a veces, tortuoso camino de realizar una Tesis Doctoral.

Es justo comenzar los agradecimientos con la persona que me ha permitido cumplir este sueño. La persona que ha confiado en mí desde el principio. A mi director de Tesis, Alejandro. Gracias por convertirme en un verdadero científico. Gracias por darme la libertad necesaria para pensar por mi mismo y llevar a cabo mis propios experimentos. Gracias por estar ahí, sabiendo reorientarme cuando la cosa se me iba un poco de las manos. Me has aportado la seguridad necesaria para la consecución de este trabajo. Te estaré eternamente agradecido.

A Francis, el que fue mi padre científico, el que me acogió con los brazos abiertos cuando solo era un niño inquieto y me permitió llevar a cabo mis primeros experimentos. Mil gracias por hacerme conocer la ciencia y enseñarme a disfrutar con ella.

A Diego, por demostrarme que el único camino hacia el éxito es el trabajo duro. Fue una suerte trabajar contigo durante un tiempo y aprender que la ambición, el esfuerzo y el no rendirse nunca es el camino a seguir para lograr grandes cosas. Gracias por ser una fuente de inspiración.



Juan Antonio, sin duda, tu pérdida nos golpeó a todos. Gracias por tu desempeño y pasión en este trabajo. Gracias por sentar las bases de lo que hoy es un gran grupo. Gracias a ti estamos todos hoy aquí. Te echamos de menos.

A Codina, porque tu sola presencia es motivo de alegría. Gracias por esas palmeras de chocolate que nos ayudan a coger energías para seguir. Por las charlas de las tardes, por los consejos.

A Lola, porque nunca te he visto una mala cara, porque transmites alegría. Gracias por tus consejos, por tu energía, por tus ánimos, por todo. Simplemente gracias por ser como eres.

A Cayo, gracias por las críticas constructivas durante los seminarios, por hacer de todos nosotros personas más críticas con nuestro propio trabajo. Por hacer de todos nosotros mejores científicos.

Y, como no, a Antonio. Los dos sabemos que si hoy estoy escribiendo estas líneas es gracias a ti. Siento que siempre estaré en deuda contigo. Me has visto reír a carcajadas, pero también me has visto llorar desconsoladamente. Has estado ahí para todo lo que he necesitado en la ciencia, pero también para todo lo que he necesitado en lo personal, que bien sabemos que no ha sido poco en estos turbulentos años. Eres una de esas personas que el mundo necesita. Gracias por hacer de este grupo mi casa y por hacer de tu despacho mi gabinete psicológico.

Llega el momento de agradecer a todas esas personas que me han acompañado en el laboratorio durante estos años. Algunos siguen a mi lado, otros labran su camino lejos de aquí, pero todos habéis aportado vuestro granito de arena. Nuria, Laura, Nacho y Víctor. Compartí pocos momentos con vosotros cuando solo era un “cachorro”, pero de todos aprendí algo. De aquella época con *Pseudomonas* recuerdo con especial cariño mis inicios con Guti. Quizás fue

la “clase” fuengiroleña o simplemente tu forma de ser, no lo sé, pero creé un vínculo especial contigo que a día de hoy conservo. Gracias por los primeros consejos y los que todavía sigues brindándome. Hoy soy lo que soy, en gran parte, gracias a ti. Hablar del inicio es hablar de mi Clau. De su incombustibilidad e inmensa paciencia. Contigo empezó todo. Contigo di los primeros pasos y aprendí mucho de lo que después me ha permitido terminar mi Tesis Doctoral. “Tu chiqui” se hace mayor. En este trabajo está tu impronta. Gracias por tanto. De mi etapa con *Pseudomonas* tengo que destacar, también, a Carmencita. Siempre trabajando duro. Siempre dispuesta a darte un consejo para que lo difícil parezca mucho más fácil.

Imposible olvidarme de Houda, puro amor, pura nobleza, pura bondad. Una de esas personas que te apetece tener cerca. Mis inicios con *Bacillus* no hubiesen sido posibles sin tu ayuda. De mis inicios en *Bacillus* se merece una mención especial Joaquín, mi “Chari”. Contigo es difícil no tener afinidad e imposible no reírse. Una persona que quieres tener a tu lado, da igual si es en un congreso, en el laboratorio en pleno agosto con música de discoteca o jugando al pádel. En esos inicios también estaba Conchita, compartiendo estoicamente la dificultad para transformar nuestros *Bacillus* sin perder la sonrisa.

Casi sin darme cuenta me iba haciendo mayor y en un abrir y cerrar de ojos me vi trabajando con *Podosphaera xanthii*, el hongo que tantas frustraciones me ha hecho pasar, pero que tanto me ha hecho aprender y desarrollarme como científico. Porque, parafraseando a mi “socio” David: “La Tesis no es más que un camino contra tu propia frustración”. Contigo comenzó una amistad que sigue perdurando a día de hoy, tras tus vueltas por el mundo y tu ansiado regreso. Contigo compartí la pasión por los productos de Apple. Me siento orgulloso de que la que fue tu mesa no haya sido mancillada con un vil PC. Cuando se habla de *Podosphaera xanthii* hay que hablar de Jesús Martínez Cruz, con nombre y

apellidos. Mi mentor, mi compañero de poyata durante todos estos años, de penas y de alegrías, de música, de Monsters y de placer por la buena comida; mi compañero de habitación en los congresos. Porque trabajar al lado del mejor, me ha hecho mejor. Eres el espejo en el que todos deberíamos mirarnos.

Cómo no, agradecer también, al resto de personas que estáis cerca, en la facultad o compartiendo laboratorio conmigo. Eva, te recuerdo con mucho cariño desde mis inicios. Rebeca, ha sido un gran placer coincidir contigo. Zahira, eres el reflejo del esfuerzo y la dedicación. Sandrita, porque siempre es una inmensa alegría compartir un momento contigo y hablar sobre nuestro futuro o sobre Rulos. France, aunque decidieses seguir tu camino lejos de la ciencia, has sido un inmenso apoyo durante todos estos años. Porque ir de congreso es mucho más seguro teniéndote cerca. Cristina, siempre dispuesta a echar una mano en todo aquello que se prestase. Yandi, tu incomparable capacidad para trabajar te echen lo que te echen y tu cercanía te hacen especial. Mariki, tu felicidad radiante y tu cariño hacen del laboratorio un lugar más feliz. Alejandra, porque tener una compañera de sufrimiento con la tecnología, los auriculares, la red Eduroam y la infinita burocracia, hace todo más llevadero. Mi compi Laura, porque eres una currante nata y, sobre todo, porque tu paciencia para resolver todas mis dudas con el inglés me ha solucionado la vida. Y hablando de personas que han estado cerca durante todo este trabajo, hay una que merece una mención especial, Irene, mi Rubia. Por mantener el orden, por permitir que todo funcione, por hacer un trabajo impresionante e imprescindible. Por no acomodarte nunca. Porque me has visto crecer como persona y como científico. Porque me has apoyado cuando más lo he necesitado. Porque te has convertido en mi hermana. Gracias.

Le toca el turno al PTA. Me da una pena tremenda que no estemos todos en un mismo edificio. Si trabajásemos en el mismo laboratorio podría compartir

con mi vecino Jesús nuestras grandes vivencias con la fauna de Maqueda o con Carlos las “ligeras” subordinaciones durante las prácticas. Podría apoyarme en Jesús Hierrezuelo cada vez que tuviese dudas sobre temas complejos de química o en Luis cuando las tuviese sobre bioinformática. Podría disfrutar de la compañía y el buen rollo de Marisa, Saray, Sara, Ana, Mari Luz y María. Podría seguir disfrutando de la compañía de Montse, una de esas personas que entran en tu vida sin hacer ruido y, una vez lo han hecho, se hacen un huequito y se quedan para siempre. Porque me has escuchado en todas y cada una de las idas de olla que he tenido. Porque has demostrado el valor de la palabra amistad. Me alegro enormemente de que puedas llevar a cabo tu sueño.

Siguiendo con los agradecimientos me gustaría hacer una parada por el Departamento. Juanjo, porque tus clases me metieron el gusanillo de la Microbiología. Carmen Vila, María Muñoz, Milena y Rocío. Porque ir a arreglar algún papeleo y charlar un rato con vosotras es un soplo de aire fresco.

Tampoco pueden faltar aquellas personas que me han acompañado durante seminarios y congresos o que me han brindado ayuda técnica. De lo genéticos me llevo grandísimos amigos e infinitas vivencias. Eloy, Adri, Carla, Alba, Javi y Diego, gracias por todas esos momentos que nunca olvidaré. Un merecidísimo hueco el que se han ganado Pedro y Elena. Pedro, con tu infinita paciencia e inquietante tranquilidad has conseguido hacerme entender algo sobre bioinformática. Porque gracias a tu trabajo, ayuda y consejos ha podido salir esta Tesis adelante. Elena, porque has dejado todo lo que tenías que hacer para echarme una mano con la insoportable burocracia pre-Tesis.

Quiero agradecer, también, a todos mis compañeros del final del pasillo, Fernando, Belén, Cañas, Alberto, Josemi, Paquito y en especial a uno de los mejores científicos que he conocido, mi *coauthor* Jorge. He aprendido

muchísimo de todos vosotros. No quiero pasar la oportunidad de mencionar a todas esas personas a las que he tenido la suerte de supervisar durante sus trabajos fin de grado o fin de máster. Juanan, Erik, Migue y Dani. Porque de todos vosotros también he aprendido mucho. Aquí también tiene un hueco Pepe. Porque tus rondas nocturnas me hacían sentir más seguro esas largas noches hasta las tantas de la madrugada en el laboratorio. Y para acabar, me gustaría reconocer el inmenso trabajo que hacen los técnicos especialistas de la UMA, con especial mención a Pepi, Rocío, David, Reme y Merche. Vuestro trabajo queda reflejado en muchas Tesis y esta es una de ellos.

La realización de una Tesis Doctoral conlleva muchísima dedicación y frustración hasta el punto de poner en aprietos las relaciones sociales fuera del laboratorio. Sin embargo, cuando tienes los mejores amigos del mundo, la cosa es mucho más fácil. Mis compis de la carrera, Eloy, Migue, Javi, Manolo, Emilio, Flo, Julio... Sois muchos los que me habéis ayudado a hacer todo esto mucho más llevadero. Sin embargo, hay tres personas que merecen un lugar especial aquí. Mi Compi Bea. Porque desde aquellas primeras prácticas de citología en el puesto 22 del laboratorio, te has convertido en una persona imprescindible en mi vida. Porque, como tu dices, eres mi roca. Porque nunca he obtenido un no por respuesta cuando he necesitado tu ayuda. Paquito, ¿quién iba a pensar que te ibas a convertir en alguien tan importante cuando te conocí? Si hay una palabra que te define es lealtad. Eres amistad en estado puro. Porque cada vez que el estrés o la frustración hacían mella en mí, sabía que solo tenía que levantar el teléfono y contar contigo. Pablo, porque nuestras desconexiones musicales han hecho que mi cerebro resetease. Por escucharme pacientemente y empujarme a seguir luchando. Por recordarme que podía hacerlo. Por confiar en mí incluso cuando ni yo mismo podía hacerlo.

A mi familia. A mis tíos, tías, primos, primas. A todos los que habéis creído en mí. A mi hermano. A Pepe, porque aunque hace muchos años que no estás con nosotros, tuviste un papel muy importante en mi pasión por la ciencia. A Pepi, Antonio, Ana, Carmen y Elena, porque me habéis acogido con los brazos abierto y me habéis hecho sentir querido y cuidado en todo momento. Porque gracias a vosotros tengo una nueva familia.

A Mamá, porque estos años la vida te ha golpeado con fuerza y, aún así, has demostrado una fortaleza increíble. Porque has sido un ejemplo a seguir de esfuerzo, lucha y superación. Porque has creído en mí. Porque sin ti, nada de esto hubiese sido posible. Te quiero.

A Papá. Te fuiste sin que me diese tiempo a despedirme. Esta Tesis va especialmente dedicada a ti. Porque cuando me suba al estrado para defenderla llevando puesta tu corbata favorita, espero que puedas estar viéndome desde algún lugar y te sientas orgulloso de mi. Te echo de menos.

A Ana, mi persona favorita. La que ocupa todos mis pensamientos. La que me ha hecho conocer el verdadero amor. Porque el solo hecho de haberte conocido hace que sumergirse de lleno en la incertidumbre de realizar una Tesis Doctoral cobre sentido. Porque has sacado la mejor versión de mi mismo. Porque me has cuidado. Porque me has acompañado durante toda la Tesis, aguantado la frustración y estrés que arrastraba conmigo, sin pedir nada a cambio. Porque no sé que me deparará el futuro, pero si sé que quiero vivirlo a tu lado. Porque eres lo mejor que me ha pasado en la vida. Porque te amo con locura.

Este trabajo está firmado con mi nombre, pero es obra de todos vosotros. Muchas gracias.



*A mis padres*  
*A Ana*





*“Puede que sea al final de una jornada... O en el laboratorio, a las cuatro de la mañana, después de haberte pasado cinco años analizando datos, pero llega un momento en el que descubres algo, ves algo o de repente algo adquiere sentido y te das cuenta de que sabes algo que aún no sabe nadie más en el mundo entero. Solo tú. Nadie más. Y te das cuenta de que eso es lo único que importa y de que lo conservarás durante poco tiempo antes de que se lo cuentes a otra persona, pero durante ese tiempo te sientes más vivo que nunca. Ese es el motivo. Por eso hacemos esto, aguantamos los sueldos bajos y los riesgos altos, las condiciones indignas y las relaciones jodidas. Lo hacemos por ese momento”*

*Aleta.*

*Christopher Moore*



*“No tengas miedo de la perfección, nunca la alcanzarás”*

*Salvador Dalí*



# CONTENTS

<b>Resumen</b>	1
<b>Chapter I: General Introduction and objectives</b>	29
THE POWDERY MILDEWS	31
THE CUCURBITS POWDERY MILDEW	32
Life cycle and establishment	36
Disease management	37
THE POWDERY MILDEW-HOST INTERACTIONS	41
The powdery mildew effectors	43
THE HAUSTORIUM	49
Haustorial development and establishment	49
Haustorial composition	51
Isolation of haustoria and gene expression studies	54
Nutrient uptake in the haustorium	57
Haustorial effectors	59
The haustorium as a gate for the introduction of genetic material in biotrophic fungi	61
REFERENCES	65
OBJECTIVES	84
<b>Chapter II: RNA-seq analysis and fluorescence imaging of melon powdery mildew disease reveal an orchestrated reprogramming of host physiology</b>	85
INTRODUCTION	89

MATERIAL AND METHODS	92
RESULTS	99
DISCUSSION	118
SUPPLEMENTAL DATA	125
REFERENCES	126

**Chapter III: The haustorial transcriptome of the cucurbit pathogen *Podosphaera xanthii* reveals new insights into the biotrophy and pathogenesis of powdery mildew fungi**

INTRODUCTION	141
MATERIAL AND METHODS	144
RESULTS	154
DISCUSSION	173
SUPPLEMENTAL DATA	182
REFERENCES	184

**Chapter IV: Two secreted haustorial acid phosphatases are key factors for *Podosphaera xanthii* development and promising targets for fungicide design**

INTRODUCTION	197
MATERIAL AND METHODS	200
RESULTS	210
DISCUSSION	229
REFERENCES	235

<b>Chapter V: Contribution of a secreted haustorial lytic polysaccharide monooxygenase of <i>Podosphaera xanthii</i> to the manipulation of chitin-triggered immunity of its host</b>	245
INTRODUCTION	249
MATERIAL AND METHODS	252
RESULTS	261
DISCUSSION	280
REFERENCES	287
<b>Chapter VI: General Discussion</b>	297
TRANSCRIPTOMICS APPROACHES TO UNRAVEL THE PLANT-PATHOGEN MOLECULAR DIALOGUE	300
THE HAUSTORIUM IS NOT ANOTHER FUNGAL CELL	305
HAUSTORIUM-SPECIFIC SECRETED PROTEINS: UNTAPPED TARGETS FOR RATIONAL FUNGICIDE DESIGN	308
REFERENCES	314
<b>Conclusions</b>	323
<b>Conclusiones</b>	327
<b>Appendix I</b>	331





## RESUMEN

Los cultivos se ven afectados por diferentes enfermedades de plantas que causan importantes pérdidas en la producción y en la calidad de los frutos y vegetales (Yang *et al.*, 2017). Estas enfermedades pueden estar producidas por nematodos, protozoos, hongos, oomicetos, bacterias, virus y viroides (Baker *et al.*, 1997), constituyendo los hongos el principal grupo de patógenos de plantas por el número de especies y su importancia económica (Doehlemann *et al.*, 2017). Entre los hongos patógenos destacan los oídios, agentes causales de las enfermedades del mismo nombre, por ser los patógenos causantes de la enfermedad de plantas más extendida, común y fácilmente reconocible, el oídio (Hacquard, 2014). Esta enfermedad se caracteriza por la aparición de manchas blancas pulverulentas en la superficie de las hojas, peciolo, tallos y raramente en frutos (Eichmann and Hüchelhoven, 2008; Pérez-García *et al.*, 2009). Los oídios son hongos biotrofos obligados, es decir, requieren células vivas del hospedador para completar su ciclo de vida. La biotrofia en estos patógenos viene determinada por la presencia de una estructura especial de parasitismo denominada haustorio (Godfrey *et al.*, 2009; Martínez-Cruz *et al.*, 2014; Ahmed *et al.*, 2015; Pennington *et al.*, 2016). Los haustorios se desarrollan dentro de las células de la planta y establecen una relación íntima con el hospedador, siendo sus principales funciones la obtención de nutrientes y la liberación de pequeñas proteínas denominadas efectores (Godfrey *et al.*, 2010; Chaudhari *et al.*, 2014; Lo Presti *et al.*, 2015). Aunque estén localizados en el interior de las células vegetales, los haustorios permanecen separados del citoplasma mediante una estructura denominada membrana extrahaustorial (EHM) (Gil and Gay, 1977; Mackie *et al.*, 1991; Martínez-Cruz *et al.*, 2014). Entre la membrana

extrahaustorial (EHM) y la pared celular del haustorio se encuentra una región denominada matriz extrahaustorial (EHMx) (Gil and Gay, 1977; Koh *et al.*, 2005), donde se produce el intercambio de moléculas entre el hongo y su huésped (Gil and Gay, 1977; Micali *et al.*, 2011) y dentro de la cual se extienden los lóbulos del haustorio, unas proyecciones con gran presencia de vesículas que sugieren una importante actividad secretora del haustorio mediada por exosomas (Martínez-Cruz *et al.*, 2014). Los efectores cuentan con diversas funciones como la modulación de la respuesta de defensa de la planta, la protección de la integridad fúngica o la alteración de la fisiología de la célula huésped (Pedersen *et al.*, 2012; Rovenich *et al.*, 2014; Lo Presti *et al.*, 2015). En el caso de los oídios, han sido caracterizados pocos efectores debido, fundamentalmente, a la especificidad de huésped de los biotrofos obligados y, por tanto, a la imposibilidad de anotación de dichos efectores por identidad de secuencia con otros hongos filamentosos.

Los oídios afectan a una amplia variedad de angiospermas tanto monocotiledóneas como dicotiledóneas (Braun and Cook, 2012, Takamatsu, 2013; Seifi *et al.*, 2014), afectando a cultivos tan importantes como el trigo, la cebada, la vid y numerosos cultivos hortícolas y ornamentales, destacando por su especial virulencia y agresividad el oídio de las cucurbitáceas. Aunque hay dos especies de hongos que provocan la enfermedad del oídio de las cucurbitáceas, *Golovinomyces cichoracearum* y *Podosphaera xanthii* (Kuzuya *et al.*, 2006; Pérez-García *et al.*, 2009; Miazzi *et al.*, 2011), es *P. xanthii* el principal agente causal de dicha enfermedad en el mundo y el único agente causal del oídio de las cucurbitáceas en el sur de España, donde es uno de los factores limitantes más importantes para la producción de estos cultivos (del Pino *et al.*, 2002; Fernández-Ortuño *et al.*, 2006). A pesar de haberse desarrollado diferentes herramientas para el manejo del oídio de las

cucurbitáceas, en la práctica, la aplicación de fungicidas sigue siendo la principal estrategia para el control de esta enfermedad (McGrath, 2010). Sin embargo, el impacto del control químico es moderado dada la gran rapidez con la *P. xanthii* desarrolla resistencia frente a los compuestos más comúnmente usados para su control (Fernández-Ortuño *et al.*, 2006; Bellón-Gómez *et al.*, 2015), haciendo que la mayoría de fungicidas se tornen ineficaces (Hollomon and Wheeler, 2002). Aunque en los últimos años los estudios sobre las bases moleculares de las enfermedades causadas por oídios han aumentado, el conocimiento de las interacciones moleculares con sus huéspedes, así como las bases moleculares del estilo de vida biotrófico, permanecen ampliamente desconocidas. En el caso concreto que nos concierne, el oídio de las cucurbitáceas, estas bases moleculares están aún menos caracterizadas todavía. Este hecho, unido a la necesidad de desarrollar nuevas estrategias de control de la enfermedad, nos ha llevado a la realización de este trabajo. En él nos hemos centrado en los cambios moleculares del huésped durante las primeras fases de la patogénesis, así como en la principal estructura de parasitismo de este hongo, el haustorio.

En primer lugar, decidimos estudiar los cambios en la expresión génica ocurridos en melón, uno de los principales huéspedes de *P. xanthii*, en uno de los cultivares más sensibles a la enfermedad, el cultivar Rochet, durante fases tempranas de la enfermedad (capítulo II). Los cambios ocurridos en un cultivar sensible durante la interacción compatible son esenciales a la hora de desarrollar nuevas estrategias de control de la enfermedad como, por ejemplo, el desarrollo de nuevos cultivares resistentes. Para estudiar los cambios ocurridos en la expresión génica, realizamos un análisis RNA-seq durante los primeros estadios de la enfermedad. Para este propósito se extrajo RNA de hojas de melón cv. Rochet altamente susceptible a oídio, de hojas control, inoculadas con agua, y

de hojas infectadas, inoculadas con *P. xanthii*, a diferentes tiempos (24, 48 y 72 h). Las extracciones de RNA se usaron para la construcción de librerías de cDNA que, posteriormente, fueron secuenciadas usando la plataforma Illumina NextSeq 550. Tras la secuenciación, el uso de Autoflow (Seoane *et al.*, 2016), nos permitió automatizar el análisis bioinformático de los datos. Este análisis incluyó un preprocesamiento de las lecturas brutas usando SeqTrimNext (Falgueras *et al.*, 2010), un posterior mapeo de las secuencias frente al transcriptoma de referencia de melón (Blanca *et al.*, 2011) y el análisis de los genes diferencialmente expresados en todas las muestras de la planta (control vs infección) usando DeSeq2 (Love *et al.*, 2014). De esta manera, se identificaron 1.114 genes de la planta diferencialmente expresados a 24 h, 3.785 a 48 h y 4.226 a 72 h. El enriquecimiento funcional de los genes diferencialmente expresados reveló diferentes procesos que se estaban viendo modulados durante la infección, la mayoría de los cuales se englobaron dentro de la fotosíntesis (metabolismo primario) y de las rutas metabólicas relacionadas con la defensa vegetal (metabolismo secundario). El posterior análisis mediante el uso del software MapMan (Thimm *et al.*, 2004) añadió más información sobre la expresión de cada uno de los genes desregulados, así como de las rutas metabólicas a las que estaban asociados dichos genes. Para corroborar estos resultados se realizaron estudios de expresión mediante RT-qPCR de algunos genes clave de estos procesos como *lhcb6*, *psbS*, *petE2*, *ohp1*, *pgr5*, *rbcS*, *rca* y *prk* para el metabolismo primario (fotosíntesis y ciclo de Calvin) y *pall*, *pal2*, *pal4* y *adt6* para el metabolismo secundario. Los resultados de expresión obtenidos mediante RT-qPCR corroboraron los datos obtenidos mediante RNA-seq.

Como complemento a los datos de expresión génica, estas fases tempranas de la enfermedad también fueron estudiadas usando técnicas de captura de imágenes como fluorescencia roja de la clorofila y fluorescencia verde-azul. Esta aproximación funcional permitió realizar un análisis fisiológico de las plantas infectadas así como entender mejor los cambios ocurridos en la expresión génica. La captación de imágenes de fluorescencia roja de la clorofila permitió obtener parámetros clave en la fotosíntesis de la planta como son  $F_v/F_M$  o máximo rendimiento cuántico del fotosistema II ( $\phi_{PSII}$ ),  $F_{PSII}$  o rendimiento cuántico del PSII y NPQ o quenching no fotoquímico.  $F_v/F_M$  es un indicador de daños en el PSII,  $\phi_{PSII}$  es un indicador de actividad fotosintética y NPQ representa la cantidad de calor que es disipada en forma de calor para evitar daños en el aparato fotosintético. Los resultados de la fluorescencia roja de la clorofila mostraron un descenso de  $\phi_{PSII}$  que se correspondió con un aumento de NPQ, mientras que  $F_v/F_M$  se mantuvo constante. Estos datos se corresponden con un descenso de la actividad fotosintética y una disipación en forma de calor de la energía no usada en fotosíntesis para evitar daños en el aparato fotosintético. La fluorescencia roja de la clorofila no solo nos permitió obtener un enfoque fisiológico de los datos de expresión génica sino que la combinación de ambas técnicas nos ayudó a dilucidar lo que está ocurriendo a nivel fotosintético. De esta manera, la propia planta estaría reprimiendo ciertos genes como *ohp1* que conllevarían una desactivación temporal del PSII y sobreexpresando otros como *lhcb6*, *petE* o *pgr5* que permitirían un transporte cíclico a nivel de PSI y una disipación de energía sobrante en forma de calor, la cual evitaría daños en el PSII. Esta estrategia de la propia planta podría venir disparada a raíz de la sobre expresión de genes del ciclo de Calvin como *rbcS*, *prk* o *rca*, que *P. xanthii* podría estar induciendo como vía para aumentar su

acceso a fotosintatos. Así, mientras que *P. xanthii* pretende acceder a más nutrientes, las plantas de melón limitarían este acceso mediante el transporte cíclico a nivel de PSI.

En cuanto a los cambios del metabolismo secundario, la captación de imágenes de fluorescencia verde y azul permite obtener un indicador de la cantidad de ciertos productos del metabolismo secundario acumulados en las plantas como fenilpropanoides, lignanos o ligninas, todos ellos relacionados directamente con la defensa. En este caso, las imágenes de fluorescencia mostraron como la infección de *P. xanthii* evita la acumulación de todos estos compuestos seguramente por bloqueo de ciertos genes clave de la ruta del shikimato y de la ruta de síntesis de fenilpropanoides. Los resultados de este capítulo, mediante la combinación de ambas técnicas, nos ha permitido comprender mejor el desarrollo de esta enfermedad desde dos enfoques diferentes, pero complementarios e integradores, así como abrir las puertas a futuros estudios que permitan, por ejemplo, la identificación de genes de susceptibilidad (*S*) que permitieran el diseño de cultivares resistentes a la enfermedad.

El capítulo II nos permitió obtener información muy valiosa sobre los cambios ocurridos en uno de los huéspedes más susceptible a la infección de *P. xanthii*, el melón. Sin embargo, los estudios referentes al propio patógeno y más concretamente a su estructura especializada de parasitismo, el haustorio, siguen siendo muy escasos. En el capítulo III, decidimos hacer un análisis transcriptómico de esta estructura teniendo en cuenta la importancia que se le presupone al haustorio y a sus proteínas secretadas en el desarrollo de la enfermedad (Oliva *et al.*, 2010). Nuestros objetivos eran obtener un mayor conocimiento de los procesos moleculares subyacentes a la biotrofia y patogénesis que ocurren en esta estructura, así como identificar proteínas

secretadas específicamente por el haustorio que pudieran estar implicadas directamente en la patogénesis de *P. xanthii*. Una de las mayores limitaciones a la hora de hacer estudios específicos de haustorios es su dificultad de aislamiento. Las técnicas de aislamiento usadas hasta la fecha como la cromatografía de afinidad usando concavalina A o la centrifugación isopícnica en gradiente de Percoll, son poco recomendables dada la gran cantidad de contaminantes de la planta que se obtienen durante el proceso (Godfrey *et al.*, 2010; Weßling *et al.*, 2012; Link *et al.*, 2014). Por ello, el primer escollo a salvar era el aislamiento de haustorios. Para tal fin, diseñamos una nueva técnica de aislamiento basada en la citometría de flujo. Para ello, las estructuras epifíticas de *P. xanthii* fueron eliminadas desde cotiledones de calabacín altamente infectados. Estos cotiledones fueron, posteriormente, homogeneizados y filtrados para obtener un lisado de restos vegetales entre los que se encontraban los haustorios en una pureza del 0,02%. Finalmente, este lisado fue separado mediante citometría de flujo tras la tinción de las estructuras fúngicas con un fluoróforo (WGA-Alexa Fluor 488) que se une exclusivamente a las paredes celulares fúngicas. De esta manera, y combinando una separación por intensidad de fluorescencia y por tamaño relativo, pudimos obtener haustorios totalmente libre de contaminantes visibles. Sin embargo, las extracciones de RNA procedentes de los haustorios presentaron una baja calidad debida, fundamentalmente, al largo proceso de aislamiento y extracción. Por ese motivo, la librería de cDNA fue realizada con el kit NuGen Ovation RNA-seq system combinando la amplificación con cebadores aleatorios y oligos dT, seguida de una eliminación de las secuencias ribosómicas conocidas mediante cebadores específicos. Finalmente, mediante una amplia profundidad de secuenciación con la plataforma Illumina NextSeq 550 se obtuvieron



531.445.575 lecturas que permitieron rescatar la máxima información posible teniendo en cuenta las limitaciones del modelo de estudio.

La realización de una aproximación bioinformática denominada TransFlow diseñada específicamente para ensamblar transcriptomas de organismos no modelo (Seoane *et al.*, 2018), nos permitió ensamblar diversos transcriptomas y compararlos con varios transcriptomas de referencia para, de esta manera, elegir el que mejor calidad presentaba. El análisis del mejor ensamblaje haustorial de *P. xanthii* y la comparación con el transcriptoma epifítico previamente realizado en nuestro laboratorio (Vela-Corcía *et al.*, 2016), nos permitieron conocer algunos genes que estaban siendo expresados en esta estructura como genes específicos de interacción con el hospedador, de protección frente a especies reactivas de oxígeno, de transportadores o de regulación de la expresión génica mediada por ncRNA o siRNA, lo que mostró la importancia del haustorio en el establecimiento de la enfermedad, en el transporte de nutrientes y en la regulación génica durante la infección. Un aspecto llamativo fue la identificación de un alto número de ncRNA, lo que sugería que la regulación génica podía ser una función muy importante de esta estructura. Por otra parte, entre los 50 genes más expresados destacaron aquellos encargados del transporte de nutrientes y de la transcripción y traducción, volviendo a apoyar que el haustorio es una estructura relacionada directamente con el transporte de nutrientes desde el hospedador así como una estructura muy activa en la síntesis de proteínas. Además, determinamos el secretoma haustorial predicho mediante la combinación de diferentes softwares como Secretool, PECAS y DeepLoc (Cortázar *et al.*, 2014; Cortazar *et al.*, 2015; Almagro Armenteros *et al.*, 2017) y lo comparamos con el secretoma predicho para las estructuras epifíticas (Vela-Corcía *et al.*, 2018), lo que nos permitió obtener un pool de 12 proteínas candidatas secretadas expresadas exclusivamente en el haustorio, la mayoría de

ellas sin función anotada, que fueron denominadas PHEC, acrónimo de “*Podosphaera haustorial effector candidates*”.

Para validar la expresión exclusiva en el haustorio de estas proteínas secretadas se realizó una RT-PCR semicuantitativa a tiempo final, obteniendo que 10 de estas 12 proteínas estaban siendo predominantemente expresadas en el haustorio. Diversos softwares de modelado proteico y predicción de motivos e interacción proteína-ligando como I-TASSER, Phyre2, CATH/Gene3D o MotifScan (Pagni *et al.*, 2007; Zhang, 2008; Kelly *et al.*, 2015; Lam *et al.*, 2016) permitieron obtener información relevante sobre la posible función de estas PHEC. De esta manera, proteínas que en un primer momento carecían de función conocida fueron predichas como una ácido fosfatasa, varias proteínas de adhesión, una monooxigenasa lítica o una dodecina, permitiendo describir posibles funciones del haustorio de *P. xanthii* desconocidas hasta la fecha. Finalmente, el análisis de expresión génica de estas proteínas secretadas mediante RT-qPCR mostró como tres de ellas, PHEC689 (predicha como fosfatasa ácida), 15569 (anotada como fosfatasa ácida) y PHEC27213 (predicha como monooxigenasa lítica), presentaban una expresión relativa bastante elevada en comparación con el resto de proteínas secretadas. Este dato junto con el hecho que se encontraban entre las 25 proteínas más expresadas del haustorio, indicaba que estas proteínas deberían tener una función relevante para el desarrollo y mantenimiento de esta estructura. Este capítulo, por tanto, aportó una aproximación novedosa para el estudio molecular de los haustorios de hongos biotrofos y nos permitió identificar procesos y funciones involucrados en la biología de *P. xanthii* que podrían ser esenciales para su biotrofia y patogénesis.

La obtención del transcriptoma haustorial de *P. xanthii*, así como la predicción del secretoma haustorial, su comparación con el transcriptoma

epifítico y los estudios de expresión génica, nos permitió identificar un conjunto de proteínas secretadas expresadas específicamente en el haustorio (Capítulo III). De ese conjunto de proteínas estudiamos más en profundidad aquellas que presentaron una mayor expresión relativa en el haustorio, entendiéndose que podrían tener un papel relevante para el haustorio y, por extensión, ser proteínas esenciales para el desarrollo de *P. xanthii*. En primer lugar seleccionamos PHEC689, que fue predicha mediante diversos modelos informáticos como una fosfatasa ácida y 15569 que estaba anotada, también, como fosfatasa ácida (capítulo IV). El modelado de estas proteínas usando I-TASSER (Zhang, 2008) y su posterior comparación usando Chimera (Pettersen *et al.*, 2004) arrojó que tanto PHEC689 como 15569 eran estructuralmente idénticas y, a su vez, muy similares a una fosfatasa ácida de *Aspergillus niger*. Además, MotifScan (Pagni *et al.*, 2007) predijo un dominio “histidina fosfatasa ácida” en las tres proteínas, sugiriendo que tanto PHEC689 como 15569 eran auténticas fosfatasas ácidas. Las fosfatasas ácidas catalizan la hidrólisis de fosfomonoésteres a pH ácido, siendo elementos clave en la liberación de fosfato inorgánico desde moléculas más complejas (Xia *et al.*, 2001). Para corroborar dicha función, utilizamos ensayos de complementación en levaduras. Para este propósito, *Saccharomyces cerevisiae* EY132, una levadura deficiente en la fosfatasa ácida secretada *pho5*, fue transformada con plásmidos de expresión en levadura que portaban los genes *PHEC689* y *15569* completos, es decir, manteniendo su péptido señal, y su actividad fue comparada con la levadura control *S. cerevisiae* EY57 que no es deficiente en *pho5*. Con este ensayo de complementación en levaduras y un medio de cultivo específico para la detección de fosfatasas ácidas secretadas, pudimos corroborar que PHEC689 y 15569 eran fosfatasas ácidas secretadas y, por tanto, fueron renombradas como PxSHAP1 y PxSHAP2, respectivamente (por sus acrónimos en inglés: “*Podospaera xanthii* secreted haustorial acid

*phosphatase 1 y 2*”). Para validar la importancia de estas proteínas en el desarrollo de *P. xanthii* realizamos ensayos de silenciamiento génico para los genes *PHEC689* y *15569* tanto individualmente como conjuntamente. Para tal fin se usó la técnica de silenciamiento génico inducido por el hospedador mediado por *Agrobacterium tumefaciens* (ATM-HIGS), previamente puesta a punto en nuestro laboratorio (Martínez-Cruz *et al.*, 2018a). Este método de silenciamiento fue capaz de reducir la expresión de los genes de estudio en torno al 50% tanto en los silenciamientos individuales como en los silenciamientos combinados. Para cuantificar la reducción del desarrollo del patógeno se utilizó tanto una estimación de la biomasa fúngica por recuento directo de puntos de penetración (haustorios), como una cuantificación de la biomasa del hongo mediante una aproximación molecular realizada por qPCR. Los ensayos de silenciamiento génico mostraron como el silenciamiento por separado de cada una de las fosfatasa ácidas hacía descender la enfermedad alrededor del 60%, lo que suponía una reducción de la enfermedad superior a la obtenida por el silenciamiento del gen control procedente del melón *CmMlo1* (Cheng *et al.*, 2012; Martínez-Cruz *et al.*, 2018a). Sin embargo, lo más llamativo se obtuvo cuando se realizó el silenciamiento conjunto de *PxSHAP1* y *PxSHAP2*, reduciéndose la enfermedad en torno al 80%. En este caso, *P. xanthii* mostraba serios problemas para desarrollarse y su crecimiento se limitó a pequeñas colonias con puntos de penetración muy pequeños y sin desarrollo de hifas secundarias. Estos datos sugieren un papel clave de las fosfatasa ácidas secretadas por el haustorio para el desarrollo de *P. xanthii*, seguramente relacionado con la obtención de fósforo, un nutriente esencial para la mayoría de procesos biológicos como la síntesis de ATP, de fosfolípidos y de ácido nucleicos, así como para la transferencia de energía, la activación y regulación de proteínas y el control de la actividad génica (Li *et al.*, 2010).

En paralelo se estudió la acumulación de peróxido de hidrógeno ( $H_2O_2$ ) por parte de células de la planta mediante el método de 3,3'-diaminobenzidina (DAB) (Thordal-Christensen *et al.*, 1997) como indicador para estimar la respuesta de defensa de la planta durante los silenciamientos de *PxSHAP1* y *PxSHAP2*. Los resultados mostraron como *PxSHAP1* y *PxSHAP2* no tenían implicación en la supresión de las defensas, ya que ni en el silenciamiento individual ni en el co-silenciamiento se obtuvo un aumento de células con acumulación de peróxido de hidrógeno. Estos resultados sugieren que *PxSHAP1* y *PxSHAP2* están más bien relacionadas con la biotrofia de *P. xanthii* que con la patogénesis, lo que viene apoyado por el gran tamaño de estas proteínas y su perfil de expresión, marcadamente diferente con respecto al de los efectores (Spanu *et al.*, 2010; Hacquard, 2014). El gran impacto de estas proteínas en el desarrollo de *P. xanthii* las convierte en dianas potenciales para el desarrollo de nuevos productos fitosanitarios. Con esa intención realizamos un ensayo de inhibición en discos de hojas (Fernández-Ortuño *et al.* 2006) probando diferentes inhibidores de fosfatasa ácida previamente descritos en bibliografía como fluoruro de sodio, ácido L(+)-tartárico, ortovanadato de sodio y molibdato de amonio (Arnold *et al.*, 1987; Lovelace *et al.*, 1997; Ullah *et al.*, 2011; Srivastava and Anand, 2015). Exceptuando el fluoruro de sodio que mostró una elevada fitotoxicidad, todos los compuestos ensayados se mostraron como potentes inhibidores del crecimiento de *P. xanthii*. En los casos concretos del ortovanadato de sodio y el molibdato de amonio a 5 mM, la enfermedad se redujo en un 100%. La relación entre estructura y actividad de estos compuestos puede suponer el camino para identificar nuevos compuestos fungicidas mediante aproximaciones químio-informáticas como la topología molecular (Zanni *et al.*, 2018). Con la vista puesta en el desarrollo de nuevos fungicidas, realizamos un análisis BLAST con la intención de buscar ortólogos de los genes

*PxSHAP1* y *PxSHAP2* en otros hongos. Este análisis nos mostró como estas proteínas están ampliamente conservadas en otros hongos ascomicetos patógenos de plantas, de insectos e incluso de mamíferos/humanos. Además, también aparecen conservadas entre hongos endofíticos y endomicorrizas, apoyando la hipótesis de obtención de fósforo como principal función de estas proteínas. Los resultados de este capítulo nos ha permitido demostrar que dos fosfatasa ácidas altamente y exclusivamente expresadas en el haustorio son puntos esenciales para el desarrollo de *P. xanthii*, siendo absolutamente claves para la obtención de fósforo vía haustorio, lo que convierte al metabolismo del fósforo en una diana muy prometedora para el desarrollo de nuevos fungicidas.

Nuestro afán por la búsqueda de proteínas clave para la patogénesis de *P. xanthii* nos llevó a seguir estudiando aquellos genes codificantes para proteínas secretadas específicas del haustorio. El gen más expresado de todas las proteínas haustoriales secretadas y el décimo tercero más expresado de todos los genes del haustorio, *PHEC27213*, se correspondió con una proteína sin función anotada que fue predicha como una monooxigenasa lítica de quitina por los diversos programas informáticos utilizados. Las monooxigenasas líticas son una clase de enzimas recientemente caracterizada que son capaces de oxidar diferentes polisacáridos recalcitrantes entre los que se encuentra la quitina (Vaaje-Kolstad *et al.*, 2010; Hemsworth *et al.*, 2015). Las monooxigenasas líticas de quitina actúan sobre la superficie de la quitina cristalina introduciendo roturas en la cadena y generando extremos oxidados (Vaaje-Kolstad *et al.*, 2010). La quitina es el principal componente de la pared celular fúngica y uno de los principales patrones moleculares asociados a patógenos (PAMP, por su acrónimo en inglés: “*pathogen-associated molecular patterns*”) (Pieterse *et al.*, 2009; Jonge *et al.*, 2010; Kombrink and Thomma, 2013; Tanaka *et al.*, 2013). Para que el patógeno, en este caso *P. xanthii*, pueda desarrollarse y causar

infección tiene que ser capaz de evadir el reconocimiento de la quitina y, de esta manera, evitar la respuesta de defensa mediada por PAMP (PTI, por su acrónimo en inglés: “*PAMP-triggered immunity*”). Con este fin, el de proteger u ocultar la quitina de los receptores de la planta, se han descrito proteínas diferentes en varios hongos fitopatógenos (van den Burg *et al.*, 2007; Bolton *et al.*, 2008; Mochizuki *et al.*, 2011; Sánchez-Vallet *et al.*, 2013; Xi *et al.*, 2014). Sin embargo, la supresión de la inmunidad disparada por PAMP está muy poco estudiada en oídios y, aunque recientemente se han descrito algunas proteínas relacionadas con esta función en hifas de *P. xanthii* (Martínez-Cruz, 2016), el mecanismo para evitar este reconocimiento por parte del haustorio continúa siendo un misterio. Dada la alta y exclusiva expresión haustorial del gen *PHEC27213* pensamos que la proteína que codifica podría tener una función relevante para el desarrollo de *P. xanthii*, estando relacionada, de algún modo, con la modificación de la quitina presente en la pared celular del haustorio. Como había sido predicho en el capítulo III, el modelo de la proteína PHEC27213 presentó una alta analogía estructural con una monooxigenasa lítica de polisacáridos de *Aspergillus oryzae*, además, MotifScan (Pagni *et al.*, 2007) predijo un dominio de unión a quitina, el cual ayudó a clarificar la quitina como posible diana. Para validar su función predicha, en primer lugar realizamos un ensayo de unión a quitina con la proteína expresada y purificada en *Escherichia coli*. Con este ensayo se demostró que PHEC27213 tenía una gran afinidad de unión a este polisacárido. Además, se realizó un ensayo de degradación de quitina y se analizaron los productos resultantes tras la reacción enzimática mediante MALDI-TOF/TOF, lo que nos permitió demostrar que, en efecto, PHEC27213 tiene actividad como monooxigenasa lítica de quitina, rompiendo ésta en pequeños oligómeros con un grado de polimerización (DP por su acrónimo en inglés: “*degree of polymerization*”) predominante de 5

(DP5). Por tanto renombramos PHEC27213 como PxSHLPMO1 (por su acrónimo en inglés “*Podosphaera xanthii secreted haustorial lytic polysaccharide monoxygenase 1*”).

A continuación, para validar la importancia del gen *PxSHLPMO1* en el desarrollo de la enfermedad, llevamos a cabo su silenciamiento mediante el sistema ATM-HIGS antes mencionado. La cuantificación del desarrollo fúngico tras el silenciamiento fue realizada del mismo modo descrito anteriormente, es decir, mediante el recuento de haustorios y mediante la estimación molecular de la biomasa del hongo por qPCR. En este caso se obtuvo un descenso del desarrollo fúngico en torno al 70%, mayor al obtenido tras el silenciamiento individual de los genes de las fosfatasa ácidas, pero menor al obtenido tras el silenciamiento conjunto de dichos genes. Sin embargo, lo más destacable fue la aparición de un gran número de células productoras de peróxido de hidrógeno, que fueron medidas con el método DAB indicado anteriormente, cuando el gen *PxSHLPMO1* fue silenciado. Con este método podemos realizar una estimación de la respuesta de defensa de la planta y determinar la implicación del gen silenciado con la supresión de dicha respuesta. De esta manera, el silenciamiento de *PxSHLPMO1* provocó una acumulación de, aproximadamente, cuatro veces más células reactivas de la planta que el control negativo, sugiriendo una implicación directa de PxSHLPMO1 en la evasión del reconocimiento fúngico mediante algún mecanismo relacionado con la modificación de la quitina. Para intentar dilucidar el mecanismo de acción de PxSHLPMO1, realizamos el silenciamiento conjunto de *PxSHLPMO1* y del gen de melón *CmCERK1*, que codifica el principal receptor encargado del reconocimiento de quitina y responsable de la activación de la inmunidad disparada por quitina. El silenciamiento conjunto de ambos genes mostró como el desarrollo de *P. xanthii* recobraba el fenotipo original, desarrollándose con



normalidad y sin producir un aumento de la respuesta de defensa de la planta. Por tanto, podemos concluir que PxSHLPMO1 se encarga de modificar la quitina de la pared celular del haustorio y, de esta manera, evadir su reconocimiento, pero ¿cómo ocurre esto? CERK1 es un receptor de membrana que es capaz de dimerizar y activar la respuesta de defensa en presencia de oligómeros de quitina con un grado de polimerización igual o superior a 8 (DP8) (Liu *et al.*, 2012). Como se pudo ver en la caracterización enzimática de PxSHLPMO1, esta proteína rompe la quitina en pequeños oligómeros de quitina, predominando aquellos con un DP5. Estos pequeños oligómeros no serían capaces de activar la dimerización de CERK1 y, por tanto, evitarían el reconocimiento de la quitina haustorial. La máxima expresión de *PxSHLPMO1*, coincidiendo con la formación del haustorio, así como la existencia de endoquitinasas de la planta sobreexpresadas en ese mismo momento, nos llevó a proponer que PxSHLPMO1 era secretada a la matriz extrahaustorial donde se encargaría de romper los fragmentos de quitina liberados por las endoquitinasas de la planta o por el crecimiento del haustorio en fragmentos que no serían capaces de activar la dimerización de CERK1. Aunque en hifas de oídio se ha demostrado la presencia de quitosano, una modificación de la quitina que es menos reconocible por los receptores de la planta (Mochizuki *et al.*, 2011; Sánchez-Vallet *et al.*, 2013; Xi *et al.*, 2014), parece ser que en haustorios no se encuentra ni esta ni ninguna otra modificación de la quitina (Micali *et al.*, 2011). Por lo tanto, PxSHLPMO1 aparece como uno de los principales mecanismos para evadir el reconocimiento de la quitina haustorial. Más aún, el análisis mediante BLASTp permitió localizar ortólogos de este gen en otros muchos ascomicetos patógenos de plantas y en hongos endofíticos y endomicorizas. Todo ello refuerza el papel de PxSHLPMO1 en la evasión del reconocimiento

del patógeno por el huésped, siendo además la primera vez que se describe una monooxigenasa lítica con un papel clave en patogénesis.

En definitiva, en esta Tesis Doctoral hemos intentado descifrar las bases moleculares de la interacción *P. xanthii* – cucurbitáceas, abordando el estudio tanto desde la perspectiva del huésped como desde la del patógeno. De esta manera, hemos realizado un estudio de los cambios de expresión génica en plantas de melón durante los primeros estadios de la interacción compatible con *P. xanthii*, centrándonos en la repercusión fisiológica que estos cambios tienen en dos procesos fundamentales de la planta como son la fotosíntesis y la síntesis de metabolitos secundarios gracias a ensayos de captación de imágenes fluorescentes (capítulo II). Los cambios en fotosíntesis parecen venir mediados por la lucha en la obtención/limitación de nutrientes durante la infección de *P. xanthii*, mientras que los cambios en el metabolismo secundario se basan en el bloqueo de ciertas rutas de síntesis de metabolitos secundarios relacionados directamente con las defensas de la planta. En cuanto al patógeno, nos centramos en estudiar su estructura clave para la patogénesis, el haustorio, desentrañando algunos de sus mecanismos moleculares e identificando algunas proteínas secretadas exclusivas de esta estructura (capítulo III). En este estudio pudimos identificar proteínas de adhesión, no descritas hasta la fecha en oídios, que podrían estar encargándose de estabilizar el haustorio dentro de la célula vegetal, así como sugerir la posible relevancia de la regulación génica mediada por RNA no codificantes. Además, la obtención del transcriptoma haustorial nos permitió identificar genes altamente expresados que codificaban proteínas secretadas exclusivamente por el haustorio. Entre estas proteínas se encontraban dos fosfatasa ácidas y una monooxigenasa lítica de quitina. Las fósfas ácidas (capítulo IV) mostraron tener un papel clave en el desarrollo de *P. xanthii*, seguramente por su implicación en la obtención de fósforo vía haustorio, y por

consiguiente, se proponen como dianas prometedoras para el desarrollo de nuevos fungicidas. Por su parte, el estudio de la monooxigenasa lítica secretada exclusivamente por el haustorio (capítulo V) nos permitió conocer uno de los principales mecanismos de esta estructura para evadir el reconocimiento de la quitina de su pared celular. Esta enzima podría estar implicada en la degradación de fragmentos grandes de quitina en pequeños oligómeros incapaces de desencadenar la respuesta de defensa de la planta.

Aunque aún nos queda mucho camino por recorrer para resolver todos los mecanismos moleculares de la interacción *P. xanthii* – cucurbitáceas, este trabajo nos ha permitido sentar las bases para el desarrollo de futuros estudios relacionados con la búsqueda de interacciones moleculares entre el patógeno y su huésped, mediante diferentes aproximaciones de biología de sistemas basadas en los datos transcriptómicos generados en este estudio, así como proponer una estrategia novedosa para la identificación de dianas basada en el análisis funcional de proteínas secretadas específicas del haustorio, que sirvan de base para el desarrollo racional de nuevos fungicidas (capítulo VI).

## REFERENCIAS

**Ahmed AA, Pedersen C, Schultz-Larsen T, Kwaaitaal M, Jørgensen HJL, Thordal-Christensen H.** 2015. The barley powdery mildew candidate secreted effector protein CSEP0105 Inhibits the chaperone activity of a small heat shock protein. *Plant Physiology* **168**, 321–333.

**Almagro Armenteros JJ, Sønderby CK, Sønderby SK, Nielsen H, Winther O.** 2017. DeepLoc: prediction of protein subcellular localization using deep learning. *Bioinformatics* **33**, 3387–3395.

**Arnold W, Sakai K, Mann L.** 1987. Selective inactivation of an extra-cytoplasmic acid phosphatase of yeast-like cells of *Sporothrix schenckii* by sodium fluoride. *Journal of General Microbiology*, 1503–1509.

**Baker B, Zambryski P, Staskawicz B, DineshKumar SP.** 1997. Signaling in plant-microbe interactions. *Science* **276**, 726–733.

**Bellón-Gómez D, Vela-Corcía D, Pérez-García A, Torés JA.** 2015. Sensitivity of *Podosphaera xanthii* populations to anti-powdery-mildew fungicides in Spain. *Pest Management Science* **71**, 1407–1413.

**Blanca JM, Cañizares J, Ziarsolo P, Esteras C, Mir G, Nuez F, Garcia-mas J, Picó MB.** 2011. Melon transcriptome characterization : Simple sequence repeats and single nucleotide polymorphisms discovery for high throughput genotyping across the species. *The Plant Genome* **4**, 118–131.

**Bolton MD, Van Esse HP, Vossen JH, et al.** 2008. The novel *Cladosporium fulvum* lysin motif effector Ecp6 is a virulence factor with orthologues in other fungal species. *Molecular Microbiology* **69**, 119–136.

**van den Burg HA, Harrison SJ, Joosten MHAJ, Vervoort J, de Wit PJGM.** 2007. *Cladosporium fulvum* Avr4 protects fungal cell walls against hydrolysis by plant chitinases accumulating during infection. *Molecular Plant-*

Microbe Interactions **19**, 1420–1430.

**Chaudhari P, Ahmed B, Joly DL, Germain H.** 2014. Effector biology during biotrophic invasion of plant cells. *Virulence* **5**, 703–709.

**Cheng H, Kun W, Liu D, Su Y, He Q.** 2012. Molecular cloning and expression analysis of *CmMlo1* in melon. *Molecular Biology Reports* **39**, 1903–1907.

**Cortázar AR, Aransay AM, Alfaro M, Oguiza JA, Lavín JL.** 2014. SECRETOOL: Integrated secretome analysis tool for fungi. *Amino Acids* **46**, 471–473.

**Cortazar AR, Oguiza JA, Aransay AM, Lavín JL.** 2015. PECAS: Prokaryotic and eukaryotic classical analysis of secretome. *Amino Acids* **47**, 2659–2663.

**Doehlemann G, Ökmen B, Zhu W, Sharon A.** 2017. Plant Pathogenic Fungi. *Microbiology Spectrum* **5**, FUNK-0023-2016.

**Eichmann R, Hückelhoven R.** 2008. Accommodation of powdery mildew fungi in intact plant cells. *Journal of plant physiology* **165**, 5–18.

**Falgueras J, Lara AJ, Fernández-pozo N, Cantón FR, Pérez-trabado G, Claros MG.** 2010. SeqTrim: a high-throughput pipeline for pre-processing any type of sequence read. *BMC Bioinformatics* **11**, 1–12.

**Fernández-Ortuño D, Pérez-García A, López-Ruiz F, Romero D, De Vicente A, Torés JA.** 2006. Occurrence and distribution of resistance to QoI fungicides in populations of *Podosphaera fusca* in south central Spain. *European Journal of Plant Pathology* **115**, 215–222.

**Gil F, Gay JL.** 1977. Ultrastructural and physiological properties of the host interfacial components of haustoria of *Erysiphe pisi* in vivo and in vitro. *Physiological Plant Pathology* **10**, 1–12.

**Godfrey D, Böhlenius H, Pedersen C, Zhang Z, Emmersen J, Thordal-**

**Christensen H.** 2010. Powdery mildew fungal effector candidates share N-terminal Y/F/WxC-motif. *BMC Genomics* **11**.

**Godfrey D, Zhang Z, Saalbach G, Thordal-Christensen H.** 2009. A proteomics study of barley powdery mildew haustoria. *Proteomics* **9**, 3222–3232.

**Hacquard S.** 2014. The genomics of powdery mildew fungi: Past achievements, present status and future prospects. *Advances in Botanical Research* **70**, 109-142.

**Hemsworth GR, Johnston EM, Davies GJ, Walton PH.** 2015. Lytic polysaccharide monooxygenases in biomass conversion. *Trends in Biotechnology* **33**, 747–761.

**Jonge R De, Esse HP Van, Kombrink A, Shinya T, Desaki Y, Bours R, Krol S Van Der, Shibuya N, Joosten MHAJ, Thomma BPHJ.** 2010. Conserved fungal LysM Effector Ecp6 prevents chitin-triggered immunity in plants. *Science* **329**, 953–955.

**Kelly LA, Mezulis S, Yates C, Wass M, Sternberg M.** 2015. The Phyre2 web portal for protein modelling, prediction, and analysis. *Nature Protocols* **10**, 845–858.

**Koh S, André A, Edwards H, Ehrhardt D, Somerville S.** 2005. *Arabidopsis thaliana* subcellular responses to compatible *Erysiphe cichoracearum* infections. *Plant Journal* **44**, 516–529.

**Kombrink A, Thomma BPHJ.** 2013. LysM effectors secreted proteins supporting fungal life. *PLoS Pathog* **9**, e1003769.

**Kuzuya M, Yashiro K, Tomita K, Ezura H.** 2006. Powdery mildew (*Podosphaera xanthii*) resistance in melon is categorized into two types based on inhibition of the infection processes. *Journal of Experimental Botany* **57**, 2093–2100.

**Lam SD, Dawson NL, Das S, Sillitoe I, Ashford P, Lee D, Lehtinen S, Orengo CA, Lees JG.** 2016. Gene3D: Expanding the utility of domain assignments. *Nucleic Acids Research* **44**, D404–D409.

**Li L, Liu C, Lian X.** 2010. Gene expression profiles in rice roots under low phosphorus stress. *Plant Molecular Biology* **72**, 423–432.

**Link TI, Lang P, Scheffler BE, et al.** 2014. The haustorial transcriptomes of *Uromyces appendiculatus* and *Phakopsora pachyrhizi* and their candidate effector families. *Molecular Plant Pathology* **15**, 379–393.

**Liu T, Liu Z, Song C, et al.** 2012. Chitin-induced dimerization activates a plant immune receptor. *Science* **336**, 1160–1164.

**Love MI, Huber W, Anders S.** 2014. Moderated estimation of fold change and dispersion for RNA-seq data with DESeq2. *Genome Biology* **15**, 550.

**Lovelace L, Lewinski K, Jakob C, Kuciel R, Ostrowski W, Lebioda L.** 1997. Prostatic acid phosphatase: structural aspects of inhibition by L-(+)-tartrate ions. *Acta Biochimica Polonica* **44**, 673–678.

**Mackie AJ, Roberts AM, Callow JA, Green JR.** 1991. Molecular differentiation in pea powdery-mildew haustoria. *Planta* **183**, 399–408.

**Martínez-Cruz,** 2016. Análisis morfológico y funcional de la interacción *Podosphaera xanthii*- cucurbitáceas. PhD thesis, University of Malaga, Malaga, Spain.

**Martínez-Cruz J, Romero D, Dávila JC, Pérez-García A.** 2014. The *Podosphaera xanthii* haustorium, the fungal Trojan horse of cucurbit-powdery mildew interactions. *Fungal genetics and biology* **71**, 21–31.

**Martínez-Cruz J, Romero D, de la Torre FN, Fernández-Ortuño D, Torés JA, de Vicente A, Pérez-García A.** 2018a. The functional characterization of *Podosphaera xanthii* candidate effector genes reveals novel target functions for fungal pathogenicity. *Molecular Plant-Microbe Interactions*

31, 914-931.

**Martínez-Cruz J, Romero D, De Vicente A, Pérez-García A.** 2018*b*. Transformation by growth onto agro-infiltrated tissues (TGAT), a simple and efficient alternative for transient transformation of the cucurbit powdery mildew pathogen *Podosphaera xanthii*. *Molecular Plant Pathology* **19**, 2502–2515.

**McGrath T.** 2010. Fungicide resistance in cucurbit powdery mildew fungi. *Plant Disease* **85**, 236–245.

**Miazzi M, Laguardia C, Faretra F.** 2011. Variation in *Podosphaera xanthii* on cucurbits in southern Italy. *Journal of Phytopathology* **159**, 538–545.

**Micali CO, Neumann U, Grunewald D, Panstruga R, O'Connell R.** 2011. Biogenesis of a specialized plant-fungal interface during host cell internalization of *Golovinomyces orontii* haustoria. *Cellular Microbiology* **13**, 210–226.

**Mochizuki S, Saitoh K ichiro, Minami E, Nishizawa Y.** 2011. Localization of probe-accessible chitin and characterization of genes encoding chitin-binding domains during rice-*Magnaporthe oryzae* interactions. *Journal of General Plant Pathology* **77**, 163–173.

**Oliva R, Win J, Raffaele S, et al.** 2010. Recent developments in effector biology of filamentous plant pathogens. *Cellular Microbiology* **12**, 705–715.

**Pagni M, Ioannidis V, Cerutti L, Zahn-Zabal M, Jongeneel CV, Hau J, Martin O, Kuznetsov D, Falquet L.** 2007. MyHits: Improvements to an interactive resource for analyzing protein sequences. *Nucleic Acids Research* **35**, W433–W437.

**Pedersen C, van Themaat EVL, McGuffin LJ, et al.** 2012. Structure and evolution of barley powdery mildew effector candidates. *BMC Genomics* **13**, 694.

**Pennington HG, Gheorghe DM, Damerum A, Pliego C, Spanu PD,**



**Cramer R, Bindschedler L V.** 2016. Interactions between the powdery mildew effector BEC1054 and barley proteins identify candidate host targets.

**Pérez-García A, Romero D, Fernández-Ortuño D, López-Ruiz F, De Vicente A, Torés JA.** 2009. The powdery mildew fungus *Podosphaera fusca* (synonym *Podosphaera xanthii*), a constant threat to cucurbits. *Molecular plant pathology* **10**, 153–160.

**Pettersen EF, Goddard TD, Huang CC, Couch GS, Greenblatt DM, Meng EC, Ferrin TE.** 2004. UCSF Chimera--a visualization system for exploratory research and analysis. *Journal of computational chemistry* **25**, 1605–1612.

**Pieterse CMJ, Leon-Reyes A, Van Der Ent S, Van Wees SCM.** 2009. Networking by small-molecule hormones in plant immunity. *Nature Chemical Biology* **5**, 308–316.

**del Pino D, Olalla L, Pérez-García A, Rivera ME, García S, Moreno R, de Vicente A, Torés JA.** 2002. Occurrence of races and pathotypes of cucurbit powdery mildew in southeastern Spain. *Phytoparasitica* **30**, 459–466.

**Lo Presti L, Lanver D, Schweizer G, Tanaka S, Liang L, Tollot M, Zuccaro A, Reissmann S, Kahmann R.** 2015. Fungal effectors and plant susceptibility. *Annual Review of Plant Biology* **66**, 513–545.

**Rovenich H, Boshoven JC, Thomma BP.** 2014. Filamentous pathogen effector functions: of pathogens, hosts and microbiomes. *Current opinion in plant biology* **20**, 96–103.

**Sánchez-Vallet A, Saleem-Batcha R, Kombrink A, Hansen G, Valkenburg D-J, Thomma BP, Mesters JR.** 2013. Fungal effector Ecp6 outcompetes host immune receptor for chitin binding through intrachain LysM dimerization. *eLife* **2**, e00790.

**Seifi A, Gao D, Zheng Z, Pavan S, Faino L, Visser RGF, Wolters AMA,**

**Bai Y.** 2014. Genetics and molecular mechanisms of resistance to powdery mildews in tomato (*Solanum lycopersicum*) and its wild relatives. *European Journal of Plant Pathology* **138**, 641–665.

**Seoane P, Espigares M, Carmona R, et al.** 2018. TransFlow: a modular framework for assembling and assessing accurate *de novo* transcriptomes in non-model organisms. *BMC Bioinformatics* **19**,(Suppl 14): 416.

**Seoane P, Ocaña S, Carmona R, Bautista R, Madrid E, M. Torres A, Gonzalo Claros M.** 2016. AutoFlow, a versatile workflow engine illustrated by assembling an optimised *de novo* transcriptome for a non-model species, such as faba bean (*Vicia faba*). *Current Bioinformatics* **11**, 440–450.

**Spanu PD, Abbott JC, Amselem J, et al.** 2010. Genome expansion and gene loss in powdery mildew fungi reveal tradeoffs in extreme parasitism. *Science* **330**, 1543–1546.

**Srivastava PK, Anand A.** 2015. The inhibitory effect of metals and other ions on acid phosphatase activity from *Vigna aconitifolia* seeds. *Preparative Biochemisstry and Biotechnology* **45**, 33–41.

**Takamatsu S.** 2013. Origin and evolution of the powdery mildews (ascomycota, eryliphales). *Mycoscience* **54**.

**Tanaka K, Nguyen CT, Liang Y, Cao Y, Stacey G, Tanaka K, Nguyen CT, Liang Y, Cao Y, Stacey G.** 2013. Role of LysM receptors in chitin-triggered plant innate immunity Role of LysM receptors in chitin-triggered plant innate immunity. *Plant Signaling & Behavior* **8**, e22598.

**Thimm O, Bläsing O, Gibon Y, Nagel A, Meyer S, Krüger P, Selbig J, Müller LA, Rhee SY, Stitt M.** 2004. MAPMAN: A user-driven tool to display genomics data sets onto diagrams of metabolic pathways and other biological processes. *Plant Journal* **37**, 914–939.

**Thordal-Christensen H, Zhang Z, Wei Y, Collinge DB.** 1997. Subcellular

localization of H<sub>2</sub>O<sub>2</sub> in plants. H<sub>2</sub>O<sub>2</sub> accumulation in papillae and hypersensitive response during the barley-powdery mildew interaction. *Plant Journal* **11**, 1187–1194.

**Ullah AH, Sethumadhavan K, Mullaney EJ.** 2011. Vanadate inhibition of fungal PhyA and bacterial AppA2 histidine acid phosphatases. *Journal of agricultural and food chemistry* **59**, 1739–1743.

**Vaaje-Kolstad G, Westereng B, Horn SJ, Liu Z, Zhai H, Sørli M, Eijsink VGH.** 2010. An oxidative enzyme boosting the enzymatic conversion of recalcitrant polysaccharides. *Science* **330**, 219–222.

**Vela-Corcía D, Bautista R, De Vicente A, Spanu PD, Pérez-García A.** 2016. *De novo* analysis of the epiphytic transcriptome of the cucurbit powdery mildew fungus *Podosphaera xanthii* and identification of candidate secreted effector proteins. *PLoS ONE* **11**, e0163379.

**Weßling R, Schmidt SM, Micali CO, Knaust F, Reinhardt R, Neumann U, Ver Loren van Themaat E, Panstruga R.** 2012. Transcriptome analysis of enriched *Golovinomyces orontii* haustoria by deep 454 pyrosequencing. *Fungal Genetics and Biology* **49**, 470–482.

**Xi Y, Pan PL, Ye YX, Yu B, Zhang CX.** 2014. Chitin deacetylase family genes in the brown planthopper, *Nilaparvata lugens* (Hemiptera: Delphacidae). *Insect Molecular Biology* **23**, 695–705.

**Xia Y, Clarkson JM, Charnley KA.** 2001. Acid phosphatases of *Metarhizium anisopliae* during infection of the tobacco hornworm *Manduca sexta*. *Archives of Microbiology* **176**, 427–434.

**Yang J, Hsiang T, Bhadauria V, Chen XL, Li G.** 2017. Plant Fungal Pathogenesis. *BioMed Research International* **2017**, 2–4.

**Zanni R, Galvez-Llompарт M, Garcia-Pereira I, Galvez J, García-Domenech R.** 2018. Molecular topology and QSAR multi-target analysis to

boost the in silico research for fungicides in agricultura chemistry. Molecular Diversity doi:10.1007/s11030-018-9879-3.

**Zhang Y.** 2008. I-TASSER server for protein 3D structure prediction. BMC bioinformatics **9**, 40.



# CHAPTER I

## General Introduction and objectives



## THE POWDERY MILDEWS

Crops around the world are affected by different plant diseases that produce losses in production yields and reductions in the quality of fruits and vegetables (Yang *et al.*, 2017). These diseases may be caused by nematodes, fungi, oomycetes, bacteria or viruses (Baker *et al.*, 1997). However, the fungi are the main causal agents of these diseases, constituting the largest number of plant pathogens (Doehlemann *et al.*, 2017). Pathogenic fungi use several strategies to infect plants. Thus, necrotrophic fungi kill their hosts for feeding from death cells whereas biotrophic fungi colonize their host to uptake nutrients from living cells (Wen, 2013). Among the latter the powdery mildew fungi stand out. These are fungi that cause the so-called powdery mildew diseases. Powdery mildews are obligate biotrophic fungi that belong to the Phylum *Ascomycota*, Class *Leotiomycetes*, Order *Erysiphales*, and Family *Erysiphaceae* (Hacquard, 2014). Nowadays, about 900 species included in sixteen genera have been described in the *Erysiphaceae* family (Braun and Cook, 2012; Hacquard, 2014).

The powdery mildew fungi cause diseases in a broad range of angiosperm hosts (Panstruga and Schulze-Lefert, 2002), including both dicotyledons and monocotyledons (Braun and Cook, 2012, Takamatsu, 2013; Seifi *et al.*, 2014). The diseases they cause are clearly recognizable by the presence of white powdery spots on both leaf surfaces (Figure 1.2), petioles, stems and, rarely, on fruits (Eichmann and Hüchelhoven, 2008; Pérez-García *et al.*, 2009). Powdery mildews act as parasites and, hence, do not directly cause the death of the plant cells, as occurs with necrotrophic fungi. This is because they need living cells to obtain nutrients and to complete their life cycles (Vogel *et al.*, 2004). However, their development may cause the indirect death of plant tissue, due to



a nutrient redistribution called “green island”, (Hückelhoven, 2005), the reduction in photosynthesis and the disruption of stomatal behavior (Prats *et al.*, 2006).

Although in the last years the studies about the molecular bases of powdery mildew diseases have increased, the typical obligate biotrophic lifestyle of these fungi has hampered research and, compared with other fungal diseases, the molecular bases of powdery mildew diseases remain virtually unknown in most cases. In this chapter, we summarized the current knowledge of the cucurbits powdery mildew disease, one of the most economically important powdery mildew diseases and one of the most devastating diseases of cucurbits. We will focus on the molecular aspects of pathogen-host interactions as well as in the main parasitism structure of these fungi, the haustorium.

## **THE CUCURBITS POWDERY MILDEW**

The cucurbit family (*Cucurbitaceae*) is a medium-size family of plants that grow in warm regions around the world, includes various species with great economic importance and comprises an important source of starch and edible fruits in many diets. The main cultivated species are melon, watermelon, zucchini, cucumber and pumpkin, although other minor species such as citron, gherkin, chayote, gourds, wild cucumber and horned cucumber also are included in this family (Pérez-García *et al.*, 2009). Nevertheless, the production of these different crops is reduced due to over 200 different diseases that affect cucurbits (Zitter *et al.* 1996). Cucurbits powdery mildew is the main disease of fungal origin that affects cucurbits under both greenhouse and open field

conditions, causing serious damage and important yield losses. Powdery mildew diseases reduce the fruit quality and can decrease crop yields by up to 50%, but under certain conditions, losses can increase to 100% (Leonar and Gianessi 2005).

There are two fungal species that cause this disease in cucurbits, *Golovinomyces cichoracearum* and *Podosphaera xanthii* (Kuzuya *et al.*, 2006; Pérez-García *et al.*, 2009; Miazzi *et al.*, 2011). The geographical distributions of these fungi are different, *G. cichoracearum* predominates in continental Europe, while *P. xanthii* prevails in Mediterranean and tropical areas. This different distribution depends on the optimum temperature for conidial germination, 15-25 °C in the case of *G. cichoracearum* and 25-30 °C in the case of *P. xanthii* (Miazzi *et al.*, 2011). Moreover, although these fungi cause the same symptoms, they are clearly distinguished from each other by visualization under light microscopy (Romero *et al.*, 2004; Fernández-Ortuño *et al.*, 2006; Pérez-García *et al.*, 2009). In this way, while *P. xanthii* shows conidia with fibrosin bodies and lateral germination, *G. cichoracearum* presents conidia without fibrosin bodies and apical germination (Figure 1.1A).

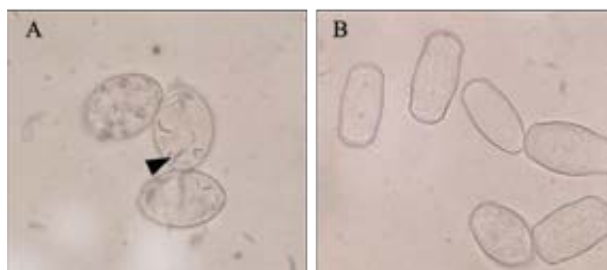


**Figure 1.1.** Micrographs showing conidia of the main fungal species that cause powdery mildew disease in cucurbits. A) Conidia from *Podosphaera xanthii*. B) Conidia from *Golovinomyces cichoracearum*. The arrow indicates the typical fibrosin bodies present in *P. xanthii* conidia.

*P. xanthii* is considered to be the major causal agent of cucurbits powdery mildew around the world and the sole cause of this disease in southern of Spain, being one the most important limiting factors for cucurbit production (del Pino *et al.*, 2002; Fernández-Ortuño *et al.*, 2006). *P. xanthii*, as a powdery mildew fungus, belongs to the *Erysiphaceae* family included in the Phylum *Ascomycota*, Class *Leotiomycetes* and Order *Erysiphales*. However, its nomenclature is not yet well standardized in the literature. In this way, *P. xanthii* has been named *Sphaeroteca fuliginea*, *Sphaeroteca fusca*, *Podosphaera fusca* and, more recently, *Podosphaera xanthii*. The reduction of the *Sphaeroteca* genus to *Podosphaera* is widely accepted according to scanning electron microscopy and molecular results (Braun *et al.*, 2002). On the other hand, the separation between *P. fusca* and *P. xanthii* was proposed based on the teleomorph morphological structure, by which the pathogen on cucurbits seems to have a larger ascumata and an ascus with a larger oculus (Braun and Takamatsu, 2000; Braun *et al.*, 2001). However, to date, this nomenclature remains controversial and many authors continue to consider *P. xanthii* and *P. fusca* as synonymous.

Like other powdery mildews diseases, the symptoms caused by *P. xanthii* are easily recognizable, with the characteristic talcum-like whitish fungal growth developed on both leaf surfaces, petioles, stems, and rarely on fruits (Sitterly 1978; Zitter *et al.*, 1996) (Figure 1.2A). These visible and typical powdery mildew colonies are composed by a weft of mycelia, conidiophores and conidia (Figure 1.2B) that reveal the growth *P. xanthii* on a susceptible host. Moreover, *P. xanthii*, like other powdery mildew fungi, also develops inside host epidermal cells (Hückelhoven and Panstruga, 2011). In this location, *P. xanthii* subsists and uptakes nutrients from the host through a specialized feeding and parasitism structure called the haustorium (Figure 1.2E).

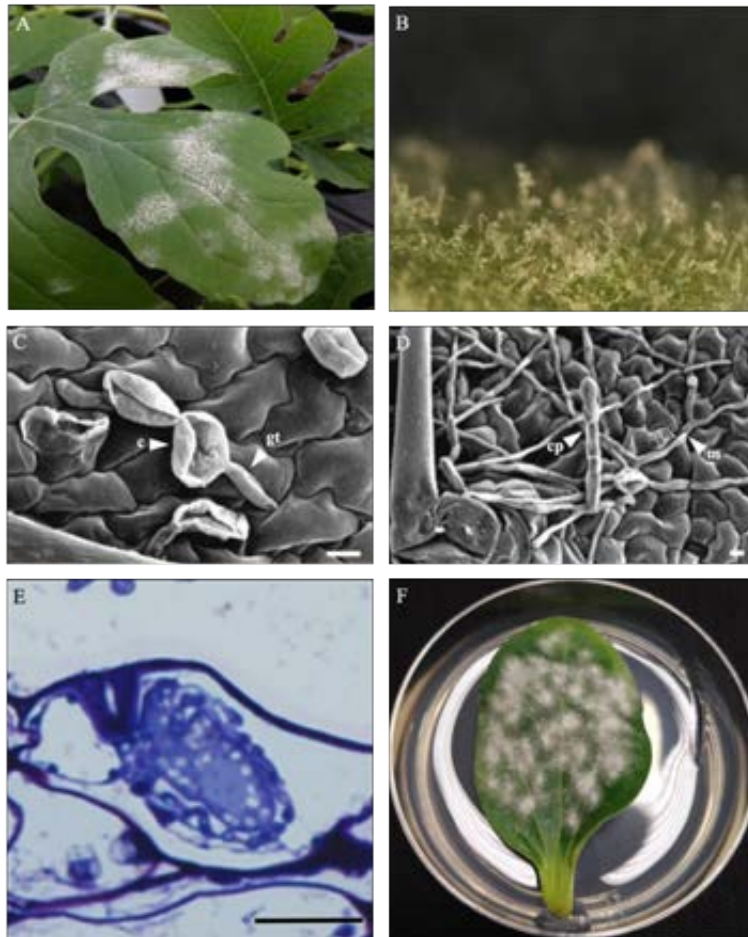


**Figure 1.2.** Typical symptoms and main development structures of the cucurbit powdery mildew agent *P. xanthii*. A) Watermelon leaf grown under greenhouse conditions with typical talcum-like whitish colonies of *P. xanthii*. B) Detail of *P. xanthii* conidiophores onto a zucchini cotyledon. C) Scanning electron micrograph of a *P. xanthii* germinated conidia (c) showing the developed of germ tube (gt). D) Scanning electron micrograph of *P. xanthii* hyphae (h) and conidiophore (cp). E) Light microscopy picture of a *P. xanthii* haustorium developed into a zucchini epidermal cell. F) A typical laboratory culture of *P. xanthii* maintained *in vitro* onto a zucchini cotyledon. Scale bars 10  $\mu\text{m}$ . Pictures C and D were taken from Pérez-García *et al.* (2001). Picture E was taken from Martínez-Cruz *et al.* (2014).

### *Life cycle and disease establishment*

*P. xanthii* is a heterothallic fungus that shows both sexual and asexual life cycles. In the first case, the reproduction occurs after the encounter of two opposite mating type hyphae. As a consequence of this encounter, a fruit body called chasmothecium is formed, which contains one ascus bearing eight sexual spores or ascospores (Figure 1.3) (McGrath, 1994). Chasmothecia are considered to be overwintering sources of inoculum in some areas (Pirondi *et al.*, 2015a). However, chasmothecia are rarely or never have been observed in several of the world's most important cucurbit areas such as Spain. For this reason, the prevalence and epidemiological relevance of the pathogen sexual reproduction remains unknown (Pérez-García *et al.*, 2009). Moreover, the *P. xanthii* populations are likely to be predominantly clonal, suggesting that asexual reproduction is the major reproduction type of this fungal species (Pirondi *et al.*, 2015b).

The asexual reproduction of *P. xanthii* is very similar to those of other powdery mildew fungi (Figure 1.3). After the landing of conidia onto a susceptible host, a short primary germ tube is produced, which senses the nature of the surface (Both *et al.*, 2005b; Pérez-García *et al.*, 2009) and ends in a primary differentiated appressorium. This appressorium is responsible of the penetration of the cuticle and the cell wall of plant epidermal cells, remaining intact the host plasma membrane (Eichman and Hukelhoven, 2008). The high turgor pressure generated in the appressorium, together with the activity of a combination of lytic enzymes such as cellobiohydrolases and cutinases, enable that a hyphal peg may penetrate into the host epidermal cell and forms a primary haustorium (Tucker and Talbot, 2002; Hükelhoven, 2005; Godfrey *et al.*, 2009). When a functional haustorium is formed, the epiphytic mycelium

proliferates forming additional secondary appressoria and, hence, further haustoria. Later, the primary hypha branches and forms the secondary hyphae. Conidiophores emerge vertically from some of the secondary hyphae as morphologically distinct structures and produce 5-10 ovoid-shaped asexual conidia in chains (Both *et al.*, 2005b). The weft of hyphae and conidia form the white colonies on the plant surface, which are visible to the naked eye about 5-6 days after inoculation.

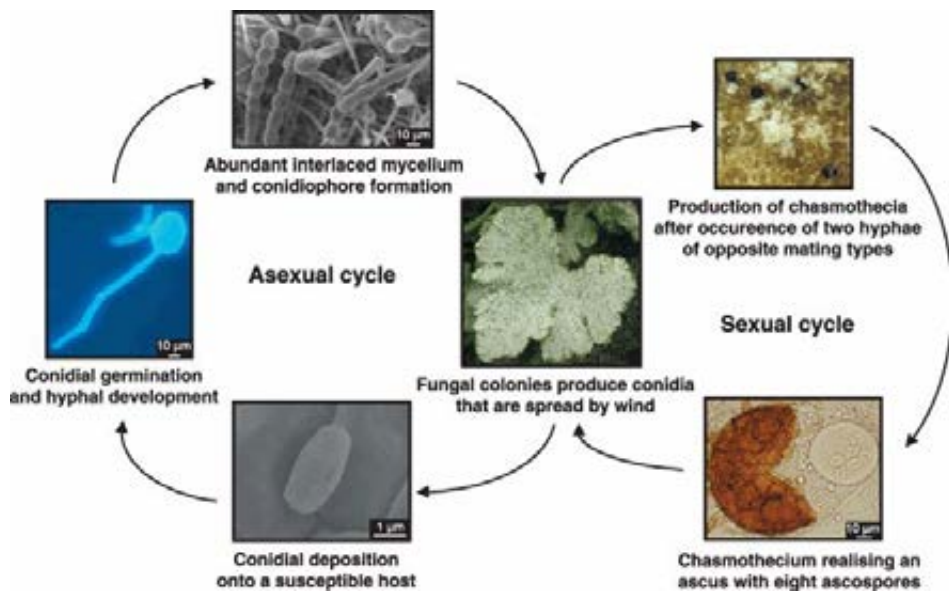


**Figure 1.3.** Life cycle of *P. xanthii*. Taken from Pérez-García *et al.* (2009).

### *Disease management*

To manage powdery mildew disease caused by *P. xanthii*, the use of several control approaches such as cultural practices, the employ of resistant cultivars, the application of fungicides and more recently, the use of biocontrol agents, are

recommended (Jahn *et al.*, 2002; Jarvis *et al.*, 2002; Romero *et al.*, 2004; Chen *et al.*, 2007).

*P. xanthii* is more damaging and frequent during high humidity periods. The high plant density and narrow row spacing, and certain management practices, may increase the relative humidity, facilitating the dispersion of the inoculum within crops and, hence, increasing the severity of the disease. For this reason, the cultural practices are one the main strategies for cucurbits powdery mildew management and have been focused on crop density and rotation, nutrition and soil conditions to cause a reduction of primary inoculum (Chen *et al.*, 2007). In addition, stubble burning may reduce, drastically, the primary inoculum of the fungus (Keinath 1996).

The genetic improvement as a strategy for powdery mildew control is a very important attribute that contributes to increase the crop yields and reduce the frequency of fungicides application, hence increasing health and environmental benefits (Pérez-García *et al.*, 2009). Breeding for resistance to powdery mildew in cucurbits has a long and successful history (Jahn *et al.*, 2002), since the use of resistant cultivars represents one of the main means of disease management, although with variable success (Zitter *et al.*, 1996). Many breeding lines and commercial varieties of squash, cucumber and melon have been released with resistance to *P. xanthii*. Several resistance genes (Pm) have been reported, especially in melon (Pitrat, 2002). Although recessive genes conferring resistance have been described, in most cases resistance is usually conferred by single dominant genes (Jahn *et al.*, 2002). In this way, a complete and updated list of resistance genes in cucurbits and supply services for researches about genetics and breeding of cucurbit species are available in databases such as Cucurbit Genetics Cooperative (CGC) (<http://cuke.hort.ncsu.edu/cgc/>). The fourth major crop, watermelon, has been traditionally considered to be resistant

to powdery mildew. Nevertheless, outbreaks of powdery mildew in watermelon have been reported that appear to be elicited by highly aggressive isolates of *P. xanthii* (Cohen *et al.*, 2000; Jahn *et al.*, 2002; del Pino *et al.*, 2002). Moreover, the development of new races of the pathogen, especially in melon, where there have been more than 30 reported sources of resistance to the 28 putative races of *P. xanthii* described so far (McCreight, 2006), hinders disease management through resistance breeding.

In practice, the application of fungicides remains as the main strategy for the control of cucurbits powdery mildew (McGrath, 2010). Fungicides are divided in two major groups, contact and systemic fungicides (Lucas 1998). Contact fungicides, such as Sulphur, dinitrophenyls or quinomethionate, have multiple modes of action and are used as preventive agents (López-Ruiz *et al.*, 2005). Nevertheless, they are highly toxic and negative for the environment. Systemic fungicides are site-specific compounds that affect a specific physiological function or metabolic pathway and they are effective both before and after the establishment of infection. Currently, systemic fungicides are the most commonly used against powdery mildews (Fraaije *et al.*, 2007). Among the fungicides registered in Spain for the control of cucurbits powdery mildew (Table 1.1) are found QoI fungicides such as azoxystrobin, which acts inhibiting mitochondrial respiration; DMI fungicides such as myclobutanil, which targets sterol 14 $\alpha$ -demethylase (CYP51) in the ergosterol biosynthetic pathway of fungi; MBC fungicides such as thiophanate-methyl, which acts inhibiting mitosis and cell division; inhibitors of signal transduction such as quinoxifen or inhibitors of nucleic acid synthesis such as bupirimate.



**Table 1.1.** Fungicides for the control of cucurbits powdery mildew registered in Spain.

Chemical group	Common name	Target
Carboxylic Acid Amides (AAC)	Dimethomorph	Cellulose synthase (cell wall byosynthesis)
Aryl-phenyl-ketones	Metrafenone	Unknown (actin/myosin/fimbrin function)
Aza-naphthalenes	Quinoxifen	Unknown (signal transduction)
Phenyl-acetamide	Cyflufenamid	Unknown
Hydroxy-(2-amino-) pyrimidines	Bupirimate	Adenosin-deaminase (nucleic acid metabolism)
Demethylation inhibitors (DMI)	Difenoconazole, fenbuconazole, myclobutanil, penconazole, tebuconazole, tetraconazole	C14- demethylase in sterol biosynthesis, <i>erg11/cyp51</i> genes (sterol biosynthesis in membranes)
Quinone outside inhibitors (Qoi)	Azoxystrobin, kresoxim-methyl, pyraclostrobin, trifloxystrobin	Complex III: cytochrome bc1 (ubiquinol oxidase) at Qo site ( <i>cyt b</i> gene) (respiration)
Succinate- dehydrogenase inhibitors (SDHI)	Boscalid, fluopyram, fluxapyroxad, isopyrazam	Complex II: succinate-dehydrogenase (respiration). Sdh subunits.
Methyl benzimidazole carbamates (MBC)	Thiophanate-methyl	<i>β-tubulin</i> gene (β-tubulin assembly in mitosis)

Unfortunately, the impact of chemical control have been moderated, since *P. xanthii* develops resistance to different compounds very rapidly (Fernández-Ortuño *et al.*, 2006; Bellón-Gómez *et al.*, 2015), making that most of fungicides become ineffective (Hollomon and Wheeler, 2002). Hence, the molecular analyses of powdery mildews-hosts interactions are necessary to identify novel targets in the fungal agent, which may allow the development of new anti-powdery mildew fungicides or resistant cultivars.

Recently, biocontrol or the use of natural enemies of the pathogens is another strategy employed in powdery mildew management. Biocontrol agents with modes of action based on induction of plant systemic resistance, parasitism or antibiosis could be efficient against powdery mildews (Paulitz and Richard, 2001). Currently, several organisms such as fungi, yeasts, arthropods or bacteria with different mechanisms of action have been described in literature. Among them, strains of the *Bacillus* genus stand out, which have been described as efficient biocontrol agents against the cucurbit powdery mildew *P. xanthii* by means of antibiosis (Romero *et al.*, 2004; 2007). Moreover, some of these

strains also showed abilities as inducers of systemic resistance and as plant growth promoting rhizobacteria (PGPR) in melon (García-Gutiérrez *et al.*, 2012). Some of these strains are being currently marketed by the Dutch company Koppert B.V. Nevertheless, the implementation in practice of biological control tools against cucurbit powdery mildew is still very limited.

## **THE POWDERY MILDEW-HOST INTERACTIONS**

Cucurbit powdery mildew remains as a major challenge in agriculture and, therefore, a deep understanding of molecular mechanisms governing this disease is necessary to identify key points that allow the development of novel control tools (Rezzonico *et al.*, 2017). Advances in new generation sequencing technologies combined with different bioinformatics approaches have allowed to obtain valuable transcriptomics information about powdery mildew-host interactions and to report whole-transcriptomic changes in several powdery mildew-infected plants. In this way, transcriptomic analyses of both sensible and resistant cultivars of grape infected with *Erysiphe necator* (Fung *et al.*, 2007; Borges *et al.*, 2013; Weng *et al.*, 2014), of a sensible strawberry cultivar infected with *Podosphaera aphanis* (Jambagi and Dunwell, 2015) and of sensible and resistant wheat cultivars infected with *Blumeria graminis* f. sp *tritici* (Xin *et al.*, 2012; Zhang *et al.*, 2014), have been developed. Moreover, in wheat infected with *B. graminis* f. sp *tritici* a proteomic analysis has been developed (Fu *et al.*, 2016). These analyses allow obtaining necessary and valuable information about the host changes as a consequence of powdery mildew infection and they are the first step on the long road towards the

development of new resistant cultivars in these crops. Nevertheless, although transcriptomes and genomes of major cucurbits crops as melon, zucchini, watermelon and cucumber are available (Huang *et al.*, 2009; Guo *et al.*, 2011; Ando *et al.*, 2012; Blanca *et al.*, 2012; Garcia-Mas *et al.*, 2012; Xu *et al.*, 2013; Montero-Pau *et al.*, 2017), only two studies that describe transcriptomic profiles of melon and pumpkin cultivars resistant to *P. xanthii* have been reported (Li *et al.*, 2015; Guo *et al.*, 2018; Zhu *et al.*, 2018) and, thus, the changes caused by *P. xanthii* in its hosts during compatible interactions remain unknown.

In the other hand, several genomes of different powdery mildew fungi such as *Oidium neolycopersici*, *Erysiphe necator*, *Golovinomyces orontii*, *B. graminis* f. sp. *tritici* and *B. graminis* f. sp. *hordei*, which are the causal agents of tomato, grape, *Arabidopsis*, wheat and barley powdery mildews, respectively (Baxter *et al.*, 2010; Spanu *et al.*, 2010; Duplessis *et al.*, 2011; Hacquard *et al.*, 2013; Wicker *et al.*, 2013; Jones *et al.*, 2014; Wu *et al.*, 2018) have been developed. These genomes, together with several transcriptomic studies of these pathogens along different stages of infection (Both *et al.*, 2005*b,a*; Weßling *et al.*, 2012; Asai *et al.*, 2014; Jones *et al.*, 2014; Bindschedler *et al.*, 2016; Vela-Corcía *et al.*, 2016), provide new insights into the pathogenesis and biotrophy of powdery mildew fungi such as the identification of missing genes and metabolic pathways, the genome expansion with the proliferation of transposable elements and the repertoire of effector candidate genes (Baxter *et al.*, 2010; Spanu *et al.*, 2010; Duplessis *et al.*, 2011; Kemen *et al.*, 2011; Wicker *et al.*, 2013).

Moreover, advances in genomics and transcriptomics as well as the recent development of several tools for gene functional analysis in powdery mildew fungi such as transient transformation and host-induced gene silencing (Nowara *et al.*, 2010; Pliego *et al.*, 2013; Martínez-Cruz *et al.*, 2017, 2018*b*), have

allowed to develop different molecular studies about biotrophic fungi – hosts interactions, standing out the study of effectors (Godfrey *et al.* 2010; Hacquard *et al.* 2012; Pedersen *et al.* 2012; Vela-Corcía *et al.* 2016) due to their importance in manipulation of the host by inhibiting their defense mechanisms (Ridout *et al.*, 2006; Block *et al.*, 2008; Göhre and Robatzek, 2008).

### *The powdery mildew effectors*

Powdery mildew fungi as well as other biotrophic fungi such as rust fungi, maintain a close relationship with its host, since they need to obtain nutrients from living plant cells. To this end, they have developed a specialized structure of parasitism termed haustorium (Godfrey *et al.*, 2009; Ahmed *et al.*, 2015; Pennington *et al.*, 2016). Moreover, to avoid being recognized and, hence, to be able to maintain this close relationship with its host, the biotrophic fungi need to manipulate the defense mechanisms of the plant. For this purpose, among others, these pathogens release a wide battery of proteins denominated effectors (Godfrey *et al.*, 2010; Chaudhari *et al.*, 2014; Lo Presti *et al.*, 2015). Effectors may be defined as proteins secreted by the pathogen, which protect the fungal integrity, alter the structure of host cell physiology and modulate plant defense response to colonize and proliferate into them (Pedersen *et al.*, 2012; Rovenich *et al.*, 2014; Lo Presti *et al.*, 2015).

Plants are able to trigger their defense responses through two different mechanisms: PAMP-triggered immunity (PTI) and effector-triggered immunity (ETI) (Figure 1.4). The PTI is the recognition of pathogen associated molecular patterns (PAMP) by specialized plant pattern recognition receptors (PRRs) (Figure 1.4A) (van Loon *et al.*, 2006). PAMPs are conserved epitopes along the pathogens such as flagellin and peptidoglycan from bacterial cell wall or a major

component of fungal cell wall, the chitin (Pozo *et al.*, 2005). For its part, the ETI consist in the recognition of the effector proteins released by a pathogen. This recognition is carried out by the host resistance (R) proteins (van Loon *et al.*, 2006) (Figure 1.4B). The PTI and ETI cause several signaling mechanisms, such as the activation of the hypersensitive response (HR), the accumulation of reactive oxygen species (ROS) and hormone signaling, during immune response. In this way, although HR is often associated to ETI (van Loon *et al.*, 2006) and ROS production to PTI (Navarro *et al.*, 2006), the two mechanisms can be activated in both PTI or ETI, like occurs with the signaling by the classical immunity hormones such as salicylic acid, jasmonic acid and ethylene (Pieterse *et al.*, 2009).

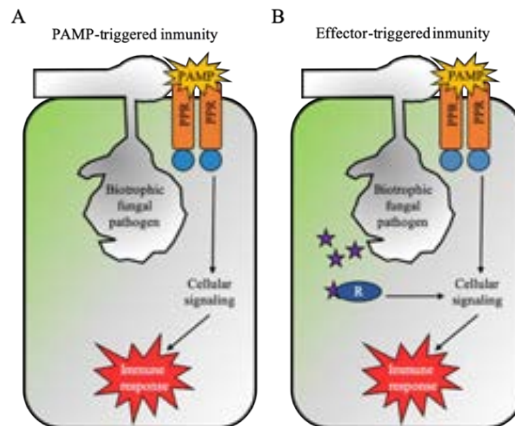


**Figure 1.4.** Schematic representation of the innate immunity in plants. A) PAMP-triggered immunity (PTI). Pathogen-associated molecular patterns (PAMPs) from pathogen are recognized by pattern-recognition receptors (PRRs) in the host, leading to a cellular signaling and resulting in immune response. C) Effector-triggered immunity (ETI). Effectors (purple stars) released by pathogen into the host cell are recognized by resistance (R) receptor, resulting in a cellular signaling and leading to immune response.

In plant pathogenic fungi, effectors are classified into cytoplasmic and apoplastic, depending on their final destination in the host. The last are small proteins (less than 300 amino acids) and highly cysteine-rich that, usually, exhibit inhibitory activity against extracellular host hydrolytic enzymes (Stergiopoulos and de Wit, 2009). The function and direct host targets of cytoplasmic effectors is little known, although some of them present a functional nuclear localization signal (NLS) that suggests the nucleus as possible target (Kemen *et al.*, 2005). Relatively few fungal effectors have been functionally characterized in comparison with oomycetes or bacterial effectors (Lo Presti *et al.*, 2015). Among the effectors analyzed in fungi, those related with the modulation of plant defense responses are found (van den Burg *et al.*, 2007; Bolton *et al.*, 2008; Jonge *et al.*, 2010; Mentlak *et al.*, 2012; Sánchez-Vallet *et al.*, 2013). This is the case of Avr4 and Ecp6 from *Cladosporium fulvum* or Slp1 from *Cladosporium fulvum*. Avr4 is an apoplastic effector with chitin-binding domain that protects the fungal cell wall against hydrolysis by plant chitinases (van den Burg *et al.*, 2006; van Esse *et al.*, 2007), while Ecp6 and Slp1 sequester free chitin oligomers produced by the degradative activity of plant chitinases, avoiding the activation of PTI by chitin recognition (Bolton *et al.*, 2008; Jonge *et al.*, 2010; Mentlak *et al.*, 2012; Sánchez-Vallet *et al.*, 2013).

Focusing on powdery mildew effectors, they usually share an Y/F/WxC N-terminal amino acid motif, which consists in a conserved aromatic amino acid (Y, F or W) followed by any amino acid and then a cysteine (Godfrey *et al.*, 2010). This motif seems to be responsible of effector translocation into plant cell as occurs with oomycetes effectors, which present two classes of consensus sequences for protein translocation, RxLR and LxFLAK (Hacquard *et al.*, 2012; Schmidt *et al.*, 2014). Another hypothesis about the function of Y/F/WxC motif is related to allow a correct folding of the effector candidate (Hacquard *et al.*,

2012), although to date there is no evidence that these motifs are necessary for translocation or folding of the effector candidate proteins. Within powdery mildew effectors, it should be note the Candidates for Secreted Effector Proteins (CSEPs), defined as proteins with a predicted signal peptide, without transmembrane domain and without homology to other proteins outside the powdery mildew fungi (*Erysiphales*) (Pedersen *et al.*, 2012). The number of effectors is very variable among the different species of powdery mildews analyzed. In this way, the number of effectors identified in the epiphytic transcriptome of *E. necator* (Jones *et al.*, 2014) was 4 times higher than in epiphytic transcriptome of *P. xanthii* (Vela-Corcía *et al.*, 2016). Moreover, only 10 candidate effectors of the initial set of 248 identified in *B. graminis* f. sp. *hordei* were conserved in *E. pisi* and *G. orontii* (Spanu *et al.*, 2010). These data suggest that the most effectors are specific of the pathogen-host interaction as consequence of host adaptation. Despite the identification of many powdery mildew effectors, to date the number of characterized effectors is very limited due, mainly, to biotrophic specificity of most of these effectors and, hence, to the impossibility of functional annotation by sequence identity with other filamentous fungi.

AVR<sub>a10</sub> and AVR<sub>k1</sub> were the firsts effectors identified in *B. graminis* f. sp. *hordei* using a map-based cloning approach, which, moreover, lack secretion signal peptide (Ridout *et al.*, 2006). Other *B. graminis* f. sp. *hordei* effectors have been characterized, among which are a putative beta-1,3 glycosyltransferase, a putative metalloprotease and two putative secreted ribonucleases (Pliego *et al.*, 2013). It is interesting to note, the putative functions of CSEP0105 and CSEP0162, which have been proved to interact with two barley small heat shock proteins (Hsps). These proteins allow the adaptation of plant cell in order to overcome the stress during abiotic changes or biotic attacks

(Ahmed et al., 2015). Recently, several effectors previously identified in epiphytic transcriptome of *P. xanthii* have been characterized (Martínez-Cruz et al., 2018a). This is the case of for example, a phospholipid-binding protein (PEC019) that could be modifying the membrane organization, an  $\alpha$ -mannosidase (PEC032) that could be modifying proteins glycosylation and a cellulose-binding protein (PEC054) that could be avoiding the immunity triggered by cellulose (Martínez-Cruz et al., 2018a) (Table 1.2). However, these results are only the tip of the iceberg, being necessary to deepen more in the effector biology, especially in those secreted by specialized parasitism structure, the haustorium, in order to decipher the function of those proteins directly related with the infective process of *P. xanthii*.

**Table 1.2.** Summary of powdery mildew effectors characterized to date.

Effector	SP <sup>a</sup>	Localization	Silencing <sup>b</sup>	Target	Function	Reference
<i>Blumeria graminis</i> f. sp. <i>hordei</i>						
AVR <sub>ai10</sub>	No	Cytoplasm	Reduces HI	-	-	Ridout et al., 2006; Pliego et al., 2013
AVR <sub>ak1</sub>	No	Cytoplasm	Reduces HI	-	-	Ridout et al., 2006; Pliego et al., 2013
BEC1	Yes	Cytoplasm	Reduces HI	-	-	Schmidt et al., 2014
BEC2	Yes	Cytoplasm	Reduces HI	-	-	Schmidt et al., 2014
BEC3	Yes	Cytoplasm	Reduces HI	Thiopurine methyltransferase	-	Schmidt et al., 2014
BEC4	Yes	Cytoplasm	Reduces HI	ARF-GTPase activating protein and ubiquitin-conjugating enzyme	-	Schmidt et al., 2014
BEC5	Yes	Cytoplasm	Reduces HI	-	Interfere with host vesicle trafficking	Schmidt et al., 2014
BEC1019	Yes	Cytoplasm	Reduces HI	-	Metalloprotease	Pliego et al., 2013
BEC1011	Yes	-	Reduces HI	-	Supress plant cell death	Pliego et al., 2013
BEC1054	Yes	-	Reduces HI	Glutathione S-transferase, Pathogenesis-related protein PR5, Elongation factor 1 gamma (EF1G) and malate dehydrogenase	Ribonuclease	Pliego et al., 2013 Ahmed et al., 2015
BEC1038	Yes	-	Reduces HI	-	-	Pliego et al., 2013
BEC1016	Yes	-	Reduces HI	-	-	Pliego et al., 2013



## General Introduction

BEC1040	Yes	-	Reduces HI	-	-	Pliego <i>et al.</i> , 2013
BEC1018	Yes	-	Reduces HI	-	-	Pliego <i>et al.</i> , 2013
BEC1005	Yes	-	Reduces HI	-	$\beta$ 1-3 glucanase	Pliego <i>et al.</i> , 2013
CSEP0055	Yes	-	Reduces HI	Pathogenesis-related protein PR17c	Hamper penetration resistance	Zhang <i>et al.</i> , 2012
CSEP0105	Yes	Cytoplasm/ nucleus	Reduces HI	Heat-shock protein Hsp16.9 and Hsp17.5	Promotes virulence	Ahmed <i>et al.</i> , 2015
CSEP0162	Yes	Cytoplasm/ nucleus	Reduces HI	Heat-shock protein Hsp16.9 and Hsp17.5	-	Ahmed <i>et al.</i> , 2015
CSEP0254	Yes	Cytoplasm/ nucleus	Reduces HI	-	-	Ahmed <i>et al.</i> , 2016
CSEP0081	Yes	Cytoplasm/ nucleus	Reduces HI	-	-	Ahmed <i>et al.</i> , 2016
CSEP0443	Yes	Cytoplasm	Reduces HI	-	-	Unpublished
<b><i>Golovinomyces orontii</i></b>						
OEC2	Yes	-	-	-	BEC2 orthologue	Weßling <i>et al.</i> , 2014
OEC54	Yes	Sub-nuclear	-	Transcription factor TCP14	-	Weßling <i>et al.</i> , 2014
OEC45	Yes	-	-	-	-	Weßling <i>et al.</i> , 2014
OEC49	Yes	-	-	Functional target	-	Weßling <i>et al.</i> , 2014
OEC78	Yes	-	-	Functional target	-	Weßling <i>et al.</i> , 2014
OEC101	Yes	-	-	Functional target	-	Weßling <i>et al.</i> , 2014
<b><i>Podosphaera xanthii</i></b>						
PEC007	Yes	-	Reduces Hn	Putative methylation of nucleic acids	Putative methyltransferase	Martinez-Cruz <i>et al.</i> , 2018a
PEC009	Yes	-	Reduces Hn	Putative regulation of gene expression	Putative transcription factor	Martinez-Cruz <i>et al.</i> , 2018a
PEC019	Yes	-	Reduces Hn	Membrane organization	Phospholipid-binding protein	Martinez-Cruz <i>et al.</i> , 2018a
PEC032	Yes	-	Reduces Hn	Glycosylation from different proteins	Exo- $\alpha$ -mannosidase	Martinez-Cruz <i>et al.</i> , 2018a
PEC034	Yes	-	Reduces Hn	Putative vesicle trafficking	Putative ALIX protein	Martinez-Cruz <i>et al.</i> , 2018a
PEC054	Yes	-	Reduces Hn	Cellopentaose	Cellulose-binding protein	Martinez-Cruz <i>et al.</i> , 2018a

<sup>a</sup> Signal peptide

<sup>b</sup> Fungal growth indicator: HI = Haustorial index; Hn = Haustorial number

## THE HAUSTORIUM

The relationships between the biotrophic fungi and their plant hosts are quite diverse, from symbiosis to parasitism. Thus, whereas the endomycorrhizal fungi maintain a symbiotic relationship with the plant roots, the rust and powdery mildew fungi have a parasitic relationship with their hosts. In the case of endomycorrhizas, the fungi obtain mainly sugars from plant cells while help plants to obtain other nutrients such as phosphorus, sulfur, nitrogen and several minerals from soil. By contrast, in the case of parasitic fungi, they compete with the plant for the use of different nutrients such as sugars and amino acids. This competition is carried out developing, into the host plant cells, a specialized structure of parasitism called the haustorium. This structure has generated great interest in plant pathologists since its first description in 1853 (von Mohl, 1853). However, despite its early description, many questions are still open and come to mind when we talk about the haustorium. The main unsolved issues of haustorium are its establishment into the host cell, its composition, its capacity to avoid the plant recognition and its manner to uptake nutrients from host cells.

### *Haustorial development and establishment*

The wide morphological spectrum of haustoria is exemplified in the case of rust fungi, which have different stages, monokaryotic and dikaryotic, associated each one to different haustorial morphologies (Mendgen *et al.*, 2000). The monokaryotic stage produces M-haustoria, which appears as an hyphal extension without morphological differentiation (Gold and Mendgen 1991), whereas the dikaryotic haustoria are developed from external haustorial mother cell and present marked structural modifications compared to hyphal cells

(Heath and Skalamera, 1997). To simplify the explanation, we are going to exemplify the process of haustorial development centered on the haustoria of powdery mildew fungi (Figure 1.5), which has been less studied than rust haustoria.

In first place, and prior to haustorium formation, it is necessary the fungal penetration into the plant cell wall, which occurs by the release of several lytic enzymes (Eichmann and Hückelhoven, 2008) as well as by the formation of a fungal structure termed appressorium. From the appressorium will emerge the so-called penetration peg, which is a specialized hypha that penetrates cuticle and plant cell wall, which finally will enlarge to produce the haustorial body (Bushnell and Bergquist, 1974). Later, the haustorial body will be completely developed together with some prolongations emerging from it, the haustorial lobes (Figure 1.5) (Gil and Gay, 1977; Mackie *et al.*, 1991; Martínez-Cruz *et al.*, 2014). The haustorium is not really an intracellular structure, since the process of its formation causes the invagination of the host plasma membrane, which remains surrounding the haustorium, giving rise to the so-called extrahaustorial membrane (EHM) (Figure 1.5) (Gil and Gay, 1977; Mackie *et al.*, 1991; Martínez-Cruz *et al.*, 2014).

The appressorium and haustorium are separated by the haustorial neck where the EHM and the haustorial membrane (HM) are sealed by two neckbands regions called A band and B band (Chong and Harder, 1980; Stumpf and Gay, 1990; Mendgen *et al.*, 2000), whereas a septum with a pore, coming from the papilla rupture (Eichmann and Hückelhoven, 2008), separates the haustorial cytoplasm and the appressorium cytoplasm (Figure 1.5A) (Gil and Gay, 1977; Mackie *et al.*, 1991; Wang *et al.*, 2009; Micali *et al.*, 2011). All this leaves a space covered by a wide amorphous matter between the EHM and the HM termed the extrahaustorial matrix (EHMx) (Gil and Gay, 1977; Koh *et al.*,

2005), which can be considered a symplastic compartment (Voegelé and Mendgen, 2003) and seems ideal for nutrient uptake from the host (Gil and Gay, 1977; Micali *et al.*, 2011) (Figure 1.5). The set of haustorial body, haustorial lobes, HM, EHM and EHMx is denominated collectively as the haustorial complex (HC) (Figure 1.5) (Mackie *et al.*, 1991; Micali *et al.*, 2011; Martínez-Cruz *et al.*, 2014).

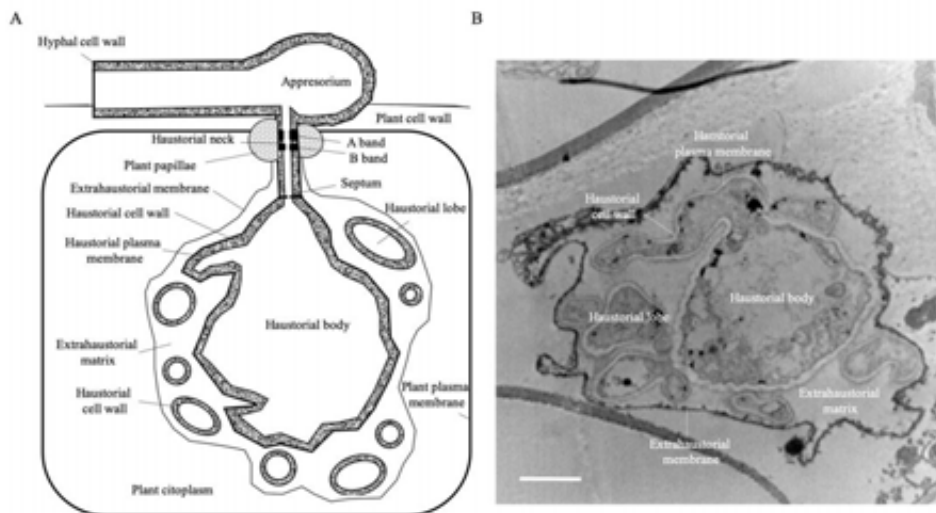


**Figure 1.5.** The powdery mildew haustorial complex. A) Schematic representation of a transversal section of a powdery mildew haustorial complex and its association with a host plant epidermal cell. B) Transverse section of a *P. xanthii* haustorial complex examined by transmission electron microscopy (TEM). Bar = 2  $\mu\text{m}$ . Modified from Martínez-Cruz *et al.* (2014).

### *Haustorial composition*

As previously indicated, the origin of the haustorium is a hypha so it seems obvious to think that its composition is the same. Nevertheless, several

particularities have been described in the haustorium (Mackie *et al.*, 1991; Micali *et al.*, 2011; Martínez-Cruz *et al.*, 2014). In first place, the EHM is, in fact, a modification of the plant plasma membrane, being its composition and structure different (Hückelhoven and Panstruga, 2011). The EHM is more convoluted and present a greater thickness than plant plasma membrane, shows a huge amount of associated polysaccharides and lacks intramembrane particles (Gil and Gay, 1977; Mackie *et al.*, 1991). Moreover, in contrast to plant plasma membrane, in the EHM there is absence of ATPase activity (Spencer-Phillips and Gay, 1981; Mackie *et al.*, 1991). Nevertheless, the resistance protein RPW8.2, which is involved in haustorium reception and accumulation of hydrogen peroxide, is localized in the EHM and is essential to haustorium reception (Wang *et al.*, 2009; Kim *et al.*, 2014). The EHM has been objective of several studies and, although its origin remains unknown, two hypotheses have been formulated in this regard. The first of them indicates that the origin of EHM is a consequence of a high modification of plant plasma membrane as a consequence of fungal activity over time, whereas the second hypothesis suggests that its origin is due a *de novo* formation during the haustorium formation (Mackie *et al.*, 1991; Wang *et al.*, 2009; Kim *et al.*, 2014). A recent study has demonstrated that the EHM shares common features with the endoplasmic reticulum membrane, but it does not depend on conventional secretion, suggesting the possibility of a non-conventional secretory pathway from endoplasmic reticulum that may provide the necessary material to this membrane (Kwaaitaal *et al.*, 2017).

On the other hand, the bands of the haustorial neck show a different composition to the fungal cell wall. They are composed mainly by iron, phosphorus,  $\beta$ -glucans, and lipidic and proteinaceous compounds (Chong and

Harder, 1980; Stumpf and Gay, 1990; Mendgen *et al.*, 2000). More specifically, the A band seems to be rich in  $\beta$ -1,3-glucans and its lipidic compounds are attached to chitin and  $\beta$ -1,3-glucans, whereas the B band seems to be rich in  $\beta$ -1,4-glucans and its lipidic compounds are bound to proteinaceous components (Stumpf and Gay, 1990).

Other evidence that suggests the molecular differentiation of the haustorium during its development is the presence of a 62 kDa N-linked glycoprotein, which has been described as unique in the haustorial membrane of pea powdery mildew, suggesting that the external composition of the haustorium differs with the composition from the rest of the fungal membranes (Mackie *et al.*, 1991). Similarly, the differences seem to be also extensible to the haustorial cell wall. This is the case of three unknown carbohydrate epitopes restricted to the haustorial cell wall, but not in other fungal structures, which have been described in flax rust by the production of monoclonal antibodies in mouse immunized with isolated haustoria (Murdoch *et al.*, 1998). Moreover, although molecular patterns associated to the fungal cell wall, such as chitin and  $\beta$ -1,3-glucans, are present in the surface of the haustorium, chitosan or any other modification of haustorial chitin does not seem to occur, as happens in the hyphal cell wall (Micali *et al.*, 2011). The chitin modification to chitosan has been described as one of the strategies employed by fungi to avoid plant recognition, since it presents a lower power of elicitation than chitin (Mochizuki *et al.*, 2011; Sánchez-Vallet *et al.*, 2013; Xi *et al.*, 2014). Therefore, the mechanism that the haustorium uses to avoid chitin recognition remains unknown.

Other striking point regarding the haustorium is the presence of a huge amount of vesicles located mostly in the haustorial lobes (Martínez-Cruz *et al.*,

2014) (Figure 1.6) as well as in the EHMx (Micali *et al.*, 2011), suggesting the existence of an specific exosome-mediated secretion pathway in the haustorium.

### *Isolation of haustoria and gene expression studies*

To perform a specific analysis of gene expression in haustoria, it is necessary a correct isolation of these cells, in order to show the genes expressed and to deduce the metabolic activities within the haustorial cells without interferences of similar activities from plant or hyphal cells. This isolation has been performed by different approaches: affinity chromatography with lectin concavalin A columns (Hahn and Mendgen, 1992), gradient centrifugation using sucrose (Tiburzy *et al.*, 1992) and isopycnic centrifugation with Percoll (Pain *et al.*, 1994), being the affinity chromatography with concavalin A and the isopycnic centrifugation with Percoll the more successfully to date. Although along the time ConA and Percoll approaches have been slightly modified (Godfrey *et al.*, 2010; Micali *et al.*, 2011; Link *et al.*, 2014; Martínez-Cruz *et al.*, 2014), to date no novel isolation approaches have been performed and they are still being used, despite the presence of plant contaminants in the haustorial preparations obtained by both techniques (Godfrey *et al.*, 2010; Weßling *et al.*, 2012; Link *et al.*, 2014).

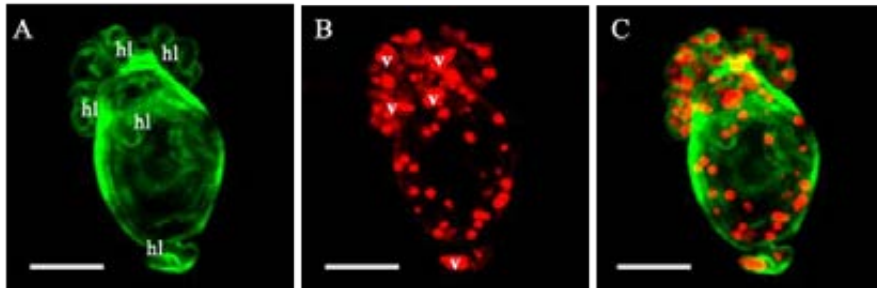


**Figure 1.6.** Detection of vesicles in an isolated haustorium of *P. xanthii* examined by confocal laser scanning microscopy. A) Specific staining of haustorial cell wall with WGA-Alexa Fluor 488 conjugate (green). B) Specific staining of membrane vesicles with FM4-64 (red). C) Overlay of pictures A and B showing the preferred location of the vesicles associated with the haustorial lobes. Abbreviations are: hl, haustorial lobe; v, vesicle. Bars, 4  $\mu$ m. Taken from Martínez-Cruz *et al.* (2014).

Despite the different approaches used for the isolation of haustoria, only a few transcriptomic studies of rust haustoria (Hahn and Mendgen, 1997; Jakupović *et al.*, 2006; Yin *et al.*, 2009; Garnica *et al.*, 2013; Link *et al.*, 2014) and only two of powdery mildew haustoria (Godfrey *et al.*, 2010; Weßling *et al.*, 2012), have been reported to date. This is surely due to the fact that all the haustorial isolation techniques are time consuming and, hence, the gene expression status can be altered (Weßling *et al.*, 2012). The first study on haustorial gene expression, which was conducted in the bean rust fungus, identified a metallothionein gene as well as genes related to thiamine biosynthesis and nutrient uptake such as amino acid transporters (Hahn and Mendgen, 1997). Subsequent works (Jakupović *et al.*, 2006; Yin *et al.*, 2009) showed that the highest proportion of genes expressed in rust haustoria were involved in protein synthesis, energy production and metabolism, being important the presence of secreted proteins (Yin *et al.*, 2009) as well as of



several nutrient transporters (Jakupović *et al.*, 2006; Yin *et al.*, 2009). However, these works only allowed studying a small portion of haustorial genes.

The emergence of high-throughput RNA sequencing has allowed us to increase the understanding of gene expression in haustoria. In this way, transcriptomic studies of rust haustoria identified that they are especially active in acquisition of amino acids, sugars, phosphorus and nitrogen compounds among others, as well as in response to stress and in protein synthesis (Garnica *et al.*, 2013; Link *et al.*, 2014). For its part, the only high-throughput RNA sequencing study of powdery mildew haustoria (Weßling *et al.*, 2012), suggested that the gene expression in both rust and powdery mildew haustoria is similar. This transcriptomic analysis showed that the powdery mildew haustoria are also active in protein metabolism, primary metabolism and energy production as well as in response to stress, ROS scavenging, vesicle-mediated transport and pathogenesis. In both rust and powdery mildew haustoria, a substantial proportion of transcripts corresponded with genes coding for secreted proteins, among which a high amount of them corresponded with effector candidates. That is, those putatively secreted proteins without homology to other proteins in databases (Weßling *et al.*, 2012; Garnica *et al.*, 2013; Link *et al.*, 2014).

In summary, the gene expression analysis of haustoria indicated that these cells present a high protein synthesis and are directly involved in nutrient uptake, energy production, plant defence suppression, ROS scavenging and pathogenesis, and probably in the release of secreted proteins.

### *Nutrient uptake in the haustorium*

One vital aspect of obligate biotrophic life style is the acquisition and mobilization of nutrients from host cells and, in relation to this, the arsenal of protein transporters and enzymes required for this purpose. In haustorium-forming fungi, the haustorium seems to be the main structure responsible for nutrient uptake and as such, the specific expression in the haustorium of several nutrient transporters has been proposed. Thus, the putative hexose transporter HXT1 and the amino acid transporters AAT1, AAT2 and ATT3 have been widely described in several studies on rust haustoria (Mendgen *et al.*, 2000; Struck *et al.*, 2002, 2004; Voegelé *et al.*, 2002; Garnica *et al.*, 2013). Biochemical studies of AAT1 and AAT3 showed that they act as amino acid transporters with specificity for L-histidine/L-Lysine and L-leucine/L-methionine/L-cysteine, respectively (Struck *et al.*, 2002, 2004). Moreover, HXT1 and AAT2 transporters were immuno-localized exclusively in the haustorial plasma membrane (Mendgen *et al.*, 2000; Voegelé *et al.*, 2002).

The main ion pumps in fungi and plants are the H<sup>+</sup>-ATPases present in the plasma membrane, which seem to play a key role in active nutrient uptake (Sondergaard *et al.*, 2004). This is the case of PMA1, a plasma membrane ATPase essential for growth of *Saccharomyces cerevisiae* (Serrano *et al.*, 1986), whose hydrolytic activity was several-fold higher in microsomal vesicles of isolated haustoria of the bean rust fungus *Uromyces fabae*, in contrast to the activity in ungerminated urediospores and germ tubes (Struck *et al.*, 1996). This fact, together with the molecular characterization of this enzyme and its suggested autoregulation (Struck *et al.*, 1998), support the function of PMA1 in nutrient uptake from host cells.

In the case of powdery mildew fungi, although nine predicted sugar transporters and six putative amino acid transporters were identified in *Arabidopsis* powdery mildew haustoria, none of them were described among the top 50 expressed genes in haustorial cells (Weßling *et al.*, 2012), as expected according to previous results obtained in rust haustoria, where those transporters were highly expressed (Hahn and Mendgen, 1997; Jakupović *et al.*, 2006; Duplessis *et al.*, 2011). This fact is worthwhile to note, since in the case of powdery mildew fungi, glucose seems to be the main carbon source obtained from host leaves (Sutton *et al.*, 1999; Fotopoulos *et al.*, 2003). Although a MFL maltose transporter and PMA1 were induced in late stages of fungal development (Weßling *et al.*, 2012) and despite that the transcript abundance does not determine the protein levels, the lack of identification of hexose transporters in a proteomic study of haustoria from barley powdery mildew *B. graminis* (Godfrey *et al.*, 2009), indicates that powdery mildews probably use a small amount of sugars transporters, suggesting that powdery mildew haustoria, in contrast to rust haustoria, may use other alternatives for carbohydrate uptake.

Although the hexoses and amino acids transporters have been the nutrient transporters more extensively studied, other different nutrient transporters have been described in haustoria. This is the case of the sulfate transporter described in wheat stripe rust haustoria (Yin *et al.*, 2009) or the inorganic phosphate transporter found among the top 50 expressed genes in the haustoria of *Arabidopsis* powdery mildew (Weßling *et al.*, 2012), suggesting the implication of powdery mildew haustoria in sulphur and phosphorus acquisition.

### *Haustorial effectors*

The presence of a high amount of transcripts coding for putative secreted proteins in both, rust and powdery mildew haustoria (Weßling *et al.*, 2012; Garnica *et al.*, 2013; Link *et al.*, 2014), suggests the participation of the haustorium in the release of effectors inside the host cells and highlights the importance of this structure not only in the acquisition of nutrients, but also, for example, in the manipulation of host plant defense mechanisms.

The rust transferred protein 1 (RTP1) was the first protein that was shown to be specifically expressed in haustorium. This protein is translocated to the host cell during the rust infection (Hahn and Mendgen, 1997; Kemen *et al.*, 2005) and acts as a protease inhibitor in the supernatants of yeast cultures, suggesting a putative role as an inhibitor of host protease activity associated to plant defense (Pretsch *et al.*, 2013). Moreover, it was also found forming filamentous structures and aggregates in EHMx and, hence, a putative function in accommodation of haustorium into the host cell was also postulated (Kemen *et al.*, 2013). Other proteins have been identified as secreted by rust haustoria. This is the case of four Avr proteins of *Melampsora lini*, which have been confirmed to be translocated into flax cells (Rafiqi *et al.*, 2010).

Recent transcriptomic studies have allowed identifying many putative secreted proteins in rust haustoria. Thus, the haustorial transcriptome of *Puccinia striiformis f. sp. tritici* has revealed the abundance of transcripts of cysteine-rich proteins among the haustorial effector candidates, as well as the fact that most of the secreted proteins identified in haustoria were differentially expressed compared to germinated spores (Garnica *et al.*, 2013), which is consistent with the major expression of effectors in haustoria, where they can directly modify host functions. The same transcriptomic study identified a

considerably high number of extracellular cell wall modifying enzymes such as chitinases, as occurs in the haustorial transcriptome of *Uromyces appendiculatus*, where these proteins and those related with response to biotic stimulus were considerably enriched (Link *et al.*, 2014). In the haustorial transcriptome of *Arabidopsis* powdery mildew *G. orontii* extracellular cell wall modifying enzymes were also identified (Weßling *et al.*, 2012), suggesting the importance of these enzymes in haustorial activity.

In contrast to rust haustorial effectors, where no characteristic sequence motifs have been identified among all predicted haustorial secreted proteins (Garnica *et al.*, 2013; Link *et al.*, 2014), the N-terminal Y/F/WxC-motif is conserved among the effector candidates identified in *B. graminis* haustoria, which is located around the first 24 amino acids after the signal peptide cleavage site (Godfrey *et al.*, 2010). This motif seems to be involved in translocation of proteins to host cells or in allowing correct folding of the effector proteins (Hacquard *et al.*, 2012). To date, these functions have not been demonstrated, however, the fact that 19 % of *B. graminis* haustorial transcriptome encodes Y/F/WxC-proteins suggests that these proteins may have key functions for the physiology of powdery mildew fungi (Godfrey *et al.*, 2010). In another study of powdery mildew haustoria, the putative importance of haustoria in effector secretion was also highlighted, since the transcripts coding for effector candidates were found overrepresented among the top expressed genes in haustoria (Weßling *et al.*, 2012).

---

*The haustorium as a gate for the introduction of genetic material in biotrophic fungi*

A major problem in the study of biotrophic fungi is the intrinsic difficulty in their genetic manipulation (Micali *et al.*, 2008). Along the time, approaches such as particle bombardment (Bhairi and Staples, 1992; Li *et al.*, 1993; Christiansen *et al.*, 1995; Webb *et al.*, 2006; Djulic *et al.*, 2011) and electroporation (Vela-Corcía *et al.*, 2018), have been used to transform both rust and powdery mildew fungi. However, these methods are poorly reproducible, unstable and with limited applicability.

In the last years, a novel system called host-induced gene silencing (HIGS) has emerged to overcome the limitations of previous approaches and is currently widely used in functional analysis of genes in obligate biotrophs (Nowara *et al.*, 2010; Pliego *et al.*, 2013). This method is based in the capability of haustorium-forming pathogens to take genetic material, in this case double-stranded RNA (dsRNA) or small interfering RNA (siRNA), through the haustorium, which leads to subsequent gene silencing of the gene of interest (Nowara *et al.*, 2010; Pliego *et al.*, 2013). Although the precise mechanism of RNA uptake by haustoria remains unknown, this tool has been successfully used in the analysis of powdery mildew and rust effectors (Nowara *et al.*, 2010; Pliego *et al.*, 2013; Panwar *et al.*, 2013). A variant of HIGS system used for the silencing of *Puccinia triticina* (Yin *et al.*, 2010) is the so-called virus-induced gene silencing (VIGS), which is based in the ability of eukaryotic organism to fight against infections caused by viruses (Waterhouse *et al.*, 2001; Unver and Budak, 2009; Kirigia *et al.*, 2014). During viral infections a dsRNA replication intermediate is produced, recognized and cleaved by Dicer, a ribonuclease that processes the dsRNA to produce siRNA. Later, this siRNA guides the RISC complex for the

degradation of mRNA corresponding to the target gene (Velásquez *et al.*, 2009). To exploit this procedure, viral vectors such as tobacco mosaic virus (TMV), tobacco rattle virus (TRV), potato virus X (PVX) and barley strip mosaic virus have been modified to carry the inserts from the genes to be silenced (Lu *et al.*, 2003).

Recently, the use of *Agrobacterium tumefaciens* has been also incorporated for the molecular analysis of powdery mildew fungi. In particular, *Agrobacterium* has been used for two purposes, gene silencing and genetic transformation. Thus, a method designated *A. tumefaciens*-mediated host-induced gene silencing (ATM-HIGS) was recently used to analyze the function of several effector candidates of *P. xanthii* (Martínez-Cruz *et al.*, 2018a). The method is based in the transformation of melon cotyledon cells with the silencing constructs via *Agrobacterium*. In this way, plant cells will produce the interfering RNA (RNAi) that will be taken up by haustoria by unknown mechanisms, leading to gene silencing. *Agrobacterium* has been also used to transform *P. xanthii*. Two methods have been proposed. The first is a variant of the typical *Agrobacterium*-mediated transformation (AMT) system; in this case *P. xanthii* conidia are directly exposed to *Agrobacterium* and transformed by the bacterium (Martínez-Cruz *et al.*, 2017). The second method has been designated “transformation by growth onto agroinfiltrated tissues” (TGAT). By this method the leaf tissue is first transformed by *Agrobacterium* and then inoculated with *P. xanthii* (Martínez-Cruz *et al.*, 2018b). In this case, according to the authors’ hypothesis, the T-DNA is transferred to *P. xanthii* via haustoria. This was supported by the co-localization of translational fluorescent fusions of Rab5 protein from *P. xanthii* and VirD2 protein from *A. tumefaciens* into small vesicles of haustoria (Figure 1.7A-C), suggesting that the endocytosis is the mechanism by which the haustoria acquire the T-DNA (Martínez-Cruz *et al.*,

2018b). VirD2 protein was shown to migrate from haustorium to nucleus of hyphal cells (Figure 1.7D-F), suggesting the possibility that hyphal cells may be also transformed. Thus, this method allowed the localization of effector proteins by means of translational fusions to fluorescent proteins (Figure 1.7G-I). However, both methods show an important limitation, the instability of the transformation. It seems that when the selection pressure is removed the T-DNAs disappear from the genome. In any case, these works on transient transformation by *Agrobacterium* of *P. xanthii* are considered an extraordinary step forward for powdery mildew research. The haustorium, the key fungal cell for gene silencing in fungal biotrophs, could also be the key for the genetic transformation of powdery mildew fungi.



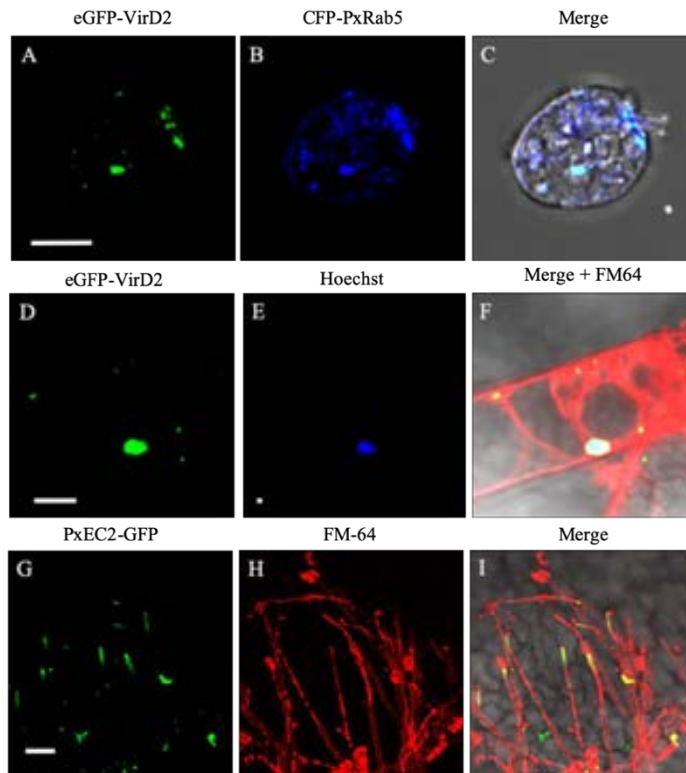


**Figure 1.7.** Confocal microscopy pictures illustrating the transformation system described for *P. xanthii* designated “transformation by growth onto agro-infiltrated tissues” (TGAT). A-C) Co-localization of VirD2 protein from *A. tumefaciens* and Rab5 endocytic vesicle-associated protein from *P. xanthii* in haustorial cells. The co-localization of eGFP-VirD2 (green) and CFP-PxRab5 (blue) allowed confirming the presence of VirD2 in endocytosis vesicles of haustoria. D-F) Subcellular localization of VirD2 protein in the nucleus of a hyphal cell. For visualization of the nucleus and *P. xanthii* hyphal membranes, staining with Hoechst (blue) and FM4-64 (red) were performed. G-I) Sub-cellular localization of the *P. xanthii* effector PxEC2 in hyphal tips. A PxEC2-GFP fusion (green) was used for transformation. Bars are: A, 5  $\mu\text{m}$ ; D, 50  $\mu\text{m}$ ; G, 10  $\mu\text{m}$ . Pictures were taken and modified from Martinez-Cruz *et al.* (2018b).

---

## REFERENCES

**Ahmed AA, Pedersen C, Schultz-Larsen T, Kwaaitaal M, Jørgensen HJL, Thordal-Christensen H.** 2015. The barley powdery mildew candidate secreted effector protein CSEP0105 Inhibits the chaperone activity of a small heat shock protein. *Plant Physiology* **168**, 321–333.

**Ahmed AA, Pedersen C, Thordal-Christensen H.** 2016. The barley powdery mildew effector candidates CSEP0081 and CSEP0254 promote fungal infection success. *PLoS ONE* **11**, e0157586.

**Ando K, Carr KM, Grumet R.** 2012. Transcriptome analyses of early cucumber fruit growth identifies distinct gene modules associated with phases of development. *BMC Genomics* **13**, 518–534.

**Asai S, Rallapalli G, Piquerez SJM, Caillaud MC, Furzer OJ, Ishaque N, Wirthmueller L, Fabro G, Shirasu K, Jones JDG.** 2014. expression profiling during *Arabidopsis*/downy mildew interaction reveals a highly-expressed effector that attenuates responses to salicylic acid. *PLoS Pathogens* **10**, e1004443

**Baker B, Zambryski P, Staskawicz B, DineshKumar SP.** 1997. Signaling in plant-microbe interactions. *Science* **276**, 726–733.

**Baxter L, Tripathy S, Ishaque N, et al.** 2010. Signatures of adaptation to obligate biotrophy in the *Hyaloperonospora arabidopsis* genome. *Science* **330**, 1549–1551.

**Bellón-Gómez D, Vela-Corcía D, Pérez-García A, Torés JA.** 2015. Sensitivity of *Podosphaera xanthii* populations to anti-powdery-mildew fungicides in Spain. *Pest Management Science* **71**, 1407–1413.

**Bhairi S., Staples RC.** 1992. Transient expression of the  $\beta$ -Glucuronidase

gene introduced into *Uromyces appendiculatus* uredosporas by particle bombardment. *Phytopathology* **82**, 986–989.

**Bindschedler L V., Panstruga R, Spanu PD.** 2016. Mildew-Omics: How global analyses aid the understanding of life and evolution of powdery mildews. *Frontiers in Plant Science* **7**, 123.

**Blanca J, Esteras C, Ziarsolo P, et al.** 2012. Transcriptome sequencing for SNP discovery across *Cucumis melo*. *BMC Genomics* **13**, 280–298.

**Block A, Li G, Fu ZQ, Alfano JR.** 2008. Phytopathogen type III effector weaponry and their plant targets. *Current Opinion in Plant Biology* **11**, 396–403.

**Bolton MD, Van Esse HP, Vossen JH, et al.** 2008. The novel *Cladosporium fulvum* lysin motif effector Ecp6 is a virulence factor with orthologues in other fungal species. *Molecular Microbiology* **69**, 119–136.

**Borges AF, Ferreira RB, Monteiro S.** 2013. Transcriptomic changes following the compatible interaction *Vitis vinifera*-*Erysiphe necator*. Paving the way towards an enantioselective role in plant defence modulation. *Plant Physiology and Biochemistry* **68**, 71–80.

**Both M, Csukai M, Stumpf MPH, Spanu PD.** 2005a. Gene expression profiles of *Blumeria graminis* indicate dynamic changes to primary metabolism during development of an obligate biotrophic pathogen. *The Plant Cell* **17**, 2107–2122.

**Both M, Eckert SE, Csukai M, Muller E, Dimopoulos G, Spanu PD.** 2005b. Transcript profiles of *Blumeria graminis* development during infection reveal a cluster of genes that are potential virulence determinants. *Molecular Plant Microbe Interaction* **18**, 125–33.

**Braun U. and Takamatsu, S.** 2000. Phylogeny of *Erysiphe*, *Microsphaera*, *Uncinula* (Erysipheae) and *Cystotheca*, *Podosphaera*, *Sphaerotheca*

(Cystothecaceae) inferred from rDNA ITS sequences a taxonomic interpretation. *Schlechtendalia* **4**, 1-33.

**Braun U, Shishkoff, N and Takamatsu, S.** 2001. Phylogeny of *Podospaera* sect. *Sphaerotheca* subsect. *Magnicellulatae* (*Sphaerotheca fuliginea* auct. S. lat.) inferred from rDNA ITS sequences a taxonomic interpretation. *Schlechtendalia* **7**, 45-52.

**Braun U, Cook RTA, Inman AJ, and Shin HD.** 2002. The taxonomy of the powdery mildew fungi. In: Belanger, R.R., Bushnell, W.R., Dik, A.J. and Carver, T.L.W. (eds) *The powdery mildews: a comprehensive treatise*. APS St. Paul, pp.13-55.

**Braun, U and Cook, RT.** 2012. Taxonomic manual of the Erysiphales (powdery mildew) Utrecht: CBS-KNAW Fungal Biodiversity Centr. Pp. 707

**van den Burg HA, Harrison SJ, Joosten MHAJ, Vervoort J, de Wit PJGM.** 2007. *Cladosporium fulvum* Avr4 protects fungal cell walls against hydrolysis by plant chitinases accumulating during infection. *Molecular Plant-Microbe Interactions* **19**, 1420–1430.

**Bushnell WR, Bergquist SE.** 1974. Aggregation of host cytoplasm and the formation of papillae and haustoria in powdery mildew of barley. *Phytopathology* **65**, 310–318.

**Chaudhari P, Ahmed B, Joly DL, Germain H.** 2014. Effector biology during biotrophic invasion of plant cells. *Virulence* **5**, 703–709.

**Chen Y, Zhang F, Tang L, Zheng Y, Li Y, Christie P, Li L.** 2007. Wheat powdery mildew and foliar N concentrations as influenced by N fertilization and belowground interactions with intercropped faba bean. *Plant and Soil* **291**, 1–13.

**Chong J, Harder DE.** 1980. Ultrastructure of haustorium development in *Puccinia coronata* avenae. I. Cytochemistry and electron probe X-ray analysis

of the haustorial neck ring. *Canadian Journal of Botany* **58**, 2496–2505.

**Christiansen SK, Knudsen S, Giese H.** 1995. Biolistic transformation of the obligate plant pathogenic fungus, *Erysiphe graminis* f.sp. hordei. *Current Genetics* **29**, 100–102.

**Cohen Y, Baider A, Petrov L, Sheck L. and Voloisky V.** 2000. Cross-infectivity of *Sphaerotheca fuliginea* to watermelon, melon and cucumber. *Acta Hort.* **510**, 85–88.

**Djelic A, Schmid A, Lenz H, Sharma P, Koch C, Wirsler SGR, Voegelé RT.** 2011. Transient transformation of the obligate biotrophic rust fungus *Uromyces fabae* using biolistics. *Fungal Biology* **115**, 633–642.

**Doehlemann G, Ökmen B, Zhu W, Sharon A.** 2017. Plant Pathogenic Fungi. *Microbiology Spectrum* **5**, doi:10.1128/microbiolspec.FUNK-0023-2016

**Duplessis S, Cuomo CA, Lin Y, et al.** 2011. Obligate biotrophy features unraveled by the genomic analysis of rust fungi. *Proceedings of the National Academy of Sciences* **108**, 9166–9171.

**Eichmann R, Hüchelhoven R.** 2008. Accommodation of powdery mildew fungus in intact plant cells. *Journal of plant physiology* **165**, 5–18.

**Fernández-Ortuño D, Pérez-García A, López-Ruiz F, Romero D, De Vicente A, Torés JA.** 2006. Occurrence and distribution of resistance to QoI fungicides in populations of *Podosphaera fusca* in south central Spain. *European Journal of Plant Pathology* **115**, 215–222.

**Fotopoulos V, Gilbert MJ, Pittman JK, Marvier AC, Buchanan AJ, Sauer N, Hall JL, Williams LE.** 2003. The monosaccharide transporter gene, AtSTP4, and the cell-wall invertase, AtBfruct1, are induced in *Arabidopsis* during infection with the fungal biotroph *Erysiphe cichoracearum*. *Plant Physiology* **132**, 821–829.

**Fraaije BA, Cools HJ, Kim SH, Motteram J, Clark WS, Lucas JA.** 2007. A novel substitution I381V in the sterol 14 $\alpha$ -demethylase (CYP51) of *Mycosphaerella graminicola* is differentially selected by azole fungicides. *Molecular Plant Pathology* **8**, 245–254.

**Fu Y, Zhang H, Mandal SN, Wang C, Chen C, Ji W.** 2016. Quantitative proteomics reveals the central changes of wheat in response to powdery mildew. *Journal of Proteomics* **130**, 108–119.

**Fung RWM, Gonzalo M, Fekete C, Kovacs LG, He Y, Marsh E, McIntyre LM, Schachtman DP, Qiu W.** 2007. Powdery mildew induces defense-oriented reprogramming of the transcriptome in a susceptible but not in a resistant grapevine. *Plant Physiology* **146**, 236–249.

**García-Gutiérrez L, Romero D, Zerriouh H, Cazorla FM, Torés JA, de Vicente A, Pérez-García A.** 2012. Isolation and selection of plant growth-promoting rhizobacteria as inducers of systemic resistance in melon. *Plant and Soil* **358**, 201–212.

**Garcia-Mas J, Benjak A, Sanseverino W, et al.** 2012. The genome of melon (*Cucumis melo* L.). *Proceedings of the National Academy of Sciences* **109**, 11872–11877.

**Garnica DP, Upadhyaya NM, Dodds PN, Rathjen JP.** 2013. Strategies for wheat stripe Rust pathogenicity identified by transcriptome sequencing. *PLoS ONE* **8**, e67150.

**Gil F, Gay JL.** 1977. Ultrastructural and physiological properties of the host interfacial components of haustoria of *Erysiphe pisi* in vivo and in vitro. *Physiological Plant Pathology* **10**, 1–12.

**Godfrey D, Böhlenius H, Pedersen C, Zhang Z, Emmersen J, Thordal-Christensen H.** 2010. Powdery mildew fungal effector candidates share N-terminal Y/F/WxC-motif. *BMC Genomics* **11**, 317.

**Godfrey D, Zhang Z, Saalbach G, Thordal-Christensen H.** 2009. A proteomics study of barley powdery mildew haustoria. *Proteomics* **9**, 3222–3232.

**Göhre V, Robatzek S.** 2008. Breaking the barriers: Microbial effector molecules subvert plant immunity. *Annual Review of Phytopathology* **46**, 189–215.

**Gold RE, Mendgen K.** 1991. Rust basidiospore germlings and disease initiation. In: Cole GT, Hoch HC, eds. *The fungal spore and disease initiation in plants and animals*. New York, USA: Plenum Press, 67-99.

**Guo W, Chen B, Chen X, Guo Y, Yang H, Li X, Wang G.** 2018. Transcriptome profiling of pumpkin (*Cucurbita moschata* Duch .) leaves infected with powdery mildew. *PLoS ONE* **13**, e0190175.

**Guo S, Liu J, Zheng Y, et al.** 2011. Characterization of transcriptome dynamics during watermelon fruit development: Sequencing, assembly, annotation and gene expression profiles. *BMC Genomics* **12**, 454.

**Hacquard S.** 2014. The genomics of powdery mildew fungi: Past achievements, present status and future prospects. *Advances in Botanical Research* **70**, 109-142

**Hacquard S, Joly DL, Lin Y-C, et al.** 2012. A comprehensive analysis of genes encoding small secreted proteins identifies candidate effectors in *Melampsora larici-populina* (poplar leaf rust). *Molecular Plant-Microbe Interactions* **25**, 279–293.

**Hacquard S, Kracher B, Maekawa T, Vernaldi S, Schulze-Lefert P, Ver Loren van Themaat E.** 2013. Mosaic genome structure of the barley powdery mildew pathogen and conservation of transcriptional programs in divergent hosts. *Proceedings of the National Academy of Sciences* **110**, E2219–E2228.

**Hahn M, Mendgen K.** 1992. Isolation by ConA binding of haustoria from

different rust fungi and comparison of their surface qualities. *Protoplasma* **170**, 95–103.

**Hahn M, Mendgen K.** 1997. Characterization of in planta-induced rust genes isolated from a haustorium-specific cDNA library. *Molecular plant-microbe interactions* : *MPMI* **10**, 427–437.

**Heath MC, Skalamera D.** 1997. Cellular Interactions between plants and biotrophic fungal parasites (JH Andrews, IC Tommerup, and JABT-A in BR Callow, Eds.). *Advances in Botanical Research* **24**, 195–225.

**Hollomon DW, Wheeler IE.** 2002 Controlling powdery mildews with chemistry. In: Bélanger RR, Bushnell WR, Dik AJ, Carver TLW (eds) *The powdery mildews, a comprehensive treatise*. APS Press, St. Paul, pp 249–255.

**Huang S, Li R, Zhang Z, et al.** 2009. The genome of the cucumber, *Cucumis sativus* L. *Nature Genetics* **41**, 1275–1281.

**Hückelhoven R.** 2005. Powdery mildew susceptibility and biotrophic infection strategies. *FEMS Microbiology Letters* **245**, 9–17.

**Hückelhoven R, Panstruga R.** 2011. Cell biology of the plant-powdery mildew interaction. *Current opinion in plant biology* **14**, 738–46.

**Jahn M, Munger HM, McCreight JD.** 2002. Breeding cucurbit crops for powdery mildew resistance. *The powdery mildews: A comprehensive treatise*. St. Paul: American Phytopathological Society (APS Press), 239–248.

**Jakupović M, Heintz M, Reichmann P, Mendgen K, Hahn M.** 2006. Microarray analysis of expressed sequence tags from haustoria of the rust fungus *Uromyces fabae*. *Fungal Genetics and Biology* **43**, 8–19.

**Jambagi S, Dunwell JM.** 2015. Global transcriptome analysis and Identification of differentially expressed genes after infection of *fragaria vesca* with powdery mildew (*Podosphaera aphanis*). *Transcriptomics* **03**, 1–10.

**Jones L, Riaz S, Morales-Cruz A, Amrine KC, McGuire B, Gubler WD,**



**Walker MA, Cantu D.** 2014. Adaptive genomic structural variation in the grape powdery mildew pathogen, *Erysiphe necator*. *BMC Genomics* **15**.

**Jonge R De, Esse HP Van, Kombrink A, Shinya T, Desaki Y, Bours R, Krol S Van Der, Shibuya N, Joosten MHJ, Thomma BPHJ.** 2010. Conserved fungal LysM effector Ecp6 prevents chitin-triggered immunity in plants. *Science* **329**, 953–955.

**Keinath AP,** 1996. Soil amendment with cabbage residue and crop rotation to reduce gummy stem blight and increase growth and yield of watermelon. *Plant Disease* **80**, 564-571.

**Kemen E, Kemen A, Ehlers A, Voegelé R, Mendgen K.** 2013. A novel structural effector from rust fungi is capable of fibril formation. *Plant Journal* **75**, 767–780.

**Kemen E, Kemen AC, Rafiqi M, Hempel U, Mendgen K, Hahn M, Voegelé RT.** 2005. Identification of a protein from rust fungi transferred from haustoria into infected plant cells. *Molecular Plant-Microbe Interactions* **18**, 1130–1139.

**Kim H, O’Connell R, Maekawa-Yoshikawa M, Uemura T, Neumann U, Schulze-Lefert P.** 2014. The powdery mildew resistance protein RPW8.2 is carried on VAMP721/722 vesicles to the extrahaustorial membrane of haustorial complexes. *Plant Journal* **79**, 835–847.

**Kirigia D, Runo S, Alakonya A.** 2014. A virus-induced gene silencing (VIGS) system for functional genomics in the parasitic plant *Striga hermonthica*. *Plant Methods* **10**, 1–8.

**Koh S, André A, Edwards H, Ehrhardt D, Somerville S.** 2005. *Arabidopsis thaliana* subcellular responses to compatible *Erysiphe cichoracearum* infections. *Plant Journal* **44**, 516–529.

**Kuzuya M, Yashiro K, Tomita K, Ezura H.** 2006. Powdery mildew

(*Podosphaera xanthii*) resistance in melon is categorized into two types based on inhibition of the infection processes. *Journal of Experimental Botany* **57**, 2093–2100.

**Kwaaitaal M, Nielsen ME, Böhlenius H, Thordal-Christensen H.** 2017. The plant membrane surrounding powdery mildew haustoria shares properties with the endoplasmic reticulum membrane. *Journal of Experimental Botany* **68**, 5731–5743.

**Leonar P, Gianessi NR** 2005. The value of fungicides in U.S crop production. CropLife Foundation. Wahington, USA.

**Li A, Altosaar I, Heath MC, Horgen PA.** 1993. Transient expression of the beta-glucuronidase gene delivered into urediniospores of *Uromyces appendiculatus* by particle bombardment. *Canadian Journal of Plant Pathology* **15**, 1–6.

**Li X, Wu J, Yin L, Zhang Y, Qu J, Lu J.** 2015. Comparative transcriptome analysis reveals defense-related genes and pathways against downy mildew in *Vitis amurensis* grapevine. *Plant Physiology and Biochemistry* **95**, 1–14.

**Link TI, Lang P, Scheffler BE, et al.** 2014. The haustorial transcriptomes of *Uromyces appendiculatus* and *Phakopsora pachyrhizi* and their candidate effector families. *Molecular Plant Pathology* **15**, 379–393.

**van Loon LC, Geraats BPJ, Linthorst HJM.** 2006. Ethylene as a modulator of disease resistance in plants. *Trends in Plant Science* **11**, 184–191.

**López-Ruiz F, Fernández-Ortuño D, Cánovas I, Pérez-García A, de Vicente A, Torés JA,** 2005. Control químico del oídio de las cucurbitáceas. *Vida Rural* **15**, 50-54

**Lu R, Martin-Hernandez AM, Peart JR, Malcuit I, Baulcombe DC.** 2003. Virus-induced gene silencing in plants. *Methods* **30**, 296–303.

**Lucas JA**, 1998 Plant pathology and plant pathogens. 3<sup>rd</sup> ed. Blackwell Science, Pxford. U.K.

**Mackie AJ, Roberts AM, Callow JA, Green JR**. 1991. Molecular differentiation in pea powdery-mildew haustoria. *Planta* **183**, 399–408.

**Martínez-Cruz J, Romero D, Dávila JC, Pérez-García A**. 2014. The *Podosphaera xanthii* haustorium, the fungal Trojan horse of cucurbit-powdery mildew interactions. *Fungal genetics and biology* **71**, 21–31.

**Martínez-Cruz**, 2016. Análisis morfológico y funcional de la interacción *Podosphaera xanthii*- cucurbitáceas. PhD thesis, University of Malaga, Malaga, Spain

**Martínez-Cruz J, Romero D, de la Torre FN, Fernández-Ortuño D, Torés JA, de Vicente A, Pérez-García A**. 2018a. The functional characterization of *Podosphaera xanthii* candidate effector genes reveals novel target functions for fungal pathogenicity. *Molecular Plant-Microbe Interactions* **31**, 914-931.

**Martínez-Cruz J, Romero D, de Vicente A, Pérez-García A**. 2017. Transformation of the cucurbit powdery mildew pathogen *Podosphaera xanthii* by *Agrobacterium tumefaciens*. *New Phytologist* **213**, 1961–1973.

**Martínez-Cruz J, Romero D, De Vicente A, Pérez-García A**. 2018b. Transformation by growth onto agro-infiltrated tissues (TGAT), a simple and efficient alternative for transient transformation of the cucurbit powdery mildew pathogen *Podosphaera xanthii*. *Molecular Plant Pathology* **19**, 2502–2515.

**McCreight JD**. 2006) Melon–powdery mildew interactions reveal variation in melon cultigens and *Podosphaera xanthii* races 1 and 2. *J. Am. Soc. Hort. Sci.* **131**, 59 – 65.

**McGrath T**. 1994. Heterothallism in *Sphaerotheca fuliginea*. *Mycologia* **86**, 517–523.

**McGrath T.** 2010. Fungicide resistance in cucurbit powdery mildew fungi. *Plant Disease* **85**, 236–245.

**Mendgen K, Struck C, Voegelé RT, Hahn M.** 2000. Biotrophy and rust haustoria. *Physiological and Molecular Plant Pathology* **56**, 141–145.

**Mentlak TA, Kombrink A, Shinya T, et al.** 2012. Effector-mediated suppression of chitin-triggered immunity by *Magnaporthe oryzae* is necessary for rice blast disease. *The Plant Cell* **24**, 322–335.

**Miazzì M, Laguardia C, Faretra F.** 2011. Variation in *Podosphaera xanthii* on cucurbits in southern Italy. *Journal of Phytopathology* **159**, 538–545.

**Micali C, Göllner K, Humphry M, Consonni C, Panstruga R.** 2008. The powdery mildew disease of *Arabidopsis*: A paradigm for the interaction between plants and biotrophic fungi. *The Arabidopsis Book* **6**, e0115.

**Micali CO, Neumann U, Grunewald D, Panstruga R, O’Connell R.** 2011. Biogenesis of a specialized plant-fungal interface during host cell internalization of *Golovinomyces orontii* haustoria. *Cellular Microbiology* **13**, 210–226.

**Mochizuki S, Saitoh K, Ichiro, Minami E, Nishizawa Y.** 2011. Localization of probe-accessible chitin and characterization of genes encoding chitin-binding domains during rice-*Magnaporthe oryzae* interactions. *Journal of General Plant Pathology* **77**, 163–173.

**von Mohl H,** 1853. Ueber die Traubenkrankheit. *Bot Z* **11**, 585–590

**Montero-Pau J, Blanca J, Bombarely A, et al.** 2017. De novo assembly of the zucchini genome reveals a whole-genome duplication associated with the origin of the *Cucurbita* genus. *Plant Biotechnology Journal* **16**, 1161–1171.

**Murdoch LJ, Kobayashi I, Hardham AR.** 1998. Production and characterisation of monoclonal antibodies to cell wall components of the flax rust fungus. *European Journal of Plant Pathology* **104**, 331–346.

**Navarro L, Dunoyer P, Jay F, Arnold B, Dharmasiri N, Estelle M, Voinnet O, Jones JDG.** 2006. A plant miRNA contributes to antibacterial resistance by repressing auxin signaling. *Science* **312**, 436–439.

**Nowara D, Gay A, Lacomme C, Shaw J, Ridout C, Douchkov D, Hensel G, Kumlehn J, Schweizer P.** 2010. HIGS: Host-induced gene silencing in the obligate biotrophic fungal pathogen *Blumeria graminis*. *The Plant Cell* **22**, 3130–3141.

**Pain NA, Green JR, Gammie F, et al.** 1994. Immunomagnetic isolation of viable intracellular hyphae of *Colletotrichum lindemuthianum* (Sacc. & Magn.) Briosi & Cav. from infected bean leaves using a monoclonal antibody. *New Phytologist* **127**, 223–232.

**Panstruga R, Schulze-Lefert P.** 2002. Micro review live and let live : insights into powdery mildew disease and. *Molecular Plant Pathology* **3**, 495–502.

**Panwar V, McCallum B, Bakkeren G.** 2013. Host-induced gene silencing of wheat leaf rust fungus *Puccinia triticina* pathogenicity genes mediated by the Barley stripe mosaic virus. *Plant Molecular Biology* **81**, 595–608.

**Paulitz TC, Richard RB.** 2001. Biological control in greenhouse systems. *Annual Review of Phytopathology* **39**, 103–133.

**Pedersen C, van Themaat EVL, McGuffin LJ, et al.** 2012. Structure and evolution of barley powdery mildew effector candidates. *BMC Genomics* **13**, 694.

**Pennington HG, Gheorghe DM, Damerum A, Pliego C, Spanu PD, Cramer R, Bindschedler L V.** 2016. Interactions between the powdery mildew effector BEC1054 and barley proteins identify candidate host targets.

**Pérez-García A, Olalla L, Rivera E, Del Pino D, Cánovas I, De Vicente A, Torés JA.** 2001. Development of *Sphaerotheca fusca* on susceptible,

resistant, and temperature-sensitive resistant melon cultivars. *Mycological Research* **105**, 1216–1222.

**Pérez-García A, Romero D, Fernández-Ortuño D, López-Ruiz F, De Vicente A, Torés JA.** 2009. The powdery mildew fungus *Podosphaera fusca* (synonym *Podosphaera xanthii*), a constant threat to cucurbits. *Molecular plant pathology* **10**, 153–160.

**Pieterse CMJ, Leon-Reyes A, Van Der Ent S, Van Wees SCM.** 2009. Networking by small-molecule hormones in plant immunity. *Nature Chemical Biology* **5**, 308–316.

**del Pino D, Olalla L, Pérez-García A, Rivera ME, García S, Moreno R, de Vicente A, Torés JA.** 2002. Occurrence of races and pathotypes of cucurbit powdery mildew in southeastern Spain. *Phytoparasitica* **30**, 459–466.

**Pirondi A, Pérez-García A, Portillo I, Battistini G, Turan C, Brunelli A, Collina M.** 2015a. Occurrence of chasmothecia and mating type distribution of *Podosphaera xanthii*, a causal agent of cucurbit powdery mildew in northern Italy. *Journal of Plant Pathology* **97**, 307–313.

**Pirondi A, Vela-Corcía D, Dondini L, Brunelli A, Pérez-García A, Collina M.** 2015b. Genetic diversity analysis of the cucurbit powdery mildew fungus *Podosphaera xanthii* suggests a clonal population structure. *Fungal Biology* **119**, 791–801.

**Pitrat M.** 2002. Gene list for melon. *Cucurbit Genet. Coop. Rep.* **25**. <http://cuke.hort.ncsu.edu/cgc/cgc25/2002toc.html>, <http://cuke.hort.ncsu.edu/cgc/cgc25/cgc25-26.pdf>

**Pliego C, Nowara D, Bonciani G, et al.** 2013. Host-induced gene silencing in barley powdery mildew reveals a class of ribonuclease-like effectors. *Molecular Plant-Microbe Interactions* **26**, 633–642.

**Pozo MJ, Van Loon LC, Pieterse CMJ.** 2005. Jasmonates - Signals in

plant-microbe interactions. *Journal of Plant Growth Regulation* **23**, 211–222.

**Prats E, Gay AP, Mur LAJ, Thomas BJ, Carver TLW.** 2006. Stomatal lock-open, a consequence of epidermal cell death, follows transient suppression of stomatal opening in barley attacked by *Blumeria graminis*. *Journal of Experimental Botany* **57**, 2211–2226.

**Lo Presti L, Lanver D, Schweizer G, Tanaka S, Liang L, Tollot M, Zuccaro A, Reissmann S, Kahmann R.** 2015. Fungal effectors and plant susceptibility. *Annual Review of Plant Biology* **66**, 513–545.

**Pretsch K, Kemen A, Kemen E, Geiger M, Mendgen K, Voegele R.** 2013. The rust transferred proteins—a new family of effector proteins exhibiting protease inhibitor function. *Molecular Plant Pathology* **14**, 96–107.

**Rafiqi M, Gan PHP, Ravensdale M, Lawrence GJ, Ellis JG, Jones DA, Hardham AR, Dodds PN.** 2010. Internalization of flax rust avirulence proteins into flax and tobacco cells can occur in the absence of the pathogen. *The Plant Cell* **22**, 2017–2032.

**Rezzonico F, Rupp O, Fahrenttrapp J.** 2017. Pathogen recognition in compatible plant-microbe interactions. *Scientific Reports* **7**, 1–12.

**Ridout CJ, Skamnioti P, Porritt O, Sacristan S, Jones JDG, Brwon KM.** 2006. Multiple avirulence paralogues in cereal powdery mildew fungi may contribute to parasite fitness and defeat of plant resistance. *The Plant Cell* **18**, 2402–2414.

**Romero D, Pérez-García A, Rivera ME, Cazorla FM, De Vicente A.** 2004. Isolation and evaluation of antagonistic bacteria towards the cucurbit powdery mildew fungus *Podosphaera fusca*. *Applied Microbiology and Biotechnology* **64**, 263–269.

**Rovenich H, Boshoven JC, Thomma BP.** 2014. Filamentous pathogen effector functions: of pathogens, hosts and microbiomes. *Current opinion in*

plant biology **20**, 96–103.

**Sánchez-Vallet A, Saleem-Batcha R, Kombrink A, Hansen G, Valkenburg D-J, Thomma BP, Mesters JR.** 2013. Fungal effector Ecp6 outcompetes host immune receptor for chitin binding through intrachain LysM dimerization. *eLife* **2**, e00790.

**Schmidt SM, Kuhn H, Micali C, Liller C, Kwaaitaal M, Panstruga R.** 2014. Interaction of a *Blumeria graminis* f. sp. hordei effector candidate with a barley ARF-GAP suggests that host vesicle trafficking is a fungal pathogenicity target. *Molecular Plant Pathology* **15**, 535–549.

**Seifi A, Gao D, Zheng Z, Pavan S, Faino L, Visser RGF, Wolters AMA, Bai Y.** 2014. Genetics and molecular mechanisms of resistance to powdery mildews in tomato (*Solanum lycopersicum*) and its wild relatives. *European Journal of Plant Pathology* **138**, 641–665.

**Serrano R, Kielland-Brandt MC, Fink GR.** 1986. Yeast plasma membrane ATPase is essential for growth and has homology with (Na<sup>+</sup> + K<sup>+</sup>), K<sup>+</sup>- and Ca<sup>2+</sup>-ATPases. *Nature* **319**, 689–693.

**Sitterly WP.** 1978. Powdery mildew of cucurbits. In: *Powdery Mildews*. Spencer D.M. (ed.) Pp. 359-379. Academic Press. London. U.K.

**Sondergaard TE, Schulz A, Palmgreen M.** 2004. Energization of transport processes in plants. roles of the plasma membrane H<sup>+</sup>-ATPase. *Plant Physiology* **136**, 2475–2482.

**Spanu PD, Abbott JC, Amselem J, et al.** 2010. Genome expansion and gene loss in powdery mildew fungi reveal tradeoffs in extreme parasitism. *Science* **330**, 1543–1546.

**Spencer-Phillips PTN, Gay JL.** 1981. Domains of ATPase in plasma membranes and transport through infected plant cells. *New Phytologist* **89**, 393–400.



**Stergiopoulos I, de Wit PJGM.** 2009. Fungal effector proteins. Annual Review of Phytopathology **47**, 233–263.

**Struck C, Ernst M, Hahn M.** 2002. Characterization of a developmentally regulated amino acid transporter (AAT1p) of the rust fungus *Uromyces fabae*. Molecular Plant Pathology **3**, 23–30.

**Struck C, Hahn M, Mendgen K.** 1996. Plasma membrane H<sup>+</sup>-ATPase activity in spores, germ tubes, and haustoria of the rust fungus *Uromyces viciae-fabae*. Fungal Genetics and Biology **20**, 30–35.

**Struck C, Mueller E, Martin H, Lohaus G.** 2004. The *Uromyces fabae* UfAAT3 gene encodes a general amino acid permease that prefers uptake of in planta scarce amino acids. Molecular Plant Pathology **5**, 183–189.

**Struck C, Siebels C, Rommel O, Wernitz M, Hahn M.** 1998. The Plasma Membrane H<sup>+</sup> -ATPase from the biotrophic rust fungus *Uromyces fabae*: Molecular characterization of the gene (PMA1) and functional expression of the enzyme in yeast. Molecular Plant-Microbe Interactions **11**, 458–465.

**Stumpf M, Gay J.** 1990. The composition of *Erysiphe pisi* haustorial complexes with special reference to the neckbands. Physiological and Molecular Plant Pathology **37**, 125–143.

**Sutton PN, Henry MJ, Hall JL.** 1999. Glucose, and not sucrose, is transported from wheat to wheat powdery mildew. Planta **208**, 426–430.

**Takamatsu S.** 2013. Origin and evolution of the powdery mildews (Ascomycota, Erysiphales). Mycoscience **54**.

**Tiburzy R, Martins E, Reisener H.** 1992. Isolation of haustoria of *Puccinia graminis* f. sp. tritici from wheat leaves. Experimental mycology **328**, 324–328.

**Tucker SL, Talbot NJ.** 2002. Surface attachment and pre-penetration stage development by plant pathogenic fungi. Annual Review of Phytopathology **39**, 385–417.

**Unver T, Budak H.** 2009. Virus-Induced gene silencing, a post transcriptional gene silencing method. *International Journal of Plant Genomics*, doi:10.1155/2009/198680.

**Vela-Corcía D, Bautista R, De Vicente A, Spanu PD, Pérez-García A.** 2016. *De novo* analysis of the epiphytic transcriptome of the cucurbit powdery mildew fungus *Podosphaera xanthii* and identification of candidate secreted effector proteins. *PLoS ONE* **11**, e0163379.

**Vela-Corcía D, Romero D, De Vicente A, Pérez-García A.** 2018. Analysis of  $\beta$ -tubulin-carbendazim interaction reveals that binding site for MBC fungicides does not include residues involved in fungicide resistance. *Scientific Reports* **8**, 7161.

**Velásquez AC, Chakravarthy S, Martin GB.** 2009. Virus-induced gene silencing (VIGS) in *Nicotiana benthamiana* and tomato. *Journal of Visualized Experiments*, doi:10.3791/1292.

**Voegelé RT, Mendgen K.** 2003. Rust haustoria : Uptake and beyond. *New Phytologist* **159**, 93–100.

**Voegelé RT, Struck C, Hahn M, Mendgen K.** 2002. The role of haustoria in sugar supply during infection of broad bean by the rust fungus *Uromyces fabae*. *Proceedings of the National Academy of Sciences* **98**, 8133–8138.

**Vogel JP, Raab TK, Somerville CR, Somerville SC.** 2004. Mutations in PMR5 result in powdery mildew resistance and altered cell wall composition. *Plant Journal* **40**, 968–978.

**Wang W, Wen Y, Berkey R, Xiao S.** 2009. Specific targeting of the *Arabidopsis* resistance protein RPW8.2 to the interfacial membrane encasing the fungal haustorium renders broad-spectrum resistance to powdery mildew. *The Plant Cell* **21**, 2898–2913.

**Waterhouse PM, Wang M, Lough T.** 2001. Gene silencing as an adaptive

defence against viruses. *Nature* **411**, 834–842.

**Webb CA, Szabo LJ, Bakkeren G, Garry C, Staples RC, Eversmeyer M, Fellers JP.** 2006. Transient expression and insertional mutagenesis of *Puccinia triticina* using biolistics. *Functional and Integrative Genomics* **6**, 250–260.

**Wen L.** 2013. Cell death in plant immune response to necrotrophs. *Plant Biochemistry & Physiology* **1**, e103.

**Weng K, Li ZQ, Liu RQ, Wang L, Wang YJ, Xu Y.** 2014. Transcriptome of *Erysiphe necator*-infected *Vitis pseudoreticulata* leaves provides insight into grapevine resistance to powdery mildew. *Horticulture Research* **1**, 1–12.

**Weßling R, Epple P, Altmann S, et al.** 2014. Convergent targeting of a common host protein-network by pathogen effectors from three kingdoms of life. *Cell Host and Microbe* **16**, 364–375.

**Weßling R, Schmidt SM, Micali CO, Knaust F, Reinhardt R, Neumann U, Ver Loren van Themaat E, Panstruga R.** 2012. Transcriptome analysis of enriched *Golovinomyces orontii* haustoria by deep 454 pyrosequencing. *Fungal Genetics and Biology* **49**, 470–482.

**Wicker T, Oberhaensli S, Parlange F, et al.** 2013. The wheat powdery mildew genome shows the unique evolution of an obligate biotroph. *Nature Genetics* **45**, 1092–1096.

**Wu Y, Ma X, Pan Z, et al.** 2018. Comparative genome analyses reveal sequence features reflecting distinct modes of host-adaptation between dicot and monocot powdery mildew. *BMC Genomics* **19**, 705.

**Xi Y, Pan PL, Ye YX, Yu B, Zhang CX.** 2014. Chitin deacetylase family genes in the brown planthopper, *Nilaparvata lugens* (Hemiptera: Delphacidae). *Insect Molecular Biology* **23**, 695–705.

**Xin M, Wang X, Peng H, Yao Y, Xie C, Han Y, Ni Z, Sun Q.** 2012. Transcriptome comparison of susceptible and resistant wheat in response to

powdery mildew infection. *Genomics, Proteomics and Bioinformatics* **10**, 94–106.

**Xu Y, Wang J, Guo S, et al.** 2013. The draft genome of watermelon (*Citrullus lanatus*) and resequencing of 20 diverse accessions. *Nature Genetics* **45**, 51–58.

**Yang J, Hsiang T, Bhadauria V, Chen XL, Li G.** 2017. Plant Fungal Pathogenesis. *BioMed Research International* **2017**, 2–4.

**Yin C, Chen X, Wang X, Han Q, Kang Z, Hulbert SH.** 2009. Generation and analysis of expression sequence tags from haustoria of the wheat stripe rust fungus *Puccinia striiformis* f. sp. *tritici*. *BMC genomics* **10**, 626.

**Yin C, Jurgenson JE, Hulbert SH.** 2010. Development of a Host-Induced RNAi System in the Wheat Stripe Rust Fungus *Puccinia striiformis* f. sp. *tritici*. *Molecular Plant-Microbe Interactions* **24**, 554–561.

**Zhang WJ, Pedersen C, Kwaaitaal M, Gregersen PL, Mørch SM, Hanisch S, Kristensen A, Fuglsang AT, Collinge DB, Thordal-Christensen H.** 2012. Interaction of barley powdery mildew effector candidate CSEP0055 with the defence protein PR17c. *Molecular Plant Pathology* **13**, 1110–1119.

**Zhang H, Yang Y, Wang C, Liu M, Li H, Fu Y, Wang Y, Nie Y, Liu X, Ji W.** 2014. Large-scale transcriptome comparison reveals distinct gene activations in wheat responding to stripe rust and powdery mildew. *BMC genomics* **15**, 898.

**Zhu Q, Gao P, Wan Y, Cui H, Fan C, Liu S, Luan F.** 2018. Comparative transcriptome profiling of genes and pathways related to resistance against powdery mildew in two contrasting melon genotypes. *Scientia Horticulturae* **227**, 169–180.

**Zitter, TA, Hopkins DL, Tomas CE.** 1996. Compendium of cucurbits disease. APS Press, St. Paul, Minnesota.

Our research group at University of Malaga is interested in deciphering the molecular basis of the pathogenesis of the main causal agent of the cucurbit powdery mildew disease, *Podosphaera xanthii*. Our ultimate goal is to develop new phytosanitary tools against this devastating plant disease that are based on suitable targets previously identified in the pathogen. Therefore, in this work, we aim to dissect the changes in gene expression occurred in the host during the compatible interaction with *P. xanthii* and to determine the role of *P. xanthii* proteins specifically secreted by the haustorium. To address these global aims, we have established the following individual objectives:

1. To study the main changes in gene expression that occur in melon (*Cucumis melo*) during the early stages of the powdery mildew disease elicited by *P. xanthii*.
2. To perform the haustorial transcriptome of *P. xanthii* and to define its associated secretome.
3. To identify haustorium-specific secreted proteins with a key role in the pathogenesis of *P. xanthii*

# CHAPTER II

## **RNA-seq analysis and fluorescence imaging of melon powdery mildew disease reveal an orchestrated reprogramming of host physiology**

Álvaro Polonio, Mónica Pineda, Rocío Bautista, Jesús Martínez-Cruz,  
María Luisa Pérez-Bueno, Matilde Barón & Alejandro Pérez-García

*Scientific Reports* (2019), 9:7978



## ABSTRACT

The cucurbit powdery mildew elicited by *Podosphaera xanthii* is one of the most important limiting factors in cucurbit production. Our knowledge of the genetic and molecular bases underlying the physiological processes governing this disease is very limited. We used RNA-sequencing to identify differentially expressed genes in leaves of *Cucumis melo* upon inoculation with *P. xanthii*, using RNA samples obtained at different time points during the early stages of infection and their corresponding uninfected controls. In parallel, melon plants were phenotypically characterized using imaging techniques. We found a high number of differentially expressed genes (DEGs) in infected plants, which allowed the identification of many plant processes that were dysregulated by the infection. Among those, genes involved in photosynthesis and related processes were found to be upregulated, whereas genes involved in secondary metabolism pathways, such as phenylpropanoid biosynthesis, were downregulated. These changes in gene expression could be functionally validated by chlorophyll fluorescence imaging and blue-green fluorescence imaging analyses, which corroborated the alterations in photosynthetic activity and the suppression of phenolic compound biosynthesis. The powdery mildew disease in melon is a consequence of a complex and multifaceted process that involves the dysregulation of many plant pathways such as primary and secondary metabolism.





## INTRODUCTION

The Cucurbitaceae or cucurbit family includes many economically important species, particularly those with edible fruits such as cucumber, melon, watermelon, zucchini and pumpkin (Pérez-García *et al.*, 2009). Unfortunately, phytopathogens hinder the production of cucurbits, leading to over 200 known diseases with diverse aetiologies (Zitter *et al.*, 1996). Cucurbit powdery mildew is the primary fungal disease that affects cucurbits under both greenhouse and open field conditions. Like other powdery mildew diseases, it is easily recognizable by characteristic symptoms such as the whitish, talcum-like, powdery fungal growth that develops on leaf surfaces, petioles and stems, and rarely on fruits (Sitterly, 1978; Zitter *et al.*, 1996). There are two species that can cause powdery mildew in cucurbits around the world, namely, *Golovinomyces orontii* and *Podosphaera xanthii*. The latter is considered to be the main causal agent of powdery mildew in cucurbits, and it is one the most important limiting factors for cucurbits production (del Pino *et al.*, 2002; Fernández-Ortuño *et al.*, 2006; Bellón-Gómez *et al.*, 2015).

The arrival of a conidium to the leaf of a susceptible host and its adhesion, penetration, nutrition and proliferation as well as plant defence response suppression, are necessary steps for the establishment of a compatible interaction (Spanu, 2006). Like most powdery mildew fungi, *P. xanthii* grows on the foliar surface, taking nutrients from the epidermal host cells through the development of a specialized parasitism-related structure called the haustorium (Martínez-Cruz *et al.*, 2014). The epiphytic transcriptome of *P. xanthii* is available (Vela-Corcía *et al.*, 2016), several molecular tools have been developed for the specific functional analysis of *P. xanthii* genes such as host-

induced gene silencing and transient transformation (Martínez-Cruz *et al.*, 2017, 2018b) and the transcriptomes and genomes of major crops such as cucumber, melon, watermelon and zucchini are also available (Huang *et al.*, 2009; Guo *et al.*, 2011; Ando *et al.*, 2012; Blanca *et al.*, 2012; Garcia-Mas *et al.*, 2012; Xu *et al.*, 2013; Montero-Pau *et al.*, 2017). However, the genetic and molecular bases of the physiological processes governing this intimate plant-fungus interaction remain largely unknown.

RNA-seq is a revolutionary tool for transcriptomics which has altered our view of the extent and complexity of eukaryotic transcriptomes (Westermann *et al.*, 2012). RNA-seq analysis has been demonstrated to be an effective approach to decipher the primary changes in gene expression, providing a far more precise measurement of transcript levels and their isoforms than other methods and allowing researchers to detect transcripts with low abundance (’t Hoen *et al.*, 2008; Marguerat and Bähler, 2010). Fungal diseases of plants remain a major challenge in agriculture. Hence, an understanding of disease mechanisms at the molecular level is of paramount importance for identifying possible intervention points for their control (Rezzonico *et al.*, 2017). For this reason, several studies have used RNA-seq analysis to obtain a more comprehensive view of the primary molecular mechanisms that are dysregulated in plants upon pathogen inoculation (Fung *et al.*, 2007; Xin *et al.*, 2012; Borges *et al.*, 2013; Weng *et al.*, 2014; Guo *et al.*, 2018). However, whole-transcriptome changes during early disease stages in susceptible plant species are less well-documented than those of resistant ones. This is the case for cucurbit-powdery mildew interactions. There are only two reports that describe the transcriptome profiles of pumpkin and melon lines resistant to powdery mildew and their comparison with susceptible cultivars (Fung *et al.*, 2007; Xin *et al.*, 2012; Borges *et al.*, 2013; Weng *et al.*, 2014; Guo *et al.*, 2018; Zhu *et al.*, 2018).

Different imaging techniques are currently widely used in plant physiology to assess the impact of biotic stress on host plants since they reveal the metabolic gradients that pathogens usually induce in infected leaves (Barón *et al.*, 2016a; Mahlein, 2016). Examples of these techniques include chlorophyll fluorescence imaging (Chl-FI) and multicolour fluorescence imaging (MCFI). Studying the red chlorophyll fluorescence (Chl-F) emitted by photosystem II (PSII) provides information on the photosynthetic performance of plants in terms of activity (Murchie and Lawson, 2013) and indirect information on the CO<sub>2</sub> assimilation rate (Baker, 2008). Similarly, MCFI is a very useful technique for monitoring the plant health status. It is based on recording the blue (F440), green (F520), red (F680) and far red (F740) fluorescence that leaves emit when they are excited with UV light. Particularly, the so-called blue-green fluorescence (BGF) is a valuable technique to study secondary metabolism, since phenolic compounds from the phenylpropanoid pathway are the primary emitters of that fluorescence (Buschmann and Lichtenthaler, 1998; Cerovic *et al.*, 1999). To date, many plant-pathogen interactions have been subject to analysis using imaging techniques (Rolfe and Scholes, 2010; Barón *et al.*, 2016a) and most of them have the primary aim of identifying specific disease identity marks.

This study is intended to elucidate the primary alterations that take place in the physiology and metabolism *P. xanthii*-inoculated melon plants during the first stages of infection. For this purpose, RNA-seq analysis was used to search for changes in leaf gene expression after pathogen inoculation. In parallel, plants were phenotypically characterized by different imaging techniques to provide experimental support for the physiological changes anticipated by RNA-seq analysis. Our findings show that photosynthesis and secondary metabolism are the primary physiological processes of the host that are altered during the initial infection stages. This study is the first step in looking for effectors of *P. xanthii*

specifically aimed at manipulating these central functions of the host physiology. Unraveling these mechanisms would be desirable as a preliminary step in the development of new melon varieties that are resistant to *P. xanthii*.

## MATERIAL AND METHODS

### *Growth conditions of plants and fungi*

Melon plants (*Cucumis melo* L.) cv Rochet (Semillas Fitó, Barcelona, Spain) susceptible to the *P. xanthii* isolate 2086 were used in all the experiments. The plants were cultivated in a growth chamber with a 16 h: 8 h, light: dark cycle at 25 °C for one month. The powdery mildew isolate was cultured on previously disinfected zucchini (*Cucurbita pepo* L.) cotyledons cv Negro Belleza (Semillas Fitó) and maintained in Bertrand medium under a 16 h: 8 h, light: dark cycle at 22 °C for one week (Álvarez and Torés, 1997).

### *Experimental design*

To elucidate the changes in the gene expression levels in these melon plants during the first stages of their compatible interactions with *P. xanthii*, we performed an RNA-seq analysis at 24 h, 48 h and 72 h post-inoculation (hpi). For the inoculation, *P. xanthii* conidia were collected by immersing infected zucchini cotyledons in 50 mL of a 0.01% Tween-20/distilled water solution. The third and fourth true leaves of 1-month-old melon plants were inoculated with a spore suspension at  $1 \times 10^6$  conidia mL<sup>-1</sup> (infected plants) or with 0.01% Tween-20 in distilled water (control plants). We used the reference transcriptome of *C. melo* to define the differentially expressed genes (DEGs)

and later orthologous annotation with *Arabidopsis thaliana* to perform GO enrichment and MapMan analysis. In parallel, the changes in the physiology of the melon plants induced by the infection were analysed using different imaging techniques and other experimental approaches as described below.

### *Confocal laser scanning microscopy (CLSM)*

To visualize the development of the fungal structures during the initial stages of the infection process, a CLSM analysis was performed. For this purpose, leaf discs were taken at the same time points selected for RNA-seq analysis and the fungal structures were stained with an aqueous solution of 100  $\mu\text{g mL}^{-1}$  propidium iodide (Zhang *et al.*, 2018). The samples were observed using a Leica SP5 II confocal microscope (Leica Microsystems, Wetzlar, Germany). The samples were excited with a 488 nm laser line and their fluorescence was detected over a 510-570 bandpass range. Bright field images were taken using the transmission channel. All the images were observed using a 40 $\times$  oil-immersion objective and were processed with Leica LAS AF software (LCS Lite, Leica Microsystems).

### *RNA isolation, cDNA library construction and Illumina sequencing*

For RNA isolation, melon leaves were collected, immediately frozen in liquid nitrogen and stored at -80 °C until use. The frozen leaves were ground with a mortar and pestle and the total RNA was extracted using TRI Reagent (Sigma-Aldrich, Saint Louis, USA) according to the manufacturer's instructions. The total RNA was quantified using a NanoDrop 2000 spectrophotometer (Thermo Fisher Scientific, Waltham, MA, USA). The quality and quantity of the RNA were measured on an Agilent Bioanalyzer 2100

using an RNA Pico 6000 chip (Agilent Technologies, Santa Clara, CA, USA). Approximately 1  $\mu\text{g}$  of each sample was used for cDNA library construction using an Illumina Stranded mRNA Sample Preparation Kit (Illumina, San Diego, CA, USA) according to the manufacturer's instructions. Finally, the cDNA libraries were sequenced by Illumina NextSeq 550 system (Illumina).

### *RNA-Seq data analysis*

The detailed strategy for the differential expression analysis is depicted in Figure 2.1. The analysis process was automatized using Autoflow (Seoane *et al.*, 2016). The raw reads were pre-processed using the SeqTrimNext pipeline (Falgueras *et al.*, 2010) (<http://www.scbi.uma.es/seqtrimnext>) available at the Plataforma Andaluza de Bioinformática (University of Málaga, Spain) using the specific NGS technology configuration parameters. This pre-processing removes low quality, ambiguous and low complexity stretches, linkers, adaptors, vector fragments, organelle DNA, polyA, polyT tails, and contaminated sequences while keeping the longest informative part of the read. SeqTrimNext also discarded sequences below 25 bp. Subsequently, the clean reads were aligned with the melon transcriptome sequence (Blanca *et al.*, 2011) (<http://melonomics.cragenomica.es/files/Transcriptome/>) with Bowtie2 (Langmead and Salzberg, 2013) in BAM files, which were then sorted and indexed using SAMtools v1.4 (Li *et al.*, 2009). The reads containing discordant alignments were rejected due to their ambiguous location. Uniquely localized reads were used to calculate the read number value for each gene. Differentially expressed genes (DEGs) between two samples were analyzed using DESeq2 (Love *et al.*, 2014), one of the R packages. For each gene, a P-value  $<0.05$  and  $\log_2$ -fold change  $>1$  or  $<-1$  were considered the significance threshold. All the

DEGs were annotated with orthologous genes in *A. thaliana* ([https://plants.ensembl.org/Arabidopsis\\_thaliana/Info/Index](https://plants.ensembl.org/Arabidopsis_thaliana/Info/Index)) using Full-LengtherNext (<http://www.scbi.uma.es/fulllengthernext>) and they were hierarchically clustered by heatmap representation.

### *Gene functional enrichment and MapMan analysis of DEGs*

The DEGs annotated with orthologous genes in *A. thaliana* were used to identify the Gene Ontology functional categories using web-based GENECODIS software (Carmona-saez *et al.*, 2007; Nogales-Cadenas *et al.*, 2009; Tabas-Madrid *et al.*, 2012) (<http://genecodis.cnb.csic.es/>). MapMan software v. 3.5.0 (Thimm *et al.*, 2004) was used to provide a graphical overview of the metabolic and regulatory pathways for the detected DEGs.

### *Quantitative reverse transcription (qRT)-PCR*

The gene expression for the selected plant genes was quantified by qRT-PCR. The total RNA was isolated from the melon plants as described above. First-strand cDNA synthesis was performed using Invitrogen Superscript III Reverse Transcriptase (Invitrogen, Carlsbad, CA, USA) with random primers according to the manufacturer's instructions. The qRT-PCR reactions were conducted in a CFX384 Touch Real-Time PCR detection system (Bio-Rad, Hercules, CA, USA) using SsoFast EvaGreen Supermix according to the manufacturer's recommendations (Bio-Rad). Gene-specific primers (Table 2.1) were designed using Primer3 (Koressaar and Remm, 2007). The *C. melo*  $\beta$ -actin gene (XM\_008462689.2) was used as a reference gene (Wu and Cao, 2010). The qRT-PCR conditions were as follows: enzyme activation step at 95 °C for



30 s, followed by 40 cycles of 5 s at 95 °C and 5 s at 55 °C. After the amplifications, the data were analyzed using CFX Manager Software (Bio-Rad). Additionally, the amplicon sizes were confirmed by visualization on 1% agarose gels.



**Figure 2.1.** Schematic workflow used to perform the RNA-seq analysis of the *P. xanthii*-melon compatible interaction.

**Table 2.1.** RT-qPCR Primers used in this study.

Gene	Primer name	Primer sequence	Amplicon size (bp)
<i>lhcb6</i>	lhcb6-F	5'-GAATCCCATGGTTCGAAGCC-3'	214
	lhcb6-R	5'-GGATACCCCTTGTTCTCCGGT-3'	
<i>psbS</i>	psbS-F	5'-GTTTCACCCCTCTTGCTGTG-3'	175
	psbS-R	5'-AATGATGCAGCAAAGCCGAT-3'	
<i>petE2</i>	petE2-F	5'-CATCCCCAAAGCTTAGCGTC-3'	201
	petE2-R	5'-ATCCCGCGTTGTTCTTGAAC-3'	
<i>pgr5</i>	pgr5-F	5'-CCTCTTTCCTCCTCCTCCA-3'	176
	pgr5-R	5'-GCAAGAACAACAACAGGTGC-3'	
<i>rbcS</i>	rbcS-2b-F	5'-GGGGAAGAGTTCAGTGCATG-3'	222
	rbcS-2b-R	5'-ATGGTCCAGTAGCGTCCATC-3'	
<i>pal1</i>	pal1-F	5'-CAAGATCGCTATGCCCTTCG-3'	164
	pal1-R	5'-CCTTGGAAAGTTGCCCTCATG-3'	
<i>pal2</i>	pal2-F	5'-GCTGAGCAACACAACCAAGA-3'	231
	pal2-R	5'-TGAAGGATCGAGTGCACCAT-3'	
<i>pal4</i>	pal4-F	5'-ACCACAATGTCACACCTTGC-3'	236
	pal4-R	5'-TCCAACACCCGTCCATTAA-3'	
<i>rca</i>	rca-F	5'-TGCTGGACTTCGACAATACG-3'	150
	rca-R	5'-CCTCCCCAAATACCCAGAAT-3'	
<i>prk</i>	prk-F	5'-AACCCATGGCTGATAACCTG-3'	152
	prk-R	5'-TCTGGATTTCACCTCTTGG-3'	
<i>ohp1</i>	ohp1-F	5'-GGGGAAGAGGGAAAGTTCTG-3'	176
	ohp1-R	5'-GGCAGAAGACCCAATTTGAA-3'	
<i>adt6</i>	adt6-F	5'-ATCCATAACTCCACCGCTTG-3'	177
	adt6-R	5'-GCCACTCACGATTACCGATT-3'	

### *Analysis of photosynthetic activity*

The photosynthetic performance in terms of PSII activity was studied by variable Chl-FI, using an Open FluorCam 700MF (Photon System Instruments, Brno, Czechia). The applied protocol was the one described as number 1 by Pineda *et al.*, (2008). Black and white images corresponding to transient chlorophyll fluorescence values were collected and used to calculate several fluorescence parameters, using FluorCam software version 5.0. The images obtained for these parameters ( $F_v/F_m$ : maximum quantum yield of PSII,  $\Phi_{PSII}$ : effective quantum yield of PSII and NPQ: non-photochemical quenching), were calculated according to Maxwell and Johnson, (2000). A false colour scale was applied to the calculated images using the Fluorcam software.

The net photosynthesis rate ( $P_N$ ) was determined using an infrared gas analyser (IRGA LI-6400, Li-Cor Inc., Lincoln, NB, USA) on a 100 mm<sup>2</sup> melon leaf area. For the measurements, radiation was supplied by a Qbeam solid state LED lighting system attached to the leaf cuvette (6400-02B LED, Li-Cor Inc.).

### *Pigment content quantification*

The pigment content was determined spectroscopically according to Lichtenthaler and Buschmann (2001). For each treatment, three leaf disks of 78 mm<sup>2</sup> each were isolated and immediately frozen under liquid nitrogen. Quantifications were performed on acetone 80% (v/v in water) leaf extracts prepared by the homogenization of the tissue in liquid nitrogen and a subsequent centrifugation at 16000 g to remove the insoluble material. The absorbance at 470, 647 and 663 nm was measured using 80% acetone as a blank. The chlorophyll *a* (Chl *a*), chlorophyll *b* (Chl *b*), total chlorophyll (Chl T), and total xanthophyll and carotenoid (Xanth + Car) contents were determined according to the equations described in Lichtenthaler and Buschmann (2001).

### *Multicolour fluorescence imaging (MCFI)*

To further investigate the plant health status, and with special interest in plant secondary metabolism, the multicolour fluorescence emission from the adaxial side of melon leaves was recorded using an Open FluorCam FC 800-O (Photon Systems Instruments), according to (Pérez-Bueno *et al.*, 2015). Images of F680, F740 and particularly, BGF (F440 and F520 emitted by phenolic compounds from the phenylpropanoid pathway) from both uninfected and *P. xanthii*-infected melon leaves were captured by FluorCam software version 7.1.0.3,

which also applied a false colour scale to the black and white images recorded here.

### *Data availability*

The complete RNA-seq sequencing data for all the samples were deposited in the NCBI Sequence Read Archive and are accessible under the accession number PRJNA434538.

## **RESULTS**

### *Visualization of the development of *P. xanthii* structures during the first stages of infection*

In parallel with the sampling of plant material for RNA-seq analysis, leaf disks were collected to visualize the development of *P. xanthii* infection structures during the period of time analyzed by RNA-seq, that is, the first 72 h of interaction (Figure 2.2). At 0 hpi (hours post-inoculation), only the conidia were visible. At 24 hpi, most of the spores had germinated. At this stage, although not observed in the pictures, the first haustoria had already developed (Martínez-Cruz *et al.*, 2014). At 48 hpi, the primary hyphae were very abundant, and the initial formation of secondary hyphae could also be detected. Finally, at 72 hpi, extensive branching was observed in the secondary hypha.

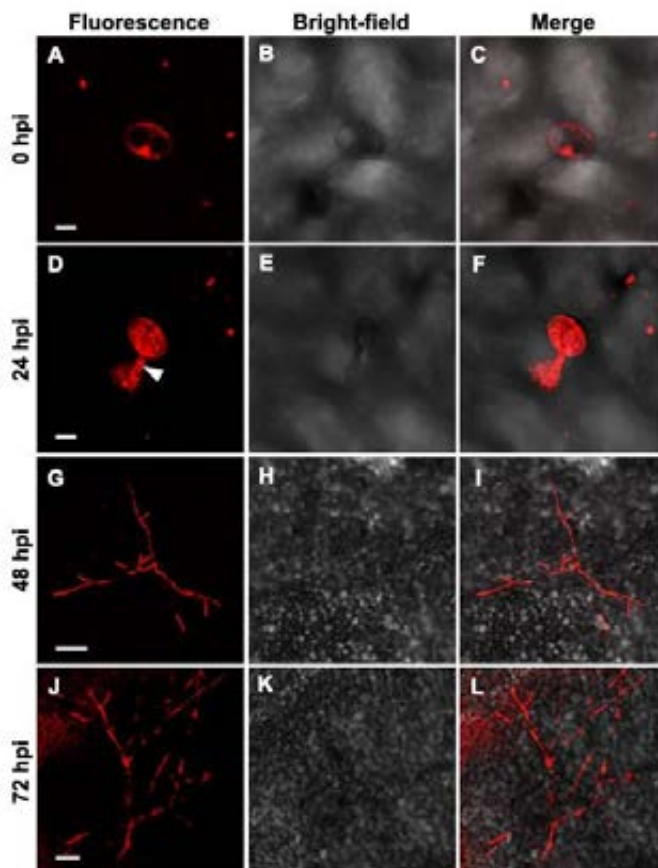


**Figure 2.2** Time-course analysis on the development of *P. xanthii* on the leaves of melon plants used for RNA-seq analysis by CLSM. Fungal structures were stained with propidium iodide. The pictures were taken at 0, 24, 48 and 72 h post-inoculation (hpi). A-C), an ungerminated conidium on the leaf surface. D-F), a conidium with a germ tube (arrowhead). G-I), a germinated spore (arrowhead) with primary hyphae and initial development of secondary hyphae. J-L), Weft of secondary hyphae. Bars: (A-F) 10  $\mu\text{m}$ ; (G-L) 100  $\mu\text{m}$ .

### *Illumina sequencing, mapping and identification of DEGs*

High-throughput sequencing produced a total of 1661.7 million short reads, of which 86.41 % (1435.9 million) passed the quality control thresholds. To

calculate the expression profile, clean reads were mapped onto the melon reference transcriptome with the Bowtie2 algorithm. The alignment results were reported in SAM/BAM format. The mapping rates for various samples are summarized in Table 2.2. The expression estimates are reported in total counts for each gene. DESeq2 software was employed to analyze the differentially expressed genes at three time points (24, 48 and 72 hpi) in infected plants relative to un-inoculated control plants. Differentially Expressed Genes (DEGs) were reported in log<sub>2</sub>FoldChange (FC) with a corresponding *p-value* for each gene. An MA plot was used to represent the DEGs of infected plants relative to control plants at 24, 48 and 72 hpi (Figure 2.3A). Among all the DEGs, 538 were common at three time points, while 237, 1870 and 2448, were exclusively exhibited at 24 hpi, 48 hpi and 72 hpi, respectively (Figure 2.3B). Furthermore, the heatmap of expression levels of all these melon DEGs showed that the expression profiles of them varied significantly in response to *P. xanthii* infection (Figure 2.3C). A total of 1114 genes showed differential expression patterns at 24 hpi, from which 863 were found to be upregulated and 251 downregulated. The number of DEGs at 48 hpi was 3785, with 2781 upregulated and 1004 downregulated genes. At 72 hpi 4226 DEGs were detected. Of these, 2697 exhibited upregulation and 1529 showed downregulation (Figure 2.3D).

**Table 2.2.** Summary mapping rates of all the samples sequenced during the RNA-seq analysis performed in this study.

<b>Samples</b>	<b>Input reads</b>	<b>Output reads</b>	<b>Rejected reads (%)</b>	<b>Reads aligned to reference (%)</b>
Uninfected24hpi_1	87,809,876	75,500,680	10.41	85.69
Uninfected24hpi_2	76,542,470	68,370,412	7.76	84.78
Uninfected24hpi_3	106,356,748	94,607,324	7.82	83.35
Uninfected48hpi_1	118,995,292	102,632,628	10.44	85.27
Uninfected48hpi_2	77,108,192	68,918,670	7.77	88.15
Uninfected48hpi_3	115,508,352	1,027,02,870	7.65	85.83
Uninfected72hpi_1	93,416,186	82,948,230	8.00	87.68
Uninfected72hpi_2	69,539,512	58,948,720	11.34	85.00
Uninfected72hpi_3	110,202,904	85,023,518	19.62	84.25
Infected24hpi_1	109,377,644	97,468,648	7.38	83.61
Infected24hpi_2	93,731,880	85,484,974	5.80	84.10
Infected24hpi_3	76,648,932	67,916,294	8.26	84.90
Infected48hpi_1	87,981,974	74,466,522	11.31	84.00
Infected48hpi_2	89,057,812	76,561,898	9.84	83.87
Infected48hpi_3	85,438,210	73,423,600	10.31	83.64
Infected72hpi_1	88,500,998	74,541,194	11.80	85.10
Infected72hpi_2	76,639,666	66,055,082	9.75	84.89
Infected72hpi_3	98,931,690	80,396,216	14.68	83.80

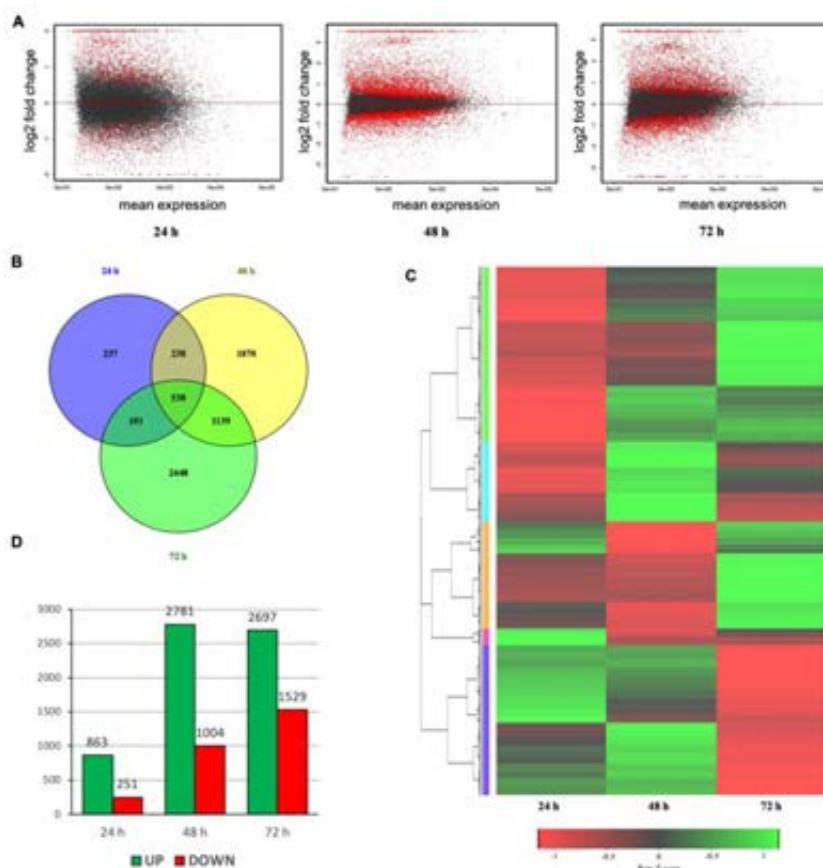


**Figure 2.3.** Summary of sequence data and the number of differentially expressed genes determined by RNA-seq in melon plants infected with *P. xanthii* versus non-infected control plants. Data were collected at 24, 48 and 72 h post-inoculation (hpi). A) log<sub>2</sub>-fold change versus a mean expression scatter plot of the RNA-seq results. B) A Venn diagram displaying the distribution of DEGs (genes with >1 or >-1 log<sub>2</sub>-fold change in expression) at each time point. C) Hierarchical clustering of DEGS at each time point. Rows are clustered using distance and average linkage. Changes of gene expression are displayed from red (lower expression) to green (higher expression). D) Number of genes up- and downregulated at each time point in infected plants compared to non-infected control plants.



### *Gene functional enrichment analysis of DEGs and metabolism overview*

To understand the primary functions of melon DEGs in response to *P. xanthii* infection, a gene functional enrichment analysis was performed using GENECODIS. A singular enrichment analysis of the GO biological process revealed a total of 33, 108 and 83 significantly enriched (adj. p-val. < 0.05) Gene Ontology (GO) terms at 24, 48 and 72 hpi, respectively (Table S2.1). These GO terms were ordered according to their hypergeometric *p-value* (Hyp), with the first positions being those with minor Hyp values. Subsequently, the GO terms were filtered to select the top 20 to reduce the amount of data and to facilitate the representation of the most enriched terms at each time point (Table 2.3). Among the first 20 GO terms over the three analysed time points, photosynthesis-related terms such as photosynthesis (GO:0015979), response to red light (GO:0010114), response to blue light (GO:0009637), response to far red light (GO:0010218) or response to light stimulus (GO:0009416) were common. Furthermore, GO terms for secondary metabolism-related genes such as response to wounding (GO:0009611), defence response to fungus (GO:0050832) or lignin biosynthesis process (GO:0009809) were also highly represented, with these GO terms being especially important at 72 hpi. In addition, other terms related to hormone signalling such as response to jasmonic acid stimulus (GO:0009753), response to abscisic acid stimulus (GO:0009757) or response to salicylic acid stimulus (GO:0009751) were also present as biological process functional enrichment.

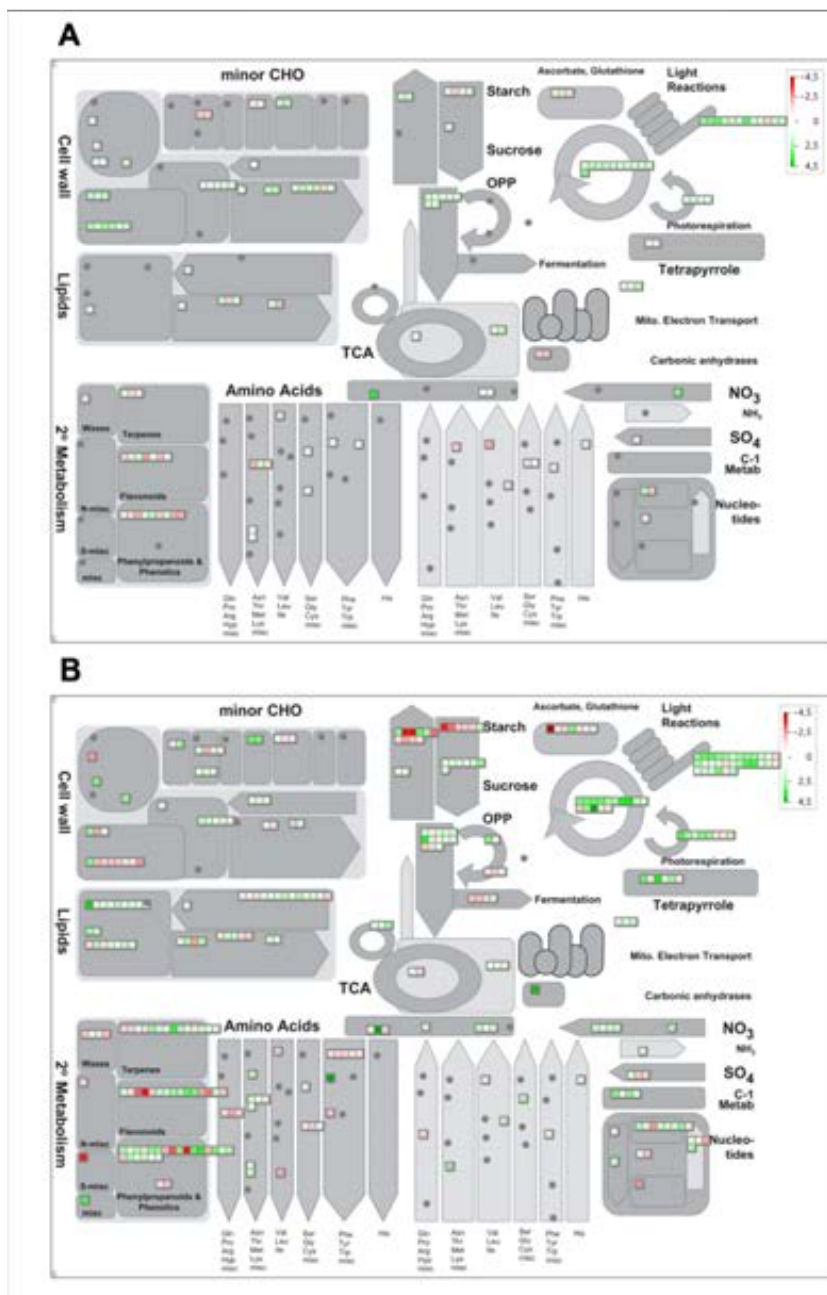
**Table 2.3.** Top 20 GO biological terms for *P. xanthii*-infected melon leaves at 24, 48 and 72 hpi, as performed by the functional enrichment of all the DEGs in web-based GENECODIS software.

24 hpi	48 hpi	72 hpi
GO:0015979 photosynthesis	GO:0015979 photosynthesis	GO:0046686 response to cadmium ion
GO:0009409 response to cold	GO:0009414 response to water deprivation	GO:0008152 metabolic process
GO:0010114 response to red light	GO:0009611 response to wounding	GO:0015979 photosynthesis
GO:0009637 response to blue light	GO:0010114 response to red light	GO:0009611 response to wounding
GO:0046686 response to cadmium ion	GO:0009409 response to cold	GO:0006979 response to oxidative stress
GO:0010218 response to far red light	GO:0009651 response to salt stress	GO:0050832 defense response to fungus
GO:0009611 response to wounding	GO:0009753 response to jasmonic acid stimulus	GO:0010114 response to red light
GO:0009416 response to light stimulus	GO:0009737 response to abscisic acid stimulus	GO:0009651 response to salt stress
GO:0019253 reductive pentose-phosphate cycle	GO:0006857 oligopeptide transport	GO:0080167 response to karrikin
GO:0015977 carbon fixation	GO:0010218 response to far red light	GO:0009737 response to abscisic acid stimulus
GO:0009744 response to sucrose stimulus	GO:0009637 response to blue light	GO:0010218 response to far red light
GO:0080167 response to karrikin	GO:0009416 response to light stimulus	GO:0055114 oxidation-reduction process
GO:0006979 response to oxidative stress	GO:0007623 circadian rhythm	GO:0019464 glycine decarboxylation via glycine cleavage system
GO:0009250 glucan biosynthetic process	GO:0080167 response to karrikin	GO:0009809 lignin biosynthetic process
GO:0009695 jasmonic acid biosynthetic process	GO:0055114 oxidation-reduction process	GO:0042128 nitrate assimilation
GO:0006857 oligopeptide transport	GO:0008152 metabolic process	GO:0009414 response to water deprivation
GO:0050832 defense response to fungus	GO:0019253 reductive pentose-phosphate cycle	GO:0010224 response to UV-B
GO:0006096 glycolysis	GO:0006096 glycolysis	GO:0009751 response to salicylic acid stimulus
GO:0009753 response to jasmonic acid stimulus	GO:0006970 response to osmotic stress	GO:0042742 defense response to bacterium
GO:0010105 negative regulation of ethylene mediated signaling pathway	GO:0015995 chlorophyll biosynthetic process	GO:0009637 response to blue light

Since the main dysregulated processes were similar at the three time points analyzed, to obtain a more comprehensive overview of the primary process dysregulation that occurred in melon plants during the first stages of *P. xanthii*

infection, we focused our study at 24 and 72 hpi and performed a MapMan analysis of DEGs at those time points (Figure 2.4). In general terms, at 24 hpi, primary metabolism-related genes such as light reaction genes, Calvin cycle genes and photorespiration genes were upregulated, whereas some secondary metabolism-related genes such as phenylpropanoid and flavonoid biosynthesis genes were slightly downregulated. Furthermore, cell wall modification-related genes were generally upregulated (Figure 2.4A). At 72 hpi, the light reaction genes, Calvin cycle genes and photorespiration genes were also upregulated. Similarly, certain secondary metabolism related genes were downregulated, and a few of them were strongly repressed. Additionally, some starch synthesis and degradation-related genes were also down-regulated. However, compared to 24 hpi, the cell wall modification-related genes were mostly downregulated at 72 hpi (Figure 2.4B). The MapMan analysis allowed us to validate that the most important GO terms were identified, completing the information and specifying the relative expression level of the primary dysregulated processes. Therefore, in general, photosynthesis and related processes were upregulated, whereas the major secondary metabolism pathways such as the phenylpropanoid biosynthesis pathway were downregulated.

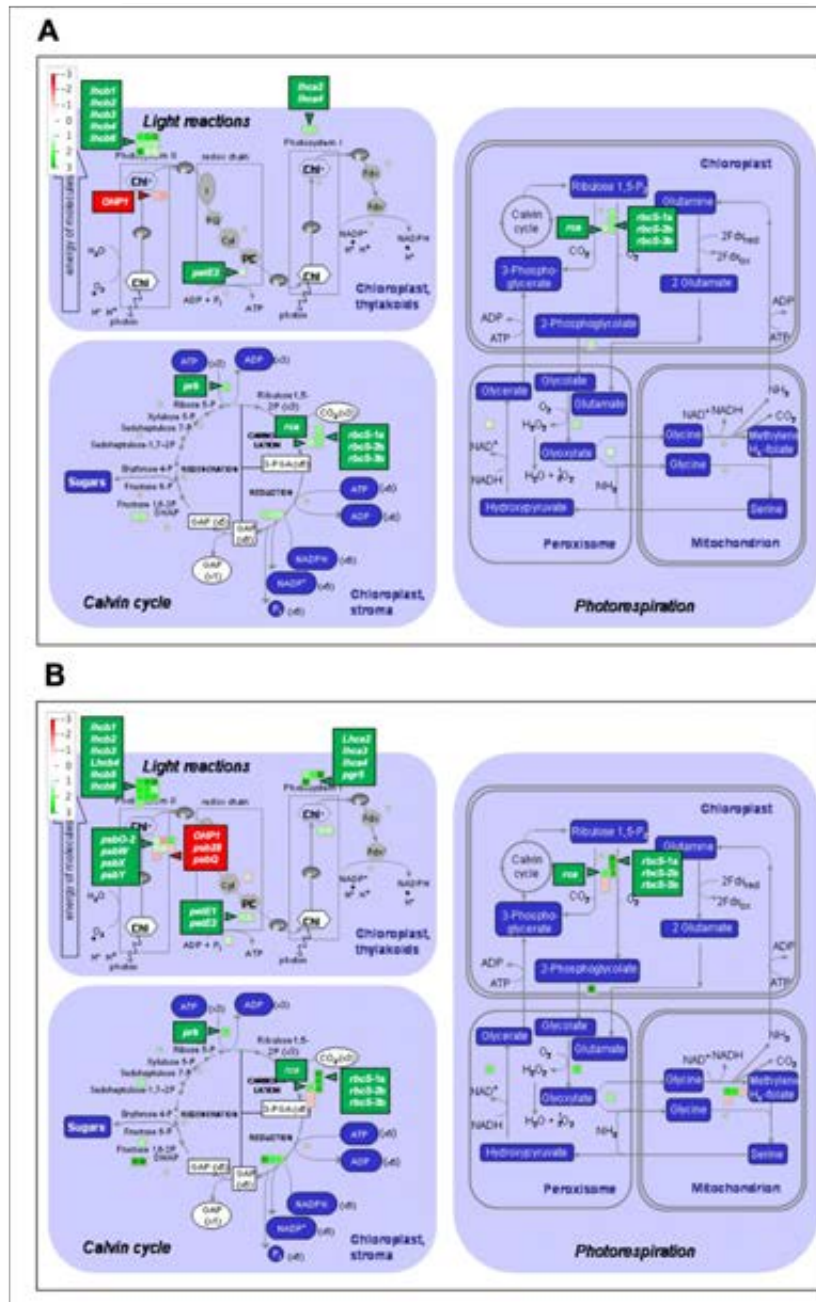
**Figure 2.4.** MapMan overview of plant metabolism in *P. xanthii*-infected melon leaves showing all DEGs at 24 A) and 72 hpi B). The analysis was performed using MapMan v.3.5.0. Individual genes are represented by small squares. The colour key represents the RPKM (Reads Per Kilobase Million)-normalized log<sub>2</sub>-transformed counts. Red represents the downregulation and green represents the upregulation of melon genes from infected plants compared to uninfected controls.



*P. xanthii* infection induces changes in the expression of melon genes involved in photosynthesis and secondary metabolism

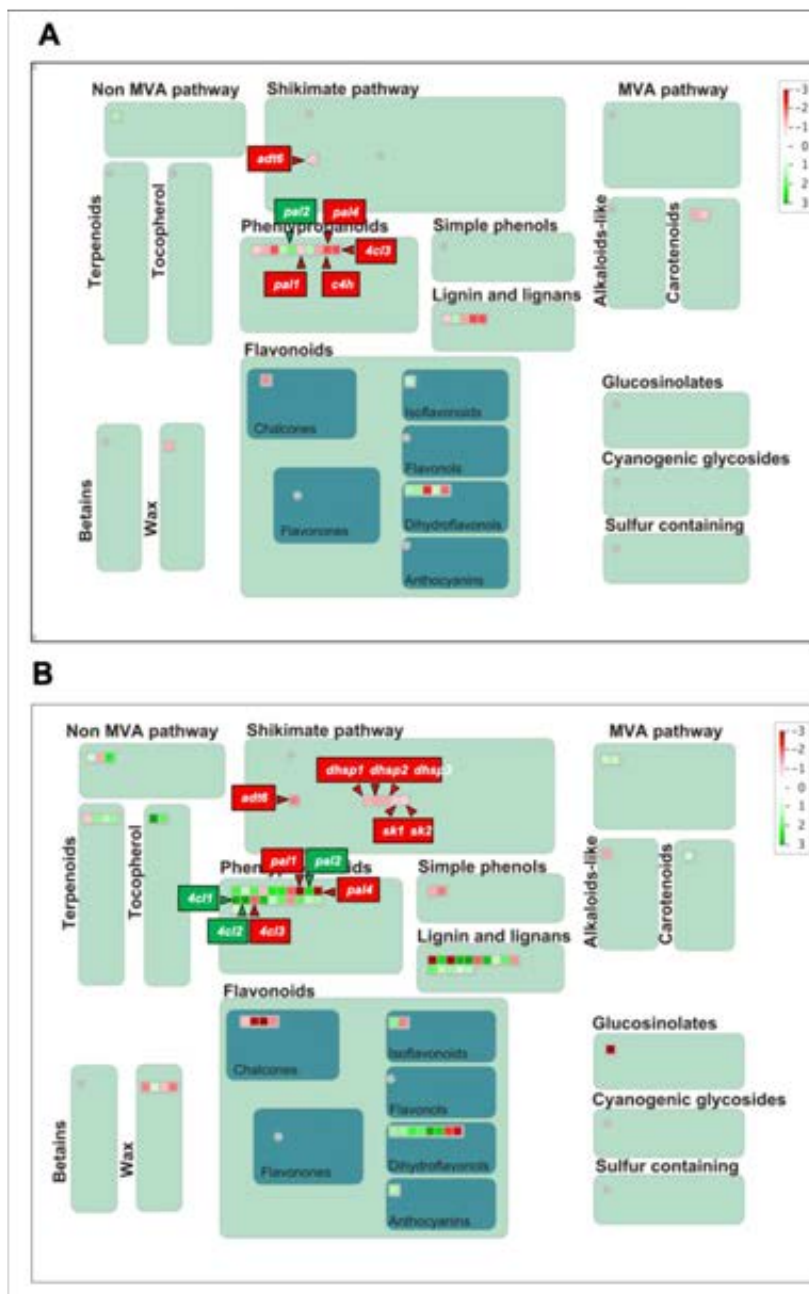
To more thoroughly visualize the genes subjected to gene expression changes in some of the primary process that were dysregulated in melon plants infected by *P. xanthii*, a MapMan analyses for photosynthesis and secondary metabolism were performed at 24 and 72 hpi (Figure 2.5). Among the 28 DEGs involved in photosynthesis at 24 hpi, 26 were upregulated, whereas only 2 were downregulated (Table S2.2). For example, several *lhc* genes that encode Lhcb and Lhca antenna proteins of PSII and PSI, respectively, or *petE2* that encodes the predominant plastocyanin isoform, were upregulated. In addition, some Calvin cycle genes such as those encoding ribulose bisphosphate carboxylase small chain (*rbcS-1a*, *rbcS-2b* and *rbcS-3b*), phosphoribulokinase (*prk*) and rubisco activase (*rca*) were also overexpressed. The only suppressed genes were *psbT* and *OHP1*, which encode the PSII 5 kDa protein subunit PSII-T and one helix protein 1, respectively (Figure 2.5A). At 72 hpi, 50 photosynthesis-related genes were DEGs. Forty-one of these genes were upregulated and 9 downregulated (Table S2.2). Among the upregulated genes, we note the other *lhc* genes (*lhcb5* and *lhca3*), *psb* genes of PSII (*psbO-2*, *psbW*, *psbX*, and *psbY*) or *petE1* and *pgr5*, codifying isoform 1 of plastocyanin and proton gradient regulation 5 protein, respectively. Although the *psbT* gene was not repressed, *psbQ* and *psb28* were downregulated at 72 hpi (Figure 2.5B).

**Figure 2.5.** MapMan of primary metabolism in *P. xanthii*-infected melon leaves showing all the DEGs at 24 A) and 72 hpi B). The analysis was performed using MapMan v.3.5.0. Individual genes are represented by small squares. The colour key represents the RPKM-normalized log<sub>2</sub>-transformed counts. Red represents downregulation and green represents upregulation of melon genes from infected plants compared to uninfected controls.



A similar approach was performed to analyse the changes in the expression of secondary metabolism-related genes in *P. xanthii*-infected melon plants (Figure 2.6). Among the 20 DEGs involved in secondary metabolism and detected at 24 hpi, 12 were downregulated and 8 were upregulated (Table S2.2). Several genes involved in the phenylpropanoid and shikimate pathways, which have a key role in the biosynthesis of different defense compounds, were repressed, including the phenylalanine ammonia lyase isoform genes *pal1* and *pal4*, which are involved in the first step of phenylpropanoids biosynthesis. By contrast, *pal2* was upregulated. Other important genes in the phenylpropanoids pathway such as *c4h* and *4cl3* were downregulated. Moreover, *adt6*, a gene related to phenylalanine biosynthesis, was also downregulated (Figure 2.6A). At 72 hpi, 62 genes involved in secondary metabolism were DEGs, of which 28 were downregulated and 34 upregulated (Table S2.2). For example, *pal4* was strongly repressed, whereas *pal2* was overexpressed. In addition, although *4cl3* remained downregulated, *4cl1* and *4cl2* were overexpressed. Furthermore, *adt6* increased its repression level and other genes in the shikimate pathway that trigger phenylalanine biosynthesis, such as *dhsp1*, *dhsp2*, *dhsp3*, *sk1* and *sk2*, were downregulated (Figure 2.6B). In summary, at 24 hpi, the phenylpropanoid pathway seems to be affected at the phenylalanine and p-coumarate biosynthesis levels, whereas at 72 hpi, the inhibition of this pathway is upstream, at the first steps of shikimate synthesis (Figure 2.7).

**Figure 2.6** MapMan of secondary metabolism in *P. xanthii*-infected melon leaves showing all DEGs at 24 A) and 72 hpi B). The analysis was performed using MapMan v.3.5.0. Individual genes are represented by small squares. The colour key represents the RPKM-normalized log<sub>2</sub>-transformed counts. Red represents downregulation and green represents upregulation of melon genes from infected plants compared to uninfected controls.





The results obtained by RNA-Seq were validated by qRT-PCR analysis. Twelve DEGs involved in photosynthesis and secondary metabolism were selected, subjected to expression analysis by qRT-PCR at the same time points and compared to the RNA-seq data. In general terms, the expression levels observed by qRT-PCR were very similar to those obtained by RNA-seq, with the only exceptions being the *OHP1* and *pgr5* at 48 hpi. These results allowed us to confirm the reliability of the RNA-seq data (Fig. 2.8).

*Fluorescence imaging analysis data from melon leaves in response to P. xanthii infection are consistent with the RNA-seq results*

To functionally validate the expression data revealed by RNA-seq analysis, the impact of the fungal infection on melon physiology was investigated by different fluorescence imaging techniques. The impact on leaf photosynthesis was investigated in terms of PSII efficiency and Calvin cycle activity (Fig. 2.9). The maximum quantum yield of PSII as measured as the  $F_V/F_M$ , did not show significant differences between infected and uninfected leaves. However, a consistent inhibition of the PSII (at 24 and 72 hpi) could be measured as a decrease in the  $\Phi_{PSII}$  of infected leaves, correlating with a reduction in the net CO<sub>2</sub> fixation rate ( $P_N$ ) of infected leaves at 72 hpi. Notably, the NPQ was significantly higher in infected leaves at 24 and 72 hpi. In addition, all these changes in the Chl-FI parameters could not be attributed to alterations in the contents of pigments such as chlorophylls, carotenoids or xanthophylls induced by the fungus, since no significant differences were found between infected and uninfected plants (Table 2.4).

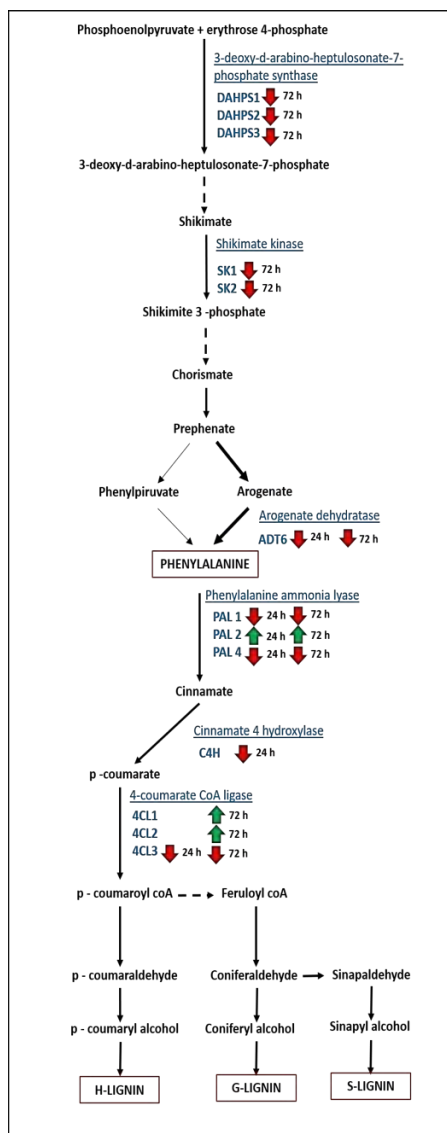


**Figure 2.7** Schematic representation of phenylpropanoids pathway of *P. xanthii*-infected melon leaves showing all DEGs at 24 and 72 hpi. The colour key represents dysregulation of melon genes from infected plants compared to uninfected controls. Green arrows represent up-regulated genes and red arrows represent down-regulated genes. Discontinuous black arrows show incomplete pathway.

**Table 2.4.** Impact of *P. xanthii* infection on pigment content of melon leaves

Pigments <sup>a</sup>	24 hpi		72 hpi	
	Uninfected	Infected	Uninfected	Infected
Chl <i>a</i>	0.84±0.12 <sup>b,c</sup>	0.78±0.03	0.73±0.04	0.65±0.05
Chl <i>b</i>	0.26±0.03	0.29±0.03	0.27±0.04	0.20±0.04
Chl T	1.10±0.12	1.08±0.06	1.00±0.09	0.85±0.09
Xant + Car	0.21±0.02	0.20±0.01	0.18±0.01	0.19±0.01

<sup>a</sup>Abbreviations are: Chl *a*, chlorophyll *a*; Chl *b*, chlorophyll *b*; Chl T, total chlorophyll content; Xant + Car, xanthophylls and carotenoids.

<sup>b</sup>Values shown are average values (n=6) in µg mg<sup>-1</sup> of fresh weight ±SE.

<sup>c</sup>No statistically significant differences between uninfected and infected samples were obtained according to two-tailed Student's *t* test.

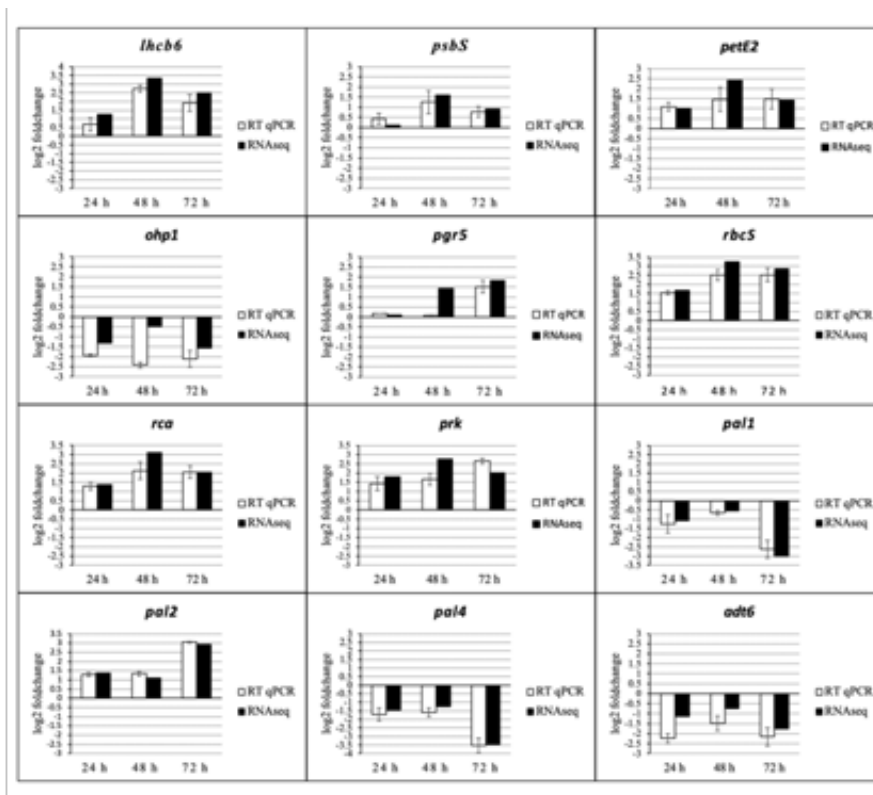


**Fig. 2.8.** Validation of RNA-Seq data from *P. xanthii*-melon compatible interactions by qRT-PCR analysis of selected primary and secondary metabolism DEGs. The relative expression ( $\log_2$ -fold change) of twelve genes at 24, 48, and 72 hpi is shown. The transcript abundance was normalized to the transcription of the endogenous control  $\beta$ -actin gene (XM\_008462689.2) and the relative expression of each gene was calibrated to the uninfected control at the corresponding time point. The qRT-PCR data (white bars) are expressed as the mean values of three experimental replicates from three independent experiments, with error bars depicting the standard error. The RNA-seq data (black bars) are also shown for comparison.

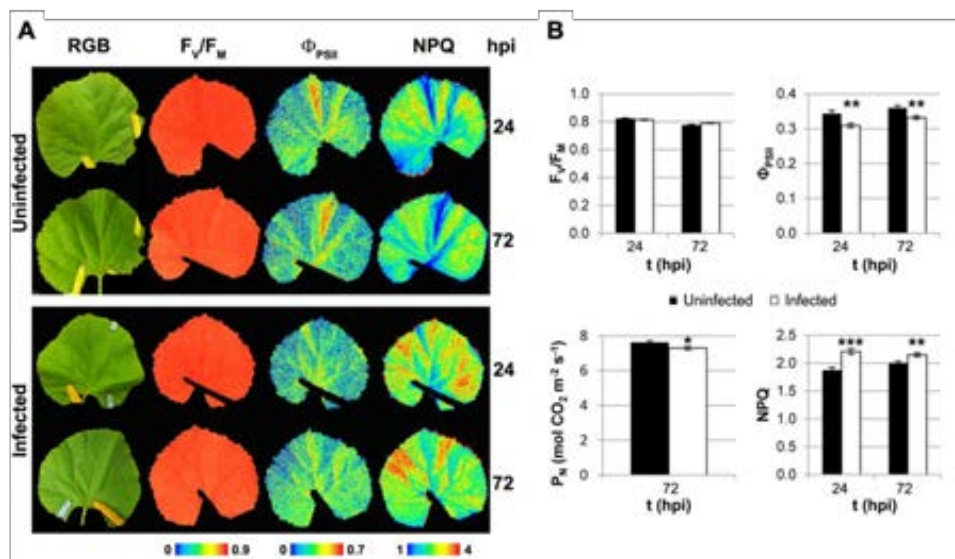


**Fig. 2.9.** Impact of *P. xanthii* infection on the primary metabolism of melon leaves. A) Standard images of the RGB,  $F_v/F_m$ ,  $\Phi_{PSII}$  and NPQ from non-infected and *P. xanthii*-infected melon leaves at 24 and 72 hpi. A false colour scale was applied for each parameter. Images from a representative experiment are shown. B) The average values of  $F_v/F_m$ ,  $\Phi_{PSII}$ , and NPQ ( $n=6$ ) and the net photosynthesis rate ( $n=10$ ) for non-infected and infected melon leaves at 24 and 72 hpi are shown, with bars representing the standard error. The asterisks indicate a statistically significant difference between the samples according to a Student's t-test (\* $P < 0.1$ , \*\* $P < 0.01$ , and \*\*\* $P < 0.001$ ). The abbreviations are:  $F_v/F_m$ , maximum quantum yield of PSII;  $\Phi_{PSII}$ , effective quantum yield of PSII; NPQ, non-photochemical quenching; and  $P_n$ , net photosynthesis rate.

The accumulation of secondary metabolites in response to fungal infection was analysed by BGFI (Fig. 2.10). The F440 and F520 emitted by the infected leaves were comparable to that released by the uninfected controls at 24 and 72 hpi. This result indicated that there was no alteration in the accumulation of phenolic compounds in response to *P. xanthii* infection. In conclusion, and as revealed by RNA-seq analysis, this fungal infection seems to alter the

photosynthesis efficiency of susceptible melon plants and manipulate the activation of the phenylpropanoid pathway.

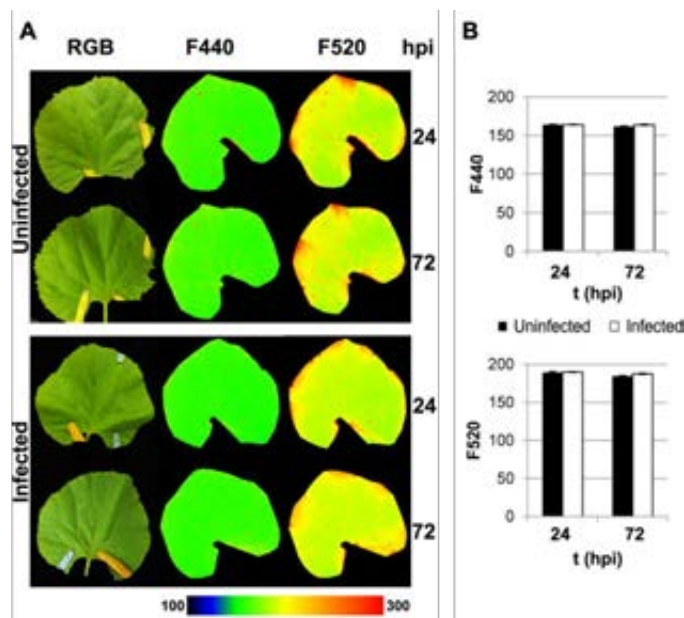


**Fig. 2.10.** Impact of *P. xanthii* infection on the secondary metabolism of melon leaves. A) Standard images of the RGB, F440 and F520 emitted by phenolic compounds from non-infected and *P. xanthii*-infected melon leaves at 24 and 72 hpi. A false colour scale was applied for each parameter. Images from a representative experiment are shown. B) The average values of F440 and F520 (n=6) for non-infected and infected melon leaves at 24 and 72 hpi are shown, with bars representing the standard error. No statistically significant differences between the samples were obtained according to a Student's t test. The abbreviations are F440, blue fluorescence and F520, green fluorescence.

## DISCUSSION

The cucurbit powdery mildew disease elicited by *P. xanthii* is one of the most important limiting factors in cucurbit production worldwide (Pérez-García *et al.*, 2009). The molecular mechanisms underlying this pathogenic interaction remain largely unknown, with only a few studies addressing the transcriptomic analysis in this fungus (Vela-Corcía *et al.*, 2016) and in resistant pumpkin and melon lines (Guo *et al.*, 2018; Zhu *et al.*, 2018). For that reason, this study is intended to decipher the primary molecular and physiological changes taking place in melon plants during the first stages of the compatible interaction with *P. xanthii*. To this end, we analyzed this interaction using a combination of RNA-seq with different imaging techniques.

RNA-seq is a sensitive and effective approach for identifying the primary changes in gene expression (’t Hoen *et al.*, 2008; Marguerat and Bähler, 2010), but it generates a large amount of data that are difficult to process. To visualize the data and to perform a more efficient analysis, tools such as GO terms enrichment or MapMan analyses were used (Gao *et al.*, 2013; Guo *et al.*, 2018). Although some terms obtained by GO enrichment analysis were different at the three time points analyzed here, most of them were related to two major physiological processes, photosynthesis and secondary metabolism. Therefore, to yield a simpler and comprehensive study, the subsequent analyses were performed using 24 and 72 hpi data points, which, on the other hand, were the time points from which image analysis data were obtained. The metabolism overview performed by MapMan yielded very similar results relative to the ones obtained through GO terms enrichment analysis, but the first approach allowed us to obtain more visual results and to identify the primary genes dysregulated

in each pathway. Therefore, by combining both analyses, it has been possible to detect different functional processes and related pathways that were being dysregulated in the melon plants infected with *P. xanthii*, with photosynthesis and secondary metabolism being the stand-outs.

Among all the photosynthesis-related DEGs, only *ohp1* was downregulated at both 24 and 72 hpi. The Ohp1 protein is required for PSII function (Beck *et al.*, 2017). Therefore, the downregulation of this gene could be part of a mechanism to decrease  $\Phi_{\text{PSII}}$  in a regulated manner. However, *lhcb6* was upregulated upon inoculation at all the data points. Lhcb6 is a subunit of the minor light harvesting complex of PSII that is involved directly in the thermal dissipation of excess energy (Passarini *et al.*, 2009; de Bianchi *et al.*, 2010). Furthermore, *psbS* was up-regulated at 48 hpi, coinciding with the maximum expression of *lhcb6*. The interaction of PsbS with the minor antenna, including Lhcb6, is crucial for the regulation of NPQ (Pérez-Bueno *et al.*, 2008; Sacharz *et al.*, 2017). Moreover, the expression of *petE2* and *pgr5* was also upregulated. Both genes encode key players in the cyclic electron flow around PSI, which dissipates the  $\Delta\text{pH}$  across the thylakoid (Munekage *et al.*, 2004; Rumeau *et al.*, 2007; Miyake, 2010), and it is essential for the photoprotection of the thylakoids (Munekage *et al.*, 2002). These transcriptomics data are consistent with those of other plants infected with powdery mildew, in which several photosynthesis-related genes were found to be upregulated (Zhang *et al.*, 2014; Fu *et al.*, 2016; Guo *et al.*, 2018).

The photosynthesis-related RNA-seq results were validated by different functional approaches such as chlorophyll fluorescence imaging (Chl-FI) and the net photosynthesis rate ( $P_N$ ). Compared to the control leaves, the *P. xanthii*-infected melon leaves showed photosynthesis inhibition at two levels, in terms



of the electron transport rate (decrease in  $\Phi_{\text{PSII}}$ ) and carbon fixation (decrease in  $P_{\text{N}}$ ) from 24 hpi onwards. Moreover, in the infected leaves, the mechanism of energy dissipation, as measured as the NPQ, was induced, although the  $F_{\text{V}}/F_{\text{M}}$  was not affected. The photosynthesis was previously shown to be inhibited, as measured as a decrease in the  $\Phi_{\text{PSII}}$  and  $P_{\text{N}}$ , while the NPQ increased during the fungal infection (Repka, 2002; Rolfe and Scholes, 2010). These photosynthetic changes were not attributed to alterations in the chlorophyll contents of melon leaves. Those data are in accordance with previously obtained results in cucumber leaves infected with *P. xanthii*, which displayed a decrease in the  $\Phi_{\text{PSII}}$  several days before a reduction in the chlorophyll content could be detected (Berdugo *et al.*, 2014). Hence, the changes in the  $\Phi_{\text{PSII}}$  and NPQ could be caused by a modification in the expression of genes such as *ohp1*, *lhcb6* and *psbS*. Swarbrick *et al.*, (2006) demonstrated downregulation in the expression of photosynthetic genes such as *rcbS* and Chl-*a/b*-binding proteins (*cab*) related to a decrease in the  $P_{\text{N}}$  of barley leaves infected by powdery mildew. However, during *P. xanthii*-melon interaction, there were increases in the expression levels of important photosynthetic genes such as *rcbS 1-a*, *2-b*, *3-b*, *rca* and *prk*. This finding could be the result of the manipulation of gene regulation by *P. xanthii* to increase the photosynthesis and photosynthates in melon plants for its own benefit; nevertheless, the plant effectively inhibited the photosynthetic activity, as a part of the plant defense program to limit carbon source availability for the pathogen (Bolton, 2009). Cyclic electron flow around PSI, for which *petE* and *pgr5* genes were found to be upregulated, could contribute to the inhibition of the Calvin cycle.

It is well known that phenylpropanoid compounds play a key role in plant defence against pathogens (Dixon *et al.*, 2002). Therefore, the repression of different DEGs related to this pathway and the shikimate pathway could be

important for the establishment of compatible interactions. Whereas *c4h*, a key gene in lignin synthesis (Yang *et al.*, 2013), was downregulated at 24 hpi, did not show expression changes at 72 hpi, suggesting that it could be affecting the phenylalanine synthesis only at very early stages of the interaction. However *adt6*, *pal1*, *pal4* and *4cl3* were downregulated at 24 and 72 hpi. The aroenate pathway has been described as the predominant pathway for phenylalanine synthesis (Maeda *et al.*, 2010, 2011), hence, enzymes such as prephenate aminotransferase (PAT) or aroenate dehydratase (ADT) become key action points. In relation to this situation, the observed downregulation of *adt6* could interfere with phenylalanine synthesis. The repression of *pal* genes could be even more important. This gene encodes enzymes that catalyse the first step in the phenylpropanoid pathway and are considered a key point of regulation between primary and secondary metabolism (Olsen *et al.*, 2008). Between the *pal1* and *pal2* genes, Rohde *et al.*, (2004) qualified *pal1* as being more important for phenylpropanoid biosynthesis. Moreover, different studies indicate that *pal1* expression is induced by wounding and pathogen attack (Ohl *et al.*, 1990; Mauch-Mani, 1996; Rookes and Cahill, 2003; Cochrane *et al.*, 2004). In addition, *pal4* has been shown to act as an important gene in lignin biosynthesis (Raes, 2003; Rohde *et al.*, 2004). In our study, both the *pal1* and *pal4* genes showed increased repression at 72 hpi, when the fungal development was more evident. The *4cl3* repression does not seem very important, since its function is related to flavonoid biosynthesis, but not to lignin biosynthesis, whose function is performed primarily by *4cl1* and *4cl2* (Li *et al.*, 2015), both of which are upregulated at 72 hpi. However, the repression of several genes in the shikimate pathway at 72 hpi, such as *dahps1*, *dahps2*, *dahps3*, *sk1* and *sk2*, was more important since they act as shikimate pathway regulators (Tzin and Galili, 2010). The *dahps* (3-Deoxy-D-arabinoheptulosonate 7-phosphate synthase)

genes act as a branch point to convert primary carbon source into the shikimate pathway and could act as a shikimate pathway key point to compete for phosphoenolpyruvate and erythrose 4-phosphate with the glycolysis and the pentose phosphate pathway (Tzin and Galili, 2010). Moreover, *dahps* genes are induced by wounding and fungal elicitors, which induce the synthesis of phenylpropanoids metabolites (McCue and Conn, 1989; Herrmann and Weaver, 1999). On the other hand, several studies have suggested that *sk* genes have an important role in plant defense response, increasing their expression in the presence of fungal elicitors (Görlach *et al.*, 1995). The repression of key genes related directly to plant defense such as *pal* or, *dahps* and *sk* when the development of *P. xanthii* increases, suggests that they are manipulated by the fungus as a strategy to favour infection development. Our RNA-seq data suggest that the phenylpropanoid synthesis is not totally blocked but is affected enough to avoid the accumulation of compounds necessary for plant defense, such as lignin or phytoalexins, resulting in a compatible interaction as described in other pathosystems (Xu *et al.*, 2011; Weng *et al.*, 2014). Similarly, secondary metabolism-related genes have been found to be commonly repressed in other plant-powdery mildew compatible interactions (Borges *et al.*, 2013; Jambagi and Dunwell, 2015; Fu *et al.*, 2016).

BGF experiments were conducted to validate the RNA-seq results on secondary metabolism. The accumulation of plant defence compounds is frequently found in diseased plants. This accumulation of host secondary metabolites could be measured as an increase in F440 and F550 in bacterial, viral and fungal infections (Barón *et al.*, 2016b). However, in *P. xanthii* infection, the F440 and F550 parameters did not display significant differences between uninfected and infected melon leaves, pointing to no changes in the accumulation of secondary metabolites in response to *P. xanthii*. This result is

in accordance with a previous study on the barley powdery mildew *Blumeria graminis* in susceptible barley plants (Swarbrick *et al.*, 2006). Furthermore, *P. xanthii* infection in zucchini plants was related to an increase of blue-green fluorescence from the leaves (Pineda *et al.*, 2017). However, in that case, the fluorescence was shown to be emitted by components of the fungal cell walls and not by plant secondary metabolites.

But what is the situation in cucurbit cultivars resistant to *P. xanthii*? Two transcriptomic studies carried out with pumpkin and melon lines resistant to *P. xanthii* showed that different genes of photosynthesis and secondary metabolism were differentially expressed (Guo *et al.*, 2018; Zhu *et al.*, 2018). Thus, most of photosynthesis related genes such as *psb27*, *psbP*, *psaK*, *psaE*, *psaH*, *psaG* or *psaN* were up-regulated in the pumpkin inbred resistant line “112-2” (Guo *et al.*, 2018), whereas in the melon resistant cultivar MR-1, carbon fixation related genes were up-regulated at the early stages of the interaction, but they were down-regulated at 72 hpi (Zhu *et al.*, 2018). However, in the melon susceptible cultivar “Rochet” examined in this work, other photosynthesis related genes were either down-regulated such as *ohp1* or up-regulated such as *lhcb6*, *petE* and *pgr5*. In addition, the carbon fixation related genes were up-regulated at all time points analyzed. With respect to the secondary metabolism related genes, in the pumpkin resistant line *4cl3* or *adt6* were up-regulated<sup>23</sup>. Aligned to this, in the melon resistant cultivar most of the pathogen-induced DEGs were enriched in pathways related to flavonoids, phytoalexins and phenylpropanoid biosynthesis, such as, for example, the *pal* genes that increased their expression after exposure to the pathogen (Zhu *et al.*, 2018). In contrast, in the melon susceptible cultivar, most of the secondary metabolism genes were down-regulated, including the *pal* genes. In other words, the genes of photosynthesis and secondary metabolism of susceptible

and resistant plants are expressed differentially and in opposite ways in response to the attack of *P. xanthii*.

Our RNA-seq and fluorescence imaging results suggest that during the first stages of infection, *P. xanthii* manipulates plant gene expression. Because of the plant-pathogen interaction, melon leaf physiology and especially photosynthesis and secondary metabolism were altered. Host manipulation is believed to be carried out by the panel of effectors secreted by the pathogen (Lo Presti *et al.*, 2015). During host colonization, *P. xanthii* secretes an important number of proteins, most of which have an unknown function (Vela-Corcía *et al.*, 2016; Martínez-Cruz *et al.*, 2018a). We believe that some of these proteins could be responsible for reprogramming the melon physiology to allow disease establishment. The catalogues of *P. xanthii* effector candidates, both epiphytic (Vela-Corcía *et al.*, 2016) and haustorial (Polonio *et al.*, unpublished results), are known. To identify *P. xanthii* effectors that specifically target photosynthesis or secondary metabolism, different approaches such as yeast two-hybrid screening (Schmidt *et al.*, 2014; Weßling *et al.*, 2014; Alkan *et al.*, 2015; Pennington *et al.*, 2016) or dual RNA-seq analysis (Alkan *et al.*, 2015; Meyer *et al.*, 2016) can be undertaken. Currently, we are resolving the melon-*P. xanthii* interactions through a dual RNA-seq approach.

---

## SUPPLEMENTAL DATA

**Table S2.1:** Gene Ontology (GO) terms related to biological processes for *P. xanthii* -infected melon leaves at 24, 46 and 72 hpi, performed by the functional enrichment analysis of all the DEGs in web-based GENECODIS software.

Available to download:

- [https://static-content.springer.com/esm/art%3A10.1038%2Fs41598-019-44443-5/MediaObjects/41598\\_2019\\_44443\\_MOESM2\\_ESM.xlsx](https://static-content.springer.com/esm/art%3A10.1038%2Fs41598-019-44443-5/MediaObjects/41598_2019_44443_MOESM2_ESM.xlsx)

**Table S2.2:** Differentially expressed genes (DEGs) related to primary and secondary metabolism from infected melon plants compared to uninfected controls at 24 and 72 hpi.

Available to download:

- [https://static-content.springer.com/esm/art%3A10.1038%2Fs41598-019-44443-5/MediaObjects/41598\\_2019\\_44443\\_MOESM3\\_ESM.xlsx](https://static-content.springer.com/esm/art%3A10.1038%2Fs41598-019-44443-5/MediaObjects/41598_2019_44443_MOESM3_ESM.xlsx)

## REFERENCES

**Alkan N, Friedlander G, Ment D, Prusky D, Fluhr R.** 2015. Simultaneous transcriptome analysis of *Colletotrichum gloeosporioides* and tomato fruit pathosystem reveals novel fungal pathogenicity and fruit defense strategies. *New Phytologist* **205**, 801–815.

**Álvarez B, Torés a.** 1997. Cultivo in vitro de *Sphaerotheca fuliginea* (Schlecht. ex Fr.), efecto de diferentes fuentes de carbono sobre su desarrollo. *Boletín de sanidad vegetal. Plagas* **23**, 283–288.

**Ando K, Carr KM, Grumet R.** 2012. Transcriptome analyses of early cucumber fruit growth identifies distinct gene modules associated with phases of development. *BMC Genomics* **13**, 518–534.

**Baker NR.** 2008. Chlorophyll Fluorescence: A Probe of Photosynthesis In Vivo. *Annual Review of Plant Biology* **59**, 89–113.

**Barón M, Pineda M, Pérez-Bueno ML.** 2016a. Picturing pathogen infection in plants. *Zeitschrift fur Naturforschung C* **71**, 355–368.

**Barón M, Pineda M, Pérez-Bueno ML.** 2016b. Picturing pathogen infection in plants. *Zeitschrift fur Naturforschung - Section C Journal of Biosciences* **71**, 355–368.

**Beck J, Lohscheider JN, Albert S, Andersson U, Mendgen KW, Rojas-Stütz MC, Adamska I, Funck D.** 2017. Small One-Helix Proteins Are Essential for Photosynthesis in Arabidopsis. *Frontiers in Plant Science* **8**, 1–14.

**Bellón-Gómez D, Vela-Corcía D, Pérez-García A, Torés JA.** 2015. Sensitivity of *Podosphaera xanthii* populations to anti-powdery-mildew fungicides in Spain. *Pest Management Science* **71**, 1407–1413.

**Berdugo CA, Zito R, Paulus S, Mahlein AK.** 2014. Fusion of sensor data

for the detection and differentiation of plant diseases in cucumber. *Plant Pathology* **63**, 1344–1356.

**Blanca JM, Cañizares J, Ziarsolo P, Esteras C, Mir G, Nuez F, Garcia-mas J, Picó MB.** 2011. Melon Transcriptome Characterization: Simple Sequence Repeats and Single Nucleotide Polymorphisms Discovery for High Throughput Genotyping across the Species. *The Plant Genome*, 118–131.

**Blanca J, Esteras C, Ziarsolo P, et al.** 2012. Transcriptome sequencing for SNP discovery across *Cucumis melo*. *BMC Genomics* **13**, 280.

**Bolton MD.** 2009. Primary Metabolism and Plant Defense—Fuel for the Fire. *Molecular Plant-Microbe Interactions* **22**, 487–497.

**Borges AF, Ferreira RB, Monteiro S.** 2013. Transcriptomic changes following the compatible interaction *Vitis vinifera*-*Erysiphe necator*. Paving the way towards an enantioselective role in plant defence modulation. *Plant Physiology and Biochemistry* **68**, 71–80.

**Buschmann C, Lichtenthaler HK.** 1998. Principles and characteristics of multi-colour fluorescence imaging of plants. *Journal of Plant Physiology* **152**, 297–314.

**Carmona-saez P, Chagoyen M, Tirado F.** 2007. GENECODIS: a web-based tool for finding significant concurrent annotations in gene lists. *Genome Biology* **8**, 1–8.

**Cerovic ZG, Samson G, Morales F, Tremblay N, Moya I.** 1999. Ultraviolet-induced fluorescence for plant monitoring: present state and prospects. *Agronomie* **19**, 543–578.

**Cochrane FC, Davin LB, Lewis NG.** 2004. The *Arabidopsis* phenylalanine ammonia lyase gene family: Kinetic characterization of the four PAL isoforms. *Phytochemistry* **65**, 1557–1564.

**de Bianchi S, Ballottari M, Dall’Osto L, Bassi R.** 2010. Regulation of



plant light harvesting by thermal dissipation of excess energy. *Biochemical Society Transactions* **38**, 651–660.

**Dixon RA, Achnine L, Kota P, Liu CJ, Reddy MSS, Wang L.** 2002. The phenylpropanoid pathway and plant defence - A genomics perspective. *Molecular Plant Pathology* **3**, 371–390.

**Falgueras J, Lara AJ, Fernández-pozo N, Cantón FR, Pérez-trabado G, Claros MG.** 2010. SeqTrim : a high-throughput pipeline for pre-processing any type of sequence read. *BMC Bioinformatics* **11**, 1–12.

**Fernández-Ortuño D, Pérez-García A, López-Ruiz F, Romero D, De Vicente A, Torés JA.** 2006. Occurrence and distribution of resistance to QoI fungicides in populations of *Podosphaera fusca* in south central Spain. *European Journal of Plant Pathology* **115**, 215–222.

**Fu Y, Zhang H, Mandal SN, Wang C, Chen C, Ji W.** 2016. Quantitative proteomics reveals the central changes of wheat in response to powdery mildew. *Journal of Proteomics* **130**, 108–119.

**Fung RWM, Gonzalo M, Fekete C, Kovacs LG, He Y, Marsh E, McIntyre LM, Schachtman DP, Qiu W.** 2007. Powdery Mildew Induces Defense-Oriented Reprogramming of the Transcriptome in a Susceptible But Not in a Resistant Grapevine. *Plant Physiology* **146**, 236–249.

**Gao Y, Xu H, Shen Y, Wang J.** 2013. Transcriptomic analysis of rice (*Oryza sativa*) endosperm using the RNA-Seq technique. *Plant Molecular Biology* **81**, 363–378.

**Garcia-Mas J, Benjak A, Sanseverino W, et al.** 2012. The genome of melon (*Cucumis melo* L.). *Proceedings of the National Academy of Sciences* **109**, 11872–11877.

**Görlach J, Raesecke HR, Rentsch D, Regenass M, Roy P, Zala M, Keel C, Boller T, Amrhein N, Schmid J.** 1995. Temporally distinct accumulation

of transcripts encoding enzymes of the prechorismate pathway in elicitor-treated, cultured tomato cells. *Proceedings of the National Academy of Sciences of the United States of America* **92**, 3166–3170.

**Guo W, Chen B, Chen X, Guo Y, Yang H, Li X, Wang G.** 2018. Transcriptome profiling of pumpkin (*Cucurbita moschata* Duch.) leaves infected with powdery mildew. *PLoS ONE*, 1–18.

**Guo S, Liu J, Zheng Y, et al.** 2011. Characterization of transcriptome dynamics during watermelon fruit development: Sequencing, assembly, annotation and gene expression profiles. *BMC Genomics* **12**, 454.

**Herrmann KM, Weaver LM.** 1999. the Shikimate Pathway. *Annual Review of Plant Physiology and Plant Molecular Biology* **50**, 473–503.

**'t Hoen PAC, Ariyurek Y, Thygesen HH, Vreugdenhil E, Vossen RHAM, de Menezes RX, Boer JM, van Ommen GJB, den Dunnen JT.** 2008. Deep sequencing-based expression analysis shows major advances in robustness, resolution and inter-lab portability over five microarray platforms. *Nucleic Acids Research* **36**.

**Huang S, Li R, Zhang Z, et al.** 2009. The genome of the cucumber, *Cucumis sativus* L. *Nature Genetics* **41**, 1275–1281.

**Jambagi S, Dunwell JM.** 2015. Global transcriptome analysis and identification of differentially expressed genes after infection of *Fragaria vesca* with powdery mildew (*Podosphaera aphanis*). *Transcriptomics: Open Access* **03**, 1–10.

**Koressaar T, Remm M.** 2007. Enhancements and modifications of primer design program Primer3. *Bioinformatics* **23**, 1289–1291.

**Langmead B, Salzberg SL.** 2013. Fast gapped-read alignment with Bowtie 2. *Nat Methods* **9**, 357–359.

**Li H, Handsaker B, Wysoker A, et al.** 2009. The Sequence Alignment /

Map format and SAMtools. *Bioinformatics Applications note* **25**, 2078–2079.

**Li Y, Kim JI, Pysh L, Chapple C.** 2015. Four isoforms of *Arabidopsis thaliana* 4-coumarate: CoA ligase (4CL) have overlapping yet distinct roles in phenylpropanoid metabolism. *Plant Physiology* **169**, pp.00838.2015.

**Lichtenthaler HK, Buschmann C.** 2001. Chlorophylls and carotenoids: measurement and characterization by UV–vis spectroscopy. *Protein Food Anal. Chem.*, 431–438.

**Love MI, Huber W, Anders S.** 2014. Moderated estimation of fold change and dispersion for RNA-seq data with DESeq2. *Genome Biology* **15**, 550.

**Maeda H, Shasany AK, Schnepf J, Orlova I, Taguchi G, Cooper BR, Rhodes D, Pichersky E, Dudareva N.** 2010. RNAi Suppression of argenatase1 reveals that phenylalanine is synthesized predominantly via the argenatase pathway in *Petunia petals*. *The Plant Cell* **22**, 832–849.

**Maeda H, Yoo H, Dudareva N.** 2011. Prephenate aminotransferase directs plant phenylalanine biosynthesis via argenatase. *Nature Chemical Biology* **7**, 19–21.

**Mahlein A-K.** 2016. Present and future trends in plant disease detection. *Plant Disease* **100**, 1–11.

**Marguerat S, Bähler J.** 2010. RNA-seq: From technology to biology. *Cellular and Molecular Life Sciences* **67**, 569–579.

**Martínez-Cruz J, Romero D, Dávila JC, Pérez-García A.** 2014. The *Podosphaera xanthii* haustorium, the fungal Trojan horse of cucurbit-powdery mildew interactions. *Fungal genetics and biology* **71**, 21–31.

**Martínez-Cruz J, Romero D, de la Torre FN, Fernández-Ortuño D, Torés JA, de Vicente A, Pérez-García A.** 2018a. The functional characterization of *Podosphaera xanthii* candidate effector genes reveals novel target functions for fungal pathogenicity. *Molecular Plant-Microbe Interactions*

31, 914-931.

**Martínez-Cruz J, Romero D, de Vicente A, Pérez-García A.** 2017. Transformation of the cucurbit powdery mildew pathogen *Podosphaera xanthii* by *Agrobacterium tumefaciens*. *New Phytologist* **213**, 1961–1973.

**Martínez-Cruz J, Romero D, De Vicente A, Pérez-García A.** 2018*b*. Transformation by growth onto agro-infiltrated tissues (TGAT), a simple and efficient alternative for transient transformation of the cucurbit powdery mildew pathogen *Podosphaera xanthii*. *Molecular Plant Pathology* **19**, 2502–2515.

**Mauch-Mani B.** 1996. Production of salicylic acid precursors is a major function of phenylalanine ammonia-lyase in the resistance of *Arabidopsis* to *Peronospora parasitica*. *the Plant Cell* **8**, 203–212.

**Maxwell K, Johnson GN.** 2000. Chlorophyll fluorescence - a practical guide. *Journal of Experimental Botany* **51**, 659–668.

**McCue KF, Conn EE.** 1989. Induction of 3-deoxy-D-arabino-heptulosonate-7-phosphate synthase activity by fungal elicitor in cultures of *Petroselinum crispum*. *Proceedings of the National Academy of Sciences* **86**, 7374–7377.

**Meyer FE, Shuey LS, Naidoo S, Mamni T, Berger DK, Myburg AA, van den Berg N, Naidoo S.** 2016. Dual RNA-Sequencing of *Eucalyptus nitens* during *Phytophthora cinnamomi* challenge reveals pathogen and host factors influencing compatibility. *Frontiers in Plant Science* **7**, 1–15.

**Miyake C.** 2010. Alternative electron flows (water-water cycle and cyclic electron flow around PSI) in photosynthesis: Molecular mechanisms and physiological functions. *Plant and Cell Physiology* **51**, 1951–1963.

**Montero-Pau J, Blanca J, Bombarely A, et al.** 2017. *De novo* assembly of the zucchini genome reveals a whole-genome duplication associated with the origin of the *Cucurbita* genus. *Plant Biotechnology Journal* **16**, 1161–1171.

**Munekage Y, Hashimoto M, Miyake C, Tomizawa KI, Endo T, Tasaka M, Shikanai T.** 2004. Cyclic electron flow around photosystem I is essential for photosynthesis. *Nature* **429**, 579–582.

**Munekage Y, Hojo M, Meurer J, Endo T, Tasaka M, Shikanai T.** 2002. PGR5 is involved in cyclic electron flow around photosystem I and is essential for photoprotection in *Arabidopsis*. *Cell* **110**, 361–371.

**Murchie EH, Lawson T.** 2013. Chlorophyll fluorescence analysis: A guide to good practice and understanding some new applications. *Journal of Experimental Botany* **64**, 3983–3998.

**Nogales-Cadenas R, Carmona-Saez P, Vazquez M, Vicente C, Yang X, Tirado F, Carazo JM, Pascual-Montano A.** 2009. GeneCodis: Interpreting gene lists through enrichment analysis and integration of diverse biological information. *Nucleic Acids Research* **37**, 317–322.

**Ohl S, Hedrick SA, Chory J, Lamb CJ.** 1990. Functional properties of a phenylalanine ammonia-lyase promoter. *The Plant Cell* **2**, 837–848.

**Olsen KM, Lea US, Slimestad R, Verheul M, Lillo C.** 2008. Differential expression of four *Arabidopsis* PAL genes; PAL1 and PAL2 have functional specialization in abiotic environmental-triggered flavonoid synthesis. *Journal of Plant Physiology* **165**, 1491–1499.

**Passarini F, Wientjes E, Hienerwadel R, Croce R.** 2009. Molecular basis of light harvesting and photoprotection in CP24. *The Journal of Biological Chemistry* **284**, 29536–29546.

**Pennington HG, Gheorghe DM, Damerum A, Pliego C, Spanu PD, Cramer R, Bindschedler L V.** 2016. Interactions between the powdery mildew effector BEC1054 and barley proteins identify candidate host targets. *Journal of Proteome Research* **15**, 826–839.

**Pérez-Bueno ML, Johnson MP, Zia A, Ruban A V., Horton P.** 2008. The

Lhcb protein and xanthophyll composition of the light harvesting antenna controls the  $\Delta$ pH-dependency of non-photochemical quenching in *Arabidopsis thaliana*. FEBS Letters **582**, 1477–1482.

**Pérez-Bueno ML, Pineda M, Díaz-Casado E, Barón M.** 2015. Spatial and temporal dynamics of primary and secondary metabolism in *Phaseolus vulgaris* challenged by *Pseudomonas syringae*. Physiologia plantarum **153**, 161–174.

**Pérez-García A, Romero D, Fernández-Ortuño D, López-Ruiz F, De Vicente A, Torés JA.** 2009. The powdery mildew fungus *Podosphaera fusca* (synonym *Podosphaera xanthii*), a constant threat to cucurbits. Molecular plant pathology **10**, 153–160.

**Pineda M, Pérez-bueno ML, Paredes V, Barón M.** 2017. Use of multicolour fluorescence imaging for diagnosis of bacterial and fungal infection on zucchini by implementing machine learning. Functional Plant Biology.

**Pineda M, Soukupová J, Matouš K, Nedbal L, Barón M.** 2008. Conventional and combinatorial chlorophyll fluorescence imaging of tobamovirus-infected plants. Photosynthetica **46**, 441–451.

**del Pino D, Olalla L, Pérez-García A, Rivera ME, García S, Moreno R, de Vicente A, Torés JA.** 2002. Occurrence of races and pathotypes of cucurbit powdery mildew in southeastern Spain. Phytoparasitica **30**, 459–466.

**Lo Presti L, Lanver D, Schweizer G, Tanaka S, Liang L, Tollot M, Zuccaro A, Reissmann S, Kahmann R.** 2015. Fungal effectors and plant susceptibility. Annual Review of Plant Biology **66**, 513–545.

**Raes J.** 2003. Genome-wide characterization of the lignification toolbox in *Arabidopsis*. Plant Physiology **133**, 1051–1071.

**Repka V.** 2002. Chlorophyll-deficient mutant in oak (*Quercus petraea* L.) displays an accelerated hypersensitive-like cell death and an enhanced resistance to powdery mildew disease **40**, 183–193.

**Rezzonico F, Rupp O, Fahrenttrapp J.** 2017. Pathogen recognition in compatible plant-microbe interactions. *Scientific Reports* **7**, 1–12.

**Rohde A, Morreel K, Ralph J, et al.** 2004. Molecular phenotyping of the *pal1* and *pal2* mutants of *Arabidopsis thaliana* reveals far-reaching consequences on phenylpropanoid, amino acid, and carbohydrate metabolism. *the Plant Cell* **16**, 2749–2771.

**Rolfe SA, Scholes JD.** 2010. Chlorophyll fluorescence imaging of plant-pathogen interactions. *Protoplasma* **247**, 163–175.

**Rookes JE, Cahill DM.** 2003. A PAL1 gene promoter – green fluorescent protein reporter system to analyse defence responses in live cells of *Arabidopsis thaliana*. *European Journal of Plant Pathology* **109**, 83–94.

**Rumeau D, Peltier G, Cournac L.** 2007. Chlororespiration and cyclic electron flow around PSI during photosynthesis and plant stress response. *Plant, Cell and Environment* **30**, 1041–1051.

**Sacharz J, Giovagnetti V, Ungerer P, Mastroianni G, Ruban A V.** 2017. The xanthophyll cycle affects reversible interactions between PsbS and light-harvesting complex II to control non-photochemical quenching. *Nature Plants* **3**.

**Schmidt SM, Kuhn H, Micali C, Liller C, Kwaaitaal M, Panstruga R.** 2014. Interaction of a *Blumeria graminis* f. sp. *hordei* effector candidate with a barley ARF-GAP suggests that host vesicle trafficking is a fungal pathogenicity target. *Molecular Plant Pathology* **15**, 535–549.

**Seoane P, Ocaña S, Carmona R, Bautista R, Madrid E, M. Torres A, Gonzalo Claros M.** 2016. AutoFlow, a versatile workflow engine illustrated by assembling an optimised *de novo* transcriptome for a non-model species, such as faba bean (*Vicia faba*). *Current Bioinformatics* **11**, 440–450.

**Sitterly W.P.** 1978. Powdery mildew of cucurbits. In: Spencer DM, ed.

Powdery mildews. London, UK: Academic Press, 359-379.

**Spanu PD.** 2006. Why do some fungi give up their freedom and become obligate dependants on their host? *New Phytologist* **171**, 447–450.

**Swarbrick PJ, Schulze-Lefert P, Scholes JD.** 2006. Metabolic consequences of susceptibility and resistance (race-specific and broad-spectrum) in barley leaves challenged with powdery mildew. *Plant, Cell and Environment* **29**, 1061–1076.

**Tabas-Madrid D, Nogales-Cadenas R, Pascual-Montano A.** 2012. GeneCodis3: A non-redundant and modular enrichment analysis tool for functional genomics. *Nucleic Acids Research* **40**, 478–483.

**Thimm O, Bläsing O, Gibon Y, Nagel A, Meyer S, Krüger P, Selbig J, Müller LA, Rhee SY, Stitt M.** 2004. MAPMAN: A user-driven tool to display genomics data sets onto diagrams of metabolic pathways and other biological processes. *Plant Journal* **37**, 914–939.

**Tzin V, Galili G.** 2010. The biosynthetic pathways for shikimate and aromatic amino acids in *Arabidopsis thaliana*. *The Arabidopsis book* **8**, 1–18.

**Vela-Corcía D, Bautista R, De Vicente A, Spanu PD, Pérez-García A.** 2016. De novo analysis of the epiphytic transcriptome of the cucurbit powdery mildew fungus *Podosphaera xanthii* and identification of candidate secreted effector proteins. *PLoS ONE* **11**, e0163379.

**Weng K, Li ZQ, Liu RQ, Wang L, Wang YJ, Xu Y.** 2014. Transcriptome of *Erysiphe necator*-infected vitis pseudoreticulata leaves provides insight into grapevine resistance to powdery mildew. *Horticulture Research* **1**, 1–12.

**Weßling R, Epple P, Altmann S, et al.** 2014. Convergent targeting of a common host protein-network by pathogen effectors from three kingdoms of life. *Cell Host Microbe* **16**, 364–375.

**Westermann AJ, Gorski SA, Vogel J.** 2012. Dual RNA-seq of pathogen



and host. *Nature Reviews Microbiology* **10**, 618–630.

**Wu T, Cao J.** 2010. Molecular cloning and expression of a bush related *CmVI* gene in tropical pumpkin. *Molecular Biology Reports* **37**, 649–652.

**Xin M, Wang X, Peng H, Yao Y, Xie C, Han Y, Ni Z, Sun Q.** 2012. Transcriptome comparison of susceptible and resistant wheat in response to powdery mildew infection. *Genomics, Proteomics and Bioinformatics* **10**, 94–106.

**Xu Y, Wang J, Guo S, et al.** 2013. The draft genome of watermelon (*Citrullus lanatus*) and resequencing of 20 diverse accessions. *Nature Genetics* **45**, 51–58.

**Xu L, Zhu L, Tu L, Liu L, Yuan D, Jin L, Long L, Zhang X.** 2011. Lignin metabolism has a central role in the resistance of cotton to the wilt fungus *Verticillium dahliae* as revealed by RNA-Seq-dependent transcriptional analysis and histochemistry. *Journal of Experimental Botany* **62**, 5607–5621.

**Yang F, Mitra P, Zhang L, et al.** 2013. Engineering secondary cell wall deposition in plants. *Plant Biotechnology Journal* **11**, 325–335.

**Zhang N, Fan Y, Li C, Wang Q, Leksawasdi N, Li F, Wang S.** 2018. Cell permeability and nuclear DNA staining by propidium iodide in basidiomycetous yeasts. *Applied Microbiology and Biotechnology* **102**, 4183–4191.

**Zhang H, Yang Y, Wang C, Liu M, Li H, Fu Y, Wang Y, Nie Y, Liu X, Ji W.** 2014. Large-scale transcriptome comparison reveals distinct gene activations in wheat responding to stripe rust and powdery mildew. *BMC genomics* **15**, 898.

**Zhu Q, Gao P, Wan Y, Cui H, Fan C, Liu S, Luan F.** 2018. Comparative transcriptome profiling of genes and pathways related to resistance against powdery mildew in two contrasting melon genotypes. *Scientia Horticulturae* **227**, 169–180.

## CHAPTER III

# **The haustorial transcriptome of the cucurbit pathogen *Podosphaera xanthii* reveals new insights into the biotrophy and pathogenesis of powdery mildew fungi**

Álvaro Polonio, Pedro Seoane, M. Gonzalo Claros & Alejandro Pérez-García

*BMC genomics* (2019), 20:543



## ABSTRACT

*Podosphaera xanthii* is the main causal agent of powdery mildew disease in cucurbits and is responsible for important yield losses in these crops worldwide. Powdery mildew fungi are obligate biotrophs. In these parasites, biotrophy is determined by the presence of haustoria, which are specialized structures of parasitism developed by these fungi for the acquisition of nutrients and the delivery of effectors. Detailed molecular studies of powdery mildew haustoria are scarce due mainly to difficulties in their isolation. Therefore, their analysis is considered an important challenge for powdery mildew research. The aim of this work was to gain insights into powdery mildew biology by analysing the haustorial transcriptome of *P. xanthii*. Prior to RNA isolation and massive-scale sequencing, flow cytometry was used to isolate *P. xanthii* haustoria free of visible contaminants. The approach used to cDNA library construction, the Illumina NextSeq sequencing and the assembly of the *de novo* haustorial transcriptome, allowed us to obtain the maximum amount of information from the low-quality RNA. The subsequent comparison with the epiphytic transcriptome revealed the importance of several biological processes for haustoria such as protection against reactive oxygen species, the acquisition of different nutrients and genetic regulation mediated by ncRNAs. In addition, we could also identify several secreted proteins expressed exclusively in haustorial cells such as cell adhesion proteins that have not been related to powdery mildew biology to date. This work provides a novel approach to study the molecular aspects of powdery mildew haustoria, allowing us to identify certain previously unknown processes and proteins involved in the biology of powdery mildews that could be essential for their biotrophy and pathogenesis.



## INTRODUCTION

*Podosphaera xanthii* is a plant-pathogenic ascomycete fungus of the *Erysiphales* order that causes powdery mildew disease in cucurbits and significantly reduces the yields of cucurbit crops (del Pino *et al.*, 2002; Fernández-Ortuño *et al.*, 2006; Pérez-García *et al.*, 2009; Bellón-Gómez *et al.*, 2015). As with other powdery mildew fungi, *P. xanthii* is an obligate biotrophic parasite that depends on living host cells for growth and reproduction. In these fungi, biotrophy is determined by the development of specialized structures of parasitism termed haustoria (Martínez-Cruz *et al.*, 2014), whose main putative functions are the uptake of nutrients from the plant and the release of effectors into the host cells (Martínez-Cruz *et al.*, 2018), that thus play a pivotal role in both biotrophy and pathogenesis (Oliva *et al.*, 2010). Since this fungal structure is the battlefield between the pathogen and the plant, the identification of physiological processes carried out by proteins expressed in the haustorium should provide key information to understand the singularities of powdery mildew fungi as well as to offer opportunities for the development of novel management tools.

Detailed molecular investigations of biotrophic fungal pathogens such as powdery mildews are not very abundant, mainly due to limitations in their growth (exclusively in host tissues) and difficulties with their genetic manipulation (Bindschedler *et al.*, 2016). Therefore, the study of powdery mildews is considered a challenge, and many aspects of their biotrophic lifestyle and pathogenesis are not yet resolved. However, next-generation sequencing technologies combined with different computational approaches have allowed us to obtain several powdery mildew genomes corresponding to different

isolates of *Blumeria graminis* f. sp. *hordei*, *B. graminis* f. sp. *tritici*, *Erysiphe necator*, *Golovinomyces orontii* and *Oidium neolycopersici*, which are the causal agents of barley powdery mildew, wheat powdery mildew, grape powdery mildew, *Arabidopsis* powdery mildew and tomato powdery mildew, respectively (Baxter *et al.*, 2010; Spanu *et al.*, 2010; Duplessis *et al.*, 2011; Hacquard *et al.*, 2013; Wicker *et al.*, 2013; Jones *et al.*, 2014; Frantzeskakis *et al.*, 2018; Wu *et al.*, 2018; Müller *et al.*, 2019). The availability of several powdery mildew genomes has allowed us to obtain new insights into the pathogenesis, such as genome size expansion with the proliferation of transposable elements and effector candidate genes (Spanu *et al.*, 2010; Wicker *et al.*, 2013), and the biotrophic lifestyle, such as the identification of missing genes and metabolic pathways, that could explain the impossibility of cultivating these fungi in artificial culture media (Baxter *et al.*, 2010; Spanu *et al.*, 2010; Duplessis *et al.*, 2011; Kemen *et al.*, 2011). The different genome assemblies have also allowed us to predict the number of effector candidate genes in the genome of powdery mildew fungi (Spanu *et al.*, 2010; Pedersen *et al.*, 2012; Wu *et al.*, 2018). Nevertheless, the prediction of effector gene catalogues from a fungal genome is error-prone and unreliable (Hacquard *et al.*, 2012), making the use of different complementary strategies necessary.

Transcriptomic analyses provide important information about those genes that are expressed during powdery mildew infection and fungal development. Moreover, these analyses allow for more accurate prediction of effector candidate genes, since short genes, often with no homology, are hard to find in genomes. Despite the fact that transcriptomes from several powdery mildew species are available (Both *et al.*, 2005*b,a*; Godfrey *et al.*, 2010; Weßling *et al.*, 2012; Hacquard *et al.*, 2013; Vela-Corcía *et al.*, 2016), specific studies on haustorial transcriptomes, which are necessary to decipher the molecular bases

of biotrophy and pathogenesis in powdery mildew species, are very limited probably due to difficulties in obtaining high-quality isolations of haustoria free of contaminants. To date, only two powdery mildew haustorial transcriptomic studies have been performed, the first from haustorial enriched barley epidermal strips (Godfrey *et al.*, 2010) and the second from haustorial fractions obtained from isopycnic Percoll centrifugation (Weßling *et al.*, 2012).

In the particular case of the cucurbit powdery mildew pathogen *P. xanthii*, the analysis of the epiphytic transcriptome (Vela-Corcía *et al.*, 2016) and the development of tools for functional gene analysis (Martínez-Cruz *et al.*, 2017, 2018), have allowed us to identify novel functions of several effector candidates and validate their role in pathogenesis (Martínez-Cruz *et al.*, 2018). Despite such advances, however, our knowledge about the biotrophic lifestyle and pathogenesis of *P. xanthii* remains incomplete because specific information about gene expression in haustoria is virtually unknown. In this study, we developed a method to isolate *P. xanthii* haustoria virtually free of debris and performed the *de novo* assembly of the *P. xanthii* haustorial transcriptome and a comparative analysis of haustorial and epiphytic transcriptomes. These analyses have allowed us to detect specific and important haustorial functions and to identify a new set of effector candidate genes specifically expressed in haustoria. Our findings provide novel information about the biotrophic lifestyle and pathogenesis of *P. xanthii* and identify previously unknown aspects of powdery mildew biology.



## MATERIAL AND METHODS

### *Fungal and plant material*

The *Podosphaera xanthii* isolate 2086 was routinely cultured on previously disinfected zucchini (*Cucurbita pepo* L.) cotyledons cv. Negro Belleza (Semillas Fitó, Barcelona, Spain) and maintained *in vitro* in Bertrand medium in 8 cm Petri dishes under a 16 h light/8 h dark cycle at 22 °C for one week. The fungal isolate deposited in our laboratory collection, was stored at -80 °C until use (Pérez-García *et al.*, 2006).

### *Isolation of P. xanthii haustorial cells*

The haustorial cells were isolated from zucchini cotyledons 10 days after inoculation with *P. xanthii* as previously described (Martínez-Cruz *et al.*, 2014) with minor modifications: after homogenization, a 40 µm nylon mesh was used. The resulting homogenate was treated with 0.025 mg/mL wheat germ agglutinin (WGA)-Alexa Fluor 488 conjugate (Thermo Fisher Scientific, Waltham, MA, USA) in PBS to label the haustorial cell walls. Fluorescence-activated cell sorting was used to separate the haustoria from other fungal structures, plant organelles and debris. For this, a Beckman Coulter MoFlo flow cytometer (Beckman Coulter, Brea, CA, USA) was employed. Cells were sorted at a rate of approximately 5000 events per sec and 25 psi of pressure. The homogenate was agitated during sorting to avoid cell aggregation. Forward scatter and green fluorescence parameters of the particles in the homogenate were used upon excitation with a laser emitting 125 mW at 48 nm to separate the haustorial cells. Green fluorescence and a dot plot of green fluorescence vs forward scatter were used to adjust electronic gating to select those particles with high green

fluorescence and forward scatter properties that corresponded to a size between 15  $\mu\text{m}$  – 20  $\mu\text{m}$ , which is equivalent to the size of the *P. xanthii* haustorium (Martínez-Cruz *et al.*, 2014). Preliminary assays to optimize threshold settings for the forward scatter were necessary. The initial homogenate and the final elution from flow cytometry were examined by confocal laser scanning microscopy (CLSM) in a Leica SP5 II confocal microscope (Leica Microsystems, Wetzlar, Germany) to determine the correct separation of collected cells. All steps, including the flow cytometry, were performed at 4 °C to avoid RNA degradation.

#### *RNA extraction, cDNA library synthesis and sequencing*

Total RNA extraction from isolated haustoria was performed immediately after cell sorting using a PicoPure RNA isolation kit (Arcturus Bioscience, Mountain View, CA USA) according to the manufacturer's instructions. Total RNA was eluted in DEPC-treated water and stored at -80 °C until use. The quantity and quality of the total RNA was measured by an Agilent 2100 bioanalyser using an RNA Pico 6000 chip (Agilent Technologies, Santa Clara, CA, USA). cDNA and Illumina library synthesis was carried out using the Ovation Universal RNA-Seq System (NuGEN Technologies, San Carlos, CA, USA) according to the manufacturer's instructions. First strand synthesis of total RNA was carried out employing an oligo (dT) primer mix and a random primer mix. For library construction, cDNA fragmentation was performed using NEBNext dsDNA Fragmentase (New England Biolabs, Ipswich, MA, USA) for 30 min at 37 °C. The Illumina adapters were then added according to the manufacturer's instructions. The ribosomal 18S and 28S sequences of *P. xanthii* (MK225523 and MK225524, respectively) were used to design custom InDA-

C primers (Table 3.1), which were necessary to deplete ribosomal sequences from the total RNA sample using the Ovation Universal RNA-Seq System (NuGEN Technologies Inc.). The libraries were then sequenced on an Illumina NextSeq 550 instrument (Illumina, San Diego, CA, USA) using the read layout 2 x 150 nt.

**Table 3.1.** Customized InDA-C primers used to deplete ribosomal sequences from total RNA extractions during the process of cDNA library synthesis.

rRNA <sup>a</sup>	Primer name	Sequence	Position <sup>b</sup>
5.8S	1_5,8S_0	5'-GATGAAGAACGACGCGAAAT-3'	0
	2_5,8S_70	5'-TCGAATCTTTGAACGCACATT-3'	70
18S	3_18S_0	5'-GGGGCCAGTCCGAAAG-3'	0
	4_18S_70	5'-TACAAAGGGCAGGACGTAA-3'	70
	5_18S_140	5'-CAATGCTCTATCCCCAGCAC-3'	140
	6_18S_210	5'-AGAAACTCGTTGGCTCTGTCA-3'	210
	7_18S_280	5'-ATTGCCTCAAAC TTCATCG-3'	280
	8_18S_350	5'-CCTGGCTATTAGCAGGTTAAGG-3'	350
	9_18S_420	5'-AACTAAGAACGCCATGCAC-3'	420
	10_18S_490	5'-TCTGGACCTGGTGAGTTTCC-3'	490
	11_18S_560	5'-GCCCTCCGTC AATTCTTT-3'	560
	12_18S_630	5'-GTAAGGTGCCGAGCGAGTC-3'	630
	13_18S_700	5'-TGATCGTCTTCGATCCCCTA-3'	700
	14_18S_770	5'-CATCCTGGCAAATGCTTTC-3'	770
	15_18S_840	5'-CATTACGGCGGTCTAGAAA-3'	840
	16_18S_910	5'-GAGCATAGGCCTGCTTTGAA-3'	910
	17_18S_980	5'-AGTCCTGGTCCCGACAC-3'	980
	18_18S_1050	5'-AGGCCCAAGGTTCAACTACG-3'	1050
	19_18S_1120	5'-TTTAATATACGCTATTGGAGCTGGA-3'	1120
	20_18S_1190	5'-CCCTCCAATTGTTCTCGTT-3'	1190
	21_18S_1260	5'-TTGTCACTACCTCCCGTGT-3'	1260
	22_18S_1330	5'-GTTTCTCAGGCTCCCTCFC-3'	1330
23_18S_1400	5'-GGGCAGAAATTTGAATGAACC-3'	1400	
24_18S_1470	5'-GCCATGCGATTCGTTAAGTT-3'	1470	
25_18S_1540	5'-GAAGTCGGGGCTTTAGCAT-3'	1540	
26_18S_1610	5'-AATGAGCCATTCGCAGTTTC-3'	1610	
28S	27_28S_0	5'-ACCTCAGTAACGGCGAGTGA-3'	0
	28_28S_70	5'-GGCCTGGCCTAAGTTCCTT-3'	70
	29_28S_140	5'-GGACGTCGTAGAGGGTGAGA-3'	140
	30_28S_210	5'-GTCGAGTTGTTGGGAATGC-3'	210
	31_28S_280	5'-AGCGCACAAGTAGAGTGATCG-3'	280
	32_28S_350	5'-TGATCCGCTAGGGTCTCTCT-3'	350

---

33_28S_420	5'-AGAATGGCTGGTGAATGTG-3'	420
34_28S_490	5'-CGCTTCGGCTAGGATGC-3'	490
35_28S_560	5'-TGAAACACGGACCAAGGAGT-3'	560
36_28S_630	5'-TAAACCCATACGCGGAATGA-3'	630
37_28S_700	5'-GGACCCGAAAGATGGTGAAC-3'	700
38_28S_770	5'-CCAGAGGAAACTCTGGTGA-3'	770
39_28S_840	5'-CCGAAGTTCCCTCAGGATAG-3'	840
40_28S_910	5'-ATTAGAGGCCTGGGGTTGA-3'	910
41_28S_980	5'-CCTTGTTACTTAATTGAACGTGGAC-3'	980
42_28S_1050	5'-GGCCATTTTGGTAAGCAGA-3'	1050
43_28S_1120	5'-ACGCTCATCAGACACCACAA-3'	1120
44_28S_1190	5'-CCGAATGAACTAGCCCTGAA-3'	1190
45_28S_1260	5'-TACTTCACCGCCAGGGTAGA-3'	1260
46_28S_1330	5'-GTCGAACGGCCTCTAGTGC-3'	1330
47_28S_1400	5'-GAAGTGGGAAAGGTTCCAT-3'	1400
48_28S_1470	5'-CGAAAGGGAAGCCGGTTAAT-3'	1470
49_28S_1540	5'-ATTCTCCACGGCAACGTAAC-3'	1540
50_28S_1610	5'-CACCTGAAATCGGTTTGTC-3'	1610
51_28S_1680	5'-GCACCTTTGTCAGGTCTGGT-3'	1680
52_28S_1750	5'-ACTCATAACCGCAGCAGGTC-3'	1750
53_28S_1820	5'-AACTTCGGGAAAAGGATTGG-3'	1820
54_28S_1890	5'-AGGTCGCCACTAGCCTCAC-3'	1890
55_28S_1960	5'-CCGGCGTACAATTAACAACC-3'	1960
56_28S_2030	5'-GGCCAGAAAGTGGTGTGAC-3'	2030
57_28S_2100	5'-TTCTGCCAGTGCTCTGAAT-3'	2100
58_28S_2170	5'-ACGCGCATGAATGGATTAAC-3'	2170
59_28S_2240	5'-CTAGCGAAACCACAGCCAAG-3'	2240
60_28S_2310	5'-AAGACCCTGTTGAGCTTGACTCT-3'	2310
61_28S_2380	5'-TTATTCAATGAAGCGGAGCTG-3'	2380
62_28S_2450	5'-GATCCGGGTTGAAGACATTG-3'	2450
63_28S_2520	5'-GGGACTCATGGAGAACAGA-3'	2520
64_28S_2590	5'-GTCCCCTGATTTTGATTTCA-3'	2590
65_28S_2660	5'-GGTGCCAGAAAAGTTACCACA-3'	2660
66_28S_2730	5'-CGACGTTGCTTTTGGATCCT-3'	2730
67_28S_2800	5'-CGGTAAGCGTTGGATTGTTTC-3'	2800
68_28S_2870	5'-CCGCAATGGTAATTCAGCTT-3'	2870
69_28S_2940	5'-TAATTGGTTTTTGGCGTGT-3'	2940

---

<sup>a</sup> Ribosomal RNA subunit depleted.

<sup>b</sup> Primer position into rRNA molecule.

### *De novo assembly and annotation of transcriptomes*

The Illumina raw reads from haustorial RNA and 975,070 Roche 454 raw single-end reads from hyphal and conidial RNA previously published by our

laboratory (Vela-Corcía *et al.*, 2016) were used to perform the *P. xanthii* transcriptomic profile. This profile comprises the haustorial transcriptome and the revised version of the epiphytic transcriptome, produced in order to compare it with the haustorial transcriptome, generated using the TransFlow workflow as described in Appendix I (Seoane *et al.*, 2018). TransFlow is a modular framework designed for 454 Roche and Illumina reads that i) pre-processes raw reads, ii) builds several tentative transcriptomes and iii) chooses the best transcriptome. The workflow was executed using the Module 1 for Illumina data, the Module 2 for the 454 Roche data, the Module 4 for assessing the reference transcriptomes and the Module 5 for assessing the putative transcriptomes and select the best candidates. Transcriptomes of *Neurospora crassa* (SRR100067) and *Candida albicans* (SRR2005826) were downloaded from ENSEMBL release 31 and used as reference transcriptomes for evaluation in Module 4. Finally, the best epiphytic (Epi) and haustorial (Hau) transcriptomes from all assemblies produced were selected according to their comparison with the reference transcriptomes. The selected transcriptomes were full annotated with orthologues in Kingdom Fungi from UniProtKB using Full-LengtherNext (<http://www.scbi.uma.es/fulllengthernext>).

### *Characterization of the P. xanthii haustorial transcriptome*

To reveal the specific functions of the haustorium, a comparison between the epiphytic and haustorial transcriptomes was carried out using the GO terms that were associated with all unigenes from both transcriptomes. In this way, GO terms retrieved from the Full-LengtherNext annotation results were compared by Venn diagram calculation performed using Venny web-based software (<http://bioinfogp.cnb.csic.es/tools/venny/>). Only those GO terms that were

present in the haustorial transcriptome were selected. To avoid redundant terms, to decrease the complexity and to obtain a visual representation of specific haustorial GO terms, REVIGO web-based software (Supek *et al.*, 2011) with a medium (0.7) allowed similarity parameter was used. REVIGO reduction analysis tool allows to condense the GO description by removing redundant terms and to cluster the closer GO terms in a two dimensional space. In addition, the top 50 most highly expressed genes in the haustorial cDNA library of *P. xanthii* were calculated by aligning the trimmed reads with respect to all contigs obtained in the assembly process. This process was carried out using Bowtie2 (Langmead and Salzberg, 2013). GO terms related to biological processes associated with these top 50 most highly expressed genes were obtained from Full-LenghterNext annotation results and visually represented by REVIGO with a medium (0.7) allowed similarity parameter.

On the other hand, due the high number of ncRNAs that were present in the haustorial transcriptome according to Full-LenghterNext annotation, and in order to avoid the possible artefacts, the trimmed reads were also aligned against all ncRNAs and only those with 10 or more mapping reads were selected. Then, an analysis of the top 50 expressed ncRNAs was performed as described above. Those ncRNAs were annotated with the non-coding RNA sequence database RNACentral (<https://rnacentral.org/>), which includes 31 databases of ncRNA. Finally, the expression pattern of some of these ncRNAs during the first steps of infection was investigated by qRT-PCR as described below.

### *Definition of predicted secretomes and selection of specific haustorial secreted proteins*

To predict the panel of secreted proteins with signal peptide produced by the epiphytic structures and the haustoria of *P. xanthii*, two web-based software programs were used. Both epiphytic and haustorial secretomes were defined using the combination of Secretool (Cortázar *et al.*, 2014) and PECAS (Prokaryotic and Eukaryotic Classical Analysis of Secretomes) software (Cortazar *et al.*, 2015). Both Secretool and PECAS are prediction pipelines that comprise a group of web tools (SignalP, TargetP among others), allowing to predict a complete secretome in a single step from amino acid sequence files. To reproduce the parameters used to predict the epiphytic secretome previously described (Vela-Corcía *et al.*, 2016), the parameters used were the following: 0.45 SignalP cut-off probability, 0 Target P cut-off probability, 1 maximum transmembrane domain and a 17 WoLF PSORT cut-off score for Kingdom Fungi. Later, to perform a more accurate prediction of candidate secreted proteins and avoid false positives, the DeepLoc web-based software (Almagro Armenteros *et al.*, 2017) was used. DeepLoc is a novel bioinformatics tool that allows predicting the subcellular localization of proteins, even those without annotated homologues, using deep learning. In addition, to discern the secreted proteins only expressed in haustoria, the UniProtKB protein identifiers of epiphytic and haustorial candidate secreted proteins were obtained from Full-LengtherNext annotation results and compared by Venn diagram. In this way, a list containing *Podosphaera* haustorium-specific secreted proteins was obtained.

### *Protein structure modelling and protein function prediction*

To gain insight into the putative functions of the *Podosphaera* haustorial effector candidates (PHECs), the website I-TASSER (<http://zhanglab.ccmb.med.umich.edu/I-TASSER/>) (Zhang, 2008) was used to perform automated protein structure homology modelling by fold recognition searches using crystal structure of proteins with known functions available in the Protein Data Bank (PDB). To measure the quality of a predicted structure, its estimated TM (template modelling) score and C (confidence) score values were used. According to I-TASSER, TM score values higher than 0.5 indicate the correct topology, and values lower than 0.17 indicate a random similarity. A C score value in the range between -5 and 2 indicates a more confident model. The website Phyre2 (<http://www.sbg.bio.ic.ac.uk/phyre2/html/page.cgi?id=index>) (Kelly *et al.*, 2015) was used to carry out the search for analogous structures. Additional software tools used to obtain more information about the putative functions or domains of PHECs were CATH/Gene3D ([http://www.cathdb.info/search/by\\_sequence](http://www.cathdb.info/search/by_sequence)) (Lam *et al.*, 2016) and MotifScan ([https://myhits.isb-sib.ch/cgi-bin/motif\\_scan#prf:SER\\_RICH](https://myhits.isb-sib.ch/cgi-bin/motif_scan#prf:SER_RICH)) (Pagni *et al.*, 2007).

### *PCR and qRT-PCR*

To validate their exclusive or preferential expression in haustoria of genes initially classified as coding for haustorium-specific secreted proteins, a PCR analysis using cDNA obtained from epiphytic and haustorial structures was carried out as previously described (Godfrey *et al.*, 2010). For this purpose, haustorial cells were isolated from infected zucchini cotyledons at 10 days after



inoculation with *P. xanthii* and total RNA was extracted as described above. Similarly, spores and hyphae were removed carefully from infected zucchini cotyledons at 10 days after inoculation with the pathogen and total RNA was isolated using TRI Reagent (Sigma-Aldrich, Saint Louis, MO, USA) according to the manufacturer's indications. The synthesis of cDNA was performed using total RNA, random primers and Superscript III Reverse Transcriptase (Thermo Fisher Scientific, Waltham, MA, USA) according to the manufacturer's instructions. PCR was carried out using the primer pairs listed in Table S11 (Additional file 1). PCR conditions were identical to those described previously (Godfrey *et al.*, 2010).

For the quantification of the expression of ncRNAs and haustorial-specific secreted protein coding genes during the early stages of infection, qRT-PCR analysis was performed. For this analysis, zucchini cotyledons inoculated with *P. xanthii* were collected at 0, 24, 48 and 72 h post-inoculation, frozen in liquid nitrogen and ground with a mortar and pestle. Total RNA extractions were carried out using TRI Reagent (Sigma-Aldrich) and cDNA synthesis was performed as described above. SsoFast EvaGreen Supermix (Bio-Rad, Hercules, CA, USA) was used to perform the qRT-PCR reactions according to the manufacturer's instructions, in a CFX384 Touch Real-Time PCR detection system (Bio-Rad) and with the primer pairs listed in Table 3.2. The qRT-PCR conditions were as follows: enzyme activation step at 95 °C for 30 s, followed by 40 cycles of 5 s at 95 °C and 5 s at 65 °C. After amplification, the data were analysed using CFX Manager software (Bio-Rad). All primers used in PCR and qRT-PCR analyses were designed using Primer3 (Koressaar and Remm, 2007). Furthermore, a clustered heat map of expression of the genes using correlation distance and average linkage was performed using ClustVis (Metsalu and Vilo, 2015).

**Table 3.2.** Primers used in this study for RT-PCR and qRT-PCR analyses.

Unigene/ ncRNA	Primer name	Sequence	Amplicon size (bp)
689	689-F	5'-AGGACTGATGGAAGCGAAGA-3'	158
	689-R	5'-GAGCCGCGTAGAACAGTTTC-3'	
15314	15314-F	5'-TGACGATCAATCACGCTCTC-3'	158
	15314-R	5'-AGGTTCCGCAGCTTTCACCTA-3'	
15509	15509-F	5'-CTCACCGGAGCAAGCTAGAC-3'	219
	15509-R	5'-AGCGCGTCAAGAAGATGTTT-3'	
15569	15569-F	5'-CTCGGCTTCTTTGGATCAAC-3'	230
	15569-R	5'-AGTCTCTTGGTTGCGGAAGA-3'	
15584	15584-F	5'-ATGGCTCAGTGCAGACAGTG-3'	211
	15584-R	5'-CACCGGGTTAACTTCCAGA-3'	
15629	15629-F	5'-CCACTCGAGACCGTGGTAAT-3'	201
	15629-R	5'-CGATTCAGGGGAGTACAGGA-3'	
15673	15673-F	5'-GCTCCAGCGAAACTTACAGG-3'	193
	15673-R	5'-AAACCTCAACGCTCTCTCCA-3'	
15694	15694-F	5'-GTCCCGGTGAGACTGTTGAT-3'	172
	15694-R	5'-GGATCGGTGAAAGCAATGTT-3'	
27213	27213 -F	5'-AGTGTGCACCAATCCACTG-3'	154
	27213-R	5'-TCCCATAACAATTGCACCAA-3'	
217529	217529-F	5'-ATATGCTGTTGCTGCTGTCG-3'	261
	217529-R	5'-TACAGCATCCAGTCCACCAG-3'	
15544	15544-F	5'-CGAATCCACCGAGATCCTTA-3'	169
	15544-R	5'-TTTCAACCCTTTCTCGGTTG-3'	
223421	223421-F	5'-AATGTGGCTCTACGGGATTG-3'	242
	223421-F	5'-GCAGAGATACCTCGGTGGAA-3'	
nc11307	11307-F	5'-GAAGTGATTGGGCCAGTTGT-3'	243
	11307-R	5'-TCGTAAGCCCGTCTCTGTTA-3'	
nc17753	17753-F	5'-TTAAGGTGGTTGGAGGTTGG	249
	17753-R	5'-CAGGCTGAGGACTACCCATC	
nc15465	15465-F	5'-TCGAACGCACACAAAACATT	186
	15465-R	5'-ACCAGGTCGAGTTGAGAACG	
nc7919	7919-F	5'-TATCCTTCCACCGACAGGAG	185
	7919-R	5'-GAGATTGGTTCAGCCATTG-3'	
nc13870	13870-F	5'-GCATCAGAAAAGCAGGACAA-3'	164
	13870-R	5'-ACTTGCTTAGGCTGCGAAAA-3'	
nc1955	1955-F	5'-CCCAGTAGTCATTAGGAGCA-3'	197
	1955-R	5'-CCACACCACCTATTCCAA-3'	

## RESULTS

### *Flow cytometry allows the isolation of haustoria free of contaminants*

To obtain preparations of total RNA from haustorial cells of the highest quality possible, a method involving the separation of haustoria by flow cytometry was conceived. The homogenate resulting from the filtration step after the homogenization of zucchini cotyledons highly infected with *P. xanthii* was stained with wheat germ agglutinin (WGA)-Alexa Fluor 488 to label haustorial cells with a green fluorescent dye (Figure 3.1A) and transferred to the cell sorter. The R1 population corresponds to fungal structures stained with WGA-Alexa Fluor 488 (Figure 3.1B). The R2 population corresponding to haustorial cells was clearly identified and separated from larger or smaller particles with green fluorescence corresponding to *P. xanthii* conidia or hyphal debris, respectively (Figure 3.1C). Only those particles combining high green fluorescence (R1) and the size properties of forward scatter equivalent to the size of *P. xanthii* haustorium (R2) were collected (Figure 3.1D). Prior to fluorescence-activated cell sorting, only 0.02% of the particles present in the homogenate were haustoria while the rest of the homogenate corresponded mainly to chloroplasts and, to a lesser extent, to spores and hyphal debris (Figure 3.1A). After separation, it was possible to obtain highly enriched haustorial preparations with a purity of 98.9% that were virtually free of visible contaminants (Figure 3.1D). These samples were then subjected to RNA isolation.

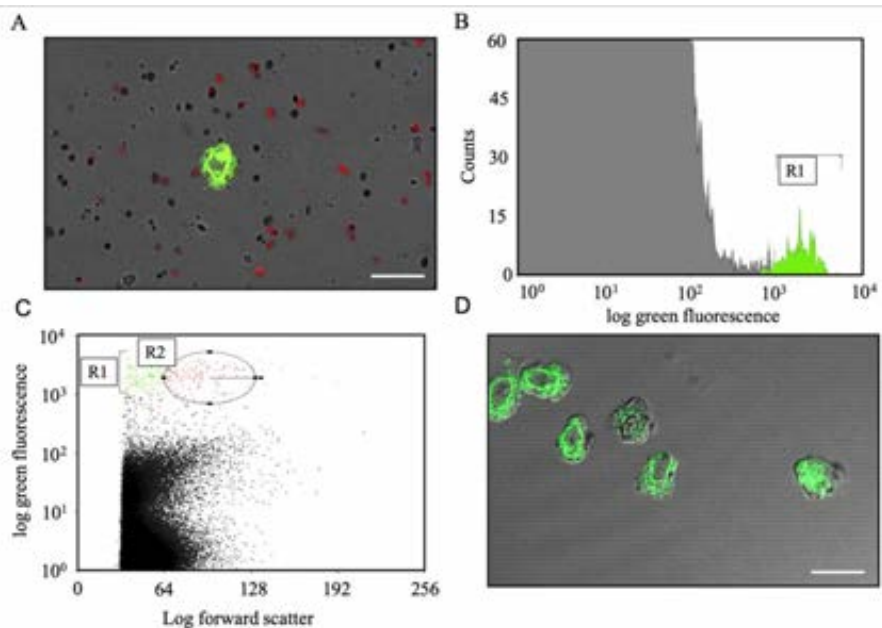


**Figure 3.1.** Isolation of *Podosphaera xanthii* haustorial cells by fluorescence-activated cell sorting. Haustoria were isolated as described in the *Methods* section, and fungal particles were stained with WGA-Alexa Fluor 488 (green fluorescence). A) A CLSM image of a haustorial homogenate before cell sorting showing a haustorial cell (green) and many particles and cell debris including chloroplasts (red). B) Counts versus log green fluorescence of particles from haustorial homogenate. The green population (R1) represents fungal particles stained with WGA-Alexa Fluor 488. C) Log green fluorescence versus log forward scatter. The red population (R2) indicates selected cells corresponding to haustoria. Events shown as green dots (e.g., hyphal debris or spores) and black (e.g., chloroplasts or plant cell wall debris) were rejected. D) A CLSM image showing purified haustoria after fluorescence-activated cell sorting. Bars, 25  $\mu\text{m}$ .

*cDNA library construction, sequencing, de novo assembly and annotation of P. xanthii transcriptomes*

From approximately 1,000 haustoria purified by flow cytometry, it was possible to isolate between 5 and 20 ng of total RNA. The quality of all RNA extractions was checked in an Agilent 2100 bioanalyser, and all RNA extractions were of a medium-low quality, obtaining RIN (RNA integrity number) values between 4 and 6.4. The best RNA extraction was used to construct the cDNA library based in a combination of oligo dT and random primers, and the Illumina library, that was subsequently sequenced on an Illumina NextSeq 550 system, yielding a total of 531,447,575 paired reads. These data are available at NCBI (BioProject PRJNA393391). These reads, along with the 975,070 raw reads previously obtained from a Roche 454 system from hyphal and conidial cDNA, which was generated by oligo dT (Vela-Corcía *et al.*, 2016), were used to generate the *P. xanthii* haustorial and epiphytic transcriptomes using the TransFlow framework (Appendix I) (Seoane *et al.*, 2018). The Module 1 performs the pre-processing of raw Illumina reads (haustorial reads in this study) and their assembly. The Module 2 does the same but with the 454 Roche reads (epiphytic reads in this study). The Module 1 yielded 140,862,905 Illumina pre-processed reads and the Module 2 yielded 687,517 Roche 454 pre-processed reads. Only 26.5% of haustorial reads were selected after the pre-processing task, while 70.5% of epiphytic reads were selected after the same task. Furthermore, with these reads, both modules generated 30 haustorial assemblies and 3 epiphytic assemblies. The top five of haustorial assemblies and all the epiphytic assemblies are shown in Table 3.3. The haustorial assemblies were more distant from the reference transcriptomes than the epiphytic transcriptomes, that could be the result of the different length

of Illumina versus 454 sequence reads and the lower quality of the haustorial RNA compared with the quality of the epiphytic RNA. Finally, the best haustorial transcriptome (scOases\_cat\_cd\_rcMin2), a scaffolded assembly from the Oases assembler, and the best epiphytic transcriptome (ctMIRA\_ctEulK29\_rcCAP3) obtained after MIRA4 and EULER-SR reconciliation of primary assemblies by CAP3 (Table 3.3), were selected to perform all the studies in this work. These transcriptomes were selected because they were the closest to the reference transcriptomes, that is, those that obtained the best parameters in comparison with the *Candida albicans* (SRR2005826) and *Neurospora crassa* (SRR100067) reference transcriptomes used for the comparative evaluation of the Module 4 of TransFlow. Both transcriptomes were annotated with Full-LengtherNext (Table S3.1). The summary of the annotation results is shown in Table 3.4.

**Table 3.3.** Summary of best epiphytic and haustorial transcriptomes generated by TransFlow. These assemblies comprise primary assemblies of 454 Roche and Illumina reads generated with several assemblers and different combinations of them.

Structure	Assembly ID	Assembly description <sup>a</sup>	MD <sup>b</sup>
Haustorium	scOases_cat_cd_rcMin2	Concatenation of two OASES assemblies with different <i>k</i> mers and sequence redundancy removal and reconciliation	0.3848
	scOases_cat	Concatenation of two OASES assemblies with different <i>k</i> mers	0.3850
	scOases_cat_cd	Concatenation of two OASES assemblies with different <i>k</i> mers and sequence redundancy removal and reconciliation	0.3861
	scSoap_cat_cd	Concatenation of two SOAP assemblies with different <i>k</i> mers and sequence redundancy removal and reconciliation	0.3887
	scOasesK35	OASES assembly with <i>k</i> -mer 35	0.3915
Epiphytic structures	ctMIRA_ctEulK29_rcCAP3	Primary assemblies (MIRA4 and EULER-SR) reconciliation using CAP3	0.0558
	ctMIRA	MIRA4-primary assembly	0.0688
	ctEulK29	EULER-SR primary assembly with <i>k</i> -mer 29	0.1435

<sup>a</sup>Summarized from Seoane et al. 2018.

<sup>b</sup>A Mean distance (MD) close to 0 means a high quality assembly and greater values show low quality assemblies.

**Table 3.4.** Summary of unigenes and ncRNAs obtained after Full-LengtherNext annotation.

Unigenes/ncRNA	Haustorial	Epiphytic
Complete unigenes	507	5217
Incomplete unigenes	8596	7745
C-terminal	983	2076
N- terminal	2189	3581
Internal	5424	2088
ncRNAs	5516	74

The poor quality of the haustorial RNA resulted in a higher number of incomplete unigenes compared to those from the epiphytic RNA (8,596 haustorial vs 7,745 epiphytic incomplete unigenes) and a considerably lower number of haustorial complete unigenes compared to those from the epiphytic RNA (507 haustorial vs 5217 epiphytic complete unigenes). Nevertheless, the number of predicted non-coding RNAs (ncRNAs) was much higher in the haustorial transcriptome than that in the epiphytic transcriptome (5,516 haustorial vs 74 epiphytic ncRNAs).

*The analysis of the P. xanthii haustorial transcriptome reveals important and specific functions of the haustorium*

GO terms, retrieved from the Full-LengtherNext annotation of epiphytic and haustorial transcriptomes (Table S3.1) were compared by Venn diagram and those that were present only in the haustorial transcriptome (Table S3.2), were visually represented by REVIGO (Figure 2A). GO terms related to biological processes such as “development of symbiont in host” (GO:0044114) or “interaction with host” (GO:0051701), reflected the intimate relationship between haustoria and plant epidermal cells. Other GO terms were related to

protection against oxidative stress, for example, “superoxide metabolism” (GO:0006801) and “response to hydrogen peroxide” (GO:0042542). GO terms such as “peptide transport” (GO:0015833) and “1,3- $\beta$ -D-glucan metabolism” (GO:0006076) indicated functions related to peptide import or cell wall modification. Furthermore, other GO terms were related to the regulation of gene expression such as “regulation of production of siRNA involved in RNA interference” (GO:0090065) and “ncRNA polyadenylation” (GO:0043629). The remaining GO terms obtained after REVIGO processing that corresponded to genes exclusively expressed in haustoria are shown in Table S3.3.

Moreover, the top 50 most highly expressed haustorial unigenes and their associated biological processes were calculated (Table S3.4). A list of the first 25 of them is shown in Table 3.5. In addition to genes involved in basic cell functions, it is interesting to note that 10 out of the top 25 most highly expressed unigenes are genes without a known function and one gene coding for an effector-like protein. GO terms related to biological processes associated with these top 50 most highly expressed haustorial unigenes (Figure 3.2B) are listed in Table S3.5. As expected, GO terms with the highest representation among the top 50 most highly expressed unigenes were “transcription” (GO:0006355, GO:0006357) and “translation” (GO:0006412, GO0006414). In addition, other GO terms that stood out were “symbiosis, encompassing mutualism through parasitism” (GO:0044403) or those related to the acquisition of nutrients such as “carbohydrate transport” (GO:0008643) and “L-lysine import across plasma” (GO:0097639).



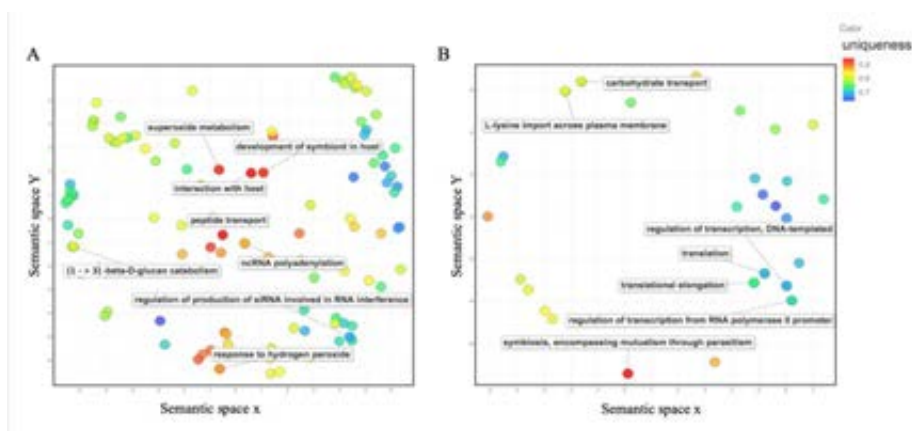


**Figure 3.2.** Visual representation of GO terms related to biological processes identified in the *Podosphaera xanthii* haustorial transcriptome. The server REVIGO, which condenses the GO description by removing redundant terms, with medium (0.7) allowed similarity parameter was used for this representation. The non-redundant GO terms were clustered in a two dimensional space according to semantic similarities to other GO terms. The colour of the bubble represents the “uniqueness” value of each GO term and indicates whether it is an outlier when compared semantically with the entire list. A) Specific non-redundant haustorial GO terms. B) Non-redundant GO terms related to biological processes of the top 50 most highly expressed haustorial genes.

**Table 3.5.** Annotation of top 25 expressed unigenes in haustoria.

	FPKM	Unigene	Length (bp)	Subject_id	Description	E-value	Identity (%)
1	3683.070	Pxanthii_hau_15484	1157	J4H557	Uncharacterized protein <i>Fibroporia radiculosa</i> .	0	65.57
2	1119.820	Pxanthii_hau_27272	1495	P15563	Uncharacterized protein. <i>Podospora anserina</i> .	1.00E-78	47.12
3	822.621	Pxanthii_hau_27283	1689	G3KEX6	Cytochrome c oxidase subunit 1 <i>Marssonina brunnea</i> f. sp. <i>multigermtubi</i> .	7.00E-32	81.25
4	609.076	Pxanthii_hau_00366852	192	A0A060QRJ0	Unassigned protein. <i>Fusarium culmorum</i> CS7071.	2.00E-05	58.33
5	182.589	Pxanthii_hau_27316	2466	H2ET44	Uncharacterized protein. <i>Candida parapsilosis</i> .	0	47
6	122.829	Pxanthii_hau_16140_1	902	P15994	ATP synthase subunit a. <i>Podospora anserina</i> .	5.00E43	75.42

7	117.173	Pxanthii_hau_15622	1462	N1JEF7	Drmip-Hesp domain-containing protein. <i>Blumeria graminis</i> f. sp. <i>hordei</i> DH14.	1.00E-36	56.1
8	80.024	Pxanthii_hau_14485	477	G2YP16	Uncharacterized protein. <i>Botryotinia fuckeliana</i> .	2.00E-15	85
9	53.860	Pxanthii_hau_27259	1389	A0A140IMW4	Laglidag endonuclease. <i>Pyronema omphalodes</i>	3.00E-109	59.88
10	44.516	Pxanthii_hau_13721	896	C5K441	Laglidag endonuclease. <i>Ajellomyces dermatitidis</i>	0.044	52.63
11	43.528	Pxanthii_hau_15600	1334	P0CY45	NADH-ubiquinone oxidoreductase. <i>Neurospora crassa</i>	3.00E-40	50
12	40.277	Pxanthii_hau_25818	257	Q08656	ATP synthase protein. <i>Neurospora crassa</i>	1.00E-18	72.92
13	37.807	Pxanthii_hau_27213	1001	C3VER8	Putative uncharacterized protein. <i>Cadophora finlandica</i> .	9.00E-61	59.49
14	32.385	Pxanthii_hau_15585	1295	A0A0B1P6R5	Uncharacterized protein. <i>Uncinula necator</i> .	0.044	90
15	30.763	Pxanthii_hau_10927	1975	L8B996	Uncharacterized protein. <i>Phlebia radiata</i> .	0.001	47.92
16	29.426	Pxanthii_hau_27286	1766	H6D5E8	Laglidag endonuclease <i>Nectria haematococca</i>	1.00E-139	54.63
17	27.922	Pxanthii_hau_12650	366	K1XD01	Acyl CoA binding protein. <i>Marssonina brunnea</i> f. sp. <i>multigermtubi</i>	3.00E-28	65.66
18	25.013	Pxanthii_hau_8297	2994	M1F6T6	Endonuclease <i>Ceratocystis cacaofunesta</i>	0.006	45.28
19	24.719	Pxanthii_hau_15673	1872	N1JQK7	Uncharacterized protein. <i>Blumeria graminis</i> f. sp. <i>hordei</i> DH14.	0	53.81
20	24.349	Pxanthii_hau_27058	599	N0A396	Uncharacterized protein. <i>Rhizoctonia solani</i> .	0.25	58.62
21	18.995	Pxanthii_hau_15091	1056	Q7RZA5	S-methyl-5'-thioadenosine phosphorylase. <i>Neurospora crassa</i> .	2.00E-156	66.88
22	17.801	Pxanthii_hau_15569	1893	A0A061HDU5	Repressible acid phosphatase <i>Blumeria graminis</i> f. sp. <i>tritici</i> 96224.	0	61.04
23	17.560	Pxanthii_hau_689	2258	N1JHJ7	CELP0015 Effector like protein <i>Blumeria graminis</i> f. sp. <i>hordei</i> DH14	0	65.35
24	13.644	Pxanthii_hau_27311	2381	P00908	Multifunctional tryptophan biosynthesis protein <i>Neurospora crassa</i>	0	62.57
25	13.521	Pxanthii_hau_27288	1835	A0A0B1PB18	Putative repressible acid phosphatase. <i>Uncinula necator</i> .	0	60.34

In addition, the trimmed reads of the haustorial transcriptome were also aligned against all ncRNAs and only those with 10 or more mapping reads were selected in order to avoid possible artefacts. Among the 5516 predicted ncRNAs by Full-LenghterNext annotation only 2143 showed 10 or more mapping reads and, hence, were selected for further analysis. The top 50 most highly expressed ncRNAs of this group of 2143 predicted ncRNAs were calculated and annotated using the RNAcentral database (Table S3.6). The annotation of these top 50 expressed ncRNAs only showed a few putative functions (Table 3.6). Among them, two ncRNAs (nc15465 and nc13870) were present in other powdery mildew fungi, *Erysiphe uncinuloides* and *Blumeria graminis*, respectively, whereas most of them were annotated with partial sequences of lncRNA from *Homo sapiens*. Moreover, the RNase function was quite represented among top 50 highly expressed ncRNAs. The expression pattern of 6 of these ncRNAs during the first stages of *P. xanthii* infection was very similar (Figure 3.3), with a very low expression at 24 and 48 h post-inoculation and a high increase in transcript levels at 72 h post-inoculation. The only exception was nc17753, which was putatively annotated as *Homo sapiens* lncRNA, which showed a wave-like expression pattern with a high expression at 24 h post-inoculation, followed by a decrease at 48 hpi and a high increase at 72 hpi. Three of the analysed ncRNAs (nc1955, nc13870 and nc15465) showed a relative high expression at 72 hpi.

**Table 3.6** Annotation of selected haustorial ncRNAs.

Sequence ID	length (bp)	RNAcentral ID	Description <sup>a</sup>	E-value	Identity (%)	Target coverage (%)
Pxanthii_hau_17753	290	URS00008C38E6	<i>Homo sapiens</i> lncRNA	3.80E-65	74.3	43
Pxanthii_hau_15465	1021	URS0000DECADB	<i>Erysiphe uncinuloides</i> miscRNA	1.50E-37	65.9	99.
Pxanthii_hau_7919	238	URS0000A7736E	<i>Arabidopsis thaliana</i> signal recognition particle (SRP)	3.30E-17	66.4	77.9
Pxanthii_hau_13870	383	URS0000BF022A	<i>Blumeria graminis</i> f. sp. <i>tritici</i> RNase P RNA	1.30E-45	69.5	99.2
Pxanthii_hau_1955	253	-	-	-	-	-
Pxanthii_hau_11307	257	URS000071105	<i>Prunus persica</i> RNase MRP RNA	5.40E-23	66.5	94.6

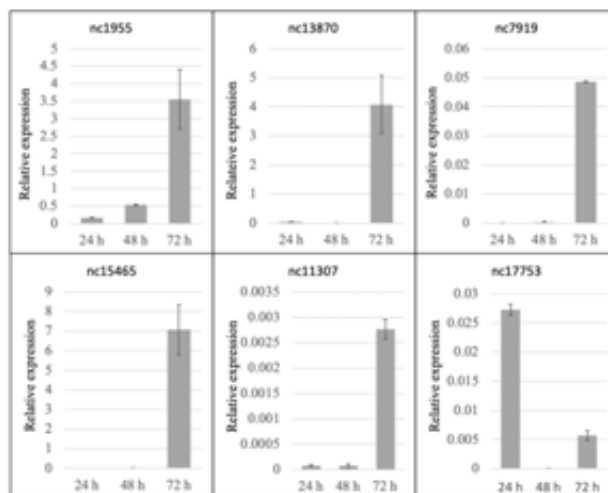


**Figure 3.3.** Analysis of the relative expression of *P. xanthii* selected ncRNAs during the first stages of infection. Total RNA was isolated from zucchini cotyledons inoculated with *P. xanthii* at 24, 48 and 72 h post-inoculation and the relative expression of ncRNAs was analysed by qRT-PCR. Transcript abundance was normalized to the transcription of the endogenous control elongation factor-1 gene *PxEF1* (MK249653). The data indicate the average values of three independent experiments with three experimental replicates. The error bars indicate the standard error.

*Ten secreted proteins are predominantly expressed in the haustorium*

The free software tools Secretool and PECAS were used to obtain the predicted haustorial and epiphytic secretomes from complete proteins. These initial secretomes were further processed by DeepLoc to obtain a more accurate prediction of secreted proteins (Figure 3.4). After Secretool and PECAS secretome processing, 26 haustorial and 140 epiphytic proteins were selected; however, only 61.5% of the haustorial proteins and 59.3% of the epiphytic proteins were validated as secreted proteins by DeepLoc (Table S3.7). In this way, a total of 16 haustorial and 83 epiphytic secreted proteins were obtained (Table S3.8), corresponding to 3.16% and 1.59% of the total of haustorial and epiphytic complete proteins, respectively.

Additionally, UniProtKB identifiers were retrieved from the Full-LengtherNext annotation results and used to compare the haustorial and epiphytic secreted proteins (Figure 3.5A). Among the 16 transcripts encoding proteins predicted to be secreted, 12 of them were represented exclusively in the haustorium according to UniProtKB identifiers (Figure 3.5A). To test the haustorial specificity of these 12 transcripts, RT-PCR analysis was conducted using cDNA obtained from epiphytic mycelia/conidia and isolated haustoria, and specific primers for each gene (Figure 3.5B). Results of this experiment showed that 10 of them were exclusively (15509, 689, 15673, 27213, 15584, 217529, 15559) or mainly (15314, 15694, 15629) expressed in haustoria and, therefore, they were denominated genes encoding haustorium-specific secreted proteins (Table 3.7). From this 10 genes, 7 of them were annotated without known function or motif. These haustorium-specific genes encoding secreted proteins without functional annotation were then designated *Podosphaera* Haustorial Effector Candidates (PHECs).

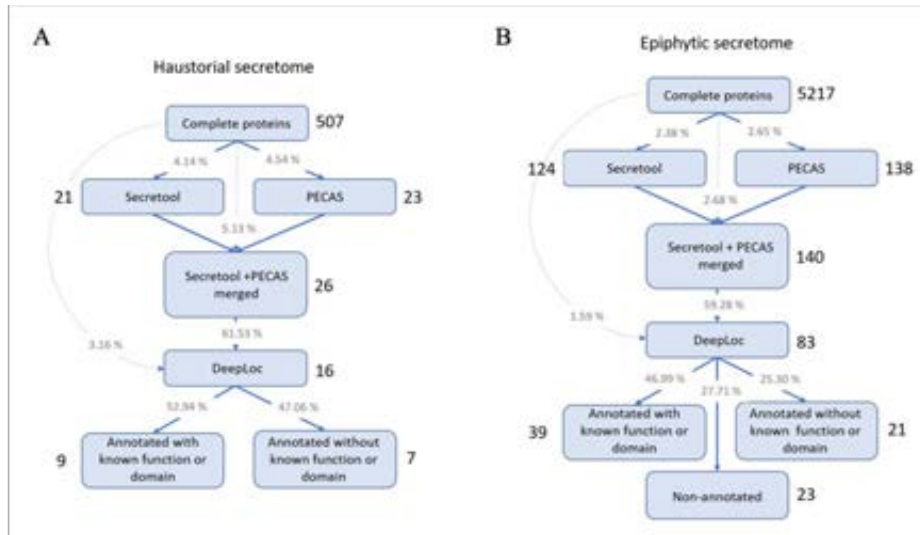


**Figure 3.4.** Workflow used to define the *Podosphaera xanthii* epiphytic and haustorial secretomes. The software used is indicated in light blue boxes, and the number of proteins selected after each software analysis is indicated with a number outside the corresponding box. The grey numbers show the percentage of secreted proteins obtained in each step of the secretome prediction workflow. A) The *P. xanthii* haustorial secretome is predicted to be composed of 16 proteins, among which 9 were annotated with known function or domain and 7 were annotated without known function or domain. B) The *P. xanthii* epiphytic secretome is predicted to be composed of 83 proteins, among which 39 were annotated with known function or domain, 21 were annotated without known function or domain and are conserved in fungi and 23 were non-annotated.

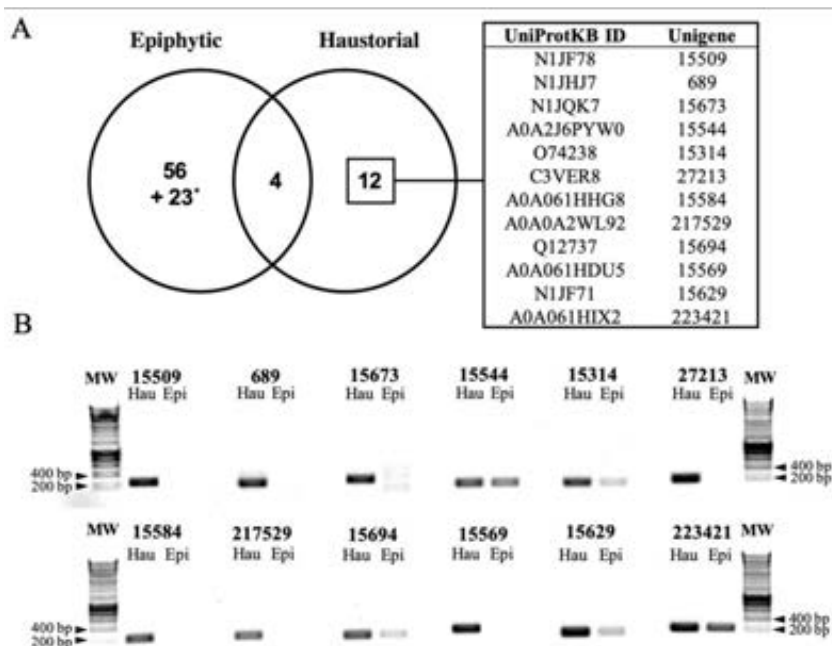


**Figure 3.5.** Identification and validation of haustorium-specific secreted proteins. A) Venn diagram showing the identification of *Podosphaera xanthii* haustorium-specific secreted proteins. The comparison was carried out using the UniProtKB protein identifiers of complete and annotated secreted proteins deduced from the revised epiphytic and the haustorial transcriptomes of *P. xanthii*. The box on the right shows the UniProtKB protein ID and unigene name of the *P. xanthii* haustorium-specific proteins. The asterisk denotes the set of non-annotated proteins detected in the epiphytic secretome. B) Detection of transcripts of *P. xanthii* haustorium-specific secreted proteins in haustorial (Hau) and epiphytic (Epi) structures. Isolation of epiphytic structures and haustorial cells, extraction of RNA and cDNA synthesis were performed as described in Methods. Detection of transcripts was carried out by PCR analysis using the specific primers listed in Table S11 (Additional file 1). The picture shows a representative image of an agarose gel with the results obtained after 3 different PCR experiments with three different RNA samples MW, molecular weight marker HyperLadder 1Kb (Bioline, London, UK).

**Table 3.7.** Annotation of *P. xanthii* genes encoding haustorium-specific secreted proteins.

Sequence ID	PHEC name	Protein <sup>a</sup>	Subject ID	Description	E-value	Identity (%)
Pxanthii_hau_689	PHEC689	457	N1JHJ7	CELP0015 Effector like protein. <i>Blumeria graminis</i> f. sp. <i>hordei</i> DH14	0.0	65.35
Pxanthii_hau_15509	PHEC15509	339	N1JF78	Uncharacterized protein <i>Blumeria graminis</i> f. sp. <i>hordei</i> DH14	1.0e-91	47.55
Pxanthii_hau_15314	-	135	O74238	Protein SnodProt1. <i>Phaeosphaeria nodorum</i>	4.0e-44	51.47
Pxanthii_hau_15629	-	401	N1JF71	Thioredoxin reductase. <i>Blumeria graminis</i> f. sp. <i>hordei</i> DH14	3.0e-137	58.07
Pxanthii_hau_15569	-	538	A0A061HDU5	Repressible acid phosphatase. <i>Blumeria graminis</i> f. sp. <i>hordei</i> 96224.	0.0	61.04
Pxanthii_hau_15584	PHEC15584	249	A0A061HHG8	Uncharacterized protein. <i>Blumeria graminis</i> f. sp. <i>hordei</i> 96224.	1.0e-43	49.34
Pxanthii_hau_15673	PHEC15673	461	N1JQK7	Uncharacterized protein. <i>Blumeria graminis</i> f. sp. <i>hordei</i> DH14	0.0	53.81
Pxanthii_hau_15694	-	602	Q12737	Bilirubin oxidase. <i>Myrothecium verrucaria</i> .	4.0e-145	47.51
Pxanthii_hau_27213	PHEC27213	209	C3VER8	Putative uncharacterized protein. <i>Cadophora finlandica</i> .	6.00e-71	53
Pxanthii_hau_000217529	PHEC217529	86	A0A0A2WL92	Uncharacterized protein. <i>Beauveria bassiana</i> D1-5	1.00E-51	99

<sup>a</sup> Number of amino acids in the unprocessed form (with signal peptide).

### *Protein modelling and protein-ligand predictions reveal putative functions for some PHECs*

To decipher the biological functions of these PHECs without known function, protein models were obtained for each PHEC using the I-TASSER server and the amino acid sequence of the mature protein (without a signal



peptide). Additionally, a set of prediction tools (Phyre2, CATH/Gene3D and Motif Scan) was used to obtain more information related to the putative functions or domains of PHECs. The resulting I-TASSER models are shown in Figure 3.6, and the main features retrieved from all software used are listed in Table 3.8. The PHEC689 model exhibited significant structural analogy with an acid phosphatase from *Aspergillus niger* (PDB code 1QFX) (Figure 3.6A; Table 3.8) and a phosphate ion as protein ligand (Table 3.8), suggesting that PHEC689 could be able to release phosphate groups from different plant molecules. The PHEC15509 model showed structural analogy with the cell adhesion protein SYS-1 from *Caenorhabditis elegans* (PDB code 3C2H) as well as a putative interaction with peptides (Figure 3.6B; Table 3.8). For its part, CATH/GENE 3D and Phyre2 indicated analogy with an integrin protein, suggesting that PHEC15509 could act as an integrin involved in cell adhesion by binding to other proteins. The resulting PHEC15584 model showed structural analogy with a cell adhesion protein from *Clostridium sporogenes* (PDB code 4QRK) and N-acetylglucosamine was predicted as a ligand (Figure 3.6C; Table 3.8), suggesting that PHEC15584 could act as a cell adhesion protein that interacts with N-acetylglucosamine residues. In the case of PHEC15673, the resulting model presented significant structural analogy with the PSCD (proline, serine, cysteine and aspartate) domain of cell wall pleuralin-1 from diatom *Cylindrotheca fusiformis* (PDB code 2NBI) as well as a serine-rich region and a possible interaction with peptides (Figure 3.6D; Table 3.6), suggesting a putative function related to adhesion. The PHEC27213 model showed high structural analogy with an A11 lytic polysaccharide monooxygenase from *Aspergillus oryzae* (PDB code 4MAH) and a chitin binding domain (Figure 3.6E; Table 3.6), suggesting, that PHEC27213 could act as a chitin-active lytic polysaccharide monooxygenase. Finally, the resulting PHEC217529 model

showed significant structural analogy with a DUF1471 domain-containing protein from *Salmonella typhimurium* (PDB code 2M2J) (Figure 3.6F; Table 3.6) whereas the predicted features retrieved from CATH/Gene3D and Phyre2 analyses indicated analogy with a flavin-binding protein dodicin.

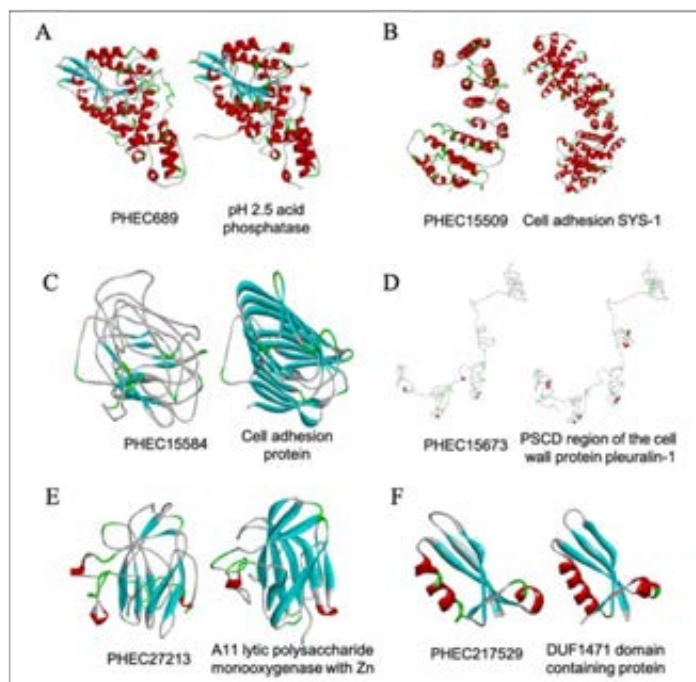


**Figure 3.6.** Predicted three-dimensional (3D) models of *Podosphaera xanthii* haustorium-specific effector candidates (PHECs) and their best structural analogues constructed using the I-TASSER server. A) PHEC689 and an acid phosphatase from *Aspergillus niger* (PDB code 1QXF). B) PHEC15509 and the cell adhesion protein SYS-1 from *Caenorhabditis elegans* (PDB code 3C2H). C) PHEC15584 and a cell adhesion protein from *Clostridium sporogenes* (PDB code 4QRK). D) PHEC15673 and the PSCD region of the cell wall protein pleuralin-1 from *Cylindrotheca fusiformis* (PDB code 2NBI). E) PHEC27213 and the A11 lytic polysaccharide monooxygenase from *Aspergillus oryzae* (PDB code 4MAH). F) PHEC217529 and the DUF1471 domain containing protein from *Salmonella typhimurium* (PDB code 2M2J).

**Table 3.8.** Principal features of PHECs obtained after structure modelling.

Protein model	Score values <sup>a</sup>		Structural analogs <sup>b</sup>		Predicted features	
	C score	TM score	PDB file	Species	Activity <sup>c</sup>	Ligands <sup>d</sup>
PHEC689	0.98	0.901	1QFX	<i>Aspergillus niger</i>	Histidine acid phosphatase	Phosphate ion
PHEC15509	-3.70	0.733	3C2H	<i>Caenorhabditis elegans</i>	Cell adhesion protein similar to integrin	Peptide
PHEC15584	-3.69	0.749	4QRK	<i>Clostridium sporogenes</i>	Cell adhesion protein	N-acetylglucosamine
PHEC15673	-0.26	0.934	2NBI	<i>Cylindrotheca fusiformis</i>	Cell wall protein pleuralin-1 with serine-rich region	Peptide
PHEC27213	-2	0.715	4MAH	<i>Aspergillus oryzae</i>	Lytic polysaccharide monoxygenase with chitin binding domain	Zinc
PHEC21752 9	0.87	0.856	2M2J	<i>Salmonella typhimurium</i>	Flavin-binding protein dodecin	Nucleic acid

<sup>a</sup> Score values represent the reliability of each model according to I-Tasser. C-score values measure the confidence of each model and are in the range of -5 to 2, where a higher value means a model with a higher confidence. TM-score values measure the structural similarity between two protein models. TM-score is in the range of 0 to 1, being 1 a perfect match between the models.

<sup>b</sup> Protein structurally close to the PHEC model according to I-TASSER prediction. PDB = Protein Data Bank.

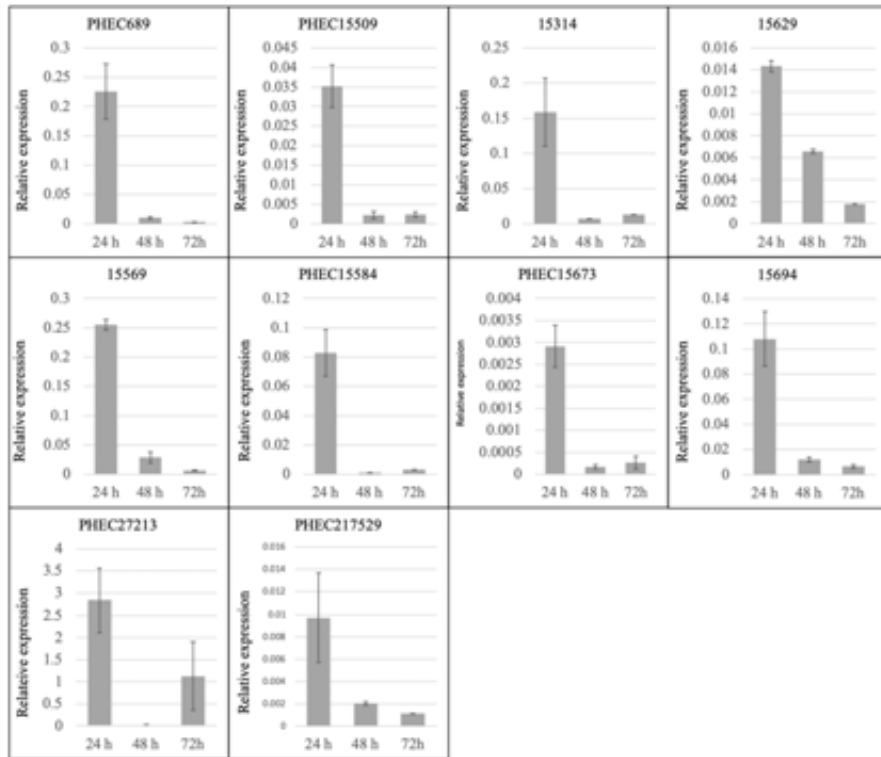
<sup>c</sup> Putative activity based on the results obtained from software tools I-TASSER, Phyre2, CATH/3D gene and Motif Scan.

<sup>d</sup> Ligand prediction according to COACH software.

### *Expression analysis of P. xanthii haustorium-specific secreted proteins*

The expression patterns of the ten *P. xanthii* genes coding for haustorium-specific secreted proteins were analysed during the first stages of pathogenesis (Figure 3.7A). In addition, these genes were grouped by hierarchical clustering according to their expression levels (Figure 3.7B). All showed a similar expression pattern with high levels of expression at 24 h followed by a sharp decrease in expression at 48 h, whereas at 72 h, the expression increased or decreased in comparison to 48 h. The genes that exhibited a second increase in expression at 72 h were grouped into cluster I. For its part, the genes that showed a slight decrease in expression at 72 h were grouped into cluster II. In the cases of *15629* and *PHEC27213*, they were not grouped in any cluster, since the decrease in expression of *15629* was attenuated in time without the abrupt decrease in expression that occurs in most genes, and the increase in expression of *PHEC27213* at 72 h was sharper than in other genes. The genes with the highest relative expression were *PHEC27213*, *15569* and *PHEC689*, which, interestingly, were found to be among the top 25 most highly expressed haustorial genes (Table 3.5).

A



B

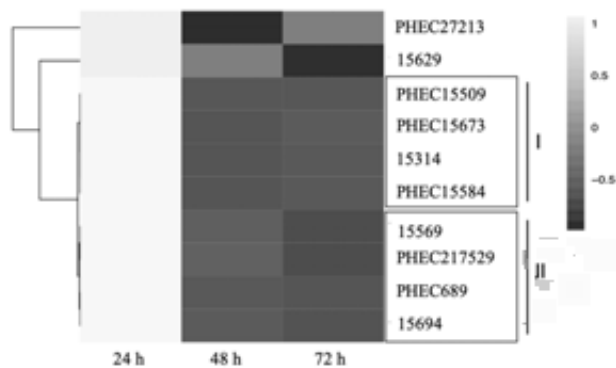


**Figure 3.7.** Analysis of the relative expression of *Podosphaera xanthii* genes coding for haustorium-specific secreted proteins during the first steps of infection. A) Relative expression of genes analysed by quantitative reverse transcription–polymerase chain reaction (qRT-PCR). Total RNA was isolated from zucchini cotyledons inoculated with *P. xanthii* at different time points (24, 48 and 72 h post-inoculation), and the relative expression of genes was analysed by qRT-PCR. Transcript abundance was normalized to the transcription of the endogenous control elongation factor-1 gene *PxEFI* (MK249653). The data shown represent average values of three experimental replicates from three independent experiments, with error bars showing the standard error. B) Hierarchical clustering of the relative expression of genes coding for haustorium-specific secreted proteins at different time points after inoculation (24, 48 and 72 h) performed by ClustVis. Rows are clustered using distance and average linkage. Changes in gene expression are displayed from white (higher expression) to black (lower expression).

## DISCUSSION

Powdery mildew is a devastating disease in cucurbits. *P. xanthii* is its main causal agent and is responsible for significant yield losses in many cucurbit crops worldwide (Pérez-García *et al.*, 2009). The haustorium, which is a specialized structure for parasitism in powdery mildew fungi, plays a pivotal role in biotrophy and pathogenesis (Oliva *et al.*, 2010) and allows an intimate interaction between the fungus and the plant cells. Therefore, it is an essential element in the establishment of powdery mildew disease. However, despite its biological importance, the only study on the *P. xanthii* haustorium is a microscopic analysis of its structure (Martínez-Cruz *et al.*, 2014). In a previous study, the role of several effector candidates secreted by *P. xanthii* during epiphytic growth in powdery mildew pathogenesis was demonstrated (Martínez-Cruz *et al.*, 2018). In this work, we sought to decipher the molecular

bases for the functions of the *P. xanthii* haustorium and find those effector candidates expressed specifically in this structure. This is, in our opinion, valuable information to help unveil the unknown aspects of the biotrophy and pathogenesis of powdery mildew fungi. For this purpose, a method to isolate haustoria free of contaminants was developed that was used together with the *de novo* assembly of the haustorial transcriptome, the corresponding secretome prediction and the comparison between the haustorial transcriptome and the epiphytic transcriptome.

Transcriptomic studies have been used to obtain relevant information about gene expression profiles in powdery mildew fungi (Both *et al.*, 2005*a,b*); thus, they have allowed for more accurate effector prediction than the prediction obtained from powdery mildew genomes (Hacquard *et al.*, 2012). However, the difficult task of isolating the haustoria is reflected in the few haustorial transcriptomic studies available to date (Godfrey *et al.*, 2010; Weßling *et al.*, 2012). Due to the high presence of plant contaminants in the haustorial preparations obtained either by isopycnic Percoll centrifugation (Godfrey *et al.*, 2010; Weßling *et al.*, 2012) or after elution from concanavalin A columns (Link *et al.*, 2014), we developed a method to isolate haustoria by flow cytometry that allowed us to obtain haustorial cells virtually free of visible contaminants. However, all these techniques require considerable time and, therefore, can alter the gene expression status of haustorial genes and/or damage the RNA quality (Weßling *et al.*, 2012) since the most unstable mRNAs have a half-life of only 5 min and could degrade, as previously described in yeast (Sachs, 1993). For this reason, the isolation of low-quality RNA is expected, although due to the difficulties in isolation and the small amount of molecular information about the haustorium currently available, the risk of the loss of sequence information is acceptable.

The sequencing of low-quality RNA is not recommended; however, it has been shown that useful data can be collected using highly degraded RNA (Gallego Romero *et al.*, 2014). A decrease in RIN values generally results in an increase in 3' bias; however, RIN values between 4 and 6 correspond with 62.2% and 58.1% 3' bias, respectively, versus the 50% 3' bias expected for an RIN of 10 (Sigurgeirsson *et al.*, 2014). Moreover, the amplification using oligo (dT) and random primers carried out by the Ovation RNA-Seq System V2 decreased this bias due to the simultaneous amplification across the whole transcriptome and at the 3' end, yielding an accurate and uniform transcriptome representation (Faherty *et al.*, 2015). In addition, the customized InDA-C primers used by the Ovation RNA-Seq System V2 to deplete ribosomal sequences considerably reduced the rRNA contamination in the final reads (Tariq *et al.*, 2011). All this, together with the yield from Illumina NextSeq 550 sequencing (531,447,575 sequence reads), became the best option to obtain as much sequence information as possible from the low-quality haustorial RNA. Despite this, only 26.5% of the haustorial reads were useful after pre-processing versus 70.5% of the epiphytic reads. This can be explained by the presence of rRNA and tRNA sequences not depleted by the InDA-C primers that, therefore, produced a large number of filtered out reads from the haustorial RNA. This, together with the lower number of complete coding unigenes obtained from the haustorial transcriptome compared with those from the epiphytic transcriptome, confirmed the difficulties associated with the isolation of haustorial RNA.

Although the haustorial transcriptome of *P. xanthii* is probably largely incomplete, its characterization and comparison with the epiphytic transcriptome have allowed us to identify certain biological processes specific to the haustorium such as “development of symbiont in host” and “interaction with host” that show the intimate relationship between the haustorium and plant



cells. Consistent with this, the transcription factor CPh2 (Pxanthii\_hau\_15645), which is related to the positive regulation of filamentous growth, virulence and invasiveness in *Candida albicans* (Lane *et al.*, 2001a,b), was found in the top 50 most highly expressed genes. Other haustorial-specific processes were “superoxide metabolism” and “response to hydrogen peroxide”, which included the specific expression of genes involved in protection against oxidative stress, suggesting a key role of the haustorium in ROS scavenging as previously described in other transcriptomic and proteomic studies of powdery mildew and rust haustoria (Jakupović *et al.*, 2006; Bindschedler *et al.*, 2009, 2011; Godfrey *et al.*, 2009; Pedersen *et al.*, 2012). Similarly, the process “1,3- $\beta$ -D-glucan catabolism” suggests the expression of specific haustorial genes related to the modification of the fungal cell wall during development of the haustorium, although some of these genes could also be involved in the degradation of plant  $\beta$ -glucans such as callose, a 1,3- $\beta$ -glucan present in papillae, as described in other fungal plant pathogens (Yang *et al.*, 2015). Nutrient uptake is a typical function of haustoria of powdery mildew and rust fungi (Hahn and Mendgen, 1997; Jakupović *et al.*, 2006; Bindschedler *et al.*, 2009, 2011; Yin *et al.*, 2009; Weßling *et al.*, 2012). The haustorial-specific process “peptide transport” corresponded to the dipeptide transport ATP-binding protein DppF, indicating the presence of a peptide uptake system (Sanz *et al.*, 2003; Asai *et al.*, 2018), which plays a key role in the human bacterial pathogen *Treponema denticola* (Asai *et al.*, 2018). With this regard, other transporters such as an amino-acid permease and a MFS sugar transporter were found among the top 50 most highly expressed genes in the *P. xanthii* haustorium.

On the other hand, the considerably high number of ncRNAs detected in haustoria, together with specific haustorial biological processes identified such as “regulation of production or siRNA involved in RNA interference” and

“ncRNA polyadenylation”, suggest the importance of this type of genetic regulation by the haustorium, making it tempting to speculate that an important part of these ncRNAs could be related to pathogenesis, as previously described in *Phytophthora infestans* (Chacko and Xiaorong, 2013). Six of these ncRNAs (five of them with high coverage and identity in comparison with the annotated ncRNA and one of them without putative function), were selected among the top 50 expressed ncRNAs and subjected to further analysis. It is noteworthy the presence among these 6 putative ncRNAs of a signal recognition particle (SRP), which catalyze targeting of nascent secretory proteins, as well as a RNase P and a RNase MRP, which are involved in tRNA and rRNA processing, respectively. The high expression of these ncRNAs support a high translation, a biological process highly represented among top 50 expressed genes. In concordance with our results, previous reports suggested that small RNAs might play a role in the plant-powdery mildew interaction (Piccinelli *et al.*, 2005; Xin *et al.*, 2010, 2011; Kusch *et al.*, 2018).

In the originally reported epiphytic transcriptome (Vela-Corcía *et al.*, 2016), 137 secreted protein candidates were identified. In the revised version of the transcriptome obtained in this work, 140 secreted protein candidates have been proposed. Despite the slight increase in the number of these proteins, the use of DeepLoc software significantly reduced the number of predicted secreted proteins. This fact demonstrated the restrictive approach used to define the predicted secretomes that allowed us to obtain a more accurate prediction and reduced the rate of false positives, despite losing several putative secreted protein candidates. The number of haustorial and epiphytic secreted proteins predicted in comparison to the total number of complete unigenes (3.2% of the complete haustorial proteins are candidate secreted proteins versus 1.6% of the complete epiphytic proteins), suggests that the haustorium contributes to the

secretion of proteins to a great extent, highlighting the contribution of this structure to the process of protein secretion (Hacquard, 2014; Vela-Corcía *et al.*, 2016) and consequently to pathogenesis (Oliva *et al.*, 2010).

The previously obtained epiphytic transcriptome (Vela-Corcía *et al.*, 2016) has allowed us to perform a comparison with the haustorial transcriptome and select those effector candidates expressed exclusively in the haustorium. Although most of them have a non-annotated function, the reliability of I-TASSER and other software in the protein function prediction of *P. xanthii* effectors had been demonstrated in a previous study (Martínez-Cruz *et al.*, 2018). In this work, a similar *in silico* analysis was carried out, revealing putative functions for several haustorium-specific secreted proteins such as phosphorous acquisition, cell adhesion, cell wall degradation/modification and defence against oxidative stress.

Regarding the latter function, the detection of 15629 and PHEC217529 transcripts, which code for a putative thioredoxin reductase and a putative flavin-binding dodecin protein, respectively, among the haustorium-specific secreted proteins emphasizes the importance of protecting the haustorium against plant oxidative stress. Thioredoxin reductase has been described as involved in defence against reactive oxygen species (Sasoni *et al.*, 2016; Liao *et al.*, 2017) and is also necessary for cell wall integrity of *Magnaporthe oryzae* during biotrophic colonization of the host (Fernandez and Wilson, 2014). Similarly, protection against oxidative stress has been suggested as a function of dodecin proteins (Bieger *et al.*, 2003). Dodecins are widely spread and found in a large variety of bacterial pathogens including plant pathogens such as *Ralstonia solanacearum*. However, their role in pathogenesis has not been identified until very recently; specifically, their role in *Mycobacterium tuberculosis* pathogenicity was identified (Bourdeaux *et al.*, 2018).

Two putative acid phosphatases (15569, PHEC689) were found among the effector candidates specifically expressed in the haustorium. The implication of these enzymes in pathogenesis has been described in intracellular bacteria such as *Francisella tularensis* (Mohapatra *et al.*, 2007, 2013), the tuberculosis agent (Puri *et al.*, 2013) and the entomopathogenic fungus *Metarhizium anisopliae* (Xia *et al.*, 2001). Moreover, their coordination (grouped in cluster II), high relative expression (among the top 50 most highly expressed haustorial genes) and function (phosphate acquisition) support their importance in biotrophy rather than in pathogenesis because they present an expression pattern and a molecular size different from those described for canonical powdery mildew effectors (Pedersen *et al.*, 2012; Hacquard, 2014). Nevertheless, pathogenesis and survival in the host follow a very thin line in biotrophic biology, and sometimes it is very difficult to distinguish what is specific for pathogenesis from basic physiological functions.

Other specific haustorial proteins in *P. xanthii* seem to be canonical effectors. This is the case for 15314, a putative homologue of SnodProt1, a virulence factor in *P. nodorum* of unknown function (Jeong *et al.*, 2007). Within this group, we could also include 15629, a putative bilirubin oxidase, and PHEC27213, a putative A11 lytic polysaccharide monooxygenase. These enzymes have been previously described in fungi but play a role in biomass conversion rather than a role in pathogenesis (Xie *et al.*; LI *et al.*, 2012; Durand *et al.*, 2012). However, the typical effector expression pattern of PHEC27213 and the fact that it was the most highly expressed haustorial effector candidate and the thirteenth most expressed haustorial gene suggest a potentially important role in *P. xanthii* pathogenesis.

Interestingly, a third of the total specific haustorial secreted proteins correspond to cell adhesion proteins (PHEC15509, PHEC15584, PHEC15673)

that present the same expression pattern (cluster I). Integrin proteins (such as putative integrin PHEC15509) have a relevant role in adhesion to host proteins in *Candida albicans* (Tronchin *et al.*, 1991; Santoni *et al.*, 1994). To date, no proteins with cell adhesion properties have been described in biotrophic fungi. Nevertheless, the high number of these proteins among all haustorium-specific secreted proteins suggests the relevance of cell adhesion proteins to the biotrophic lifestyle, perhaps as haustorial-stabilizing proteins during the development and accommodation of the haustorium inside the plant cell.

The results of this study, the third study on powdery mildew haustoria, raise an interesting question: is it possible to identify gene sets that are generally haustorium-specific? The most expressed biological processes identified in the *P. xanthii* haustorium such as transcription and translation, have been described in *G. orontii* haustorial transcriptome (Weßling *et al.*, 2012), supporting the high protein turn-over in haustoria. However, the same is not true for most haustorium-specific secreted proteins. Only two proteins with similar functions to those described in *P. xanthii*, ROS scavenging, such as a Cu/Zn superoxide dismutase, and chitin modification, such as a chitinase, were described in the *G. orontii* haustoria (Weßling *et al.*, 2012), whereas none of them were described in the haustorial transcriptome of *B. graminis* (Godfrey *et al.*, 2010). This difference can be due in part to the high number of secreted proteins without functional annotation in those transcriptomic studies. In addition, the quality of haustorial transcriptomes is often poor, so it is easy to assume that substantial information is missing. However, the fact that for most of the genes encoding haustorial-specific *P. xanthii* secreted proteins is possible to find orthologues in the genomes of other powdery mildew fungi, suggests that there is a possibility that haustorial core genes will be found in the future.

Despite the difficulties in obtaining preparations of haustoria free of contaminants and in isolating good quality RNA from these cells, the assembly of a *de novo* haustorial transcriptome of *P. xanthii* and its comparison with a revised version of an epiphytic transcriptome previously developed allowed us to gain new insights into the biotrophy and pathogenesis of *P. xanthii*. According to specifically expressed genes, major biological functions associated with the haustorium such as protection against reactive oxygen species and the acquisition of nutrients were supported. However, additional important functions such as the secretion of cell adhesion proteins have not been described to date. A schematic representation of the functions of the *P. xanthii* haustorium according to the results obtained in this work is shown in Figure 3.8. The analysis of these functions could be a nice starting point to unravel the unknown aspects of powdery mildew biology.

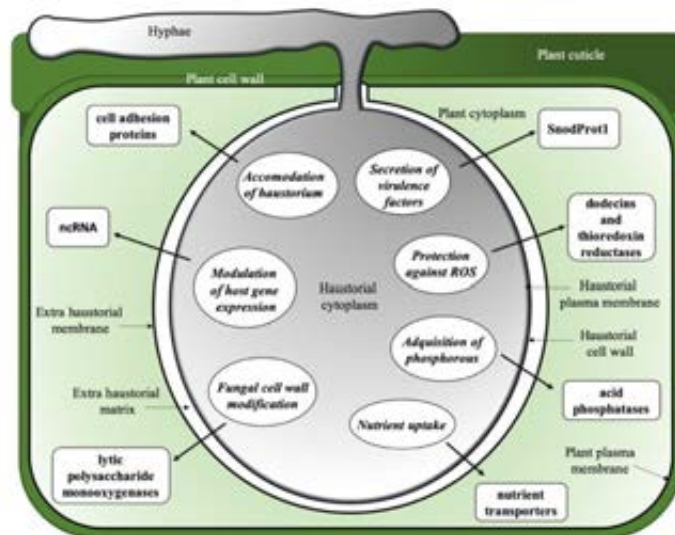


**Figure 3.8.** Schematic representation of the physiological processes specific to the *P. xanthii* haustorium according to the results obtained in this work.

## SUPPLEMENTAL DATA

Available to download:

- [https://static-content.springer.com/esm/art%3A10.1186%2Fs12864-019-5938-0/MediaObjects/12864\\_2019\\_5938\\_MOESM2\\_ESM.xlsx](https://static-content.springer.com/esm/art%3A10.1186%2Fs12864-019-5938-0/MediaObjects/12864_2019_5938_MOESM2_ESM.xlsx)

**Table S3.1:** Full annotation of *P. xanthii* haustorial and epiphytic transcriptomes (corresponding to Table S2).

**Table S3.2:** Comparison of haustorial and epiphytic GO terms performed by Venn diagram (corresponding to Table S3).

**Table S3.3:** Non-redundant GO terms related to biological processes specific to *P. xanthii* haustoria obtained by REVIGO (corresponding to Table S4).

**Table S3.4:** Top 50 expressed unigenes in *P. xanthii* haustoria (corresponding to Table S5).

**Table S3.5:** Non-redundant GO terms related to biological processes of the top 50 expressed haustorial unigenes obtained by REVIGO (corresponding to Table S6).

**Table S3.6:** Top 50 expressed ncRNAs in *P. xanthii* haustorial transcriptome (corresponding to Table S7).

**Table S3.7:** Subcellular localization analysis of haustorial and epiphytic candidate secreted proteins of *P. xanthii* performed by DeepLoc (corresponding to Table S8).

**Table S3.8:** Annotation of *P. xanthii* haustorial and epiphytic secretomes (corresponding to Table S9).



## REFERENCES

**Almagro Armenteros JJ, Sønderby CK, Sønderby SK, Nielsen H, Winther O.** 2017. DeepLoc: prediction of protein subcellular localization using deep learning. *Bioinformatics* **33**, 3387–3395.

**Asai T, Okamoto-Shibayama K, Kikuchi Y, Ishihara K.** 2018. Characterization of a novel potential peptide import system in *Treponema denticola*. *Microbial Pathogenesis* **123**, 467–472.

**Baxter L, Tripathy S, Ishaque N, et al.** 2010. Signatures of adaptation to obligate biotrophy in the *Hyaloperonospora arabidopsis* genome. *Science* **330**, 1549–1551.

**Bellón-Gómez D, Vela-Corcía D, Pérez-García A, Torés JA.** 2015. Sensitivity of *Podosphaera xanthii* populations to anti-powdery-mildew fungicides in Spain. *Pest Management Science* **71**, 1407–1413.

**Bieger B, Essen LO, Oesterhelt D.** 2003. Crystal structure of halophilic dodecin: A novel, dodecameric flavin binding protein from *Halobacterium salinarum*. *Structure* **11**, 375–385.

**Bindschedler L V., Burgis TA, Mills DJS, Ho JTC, Cramer R, Spanu PD.** 2009. In planta proteomics and proteogenomics of the biotrophic barley fungal pathogen *Blumeria graminis* f. sp. *hordei*. *Molecular & Cellular Proteomics* **8**, 2368–2381.

**Bindschedler L V., McGuffin LJ, Burgis TA, Spanu PD, Cramer R.** 2011. Proteogenomics and in silico structural and functional annotation of the barley powdery mildew *Blumeria graminis* f. sp. *hordei*. *Methods* **54**, 432–441.

**Bindschedler L V., Panstruga R, Spanu PD.** 2016. Mildew-Omics: How global analyses aid the understanding of life and evolution of powdery mildews.

Frontiers in Plant Science 7, 123.

**Both M, Csukai M, Stumpf MPH, Spanu PD.** 2005a. Gene expression profiles of *Blumeria graminis* indicate dynamic changes to primary metabolism during development of an obligate biotrophic pathogen. *The Plant Cell* 17, 2107–2122.

**Both M, Eckert SE, Csukai M, Muller E, Dimopoulos G, Spanu PD.** 2005b. Transcript profiles of *Blumeria graminis* development during infection reveal a cluster of genes that are potential virulence determinants. *Molecular Plant Microbe Interaction* 18, 125–33.

**Bourdeaux F, Hammer CA, Vogt S, Schweighöfer F, Nöll G, Wachtveitl J, Grininger M.** 2018. Flavin storage and sequestration by *Mycobacterium tuberculosis* dodecin. *ACS Infectious Diseases* 4, 1082–1092.

**Chacko N, Xiaorong L.** 2013. Non-coding RNAs in the development and pathogenesis of eukaryotic microbes. *Applied Microbiology and Biotechnology* 97, 7989–7997.

**Cortázar AR, Aransay AM, Alfaro M, Oguiza JA, Lavín JL.** 2014. SECRETOOL: Integrated secretome analysis tool for fungi. *Amino Acids* 46, 471–473.

**Cortazar AR, Oguiza JA, Aransay AM, Lavín JL.** 2015. PECAS: Prokaryotic and eukaryotic classical analysis of secretome. *Amino Acids* 47, 2659–2663.

**Duplessis S, Cuomo CA, Lin Y, et al.** 2011. Obligate biotrophy features unraveled by the genomic analysis of rust fungi. *Proceedings of the National Academy of Sciences* 108, 9166–9171.

**Durand F, Gounel S, Kjaergaard CH, Solomon EI, Mano N.** 2012. Bilirubin oxidase from *Magnaporthe oryzae*: an attractive new enzyme for biotechnological applications. *Applied Microbiology and Biotechnology* 96,

1489–1498.

**Faherty SL, Campbell CR, Larsen PA, Yoder AD.** 2015. Evaluating whole transcriptome amplification for gene profiling experiments using RNA-Seq. *BMC Biotechnology* **15**.

**Fernández-Ortuño D, Pérez-García A, López-Ruiz F, Romero D, De Vicente A, Torés JA.** 2006. Occurrence and distribution of resistance to QoI fungicides in populations of *Podosphaera fusca* in south central Spain. *European Journal of Plant Pathology* **115**, 215–222.

**Fernandez J, Wilson RA.** 2014. Characterizing roles for the glutathione reductase, thioredoxin reductase and thioredoxin peroxidase-encoding genes of *Magnaporthe oryzae* during rice blast disease. *PLoS ONE* **9**, e87300.

**Frantzeskakis L, Kracher B, Kusch S, Yoshikawa-Maekawa M, Bauer S, Pedersen C, Spanu PD, Maekawa T, Schulze-Lefert P, Panstruga R.** 2018. Signatures of host specialization and a recent transposable element burst in the dynamic one-speed genome of the fungal barley powdery mildew pathogen. *BMC Genomics* **19**, 381.

**Gallego Romero I, Pai AA, Tung J, Gilad Y.** 2014. RNA-seq: impact of RNA degradation on transcript quantification. *BMC biology* **12**, 42.

**Godfrey D, Böhlenius H, Pedersen C, Zhang Z, Emmersen J, Thordal-Christensen H.** 2010. Powdery mildew fungal effector candidates share N-terminal Y/F/WxC-motif. *BMC Genomics* **11**.

**Godfrey D, Zhang Z, Saalbach G, Thordal-Christensen H.** 2009. A proteomics study of barley powdery mildew haustoria. *Proteomics* **9**, 3222–3232.

**Hacquard S.** 2014. The genomics of powdery mildew fungi: Past achievements, present status and future prospects. *Advances in Botanical Research* **70**, 109-142

**Hacquard S, Joly DL, Lin Y-C, et al.** 2012. A comprehensive analysis of genes encoding small secreted proteins identifies candidate effectors in *Melampsora larici-populina* (poplar leaf rust). *Molecular Plant-Microbe Interactions* **25**, 279–293.

**Hacquard S, Kracher B, Maekawa T, Vernaldi S, Schulze-Lefert P, Ver Loren van Themaat E.** 2013. Mosaic genome structure of the barley powdery mildew pathogen and conservation of transcriptional programs in divergent hosts. *Proceedings of the National Academy of Sciences* **110**, E2219–E2228.

**Hahn M, Mendgen K.** 1997. Characterization of in planta-induced rust genes isolated from a haustorium-specific cDNA library. *Molecular plant-microbe interactions* : *MPMI* **10**, 427–437.

**Jakupović M, Heintz M, Reichmann P, Mendgen K, Hahn M.** 2006. Microarray analysis of expressed sequence tags from haustoria of the rust fungus *Uromyces fabae*. *Fungal Genetics and Biology* **43**, 8–19.

**Jeong JS, Mitchell TK, Dean RA.** 2007. The *Magnaporthe grisea* snodprot1 homolog, MSP1, is required for virulence. *FEMS Microbiology Letters* **273**, 157–165.

**Jones L, Riaz S, Morales-Cruz A, Amrine KC, McGuire B, Gubler WD, Walker MA, Cantu D.** 2014. Adaptive genomic structural variation in the grape powdery mildew pathogen, *Erysiphe necator*. *BMC Genomics* **15**.

**Kelly LA, Mezulis S, Yates C, Wass M, Sternberg M.** 2015. The Phyre2 web portal for protein modelling, prediction, and analysis. *Nature Protocols* **10**, 845–858.

**Kemen E, Gardiner A, Schultz-Larsen T, et al.** 2011. Gene gain and loss during evolution of obligate parasitism in the white rust pathogen of *Arabidopsis thaliana*. *PLoS Biology* **9**, e1001094.

**Koressaar T, Remm M.** 2007. Enhancements and modifications of primer

design program Primer3. *Bioinformatics* **23**, 1289–1291.

**Kusch S, Frantzeskakis L, Thieron H, Panstruga R.** 2018. Small RNAs from cereal powdery mildew pathogens may target host plant genes. *Fungal Biology* **122**, 1050–1063.

**Lam SD, Dawson NL, Das S, Sillitoe I, Ashford P, Lee D, Lehtinen S, Orenge CA, Lees JG.** 2016. Gene3D: Expanding the utility of domain assignments. *Nucleic Acids Research* **44**, D404–D409.

**Lane S, Birse C, Zhou S, Matson R, Liu H.** 2001*a*. DNA array studies demonstrate convergent regulation of virulence factors by Cph1, Cph2, and Efg1 in *Candida albicans*. *Journal of Biological Chemistry* **276**, 48988–48996.

**Lane S, Zhou S, Pan T, Dai Q, Liu H.** 2001*b*. The basic helix-loop-helix transcription factor Cph2 regulates hyphal development in *Candida albicans* partly via Tec1. *Molecular and Cell Biology* **21**, 6418–6428.

**Langmead B, Salzberg SL.** 2013. Fast gapped-read alignment with Bowtie 2. *Nat Methods* **9**, 357–359.

**LI X, Beeson WT, Phillips CM, Marletta MA, Cate JH.** 2012. Structural basis for substrate targeting and catalysis by fungal polysaccharide monooxygenases. *Structure* **20**, 1051–1061.

**Liao X, Yang F, Li H, So PK, Yao Z, Xia W, Sun H.** 2017. Targeting the thioredoxin reductase-thioredoxin system from *Staphylococcus aureus* by silver ions. *Inorganic Chemistry* **56**, 14823–14830.

**Link TI, Lang P, Scheffler BE, et al.** 2014. The haustorial transcriptomes of *Uromyces appendiculatus* and *Phakopsora pachyrhizi* and their candidate effector families. *Molecular Plant Pathology* **15**, 379–393.

**Martínez-Cruz J, Romero D, Dávila JC, Pérez-García A.** 2014. The *Podosphaera xanthii* haustorium, the fungal Trojan horse of cucurbit-powdery mildew interactions. *Fungal genetics and biology* **71**, 21–31.

**Martínez-Cruz J, Romero D, de la Torre FN, Fernández-Ortuño D, Torés JA, de Vicente A, Pérez-García A.** 2018. The functional characterization of *Podosphaera xanthii* candidate effector genes reveals novel target functions for fungal pathogenicity. *Molecular Plant-Microbe Interactions* **31**, 914-931.

**Martínez-Cruz J, Romero D, de Vicente A, Pérez-García A.** 2017. Transformation of the cucurbit powdery mildew pathogen *Podosphaera xanthii* by *Agrobacterium tumefaciens*. *New Phytologist* **213**, 1961–1973.

**Metsalu T, Vilo J.** 2015. ClustVis: A web tool for visualizing clustering of multivariate data using Principal Component Analysis and heatmap. *Nucleic Acids Research* **43**, W566–W570.

**Mohapatra NP, Balagopal A, Soni S, Schlesinger LS, Gunn JS.** 2007. AcpA is a *Francisella* acid phosphatase that affects intramacrophage survival and virulence. *Infection and Immunity* **75**, 390–396.

**Mohapatra NP, Soni S, Rajaram MVS, Strandberg KL, Gunn JS.** 2013. Type A *Francisella tularensis* acid phosphatases contribute to pathogenesis. *PLoS ONE* **8**, e56834.

**Müller MC, Praz CR, Sotiropoulos AG, et al.** 2019. A chromosome-scale genome assembly reveals a highly dynamic effector repertoire of wheat powdery mildew. *New Phytologist* **221**, 2176–2189.

**Oliva R, Win J, Raffaele S, et al.** 2010. Recent developments in effector biology of filamentous plant pathogens. *Cellular Microbiology* **12**, 705–715.

**Pagni M, Ioannidis V, Cerutti L, Zahn-Zabal M, Jongeneel CV, Hau J, Martin O, Kuznetsov D, Falquet L.** 2007. MyHits: Improvements to an interactive resource for analyzing protein sequences. *Nucleic Acids Research* **35**, W433–W437.

**Pedersen C, van Themaat EVL, McGuffin LJ, et al.** 2012. Structure and

evolution of barley powdery mildew effector candidates. *BMC Genomics* **13**.

**Pérez-García A, Mingorance E, Rivera ME, Del Pino D, Romero D, Torés JA, De Vicente A.** 2006. Long-term preservation of *Podosphaera fusca* using silica gel. *Journal of Phytopathology* **154**, 190–192.

**Pérez-García A, Romero D, Fernández-Ortuño D, López-Ruiz F, De Vicente A, Torés JA.** 2009. The powdery mildew fungus *Podosphaera fusca* (synonym *Podosphaera xanthii*), a constant threat to cucurbits. *Molecular plant pathology* **10**, 153–160.

**Piccinelli P, Rosenblad MA, Samuelsson T.** 2005. Identification and analysis of ribonuclease P and MRP RNA in a broad range of eukaryotes. *Nucleic Acids Research* **33**, 4485–4495.

**del Pino D, Olalla L, Pérez-García A, Rivera ME, García S, Moreno R, de Vicente A, Torés JA.** 2002. Occurrence of races and pathotypes of cucurbit powdery mildew in southeastern Spain. *Phytoparasitica* **30**, 459–466.

**Puri RV, Reddy PV, Tyagi AK.** 2013. Secreted acid phosphatase (SapM) of *Mycobacterium tuberculosis* is indispensable for arresting phagosomal maturation and growth of the pathogen in Guinea pig tissues. *PLoS ONE* **8**, e70514.

**Sachs A.** 1993. Messenger RNA degradation in eukaryotes. *Cell* **74**, 413–421.

**Santoni G, Gismondi A, Liu JH, Punturieri A, Santoni A, Frati L, Piccoli M, Djeu JY.** 1994. *Candida albicans* expresses a fibronectin receptor antigenically related to  $\alpha 5\beta 1$  integrin. *Microbiology* **140**, 2971–2979.

**Sanz Y, Toldrá F, Renault P, Poolman B.** 2003. Specificity of the second binding protein of the peptide ABC-transporter (Dpp) of *Lactococcus lactis* IL1403. *FEMS Microbiology Letters* **227**, 33–38.

**Sasoni N, Iglesias AA, Guerrero SA, Arias DG.** 2016. Functional

thioredoxin reductase from pathogenic and free-living *Leptospira* spp. Free Radical Biology and Medicine **97**, 1–13.

**Seoane P, Espigares M, Carmona R, et al.** 2018. TransFlow: a modular framework for assembling and assessing accurate de novo transcriptomes in non-model organisms. BMC Bioinformatics. 2018;19(Suppl 14):416.

**Sigurgeirsson B, Emanuelsson O, Lundeberg J.** 2014. Sequencing degraded RNA addressed by 3' tag counting. PLoS ONE **9**, e91851.

**Spanu PD, Abbott JC, Amselem J, et al.** 2010. Genome expansion and gene loss in powdery mildew fungi reveal tradeoffs in extreme parasitism. Science **330**, 1543–1546.

**Supek F, Bosnjak M, Skunca N, Tomislav S.** 2011. REVIGO Summarizes and visualizes long lists of gene ontology terms. PLoS ONE **6**, e21800.

**Tariq MA, Kim HJ, Jejelowo O, Pourmand N.** 2011. Whole-transcriptome RNAseq analysis from minute amount of total RNA. Nucleic Acids Research **39**, e120.

**Tronchin G, Bouchara JP, Annaix V, Robert R, Senet JM.** 1991. Fungal cell adhesion molecules in *Candida albicans*. European Journal of Epidemiology **7**, 23–33.

**Vela-Corcía D, Bautista R, De Vicente A, Spanu PD, Pérez-García A.** 2016. De novo analysis of the epiphytic transcriptome of the cucurbit powdery mildew fungus *Podosphaera xanthii* and identification of candidate secreted effector proteins. PLoS ONE **11**, e0163379.

**Weßling R, Schmidt SM, Micali CO, Knaust F, Reinhardt R, Neumann U, Ver Loren van Themaat E, Panstruga R.** 2012. Transcriptome analysis of enriched *Golovinomyces orontii* haustoria by deep 454 pyrosequencing. Fungal Genetics and Biology **49**, 470–482.

**Wicker T, Oberhaensli S, Parlange F, et al.** 2013. The wheat powdery



mildew genome shows the unique evolution of an obligate biotroph. *Nature Genetics* **45**, 1092–1096.

**Wu Y, Ma X, Pan Z, et al.** 2018. Comparative genome analyses reveal sequence features reflecting distinct modes of host-adaptation between dicot and monocot powdery mildew. *BMC Genomics* **19**, 705.

**Xia Y, Clarkson JM, Charnley KA.** 2001. Acid phosphatases of *Metarhizium anisopliae* during infection of the tobacco hornworm *Manduca sexta*. *Archives of Microbiology* **176**, 427–434.

**Xie N, Ruprich-Robert G, Silar P, Chapeland-Leclerc F.** Bilirubin oxidase-like proteins from *Podospora anserina*: promising thermostable enzymes for application in transformation of plant biomass. *Environmental Microbiology* **17**, 866–875.

**Xin M, Wang Y, Yao Y, et al.** 2010. Diverse set of microRNAs are responsive to powdery mildew infection and heat stress in wheat (*Triticum aestivum* L.). *BMC Plant Biology*, 123.

**Xin M, Wang Y, Yao Y, Song N, Hu Z, Qin D, Xie C, Peng H, Ni Z, Sun Q.** 2011. Identification and characterization of wheat long non-protein coding RNAs responsive to powdery mildew infection and heat stress by using microarray analysis and SBS sequencing. *BMC Plant Biology* **11**, 61.

**Yang L, Xie L, Xue B, et al.** 2015. Comparative transcriptome profiling of the early infection of wheat roots by *Gaeumannomyces graminis* var. *tritici*. *PLoS ONE* **10**, e0120691.

**Yin C, Chen X, Wang X, Han Q, Kang Z, Hulbert SH.** 2009. Generation and analysis of expression sequence tags from haustoria of the wheat stripe rust fungus *Puccinia striiformis* f. sp. *tritici*. *BMC genomics* **10**, 626.

**Zhang Y.** 2008. I-TASSER server for protein 3D structure prediction. *BMC bioinformatics* **9**, 40.

# CHAPTER IV

**Two secreted haustorial acid  
phosphatases are key factors for  
*Podosphaera xanthii* development and  
promising targets for fungicide design**



## ABSTRACT

*Podosphaera xanthii* is the main causal agent of powdery mildew in cucurbits and a disease that causes significant yield losses. The control of the disease is fundamentally based on the use of fungicides. Unfortunately, *P. xanthii* has developed a rapid resistance against many of the compounds currently used for disease management. In this scenario, the development of new phytosanitary tools against cucurbit powdery mildew is strongly demanded. The aim of this work has been the search for novel potential targets for fungicide development, focusing in the haustorium, the fungal structure most closely associated with the plant cells, from which powdery mildew fungi obtain nutrients and release effectors. We have studied two secreted proteins highly and exclusively expressed in the haustorium to determine their role and importance for *P. xanthii* development. These proteins were predicted as secreted acid phosphatases, one by annotation and the other by 3D modelling, and accordingly, a yeast complementation assay was performed to validate their predicted function. In addition, gene silencing experiments demonstrated a key role of these enzymes for *P. xanthii* growth, presumably due to their participation in the acquisition of phosphorus from different plant substrates. With this regard, fungal growth inhibition assays with different acid phosphatase inhibitors also showed significant disease control. Moreover, BLAST searches showed that similar proteins are widely presented in pathogenic Ascomycota fungi. Taken together, our results indicate that acid phosphatases are essential enzymes for phosphorous uptake and parasitic growth of *P. xanthii* and possibly other phytopathogenic fungi, and identify phosphate metabolism as a promising target for novel fungicide design.



## INTRODUCTION

*Podosphaera xanthii* is a plant pathogenic obligate biotrophic fungus and the main causal agent of cucurbits powdery mildew disease, which causes a serious decrease in yields of both open field and greenhouse crops (del Pino *et al.*, 2002; Fernández-Ortuño *et al.*, 2006; Pérez-García *et al.*, 2009; Bellón-Gómez *et al.*, 2015). Like other powdery mildew fungi, *P. xanthii* needs living plant cells to complete its asexual life cycle (Spanu, 2006). In this cycle, first, a conidium deposited onto a susceptible host germinates developing a germ tube which elongates until creates an appressorium. Then, the appressorium breaks the cuticle and the plant cell wall to allow the fungus to enter inside the epidermal plant cell where the haustorium, the specialized structure of parasitism of these fungi, is developed (Micali *et al.*, 2011; Martínez-Cruz *et al.*, 2014). During their life cycle, powdery mildew fungi employ the haustoria to uptake nutrients from host cells and to release effectors to manipulate host physiology (Martínez-Cruz *et al.*, 2018a). Therefore, the haustorium has a pivotal role in pathogenesis and in biotrophy of these fungi, becoming the fungal structure most closely associated with the plant cells and an important subject to study in the battle against these diseases (Oliva *et al.*, 2010).

Several control tools such as cultural practices, resistant crops, chemical fungicides and more recently biocontrol agents, have been used to manage the powdery mildew diseases (Jahn *et al.*, 2002; Jarvis *et al.*, 2002; Chen *et al.*, 2007; Magno-Pérez-Bryan *et al.*, 2015). However, in practice, the repeated application of fungicides is the main strategy used for the control of these diseases (McGrath, 2010). Unfortunately, powdery mildew fungi develop rapid resistance to most of the compounds currently used against them (Fernández-

Ortuño *et al.*, 2006; Bellón-Gómez *et al.*, 2015), since most of these compounds have very specific mechanisms of action (McGrath, 2010). Hence, molecular studies of powdery mildew-host interactions are necessary to identify key aspects of pathogenesis and biotrophy that could allow the development of new strategies for the specific management of powdery mildew diseases.

Among the molecular aspects analysed in several powdery mildew-host interactions stand out the study of effectors (Godfrey *et al.*, 2010; Hacquard *et al.*, 2012; Pedersen *et al.*, 2012; Vela-Corcía *et al.*, 2016), mostly due to their importance in pathogenesis for manipulating host defence mechanisms (Ridout *et al.*, 2006; Block *et al.*, 2008; Göhre and Robatzek, 2008). Regarding *P. xanthii*, the recent development of several molecular tools for gene functional analysis, such as transient transformation and host-induced gene silencing (Martínez-Cruz *et al.*, 2017, 2018b), has allowed to demonstrate the importance of certain effectors for *P. xanthii* development (Martínez-Cruz *et al.*, 2018a). In addition, transcriptomic and genomic studies carried out in different powdery mildew species have been essential to obtain valuable information about the biotrophy of these fungi. In this way, it has been possible to identify certain missing genes and metabolic pathways such as nitrate and sulphate assimilation pathways or molybdopterin and thiamine biosynthesis pathways, (Baxter *et al.*, 2010; Spanu *et al.*, 2010; Duplessis *et al.*, 2011; Kemen *et al.*, 2011). Therefore, these fungi depend on obtaining reduced nitrogen (amino acids or  $\text{NH}_4^+$ ), sulphur, thiamine and molybdopterin, among other compounds, from the host cells, resulting in the obligate biotrophy attribute which is typical of powdery mildews. These features have been partially confirmed by the identification of amino acid transporters present in powdery mildews and other obligate biotrophs such as oomycetes and rusts (Hahn and Mendgen, 1997; Divon and Fluhr, 2006; Duplessis *et al.*, 2011; Kemen *et al.*, 2011), as well as by the

induction of nitrate/nitrite transporters of the grape powdery mildew *Erysiphae necator* on *Vitis vinifera* leaves (Pike *et al.*, 2014), indicating the capability of biotrophic fungi for nitrogen uptake from plant cells.

Obligate biotrophic fungi need to obtain other nutrients from plant cells such as phosphorus or carbohydrates. In the case of powdery mildews, glucose is the main carbon source obtained from host leaves (Sutton *et al.*, 1999; Fotopoulos *et al.*, 2003). Thus, glucose transporters have been described in different powdery mildew fungi (Zhang *et al.*, 2005; Weßling *et al.*, 2012) and one of them, together an amino acid transporter, have been found among the top 50 expressed genes in *P. xanthii* haustoria (see chapter III). Regarding phosphorus, the mechanisms by which powdery mildews obtain this element remain unknown, however, the presence of a member of Pho88 group of inorganic phosphate transporters among the top 50 expressed genes in the haustoria of the *Arabidopsis* powdery mildew *Golovinomyces orontii* (Weßling *et al.*, 2012), suggests the implication of this specialized fungal structure in phosphorus acquisition. With this regard, in the haustorial transcriptome of *P. xanthii*, an annotated acid phosphatase and a predicted acid phosphatase, both candidates to be secreted and exclusively present in haustoria, were found among the top 50 expressed genes (see chapter III). Acid phosphatases catalyse the phosphomonoesters hydrolysis at acidic pH, being key elements in the release of inorganic phosphate from more complex molecules (Xia *et al.*, 2001). Phosphorus is essential for cell viability due to its huge importance in many biological processes such as ATP, phospholipids and nucleic acids synthesis as well as energy transfer, protein activation and regulation, control of gene activity or amino acid and carbon metabolic processes (Li *et al.*, 2010). Considering the essential role of phosphorus for life, in this work we have analysed the role of those two putative acid phosphatases of *P. xanthii* by



different molecular approaches. Our results indicate that these enzymes are key proteins for fungal development and appear as potential targets for the development of novel antifungal phytotherapies.

## MATERIAL AND METHODS

### *Plants, fungi, bacteria and culture conditions*

*Podospaera xanthii* isolate 2086 was cultured on disinfected cotyledons of zucchini (*Cucurbita pepo* L.) cv. Negro Belleza (Semillas Fitó, Barcelona, Spain) and was maintained in 8 cm Petri dishes with Bertrand medium at 24 °C under a 16 h light/8 h dark cycle (Álvarez and Torés, 1997). The isolate was maintained at -80 °C until use. Melon plants (*Cucumis melo* L.) cv. Rochet (Semillas Fitó, Barcelona, Spain), were cultivated in a growth chamber at 24 °C under a 16 h light/8 h dark cycle and used in gene silencing experiments. *Agrobacterium tumefaciens* strain C58C1 also used in gene silencing assays was grown in LB medium at 28 °C supplemented with rifampicin (50 µg·mL<sup>-1</sup>) and spectinomycin (100 µg·mL<sup>-1</sup>) when required. *Escherichia coli* strain DH5α was used for vector construction and propagation and was grown in LB medium at 37 °C, adding ampicillin (100 µg·mL<sup>-1</sup>), spectinomycin (100 µg·mL<sup>-1</sup>) or kanamycin (50 µg·mL<sup>-1</sup>) when required. *Saccharomyces cerevisiae* strain EY57 and strain EY157 (courtesy of Prof. Dennis Wykoff, Villanova University, PA, USA) were used in yeast complementation experiments and were grown in YNB without uracil and supplemented with 2 % glucose, 1% raffinose or 2% galactose when required.

### *Protein modelling, sequence and phylogenetic analyses*

From the previously predicted *P. xanthii* haustorial secretome (see chapter III), one unigene that was annotated as repressible acid phosphatase (15569) and a second unigene (PHEC689) that was annotated without known function but with a predicted protein model with high analogy to an *Aspergillus niger* acid phosphatase, were selected. SignalP 4.1 server (Petersen *et al.*, 2011) was used to analyse the signal peptide and select the mature protein sequences. 3D models of PHEC689 and 15569 were performed using I-TASSER (Zhang, 2008) and were compared with the crystal model of *A. niger* acid phosphatase protein (1QFX) obtained from Protein Data Bank (PDB). Chimera software (Pettersen *et al.*, 2004) was used to develop a structural alignment of predicted protein models with the crystallised acid phosphatase from *A. niger*. Alignments of amino acids sequences from mature proteins were conducted by Clustal Omega software (Sievers and Higgins, 2014) and the protein motifs were predicted by MotifScan (Pagni *et al.*, 2007). To determine the presence of putative orthologous genes in other fungi, a BLASTp analysis was carried out using the amino acid sequences of PHEC689 and 15569 as query sequences.

### *DNA and RNA isolation and cDNA synthesis*

From infected melon cotyledons, genomic DNA was extracted using the Epicentre MasterPure™ Yeast DNA Purification Kit (Epicentre, Madison, WI, USA) and total RNA was isolated using TRI Reagent (Sigma-Aldrich, Saint Louis, MO, USA), according to the manufacturer's instructions. The quantification of total RNA was carried out using a NanoDrop 2000 spectrophotometer (Thermo Fisher Scientific, Waltham, MA, USA). The cDNA synthesis was performed using Superscript III Reverse Transcriptase (Thermo

Fisher Scientific) with random primers (Thermo Fisher Scientific), according to the manufacturer's recommendations.

### *Plasmids used and construction of gene silencing and expression vectors*

The plasmids used in this study are listed in Table 4.1 and depicted in Figure 4.1. For gene silencing experiments, the plasmid pB7GWIWG2(II) (Karimi *et al.*, 2002) was used to construct the different gene silencing vectors. The plasmid pGWB2 (Nakagawa *et al.*, 2007) was used as a negative control (empty vector) and the plasmid pCmMlo1-RNAi (Martínez-Cruz *et al.*, 2018a) was used as a positive control. These plasmids carry the T-DNA region under the control of the cauliflower mosaic virus (CaMV) 35S promoter (Figure 4.1). For the construction of gene silencing vectors, the Gateway system (Thermo Fisher Scientific) was used. First, fragments of *PHEC689* and *15569* were amplified from cDNA, previously obtained as described above, using specific primers with attB1 or attB2 tails (Table 4.2). Subsequently, these PCR amplicons were re-amplified with complete attB1 or attB2 primers (Table 4.2) to add the complete tails necessary to clone the PCR fragments in pDONR207 donor vector (Thermo Fisher Scientific) through the BP reaction using the manufacturer's indications (Thermo Fisher Scientific). After, the gene fragments contained into pDONR207 vectors were integrated into pB7GWIWG2(II) plasmid through the LR reaction according the manufacturer's recommendations (Thermo Fisher Scientific). The resulting silencing plasmids pPHEC689-RNAi and p15569-RNAi were checked by PCR amplification and sequencing. These plasmids were constructed, propagated and maintained into *E. coli* DH5 $\alpha$ . Finally, for gene silencing experiments, the plasmids were introduced by electroporation into *A. tumefaciens* C58C1.

**Table 4.1.** Plasmids used in this study

Plasmid <sup>a</sup>	Characteristics <sup>b</sup>	Reference
pGWB2	Empty vector. Negative control for gene silencing experiments.	Nakagawa <i>et al.</i> , 2007
pCmMlo1-RNAi	Positive control for gene silencing experiments. Silencing vector containing a RNA hairpin with a 412 bp fragment of <i>CmMlo1</i> .	Martínez-Cruz <i>et al.</i> , 2018
pPHEC689-RNAi	Silencing vector containing a RNA hairpin with a 360 bp fragment of <i>PHEC689</i> .	This study
p15569-RNAi	Silencing vector containing a RNA hairpin with a 337 bp fragment of <i>15569</i> .	This study
pYES-DEST52-689	Yeast expression vector carrying the complete ORF of <i>PHEC689</i> with SP and stop codon.	This study
pYES-DEST52-15569	Yeast expression vector carrying the complete ORF of <i>15569</i> with SP and stop codon.	This study

<sup>a</sup>RNAi= RNA interference

<sup>b</sup>SP = Secretion signal peptide

For yeast *in vivo* complementation experiments, the yeast expression vector pYES-DEST52 (Thermo Fisher Scientific) was used. In this case, the complete *PHEC689* and *15569* gene sequences with signal peptide were amplified from previously synthesized cDNA using the specific primers with attB1 or attB2 tails (Table 4.2). Next, these PCR amplicons were integrated into pDONR207 donor vector through the BP reaction and, subsequently, into pYES-DEST52 destination vector through the LR reaction as described above. The resulting yeast expression vectors pYES-DEST52-689 and pYES-DEST52-15569 were verified by PCR amplification and sequencing. These plasmids were constructed, propagated and maintained into *E. coli* DH5 $\alpha$ . To perform the yeast complementation experiments, these vectors were introduced into the strain *Saccharomyces cerevisiae* EY132 by electroporation.

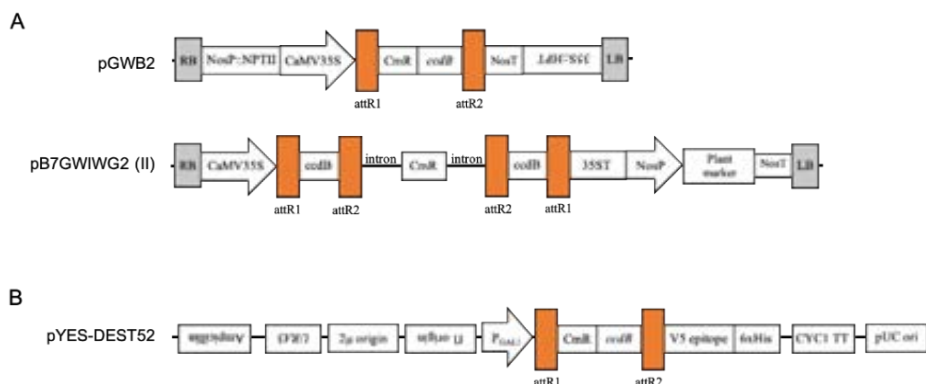


**Figure 4.1.** Graphic representation of destination Gateway vectors used for construction of silencing vectors and yeast expression vectors. Promoters are indicated as arrows. The flipped names indicate the gene localization in complementary strand. A) T-DNA region of gateway destination vectors used in gene silencing experiments. pGWB2 was used as a negative control (empty vector) and pB7GWIWG2 (II) was used to construct pPHEC689-RNAi and p15569-RNAi silencing vectors. LB: left border of T-DNA; RB: right border of T-DNA; NosP::NPTII: kanamycin resistance marker; CaMV35S: Cauliflower mosaic virus 35S promoter; attR1 and attR2: recombination sites for LR reaction; CmR: chloramphenicol resistance marker; *ccdB*: lethal gene for negative selection in bacteria; NosT: nopaline synthase terminator; 35S::HPT: hygromycin B resistance marker; 35ST: 35S terminator; NosP: nopaline synthase promoter; Plant marker: glufosinate ammonium resistance marker. B) Yeast expression vector used in *in vivo* complementation experiments. Ampicillin: ampicillin resistance gene; *URA3*: *URA3* gene; 2μ origin: origin of DNA replication; fl origin: origin of DNA replication; P<sub>GAL1</sub>: *GAL1* promoter. V5 epitope: V5 tag from RNA polymerase alpha subunit of simian virus 5 for immunochemical analyses of tagged protein; 6xHis: His tag for protein purification; CYC1 TT: cytochrome c isoform 1 transcription termination region; pUC ori: pUC type origin of DNA replication.

### *Yeast complementation assay*

To test the functionality of PHEC689 and 15569 as acid phosphatases, an *on plate* yeast complementation assay was performed. For this assay, the full length

open reading frames of *PHEC689* and *15569* were cloned into the pYES-DEST52 yeast expression vector (Thermo Scientific) using the Gateway system and transformed into the *S. cerevisiae pho5* mutant strain EY132. This strain has a deletion in the endogenous acid phosphatase gene *pho5*, and exhibits very low levels of secreted acid phosphatase activity, being suitable for *in vivo* complementation of putative secreted acid phosphatases (Wykoff *et al.*, 2007). The *pho5* wild type strain EY57 was used as a positive control for secreted acid phosphatase. The yeast transformants with the corresponding constructs were plated onto yeast nitrogen base medium (YNB) with 2% glucose without uracil. Later, yeast transformant colonies were grown overnight in liquid YNB supplemented with 1% raffinose, centrifuged, washed and re-suspended in water. The optical density of the cell suspensions was then adjusted to an  $OD_{600nm}$  of 0.3 and serial dilutions were then spotted onto YNB agar plates supplemented with 2% galactose. After two days of incubation, the plates were covered with an agar overlay, based on the description provided by Toh-E & Oshima (1974) with some modifications, containing 0.5 mg/mL of 1-naphthyl phosphate, 1 mg/mL of Fast Blue Salt B stain and 1% agarose in 50 mM of glycine buffer (pH 3.0). Plates were incubated at 30° C in the dark until colonies developed a brown/orange colour.

#### *Agrobacterium tumefaciens mediated-host induced gene silencing (ATM-HIGS) assay*

To determine the essential role of *PHEC689* and *15569* for *P. xanthii* development, the ATM-HIGS assay recently described by Martínez-Cruz *et al.* (2018) was employed. Briefly, the silencing plasmids pPHEC689-RNAi and p15569-RNAi, the RNAi-positive control pCmMlo1-RNAi, and the negative

control pGWB2 (empty vector) were introduced into *A. tumefaciens* C58C1 by electroporation. Before agro-infiltration, *A. tumefaciens* derivatives were induced with 200  $\mu\text{M}$  of acetosyringone and were grown in 5 mL of LB medium with rifampicin (50  $\mu\text{g}/\text{mL}$ ) and spectinomycin (100  $\mu\text{g}/\text{mL}$ ) or tetracyclin (50  $\mu\text{g}/\text{mL}$ ) over night at 28 °C and 200 rpm in an orbital shaker. Then, the different bacterial cultures corresponding with the different silencing constructs were washed twice in washing buffer and 200  $\mu\text{M}$  of acetosyringone. Subsequently, the *A. tumefaciens* cells were incubated for 2 h in the same washing buffer at room temperature and without agitation in order to induce the Vir proteins. Last, the *Agrobacterium* cells were centrifuged 10 min at 4000 rpm and 28 °C, re-suspended in MES buffer and their  $\text{OD}_{600\text{nm}}$  were adjusted at 0.5-1.0 in the MES buffer. The agro-infiltration was performed using a 1-mL syringe without the needle. Injections were performed into abaxial surface of melon cotyledons with the different *Agrobacterium* suspensions. For co-silencing experiments, before agro-infiltration, equal volumes of the *Agrobacterium* cell suspensions carrying the pPHEC689-RNAi and p15569-RNAi silencing constructs were mixed. After agro-infiltration, the agro-infiltrated cotyledons were maintained in a growth chamber at 24 °C under a 16 h light/8 h dark cycle for 24 h. Finally, the agro-infiltrated cotyledons were pulverized with a fresh *P. xanthii* conidial suspension ( $1 \cdot 10^5$  conidia  $\text{mL}^{-1}$ ) and maintained under the same conditions until analysis.

### *RT-qPCR and qPCR*

The analysis of expression pattern, the quantification of gene expression after silencing as well as the molecular estimation of *P. xanthii* biomass, were carried out by qPCR. The primers pairs used for these purposes were designed

using Primer3 software (Koressaar and Remm, 2007; Thornton and Basu, 2011) and are listed in Table 4.2. For gene expression analysis, total RNA from infected zucchini cotyledons or from agro-infiltrated and infected melon cotyledons was extracted and used to synthesize the cDNA as described above. The RT-qPCR reactions were conducted in a CFX384 Touch Real-Time PCR detection system (Bio-Rad, Hercules, CA, USA) using SsoFast EvaGreen Supermix (Bio-Rad) according to the manufacturer's instructions. The *P. xanthii* elongation factor-1 gene (MK249653) was used as a normalization reference gene (Zarivi *et al.*, 2015). For molecular estimation of *P. xanthii* biomass, total DNA from agro-infiltrated and infected melon cotyledons was isolated as described above. The qPCR reactions were carried out using SsoFast EvaGreen Supermix according to the manufacturer's instructions in a CFX384 Touch Real-Time PCR detection system. The *P. xanthii*  $\beta$ -tubulin gene (KC333362) and the *C. melo* actin gene (XM\_008462689.2) were used for this quantification. The ratio between *P. xanthii* and *C. melo* genomic DNA was calculated as described by Vela-Corcía *et al.* (2016). The conditions of both, RT-qPCR and qPCR, reactions were as follows: enzyme activation step for 30 s at 95 °C followed by 40 cycles at 95 °C for 5 s and 65 °C for 5 s. The data obtained after amplification were analysed using CFX Manager Software (Bio-Rad). Additionally, the amplicon sizes were confirmed by visualization on 2% agarose gels.



**Table 4.2.** Primers used in this study

Primer name	Sequence
Plasmid construction	
689si-F	5'- <u>AAAAAGCAGGCTCT</u> TCCACCTTCCGATGCTGATG-3'
689si-R	5'- <u>AGAAAGCTGGGTG</u> TACCGTGCCTTCGGATGATG-3'
15569si-F	5'- <u>AAAAAGCAGGCTCT</u> ATGGCGTTGAATATGGAGGG-3'
15569si-R	5'- <u>AGAAAGCTGGGTG</u> TGGATCGTAGGCCAGCTGAC-3'
689yeast-F	5'- <u>AAAAAGCAGGCTCT</u> ATGTATACTTTCGACCCATTG-3'
689yeast-R	5'- <u>AGAAAGCTGGGTG</u> TAA GTCGTTATAGATGGTCAGATG-3'
15569yeast-F	5'- <u>AAAAAGCAGGCTCT</u> ATGGAGTATGTCAGCCTTCTT-3'
15569yeast-R	5'- <u>AGAAAGCTGGGTG</u> TAA GGATAATCTGCCATCATAGTC-3'
attb1	5'-GGGGACAAGTTTGTACAAAAAAGCAGGCT-3'
attb2	5'-GGGGACCACTTTGTACAAGAAAGCTGGGT-3'
Gene expression analysis	
689q-F	5'-AGGAACTGATGGAAGCGAAGA-3'
689q-R	5'-GAGCCGCGTAGAACAGTTTC-3'
15569q-F	5'-TTCCGACTGTTCAACCCTTC-3'
15569-R	5'-GGCGAGTTGCAACCAATAGT-3'
Molecular estimation of fungal growth	
Tubg-F	5'-TTGTAGGAATCACATCCCTTTCTC-3'
Tubg-R	5'-TTCTTCCGTTGCATGGGTGGTTC-3'
Acting-F	5'-GGCTGGATTGCCGGTGATGATGC-3'
Acting-R	5'-GGAAGGAGGAAATCAGTGTGAACC-3'

<sup>a</sup> Underlined sequences correspond to the attb1 or attb2 primers adapter

### *Visualization of fungal development and reactive oxygen species, and haustorial count*

The histochemical detection of the accumulation of hydrogen peroxide (H<sub>2</sub>O<sub>2</sub>) by the 3,3'-diaminobenzidine (DAB) method (Thordal-Christensen *et al.*, 1997) was used to analyze the activation of plant responses as well as to visualize fungal growth and quantify the formation of haustoria after gene

silencing (Martínez-Cruz *et al.*, 2018). Briefly, discs of 1 cm diameter were taken from agro-infiltrated melon cotyledons at 24, 48 and 72 h after inoculation with *P. xanthii* and incubated over night with 1 mg/ mL of DAB (pH 3.8) (Sigma-Aldrich) at room temperature in dark. Subsequently, the discs were decoloured in boiling ethanol and examined under a Nikon Eclipse E800 light microscope searching for brown hyphae and black spots, which correspond to haustoria, and brown-red precipitates in epidermal cells, which correspond to H<sub>2</sub>O<sub>2</sub> accumulation.

#### *Inhibitor sensitivity assay*

To test the ability of certain acid phosphatases inhibitors, such as sodium fluoride, L(+)-tartaric acid, sodium orthovanadate and ammonium molybdate (Arnold *et al.*, 1987; Lovelace *et al.*, 1997; Ullah *et al.*, 2011; Srivastava and Anand, 2015), to suppress *P. xanthii* development, the fungicide sensitivity assay previously described by Fernández-Ortuño *et al.* (2006) was used. Essentially, discs of 1-cm diameter from zucchini cotyledons previously disinfected were obtained. Next, the discs were submerged into the solutions of the different compounds for 1 h and subsequently placed in 8 cm Petri dishes in Bertrand medium at room temperature until the complete drying. Finally, the treated cotyledons were inoculated with a 5- $\mu$ L drop of a *P. xanthii* conidial suspension ( $1 \times 10^5$  mL<sup>-1</sup>) and incubated at 16 h light/ 8 dark cycle at 24 °C for 10 days. Water was used as a negative control for *P. xanthii* inhibition. Each compound and concentration was tested in triplicate in 8 cm Petri dishes with Bertrand medium containing eight cotyledon discs. After incubation, pictures from each individual disc were taken and processed by Fiji image software and *P. xanthii* growth was recorded as the total pixels occupied by the *P. xanthii*

colonies. Results were expressed as percentages of disease reduction relative to water control.

### *Statistical analysis*

When required the data were statistically analysed by Fisher's least significant difference (LSD) test using IBM SPSS v20 (SPSS, Chicago, IL, USA).

## **RESULTS**

### *PHEC689 and 15569 share predicted protein models but do not share sequence identity*

The amino acid sequences from PHEC689 and 15569 proteins were obtained from Full-LenghterNext annotation of exclusive *P. xanthii* haustorial secretome. The signal peptides were removed in order to work with the mature sequence of both proteins. The proteins were modelled using I-TASSER and their predicted models were structural aligned with the crystal model of *A. niger* acid phosphatase (1QFX) showing that both models were very similar to each other and highly similar to the *A. niger* acid phosphatase (Figure 4.2). However, the alignment of amino acid sequences showed that these proteins did not share sequence identity, although the domain prediction revealed the presence of a conserved histidine acid phosphatase domain in PHEC689 (amino acids 34 - 377), in 15569 (amino acids 42 - 452) and acid phosphatase from *A. niger* (amino acids 53 - 385), as well as the presence of conserved catalytic residues

in all sequences (Figure 4.3), supporting the putative acid phosphatase function for PHEC689 and 15569 proteins.

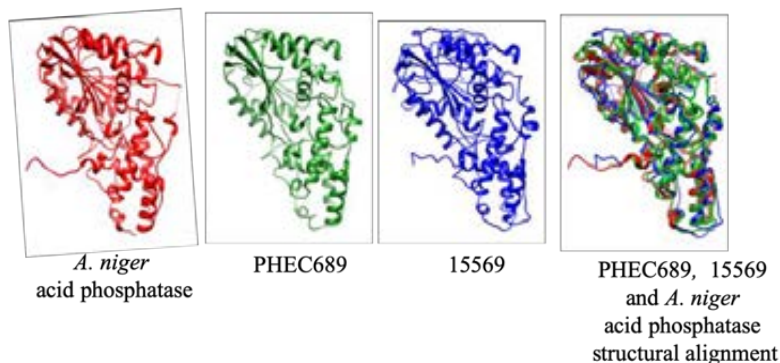


**Figure 4.2.** Comparison of PHEC689 and 15569 predicted models with the *Aspergillus niger* acid phosphatase protein. The *A. niger* acid phosphatase 3D model corresponds to the crystal 1QFX obtained from Protein Data Bank (PDB).

### *PHEC689 and 15569 are secreted acid phosphatases*

In order to validate their function as putative secreted acid phosphatases, PHEC689 and 15569 were expressed in the *S. cerevisiae* strain EY132, which is a yeast mutant deficient in the endogenous secreted acid phosphatase PHO5. The results of the yeast complementation assay for extracellular acid phosphatase activity showed that strain EY132 transformed with the expression plasmids pYES-DEST52-689 (EY132::PHEC689) and pYES-DEST52-15569 (EY132::15569) presented such activity at similar levels than the wild type strain (EY57) under the same conditions (Figure 4.4). In addition, the *on plate* assay confirmed that both proteins were secreted to the medium, confirming the functionality of their putative N-terminal secretion peptides. According to these results, PHEC689 and 15569 were re-named as PxSHAP1 and PxSHAP2, respectively (*P. xanthii* secreted haustorial acid phosphatase 1 and 2).

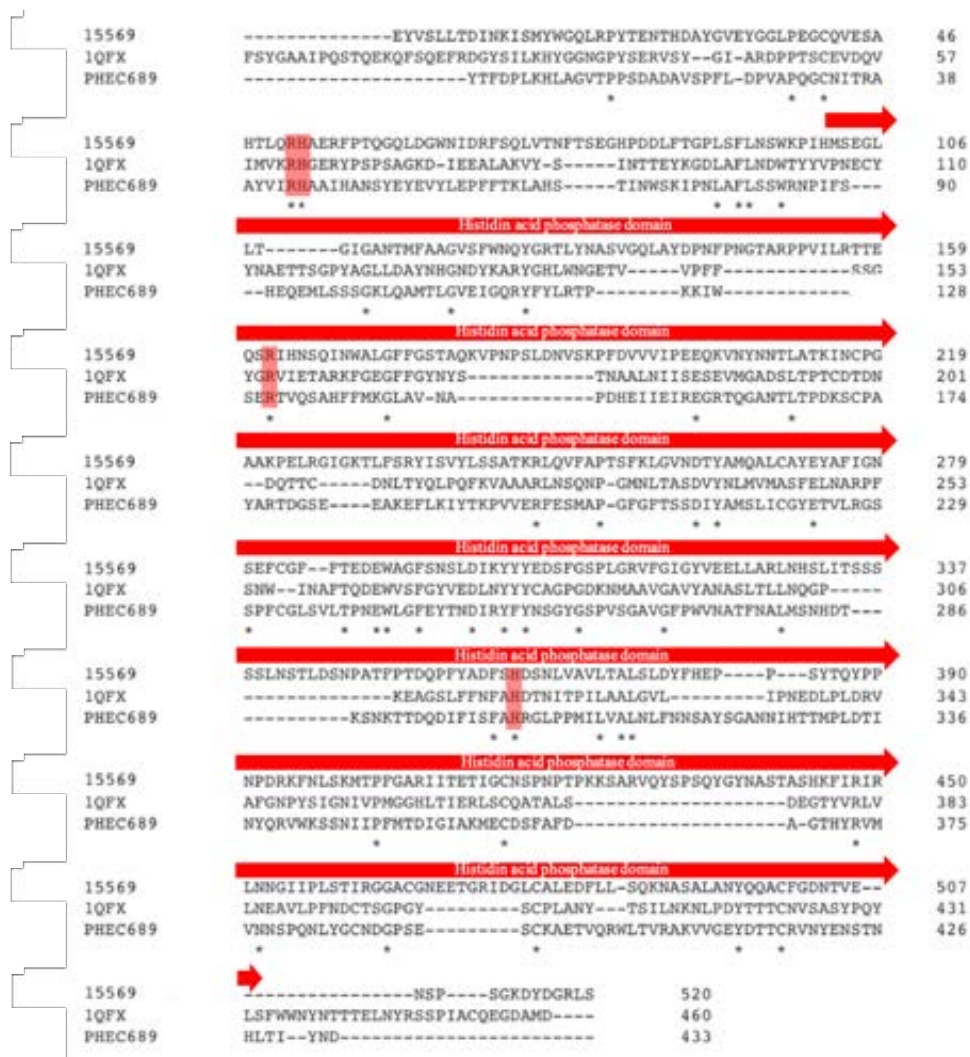


**Figure 4.3.** Comparison of the amino acid sequences from PHEC689, 15569 and *A. niger* acid phosphatase (1QFX) mature proteins. Conserved amino acids are indicated by asterisks and conserved catalytic residues are indicated by red boxes. Histidine acid phosphatase domain is marked with a red arrow. The comparison was carried out by Clustal Omega.

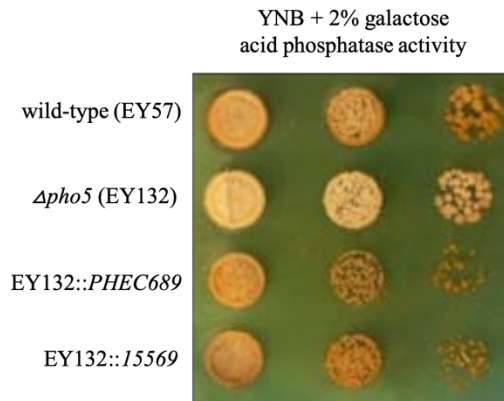


**Figure 4.4.** Yeast complementation assay for secreted acid phosphatase activity. PHEC689 and 15569 were expressed in EY132, a yeast acid phosphatase deficient mutant. The *S. cerevisiae* wild-type EY57 was used as a positive control for secreted acid phosphatase and *S. cerevisiae* EY132, deficient in *pho5* secreted acid phosphatase, was used as a negative control. The YNB medium was overlaid with 0.5 mg/mL of 1-naphthyl phosphate, 1 mg/mL of Fast Blue Salt B stain and 1% agarose in 50 mM of glycine buffer (pH 3.0) to detect acid phosphatase activity. The secreted acid phosphatase activity was shown as a brown/orange colour in the yeast colonies.

#### *PxSHAP1 and PxSHAP2 are key enzymes for P. xanthii development*

The high relative expression of *PxSHAP1* and *PxSHAP2* genes (Figure 4.5A), which were found among the top 25 most expressed genes in haustoria (see chapter III), suggested an important role of the corresponding coding proteins in the development of *P. xanthii*. Therefore, their precise role was determined by gene silencing experiments using the *A. tumefaciens*-mediated host-induced gene silencing (ATM-HIGS) assay. To check the efficacy of the ATM-HIGS system to reduce the expression levels of *PxSHAP1* and *PxSHAP2* during the individual gene silencing and co-silencing experiments, transcript levels were quantified by RT-qPCR. For both genes, the decrease in transcript

levels was around 50% in both individual gene silencing and co-silencing experiments (Figure 4.5B).

In these assays we first evaluated the visible symptoms of powdery mildew in melon cotyledons 10 days after the inoculation with *P. xanthii* conidia of agro-infiltrated cotyledons with the silencing constructs (Figure 4.6). The silencing of *PxSHAP1* and *PxSHAP2* resulted in a clear negative impact on *P. xanthii* development, since the cotyledons agro-infiltrated with silencing constructs showed more areas without powdery mildew symptoms than the cotyledons agro-infiltrated with the empty vector (negative control), and similar to the gene silencing positive control, the silencing of melon *CmMlo1* gene. The impact on powdery mildew symptoms was even more evident when *PxSHAP1* and *PxSHAP2* were co-silenced, being the reduction of the powdery mildew symptoms clearly higher than that of the silencing of individual genes (Figure 4.6).

Besides the symptoms, the fungal growth was analysed in terms of haustorial counting (number of haustoria per mm<sup>2</sup> as indicator of *P. xanthii* development) using the DAB-method for the histochemical analysis of the production of hydrogen peroxide as previously described by Martínez-Cruz *et al.*, (2018) (Figure 4.7, Figure 4.8, Figure 4.9). As shown Figure 4.7, the number of *P. xanthii* haustoria in the first steps of infection decreased after the individual silencing of *PxSHAP1* and *PxSHAP2* genes, being this decrease even higher than the RNAi positive control (*CmMlo1* gene). In the case of the co-silencing of *PxSHAP1* and *PxSHAP2* genes, the effect observed was even more evident, displaying a considerable decrease in the number and the size of haustoria, also revealing the huge difficulties of *P. xanthii* to develop the secondary hyphae. Figure 4.8 shows a general vision of *P. xanthii* development when the growth reduction was more evident. At 72 h after inoculation of agro-infiltrated

cotyledons with a mixture of *PxSHAP1* and *PxSHAP2* silencing constructs, *P. xanthii* development was considerably arrested, showing small colonies with a low number of haustoria and a reduced size compared to cotyledons infiltrated with the empty vector.

The number of haustoria per square millimeter in agro-infiltrated melon cotyledons inoculated with *P. xanthii* was counted after DAB staining and graphically represented as an estimation of fungal biomass (Figure 4.9). The individual silencing of *PxSHAP1* and *PxSHAP2* genes caused a reduction in fungal growth similar to *CmMlo1* silencing (positive control), with a less number of haustoria number at 48 and 72 h after inoculation than negative control (empty vector). In the case of the co-silencing of *PxSHAP1* and *PxSHAP2* genes, as expected, the reduction in the haustoria number was even higher than in the individual silencing experiments, showing a decrease of around twice compared to the silencing of *CmMlo1* and about 5 times compared to the empty vector.



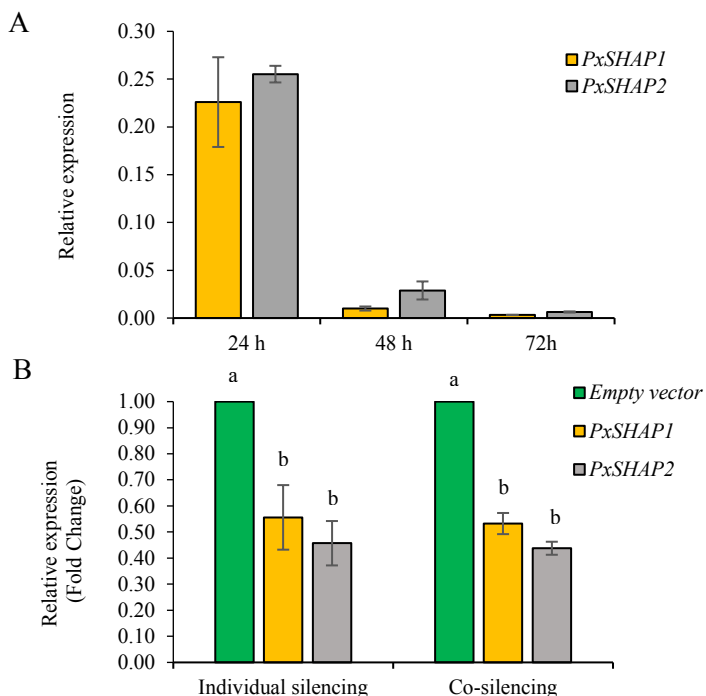


**Figure 4.5.** Expression analyses of *PxSHAP1* and *PxSHAP2* determined by RT-qPCR A) Expression pattern analysis of *PxSHAP1* and *PxSHAP2* during the first step of fungal development. Total RNA was isolated from zucchini cotyledons inoculated with *P. xanthii* at 24, 48 and 72 h post-inoculation. The change in gene expression levels was represented as the relative expression against transcription of *P. xanthii* elongation factor 1 gene *PxEF1* (MK249653). B) Efficacy of ATM-HIGS system for silencing of *PxSHAP1* and *PxSHAP2* genes. Total RNA was isolated from agro-infiltrated melon cotyledons 24 h after inoculation with *P. xanthii*. The change in gene expression levels was represented as fold change between silencing construct and empty vector sample pairs after normalization to the expression of *PxEF1* (MK249653). Bars indicate the standard error of three different experiments with three technical replicates. Bars with different letter are significantly different at  $P=0.05$  according to Fisher's least significant difference test (LSD).

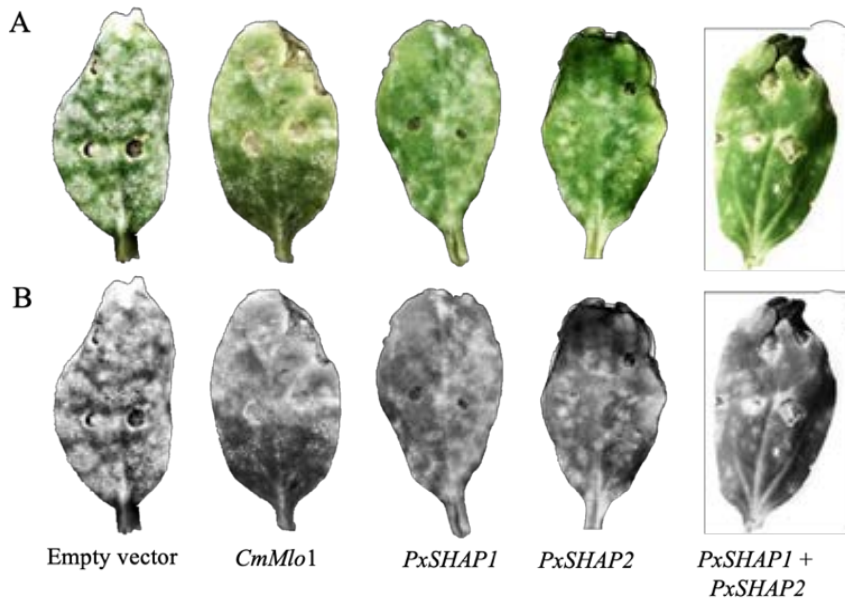


**Figure 4.6.** Effect of silencing of *PxSHAP1* and *PxSHAP2* genes on powdery mildew symptom development. Gene silencing was performed using *A. tumefaciens*-mediated host-induced gene silencing (ATM-HIGS). Melon cotyledons were agro-infiltrated with the different constructs, empty vector (negative control), pCmMlo1-RNAi (*CmMlo1*, RNAi-induced gene silencing positive control), pPHEC689-RNAi (*PxSHAP1*) and p15569-RNAi (*PxSHAP2*) or with a mixture of the latest (*PxSHAP1* and *PxSHAP2*). Pictures were taken 10 days after inoculation of *P. xanthii*. A) Colour pictures showing powdery mildew symptoms. B) Same pictures in grey scale for a better visualization of powdery mildew growth.

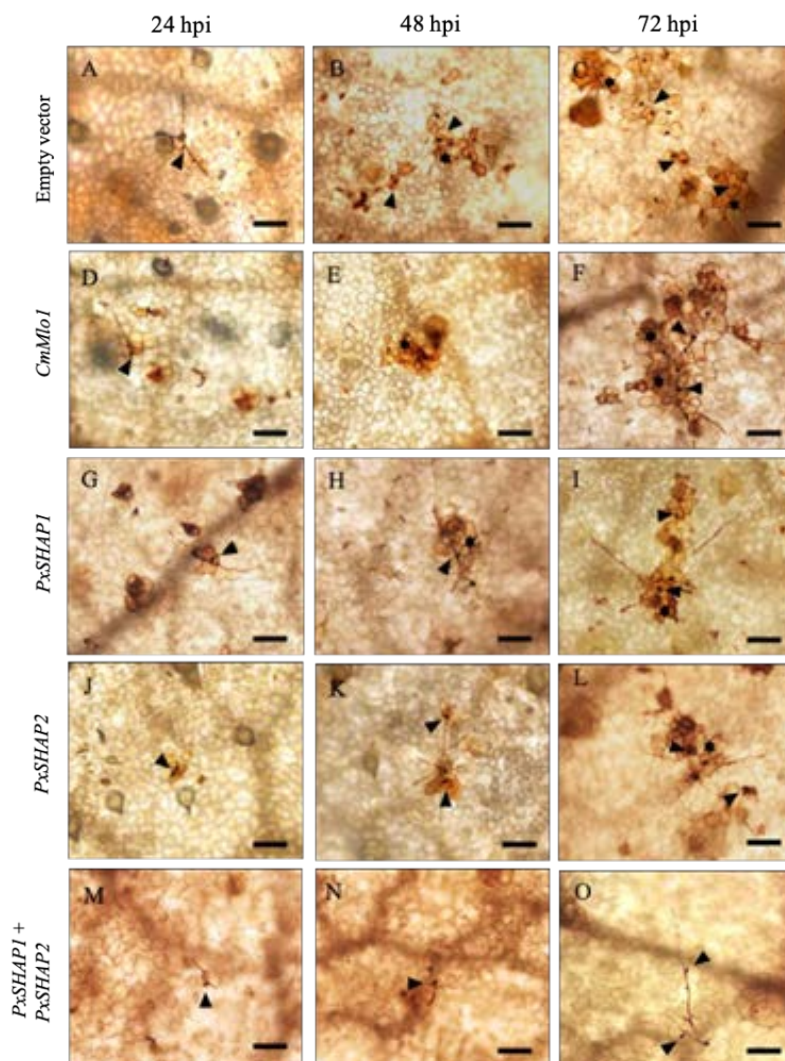


**Figure 4.7.** Time-lapse microscopy of first infection structures of *P. xanthii* after silencing of *PxSHAP1* and *PxSHAP2* genes. Empty vector was used as negative control and silencing of melon *CmMlo1* gene was used as a positive control. Arrowheads indicate penetration points corresponding with haustoria and asterisks indicate epidermal cells with accumulation of hydrogen peroxide. Bars = 100  $\mu$ m.

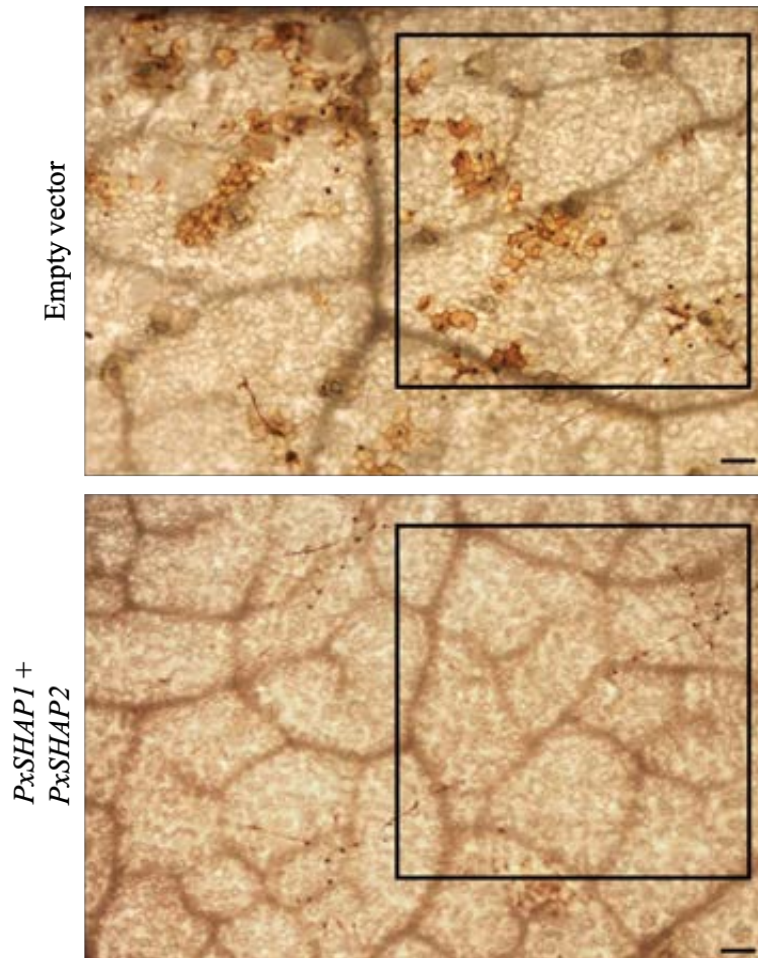


**Figure 4.8.** General view of *P. xanthii* development 72 h after co-silencing of *PxSHAP1* and *PxSHAP2* genes compared to empty vector control. Black squares indicate the surface of 1 square millimeter of melon cotyledon. Bars = 100  $\mu$ m.

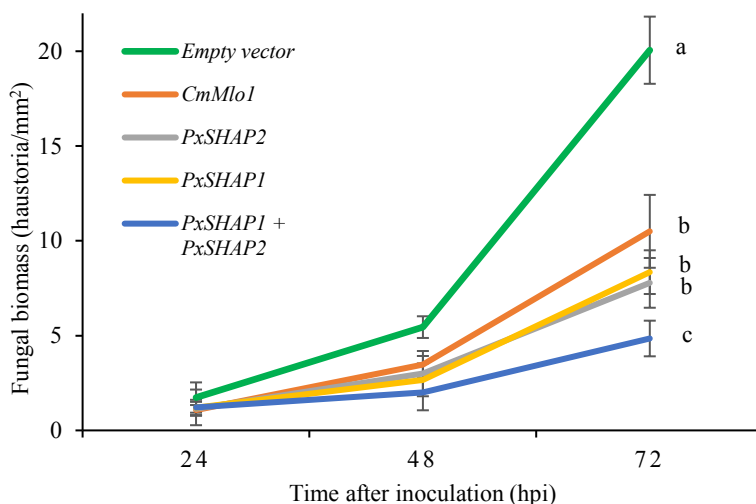


**Figure 4.9.** Analysis of the effect of silencing of *PxSHAP1* and *PxSHAP2* genes on fungal growth in terms of formation of *P. xanthii* haustoria. RNA interference (RNAi) silencing was performed using ATM-HIGS and the haustorial count was carried out in the discs prepared for H<sub>2</sub>O<sub>2</sub> detection. As a negative control the same vector used for RNAi silencing was employed without insert (empty vector). As a positive control for RNAi-induced resistance, the RNAi silencing of the melon *CmMlo1* gene was used. The estimation of fungal biomass is expressed as the number of haustoria per square millimeter of agro-infiltrated tissue. Values represent the mean values of 30 samples from three independent experiments. Bars indicate the standard error. Values with the same letter are not significantly different at  $P=0.05$  according to Fisher's least significant difference test (LSD).

Last, *P. xanthii* development was also measured using a molecular estimation method of fungal biomass based on qPCR (Figure 4.10). For this purpose, genomic DNA from agro-infiltrated melon cotyledons 72 h after inoculation with *P. xanthii*, was isolated and quantified as *P. xanthii* tubulin/*C. melo* actin ratio. This molecular approach corroborated the data obtained by haustorial counts, showing a strong reduction of *P. xanthii* development after

individual and, specially, after co-silencing of *PxSHAP1* and *PxSHAP2* genes (Figure 4.10).

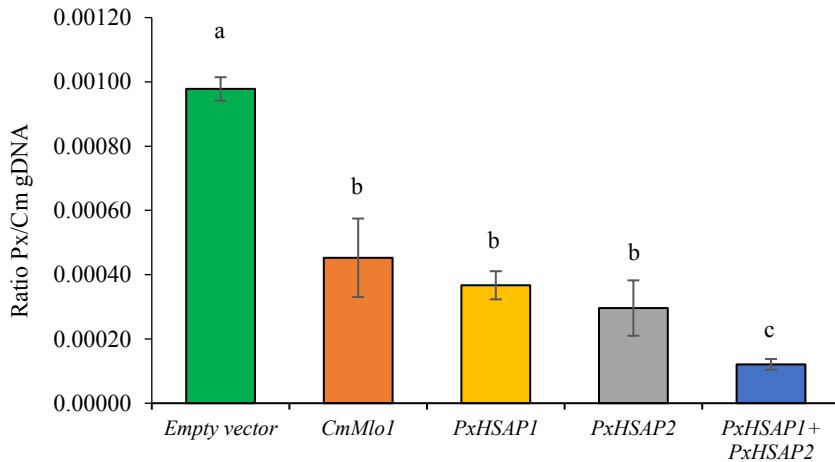


**Figure 4.10.** Analysis of the effect of silencing of *PxSHAP1* and *PxSHAP2* genes on fungal growth. A molecular estimation of *P. xanthii* growth by qPCR is shown. RNA interference (RNAi) silencing was performed using ATM-HIGS. As a negative control the same vector used for RNAi silencing was employed without insert (empty vector). As a positive control for RNAi-induced resistance RNAi silencing of the melon *CmMlo1* gene was used. DNA from agro-infiltrated melon cotyledons was isolated 72 h after inoculation of *P. xanthii*. Fungal biomass is expressed as the ratio of *P. xanthii* to melon cotyledon genomic DNA (ratio Px/Cm gDNA) determined by qPCR using the primers listed in Table 4.3 to amplify *P. xanthii*  $\beta$ -tubulin and *C. melo* actin genes. Bars indicate the mean  $\pm$  standard error of three DNA samples, with three technical replicates from three different cotyledons. Bars with different letter are significantly different at  $P=0.05$  according to Fisher's least significant difference test (LSD).

The haustorial counts corresponding to 72 h after inoculation (Figure 4.9) and the molecular estimation of fungal biomass at the same time point (Figure 4.10) were used to calculate the percentages of reduction of fungal growth produced by the silencing of *PxSHAP1* and *PxSHAP2* genes (Table 4.3). The

percentage of fungal growth reduction obtained by both approaches was certainly similar, although the molecular approach showed growth reductions slightly higher in all cases. The reductions obtained were around 60% when *PxSHAP1* and *PxSHAP2* were individually silenced and around 80% when the genes were co-silenced, demonstrating the key role of these genes in *P. xanthii* development.

**Table 4.3.** Effect of silencing of *PxSHAP1* and *PxSHAP2* genes on fungal development

Silenced gene	Microscopic estimation <sup>a</sup>		Molecular estimation <sup>a</sup>	
	Number of haustoria <sup>b</sup>	Reduction (%) <sup>c</sup>	<i>P. xanthii</i> / <i>C. melo</i> <sup>d</sup>	Reduction (%) <sup>c</sup>
Empty vector (negative control)	20.05 ± 1.77 a <sup>e</sup>	-	0.00098 ± 3.634E-5 a	-
<i>CmMlo1</i> (positive control)	9.96 ± 1.92 b	50.32	0.00045 ± 1.222E-4 b	54.08
<i>PxSHAP1</i>	8.35 ± 1.15 b	58.35	0.00037 ± 4.379E-5 b	62.24
<i>PxSHAP2</i>	7.78 ± 1.31 b	61.19	0.00030 ± 8.619E-5 b	69.39
<i>PxSHAP1</i> + <i>PxSHAP2</i>	4.85 ± 0.94 c	75.81	0.00012 ± 1.684E-5 c	87.75

<sup>a</sup> Fungal growth data were recorded 72 h after inoculation of *P. xanthii*.

<sup>b</sup> Data show the mean number of haustoria from 30 samples from three different experiments ± standard error.

<sup>c</sup> Percentage of fungal growth reduction achieved by the silencing of *PxSHAP1* and *PxSHAP2* genes referred to values obtained with empty vector (negative control).

<sup>d</sup> Data indicate the mean ± standard error of *P. xanthii* / *C. melo* genomic DNA ratio of three samples with three technical replicates from three different cotyledons.

<sup>e</sup> Values with different letter indicate significant differences at  $P=0.05$  according to Fisher's least significant difference test (LSD).

*Silencing of PxSHAP1 and PxSHAP2 genes have no effect in the release of reactive oxygen species by the host*

In parallel to haustorial counts, the same DAB histochemical analysis was used to determine the accumulation of hydrogen peroxide ( $H_2O_2$ ) in melon cotyledon epidermal cells as an estimation of the activation of plant defense responses. This quantification was performed at 24, 48 and 72 h after inoculation of *P. xanthii* on melon cotyledons previously agro-infiltrated with the silencing constructs. The plant cells with hydrogen peroxide accumulation were visualized under a light microscope as brown-red precipitates (Figure. 4.7, asterisks) and then counted and graphically represented (Figure 4.11).

The accumulation of hydrogen peroxide in melon epidermal cells inoculated with *P. xanthii* after silencing of individual *PxSHAP1* and *PxSHAP2* genes did not show significantly differences over time compared to the cotyledons agro-infiltrated with the empty vector. In the case of the co-silencing of *PxSHAP1* and *PxSHAP2* genes, a significantly decrease in accumulation of reacting cells compared to empty vector and *CmMlo1* (positive control) was observed, which is a consequence of the strong reduction of fungal growth.



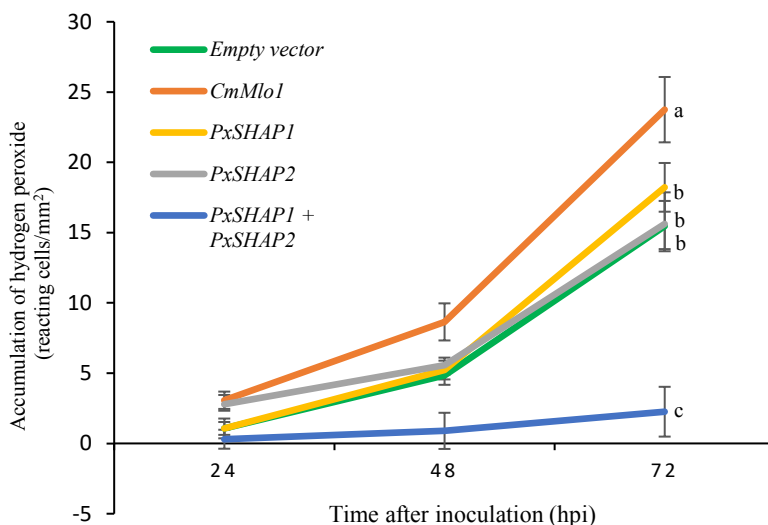


**Figure 4.11.** Time course analyses of accumulation of hydrogen peroxide in epidermal cells of melon cotyledons in response to *P. xanthii* after silencing *PxSHAP1* and *PxSHAP2* genes. RNA interference (RNAi) silencing was performed using ATM-HIGS. As a negative control the same vector used for RNAi silencing was employed without insert (empty vector). As a positive control for RNAi-induced resistance RNAi silencing of the melon *CmMlo1* gene was used. The epidermal cells with accumulation of hydrogen peroxide were identified as containing brow-red precipitates (asterisks in Figure 4.6). Data indicate the mean of 30 samples from three different experiments. Bars represent  $\pm$  standard error. Values with the same letter are not significantly different at  $P=0.05$  according to Fisher's least significant difference test (LSD).

#### *Treatments with acid phosphatase inhibitors arrested P. xanthii growth*

Since the silencing of *PxSHAP1* and *PxSHAP2* genes had a great impact on fungal growth, we wondered whether applications of enzyme inhibitors to inoculated plant tissues should also result in reductions of fungal growth. Several acid phosphatase inhibitors such as sodium fluoride, L(+)-tartaric acid, sodium orthovanadate and ammonium molybdate were tested using a leaf disc assay in order to determine their abilities to suppress *P. xanthii* development

(Figure 4.12). In the case of sodium fluoride, the compound showed a phytotoxic activity at the assayed concentrations. For its part, L-(+) tartaric acid inhibited fungal growth, causing percentages of disease reduction of 59.45% and 95.38% at 10 mM and 20 mM, respectively (Table 4.4). Ammonium molybdate and sodium orthovanadate showed the strongest fungicidal activity, reaching in both cases percentages of disease reduction of 100% at 5 mM (Table 4.4). At 1 mM, ammonium molybdate exhibited a better performance, reducing the disease by 88% compared to 61.87% of disease reduction caused by sodium orthovanadate (Table 4.4).

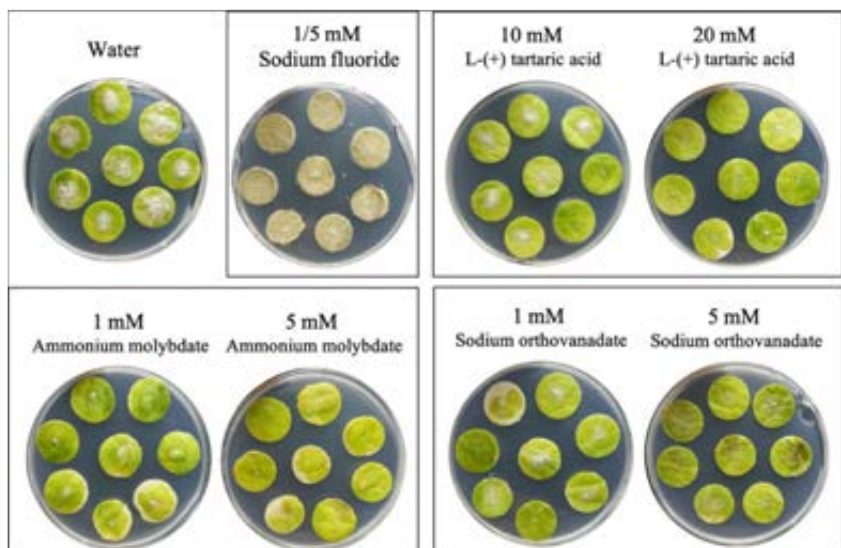


**Figure 4.12.** Fungicidal effect of acid phosphatase inhibitors on *P. xanthii* development. Zucchini cotyledon discs were treated for 1 h with the different inhibitors at different concentrations and *P. xanthii* conidia were inoculated after the complete drying. Water was used as a negative control for fungicidal activity. Pictures were taken 10 days after inoculation and used for disease quantification.

**Table 4.4.** Quantification of fungicidal effect of acid phosphatase inhibitors on *P. xanthii* development.

Treatment	Concentration	Leaf surface covered by powdery mildew (Number of square pixels) <sup>a</sup>	Disease reduction (%) <sup>b</sup>
Water	-	38306.38 ± 652.31 a <sup>c</sup>	-
L-(+) tartaric acid	10 mM	15533.75 ± 941.70 b	59.45
	20 mM	1768.12 ± 449.55 f	95.38
Ammonium molybdate	1 mM	4593 ± 391.70 d	88.00
	5 mM	0.00 ± 0.00 e	100
Sodium orthovanadate	1 mM	14068.20 ± 703.55 b	61.87
	5 mM	0.00 ± 0.00 e	100

<sup>a</sup> Data show the mean area covered by powdery mildew of 24 treated disc cotyledons from three different experiments ± standard error.

<sup>b</sup> Percentage of disease reduction achieved by each treatment referred to values of untreated discs (water, negative control)

<sup>c</sup> Values with different letter indicate significant differences at  $P=0.05$  according to Fisher's least significant difference test (LSD).

### *PxSHAP1 and PxSHAP2 orthologs are widely distributed in pathogenic ascomycete fungi*

The presence of orthologues for *PxSHAP1* and *PxSHAP2* in the genomes of other fungi was investigated by BLASTp analysis using the deduced amino acid sequences of *PxSHAP1* and *PxSHAP2* as query sequences. As shown in Table 4.5, these genes are widely present in pathogenic fungi, mostly in plant pathogens, but also in insect pathogens and even in mammalian/human pathogens. Among the plant pathogenic fungi, these genes were widely distributed in obligate biotrophic fungi. Moreover, putative orthologues were

also found in endophytic/endomycorrhizal fungi. Furthermore, these genes were also present in ubiquitous saprophytic fungi.

**Table 4.5.** Fungal species assessed for the presence of PxSHAP1 and PxSHAP2 orthologues.

Species	Pathogenicity	PxSHAP1		PxSHAP2	
		Identity (%)	Accession no.	Identity (%)	Accession no.
<b>Leotiomyces</b>					
<i>Rhynchosporium commune</i>	Plant pathogen	59	CZS95705.1	-	-
<i>Rhynchosporium secalis</i>	Plant pathogen	59	CZT50469.1	-	-
<i>Rhynchosporium agropyri</i>	Plant pathogen	59	CZT02085.1	-	-
<i>Cadophora</i> sp.	Plant pathogen	59	PVH82247.1	-	-
<i>Phialocephala subalpina</i>	endophytic/endomy corrhizal	61	CZR54627.1	-	-
<i>Phialocephala scopiformis</i>	endophytic/endomy corrhizal	59	XP_001591576.1	58.41	XP_018078177.1
<i>Hyaloscypha variabilis</i>	endophytic/endomy corrhizal	61	PMD36774.1	-	-
<i>Coleophoma cylindrospora</i>	endophytic/endomy corrhizal	59	RDW64972.1	57.67	RDW69677.1
<i>Coleophoma crateriformis</i>	endophytic/endomy corrhizal	60	RDW68308.1	58.64	RDW80800.1
<i>Diplocarpon rosae</i>	Plant pathogen	57	PBP19915.1	-	-
<i>Erysiphe pulchra</i>	Plant pathogen	66	POS85329.1	60.08	POS88371.1
<i>Erysiphe necator</i>	Plant pathogen	65	KHJ31127.1	60.57	KHJ34543.1
<i>Oidium neolycopersici</i>	Plant pathogen	63	RKF56541.1	57.91	RKF61237.1
<i>Blumeria graminis</i> f. sp. <i>hordei</i>	Plant pathogen	65	CCU82653.1	64.26	SZF00594.1
<i>Blumeria graminis</i> f. sp. <i>tritici</i>	Plant pathogen	65	EPQ63976.1	61.04	EPQ67490.1
<i>Golovinomyces cichoracearum</i>	Plant pathogen	63	RKF81351.1	61.11	RKF80194.1
<i>Glarea lozoyensis</i>	Saprophytic		XP_008082946.1	57.83	XP_024719745.1
<i>Rutstroemia</i> sp.	Saprophytic	64	PQE32035.1	57.73	PQE30117.1
<i>Pezoloma ericae</i>	endophytic/endomy corrhizal	-	-	57.09	PMD13690.1
<i>Meliniomyces bicolor</i>	endophytic/endomy corrhizal	-	-	55.51	XP_024729518.1
<b>Dothiideomycetes</b>					
<i>Monilinia fructigena</i>	Plant pathogen	61	RAL60782.1	-	-
<i>Sclerotinia borealis</i>	Plant pathogen	60	ESZ90795.1	58.80	ESZ93260.1
<i>Sclerotinia sclerotiorum</i>	Plant pathogen	59	XP_001591576.1	59.24	XP_001596570.1
<i>Botrytis cinerea</i>	Plant pathogen	60	XP_001549993.1	60.57	CCDS56896.1
<i>Marssonina brunnea</i> f. sp. <i>mmiltigermtubi</i>	Plant pathogen	58	XP_007290256.1	-	-

## Two secreted haustorial acid phosphatases are key factors for *P. xanthii* development

<i>Marsonina coronariae</i>	Plant pathogen	51	OWP05828.1	-	-
<i>Corynespora cassicola</i>	Plant pathogen	48	PSN70322.1	-	-
<i>Venturia inaequalis</i>	Plant pathogen	50	RD183696.1	55.54	RD176411.1
<i>Aureobasidium melanogenum</i>	Animal/human pathogen	49	KEQ63375.1	56.72	KEQ61592.1
<i>Aureobasidium namibiae</i>	Saprophytic	48	XP_013424789.1	57.53	XP_013427463.1
<i>Aerobasidium subglaciale</i>	Saprophytic	-	-	56.37	XP_013348286.1
<i>Paraphaesphaeria sporulosa</i>	Saprophytic	49	XP_018037011.1	-	-
<i>Clohesyomyces aquaticus</i>	Saprophytic	50	ORY14488.1	-	-
<i>Glonium stellatum</i>	Saprophytic	54	OCL14268	-	-
<i>Verruconis gallopava</i>	Animal/human pathogen	-	-	55.47	KEQ89980.1
<i>Ramularia collo-cygni</i>	Plant pathogen	-	-	54.23	XP_023623785.1
<i>Neofusicoccum parvum</i>	Plant pathogen	-	-	52.03	EOD42999.1
<i>Macrophomina phaseolina</i>	Plant pathogen	-	-	53.76	EKG18381.1
<i>Lepidopterella palustris</i>	Saprophytic	-	-	54.05	OCK74404.1
<b>Eurotiomycetes</b>					
<i>Aspergillus turcosus</i>	Saprophytic	49	RHZ58996.1	-	-
<i>Aspergillus thermotutus</i>	Animal/human pathogen	50	XP_026615679.1	-	-
<i>Amorphoteca resiniae</i>	Saprophytic	-	-	62.28	XP_024719745.1
<i>Exophiala spinifera</i>	Animal/human pathogen	-	-	55.34	XP_016238286.1
<b>Sodariomycetes</b>					
<i>Moelleriella libera</i>	Entomopathogen	48	KZZ91685.1	-	-
<i>Pochonia chlamydsporia</i>	Entomopathogen	48	XP_018141606.1	-	-
<i>Metarhizium album</i>	Entomopathogen	49	PBP28790.1	-	-
<i>Metarhizium acridum</i>	Entomopathogen	48	XP_007813842.1	52.89	XP_007815624.1
<i>Metarhizium majus</i>	Entomopathogen	48	KID84255.1	-	-
<i>Metarhizium anisopliae</i>	Entomopathogen	49	KFG86491.1	54.83	KFG86020.1
<i>Metarhizium robertsii</i>	Entomopathogen	49	XP_007816314.1	53.64	XP_007822815.1
<i>Metarhizium brunneum</i>	Entomopathogen	49	XP_014543980.1	54.44	XP_014540446.1
<i>Claviceps purpurea</i>	Plant pathogen	49	CCE26934.1	-	-
<i>Ustilaginoidea virens</i>	Plant pathogen	49	KDB18017	55.36	KDB13610.1
<i>Tolyposcladium ophioglossoides</i>	Saprophytic	-	-	55.49	KND91048.1
<b>Lecanoromycetes</b>					
<i>Umbilicaria postulata</i>	Saprophytic	-	-	57.39	SLM40567.1
<b>Xylonomycetes</b>					
<i>Xylona heveae</i>	Saprophytic	-	-	57.36	XP_018185964.1

## DISCUSSION

The control of cucurbit powdery mildew disease remains a problem due, mainly, to the great capability exhibited by *P. xanthii* for fungicide resistance developing (Fernández-Ortuño *et al.*, 2006; Bellón-Gómez *et al.*, 2015). For this reason, the in deep study of the molecular mechanisms governing the *P. xanthii*-cucurbits interactions becomes a necessary step in the pathway to develop new tools for powdery mildew management. The intimate relationship between the *P. xanthii* haustorium and the host plant cell, the essential role of this structure in disease establishment and the importance of certain effectors of *P. xanthii* secreted during epiphytic growth (Martínez-Cruz *et al.*, 2018a), make the haustorial effectors a promising element in the search of novel targets for the design of new mildewicides. The assembly of the *P. xanthii* haustorial transcriptome, the prediction of its associated secretome (see chapter III) and the comparative study with the previously developed epiphytic secretome (Vela-Corcía *et al.*, 2016), have allowed the identification of several transcripts that encode secreted proteins exclusively expressed in the *P. xanthii* haustorium. This was the case of the transcripts *PHEC689* (annotated without known function but with a protein model analogous to an *A. niger* acid phosphatase) and *15569* (annotated as an acid phosphatase gene), which were found among the top 25 expressed genes in haustoria and among the three more expressed genes encode haustorium-specific secreted proteins (see chapter III). The exclusive haustorial expression of these genes and their high relative expression, suggested a functional importance of these genes for the infection process. For these facts, in this work we analyzed the functions of PHEC689 and 15569, their

role in *P. xanthii* pathogenesis and/or biotrophy as well as their potential utilization as novel targets for new antifungal phytotherapies.

*PHEC689* and *15569* encode proteins whose 3D models presented high structural similarity between them and with an *A. niger* acid phosphatase, however, they did not share sequence identity. On the other hand, the yeast complementation assays demonstrated the acid phosphatase function and the secretion of both proteins. Hence, *PHEC689* and *15569*, renamed as *PxSHAP1* and *PxSHAP2* for *P. xanthii* secreted haustorial acid phosphatases, could be catalyzing the same enzymatic reaction although with very different amino acid sequences, indicating that they have independent evolutionary origins (Galperin and Koonin, 2012). That is, they are analogous proteins or non-homologous isofunctional enzymes (NISE) (Omelchenko *et al.*, 2010). These analogous proteins, therefore, seem to act with a redundant function that could be related to the release of phosphorus from the same or different phosphorylated plant substrates. The redundancy in effector functions have been related to the pathogenesis and intracellular survival in the human bacterial pathogen *Legionella pneumoniae* (Bardill *et al.*, 2005; Qiu *et al.*, 2016; Ling, 2017). Although in the case of *L. pneumoniae* the redundancy is due the presence of paralogues in its genome, the redundancy of acid phosphatase analogues in *P. xanthii* haustorium could be similarly related to the pathogenesis and survival into the host plant cell.

All this suggested a key role of these acid phosphatases in *P. xanthii* biotrophy and/or pathogenesis. To validate this hypothesis, individual silencing and co-silencing of *PxSHAP1* and *PxSHAP2* genes were carried out by the ATM-HIGS system. This approach has been previously used for the functional characterization of epiphytic *P. xanthii* effectors (Martínez-Cruz *et al.*, 2018a) and have allowed us to demonstrate the importance of both acid phosphatases

in *P. xanthii* development. Individual gene silencing caused a notable reduction of fungal growth similar to the reduction caused by silencing of *CmMlo1* gene from *C. melo* (Cheng *et al.*, 2012) used as a RNAi-mediated resistance positive control (Martínez-Cruz *et al.*, 2018a). However, the co-silencing of both acid phosphatase genes caused a dramatic reduction of *P. xanthii* growth, obtaining a reduction significantly higher than the reduction caused by silencing of *CmMlo1* gene and the reductions obtained after silencing of several epiphytic effector genes (Martínez-Cruz *et al.*, 2018a), revealing the huge importance of these enzymes in *P. xanthii* development. It has been described that in effectors with redundant functions, individual gene disruptions do not result in a clear phenotype while the combined gene disruption usually impairs the pathogenesis (Ling, 2017). In the case of *P. xanthii* acid phosphatases, although the co-silencing of both genes impaired fungal development, the individual silencing of each gene also resulted in a sharp decrease of fungal growth. This fact, and the broad spectrum of substrates of acid phosphatases (Saleh and Belisle, 2000; Coker *et al.*, 2013) suggest that, although these proteins share the same mechanism of action, could be acting synergistically in phosphorus acquisition from different plant molecules. For example, these enzymes could be obtaining phosphorus from phytic acid (Saleh and Belisle, 2000), the major compound of phosphorus storage in plants (Alkarawi and Zotz, 2014; Hadi Alkarawi and Zotz, 2014), and a compound also involved in plant hormone signalling and in plant resistance against pathogens (Murphy *et al.*, 2008; Blüher *et al.*, 2017). Other plant molecules containing phosphorus that can substrates for acid phosphatases can be glucose 6 phosphate, phosphoenolpyruvate or glycerol 3 phosphate (Saleh and Belisle, 2000). The substrate specificity of PxSHAP1 and PxSHAP2 has yet to be determined. As a necessary step to address this, we tried to express these proteins *in vitro* in different *E. coli* expression systems as well



as in yeast and *Nicotiana benthamiana* expression systems but we failed in producing active proteins. Nevertheless, regardless of the specific substrates used by these enzymes, our results undoubtedly show that these enzymes are essential factors for *P. xanthii* biology.

Acid phosphatases have been related to pathogenesis in other intracellular pathogens such as the bacterial pathogens *Francisella tularensis* (Mohapatra *et al.*, 2007, 2013) and *Mycobacterium tuberculosis* (Puri *et al.*, 2013) and the parasite *Trypanosoma cruzi* (Neves and Fernandes, 2014). In fungi, the acid phosphatases of the insect pathogen *Metarhizium anisopliae* play a key role in fungal development, being necessary for the growth in its host (Xia *et al.*, 2001). It is evident the key role of phosphorus in many biological processes (Li *et al.*, 2010) and, hence, the need of biotrophic fungi for the acquisition of this essential nutrient from plants. In barley plants infected with powdery mildew the phosphate uptake is increased, suggesting that the fungus could be involved in the induction of this process (Walters and Ayres, 1981). Moreover, an homolog of the phosphate transporter PHO87 of *Neurospora crassa* has been identified in *Blumeria graminis* f. sp. *hordei* whose expression correlates with virulence-related genes (Both *et al.*, 2005) and more recently, the presence of a member of Pho88 group of inorganic phosphate transporters has been described among the top 50 expressed genes in the haustoria of *Golovinomyces orontii* (Weßling *et al.*, 2012), underlining the importance of phosphorus acquisition via haustoria in powdery mildews. The fact that *P. xanthii* like other powdery mildews only can uptake nutrients from plant cells, suggests that these enzymes could be participating in phosphorus acquisition from the host as occurred in *M. anisopliae* (Xia *et al.*, 2001). Therefore, strictly speaking, they should be related to biotrophy rather than to pathogenesis. Moreover, the predicted size of PxSHAP1 and PxSHAP2 mature proteins and their expression pattern do not

match with that described for canonical effectors (Godfrey *et al.*, 2010; Pedersen *et al.*, 2012; Hacquard, 2014). In addition, the histochemical analyses revealed that the individual silencing and co-silencing of the *PxSHAP* genes did not result in an increase of hydrogen peroxide accumulation in plant cells, indicating that these enzymes are not involved in manipulation plant responses as other effectors previously identified in *P. xanthii* (Martínez-Cruz *et al.*, 2018a). All these evidence support the function in biotrophy of *P. xanthii* acid phosphatases rather than a role in pathogenesis. In any case, it is very difficult to discern between survival in the host and pathogenesis in the case of obligate biotrophs.

On the other hand, after ATM-HIGS experiments, which resulted in a significant decrease of *P. xanthii* growth when the acid phosphatases genes were silenced, we tested the capability of several acid phosphatase inhibitors to reduce the powdery mildew disease in melon cotyledons. The results were certainly promising; compounds such as ammonium molybdate or sodium orthovanadate caused a total suppression of the disease. Although only two concentrations of these compounds have been tested, in the case of ammonium molybdate a disease reduction close to 90% was obtained at 1 mM and a total control of the disease was obtained at 5 mM. In principle, these doses can be considered high and the direct use of these inhibitors, therefore, discharged for practical reasons, but these results reveal that phosphorous metabolism and acid phosphatases can be a promising target to design new fungicides. The structure-activity relationships of compounds such as L-(+)-tartaric acid, ammonium molybdate or sodium orthovanadate could be the beginning of the pathway to identify novel fungicidal compounds by cheminformatics approaches such as molecular topology (Zanni *et al.*, 2018).

Finally, BLAST analyses revealed that orthologs of *PxSHAP1* and *PxSHAP2* genes were widely present in the genomes of ascomycete fungi, especially in fungal pathogens among which stood out several powdery mildew species and intracellular entomopathogens such as *M. anisopliae* (Xia *et al.*, 2001). Moreover, orthologues were also present in non-pathogenic endophytic fungi, suggesting that, as observed in this study, they could be involved in phosphorus acquisition and be essential for survival and growth into the host plant. The high conservation of these enzymes among ascomycete fungi suggests the possibility of using them as targets for development of new fungicides against biotrophic and non-biotrophic plant pathogenic fungi. Phosphorus metabolism is essential for all organism and regarding acid phosphatases, they have been widely described in phosphorous acquisition in several soil microorganisms (Abd-Alla, 1994; Rodríguez and Fraga, 1999; Chuan-Qing *et al.*, 2014; Rombola *et al.*, 2014). However, their role in pathogenesis or growth into the host has been poorly documented. As shown here, the secreted haustorial acid phosphatases *PxSHAP1* and *PxSHAP2* are essential factors for *P. xanthii* development. The disease control achieved by acid phosphatase inhibitors and the wide conservation of these enzymes among phytopathogenic ascomycete fungi support the potential of phosphorous metabolism and acid phosphatases as a promising target for novel fungicide design.

---

## REFERENCES

**Abd-Alla MH.** 1994. Use of organic phosphorus by *Rhizobium leguminosarum* biovar *viceae* phosphatases. *Biology and Fertility of Soils* **18**, 216–218.

**Alkarawi HH, Zotz G.** 2014. Phytic acid in green leaves of herbaceous plants-temporal variation in situ and response to different nitrogen/phosphorus fertilizing regimes. *AoB PLANTS* **6**, 1–7.

**Álvarez B, Torés JA.** 1997. Cultivo in vitro de *Sphaerotheca fuliginea* (Schlecht. ex Fr.), efecto de diferentes fuentes de carbono sobre su desarrollo. *Boletín de sanidad vegetal. Plagas* **23**, 283–288.

**Arnold W, Sakai K, Mann L.** 1987. Selective inactivation of an extra-cytoplasmic acid phosphatase of yeast-like cells of *Sporothrix schenckii* by sodium fluoride. *Journal of General Microbiology*, 1503–1509.

**Bardill JP, Miller JL, Vogel JP.** 2005. IcmS-dependent translocation of SdeA into macrophages by the *Legionella pneumophila* type IV secretion system. *Molecular Microbiology* **56**, 90–103.

**Baxter L, Tripathy S, Ishaque N, et al.** 2010. Signatures of adaptation to obligate biotrophy in the *Hyaloperonospora arabidopsis* genome. *Science* **330**, 1549–1551.

**Bellón-Gómez D, Vela-Corcía D, Pérez-García A, Torés JA.** 2015. Sensitivity of *Podosphaera xanthii* populations to anti-powdery-mildew fungicides in Spain. *Pest Management Science* **71**, 1407–1413.

**Block A, Li G, Fu ZQ, Alfano JR.** 2008. Phytopathogen type III effector weaponry and their plant targets. *Current Opinion in Plant Biology* **11**, 396–403.

**Blüher D, Laha D, Thieme S, et al.** 2017. A 1-phytase type III effector interferes with plant hormone signaling. *Nature Communications* **8**.

**Both M, Eckert SE, Csukai M, Muller E, Dimopoulos G, Spanu PD.** 2005. Transcript profiles of *Blumeria graminis* development during infection reveal a cluster of genes that are potential virulence determinants. *Molecular Plant Microbe Interaction* **18**, 125–33.

**Chen Y, Zhang F, Tang L, Zheng Y, Li Y, Christie P, Li L.** 2007. Wheat powdery mildew and foliar N concentrations as influenced by N fertilization and belowground interactions with intercropped faba bean. *Plant and Soil* **291**, 1–13.

**Cheng H, Kun W, Liu D, Su Y, He Q.** 2012. Molecular cloning and expression analysis of *CmMlo1* in melon. *Molecular Biology Reports* **39**, 1903–1907.

**Chuan-Qing Z, Guang-Xiang C, Wei-Yi H, Xing-She L, Yi-Fei Y.** 2014. Dissolving mechanism of strain P17 on insoluble phosphorus of yellow-brown soil. *Brazilian Journal of Microbiology* **45**, 937–943.

**Coker OO, Warit S, Rukseree K, Sumpunn P.** 2013. Functional characterization of two members of histidine phosphatase superfamily in *Mycobacterium tuberculosis*. *BMC Microbiology* **13**, 292.

**Divon HH, Fluhr R.** 2006. Nutrition acquisition strategies during fungal infection of plants. *FEMS Microbiology Letters* **266**, 65–74.

**Duplessis S, Cuomo CA, Lin Y, et al.** 2011. Obligate biotrophy features unraveled by the genomic analysis of rust fungi. *Proceedings of the National Academy of Sciences* **108**, 9166–9171.

**Fernández-Ortuño D, Pérez-García A, López-Ruiz F, Romero D, De Vicente A, Torés JA.** 2006. Occurrence and distribution of resistance to QoI fungicides in populations of *Podosphaera fusca* in south central Spain.

European Journal of Plant Pathology **115**, 215–222.

**Fotopoulos V, Gilbert MJ, Pittman JK, Marvier AC, Buchanan AJ, Sauer N, Hall JL, Williams LE.** 2003. The monosaccharide transporter gene, AtSTP4, and the cell-wall invertase, AtBfruct1, are induced in *Arabidopsis* during infection with the fungal biotroph *Erysiphe cichoracearum*. Plant Physiology **132**, 821–829.

**Galperin MY, Koonin E V.** 2012. Divergence and convergence in enzyme evolution. Journal of Biological Chemistry **287**, 21–28.

**Godfrey D, Böhlenius H, Pedersen C, Zhang Z, Emmersen J, Thordal-Christensen H.** 2010. Powdery mildew fungal effector candidates share N-terminal Y/F/WxC-motif. BMC Genomics **11**.

**Göhre V, Robatzek S.** 2008. Breaking the barriers: Microbial effector molecules subvert plant Immunity. Annual Review of Phytopathology **46**, 189–215.

**Hacquard S.** 2014. The genomics of powdery mildew fungi: Past achievements, present status and future prospects. Advances in Botanical Research **70**, 109-142

**Hacquard S, Joly DL, Lin Y-C, et al.** 2012. A comprehensive analysis of genes encoding small secreted proteins identifies candidate effectors in *Melampsora larici-populina* (poplar leaf rust). Molecular Plant-Microbe Interactions **25**, 279–293.

**Hadi Alkarawi H, Zotz G.** 2014. Phytic acid in green leaves. Plant Biology **16**, 697–701.

**Hahn M, Mendgen K.** 1997. Characterization of in planta-induced rust genes isolated from a haustorium-specific cDNA library. Molecular plant-microbe interactions : MPMI **10**, 427–437.

**Jahn M, Munger HM, McCreight JD.** 2002. Breeding cucurbit crops for

powdery mildew resistance. The powdery mildews: a comprehensive treatise. St. Paul: American Phytopathological Society (APS Press), 239–248.

**Karimi M, Inzé D, Depicker A.** 2002. GATEWAY™ vectors for *Agrobacterium*-mediated plant transformation. *Trends in Plant Science* **7**, 193–195.

**Kemen E, Gardiner A, Schultz-Larsen T, et al.** 2011. Gene gain and loss during evolution of obligate parasitism in the white rust pathogen of *Arabidopsis thaliana*. *PLoS Biology* **9**, e1001094.

**Koressaar T, Remm M.** 2007. Enhancements and modifications of primer design program Primer3. *Bioinformatics* **23**, 1289–1291.

**Li L, Liu C, Lian X.** 2010. Gene expression profiles in rice roots under low phosphorus stress. *Plant Molecular Biology* **72**, 423–432.

**Ling S.** 2017. Beyond paralogs: The multiple layers of redundancy in bacterial pathogenesis. *Frontiers in cellular and infection Microbiology* **7**, 467. doi: 10.3389/fcimb.2017.00467.

**Lovelace L, Lewinski K, Jakob C, Kuciel R, Ostrowski W, Lebioda L.** 1997. Prostatic acid phosphatase: structural aspects of inhibition by L-(+)-tartrate ions. *Acta Biochimica Polonica* **44**, 673–678.

**Magno-Pérez-Bryan MC, Martínez-García PM, Hierrezuelo J, Rodríguez-Palenzuela P, Arrebola E, Ramos C, de Vicente A, Pérez-García A, Romero D.** 2015. Comparative genomics within the *Bacillus* Genus reveal the singularities of two robust *Bacillus amyloliquefaciens* biocontrol strains. *Molecular Plant-Microbe Interactions* **28**, 1102–1116.

**Martínez-Cruz J, Romero D, Dávila JC, Pérez-García A.** 2014. The *Podospaera xanthii* haustorium, the fungal Trojan horse of cucurbit-powdery mildew interactions. *Fungal genetics and biology* **71**, 21–31.

**Martínez-Cruz J, Romero D, de la Torre FN, Fernández-Ortuño D,**

**Torés JA, de Vicente A, Pérez-García A.** 2018a. The functional characterization of *Podosphaera xanthii* candidate effector genes reveals novel target functions for fungal pathogenicity. *Molecular Plant-Microbe Interactions* **31**, 914-931.

**Martínez-Cruz J, Romero D, de Vicente A, Pérez-García A.** 2017. Transformation of the cucurbit powdery mildew pathogen *Podosphaera xanthii* by *Agrobacterium tumefaciens*. *New Phytologist* **213**, 1961–1973.

**Martínez-Cruz J, Romero D, De Vicente A, Pérez-García A.** 2018b. Transformation by growth onto agro-infiltrated tissues (TGAT), a simple and efficient alternative for transient transformation of the cucurbit powdery mildew pathogen *Podosphaera xanthii*. *Molecular Plant Pathology* **19**, 2502–2515.

**McGrath T.** 2010. Fungicide resistance in cucurbit powdery mildew fungi. *Plant Disease* **85**, 236–245.

**Micali CO, Neumann U, Grunewald D, Panstruga R, O'Connell R.** 2011. Biogenesis of a specialized plant-fungal interface during host cell internalization of *Golovinomyces orontii* haustoria. *Cellular Microbiology* **13**, 210–226.

**Mohapatra NP, Balagopal A, Soni S, Schlesinger LS, Gunn JS.** 2007. AcpA is a *Francisella* acid phosphatase that affects intramacrophage survival and virulence. *Infection and Immunity* **75**, 390–396.

**Mohapatra NP, Soni S, Rajaram MVS, Strandberg KL, Gunn JS.** 2013. Type A *Francisella tularensis* acid phosphatases contribute to pathogenesis. *PLoS ONE* **8**, e56834.

**Murphy AM, Otto B, Brearley CA, Carr JP, Hanke DE.** 2008. A role for inositol hexakisphosphate in the maintenance of basal resistance to plant pathogens. *Plant Journal* **56**, 638–652.

**Nakagawa T, Kurose T, Hino T, Tanaka K, Kawamukai M, Niwa Y,**



**Toyooka K, Matsuoka K, Jinbo T, Kimura T.** 2007. Development of series of gateway binary vectors, pGWBs, for realizing efficient construction of fusion genes for plant transformation. *Journal of bioscience and bioengineering* **104**, 34–41.

**Neves RFC, Fernandes ACS.** 2014. Trypanosoma cruzi -secreted vesicles have acid and alkaline phosphatase activities capable of increasing parasite adhesion and infection. *Parasitology Research* **113**, 2961–2972.

**Oliva R, Win J, Raffaele S, et al.** 2010. Recent developments in effector biology of filamentous plant pathogens. *Cellular Microbiology* **12**, 705–715.

**Omelchenko M V., Galperin MY, Wolf YI, Koonin E V.** 2010. Non-homologous isofunctional enzymes: A systematic analysis of alternative solutions in enzyme evolution. *Biology Direct* **5**, 1–20.

**Pagni M, Ioannidis V, Cerutti L, Zahn-Zabal M, Jongeneel CV, Hau J, Martin O, Kuznetsov D, Falquet L.** 2007. MyHits: Improvements to an interactive resource for analyzing protein sequences. *Nucleic Acids Research* **35**, W433–W437.

**Pedersen C, van Themaat EVL, McGuffin LJ, et al.** 2012. Structure and evolution of barley powdery mildew effector candidates. *BMC Genomics* **13**.

**Pérez-García A, Romero D, Fernández-Ortuño D, López-Ruiz F, De Vicente A, Torés JA.** 2009. The powdery mildew fungus *Podosphaera fusca* (synonym *Podosphaera xanthii*), a constant threat to cucurbits. *Molecular plant pathology* **10**, 153–160.

**Petersen TN, Brunak S, von Heijne G, Nielsen H.** 2011. SignalP 4.0: discriminating signal peptides from transmembrane regions. *Nature Methods* **8**, 785.

**Pettersen EF, Goddard TD, Huang CC, Couch GS, Greenblatt DM, Meng EC, Ferrin TE.** 2004. UCSF Chimera--a visualization system for

exploratory research and analysis. *Journal of computational chemistry* **25**, 1605–1612.

**Pike S, Gao F, Kim MJ, Kim SH, Schachtman DP, Gassmann W.** 2014. Members of the NPF3 transporter subfamily encode pathogen-inducible nitrate/nitrite transporters in grapevine and *Arabidopsis*. *Plant and Cell Physiology* **55**, 162–170.

**del Pino D, Olalla L, Pérez-García A, Rivera ME, García S, Moreno R, de Vicente A, Torés JA.** 2002. Occurrence of races and pathotypes of cucurbit powdery mildew in southeastern Spain. *Phytoparasitica* **30**, 459–466.

**Puri RV, Reddy PV, Tyagi AK.** 2013. Secreted acid phosphatase (SapM) of *Mycobacterium tuberculosis* is indispensable for arresting phagosomal maturation and growth of the pathogen in Guinea pig tissues. *PLoS ONE* **8**, e70514.

**Qiu J, Sheedlo MJ, Yu K, Tan Y, Nakayasu ES, Das C, Liu X, Luo ZQ.** 2016. Ubiquitination independent of E1 and E2 enzymes by bacterial effectors. *Nature* **533**, 120–124.

**Ridout CJ, Skamnioti P, Porritt O, Sacristan S, Jones JDG, Brwon KM.** 2006. Multiple avirulence paralogues in cereal powdery mildew fungi may contribute to parasite fitness and defeat of plant resistance. *The Plant Cell* **18**, 2402–2414.

**Rodríguez H, Fraga R.** 1999. Phosphate solubilizing bacteria and their role in plant growth promotion. *Biotechnology Advances* **17**, 319–339.

**Rombola TH, Aparecida E, Pedrinho N, Gertrudes E, Lemos DM.** 2014. Identification and enzymatic characterization of acid phosphatase from *Burkholderia gladioli*. *BMC Research Notes* **7**, 221.

**Saleh MT, Belisle JT.** 2000. Secretion of an acid phosphatase (SapM) by *Mycobacterium tuberculosis* that is similar to eukaryotic acid phosphatases.

Journal of Bacteriology **182**, 6850–6853.

**Sievers F, Higgins DG.** 2014. Clustal omega. Current protocols in bioinformatics **48**, 3.13.1-16.

**Spanu PD.** 2006. Why do some fungi give up their freedom and become obligate dependants on their host? New Phytologist **171**, 447–450.

**Spanu PD, Abbott JC, Amsellem J, et al.** 2010. Genome expansion and gene loss in powdery mildew fungi reveal tradeoffs in extreme parasitism. Science **330**, 1543–1546.

**Srivastava PK, Anand A.** 2015. The inhibitory effect of metals and other ions on acid phosphatase activity from *Vigna aconitifolia* seeds. Preparative Biochemistry and Biotechnology **45**, 33–41.

**Sutton PN, Henry MJ, Hall JL.** 1999. Glucose , and not sucrose , is transported from wheat to wheat powdery mildew. Planta **208**, 426–430.

**Thordal-Christensen H, Zhang Z, Wei Y, Collinge DB.** 1997. Subcellular localization of H<sub>2</sub>O<sub>2</sub> in plants. H<sub>2</sub>O<sub>2</sub> accumulation in papillae and hypersensitive response during the barley-powdery mildew interaction. Plant Journal **11**, 1187–1194.

**Thornton B, Basu C.** 2011. Real-time PCR (qPCR) primer design using free online software. Biochemistry and Molecular Biology Education **39**, 145–154.

**Toh-E A, Oshima Y.** 1974. Characterization of a dominant, constitutive mutation, PHOO, for the repressible acid phosphatase synthesis in *Saccharomyces cerevisiae*. Journal of Bacteriology **120**, 608–617.

**Ullah AH, Sethumadhavan K, Mullaney EJ.** 2011. Vanadate inhibition of fungal PhyA and bacterial AppA2 histidine acid phosphatases. Journal of agricultural and food chemistry **59**, 1739–1743.

**Vela-Corcía D, Bautista R, De Vicente A, Spanu PD, Pérez-García A.**

2016. De novo analysis of the epiphytic transcriptome of the cucurbit powdery mildew fungus *Podosphaera xanthii* and identification of candidate secreted effector proteins. PLoS ONE **11**, e0163379.

**Walters DR, Ayres PG.** 1981. Phosphate uptake and translocation by roots of powdery mildew infected barley. Physiological Plant Pathology **18**, 195–205.

**Weßling R, Schmidt SM, Micali CO, Knaust F, Reinhardt R, Neumann U, Ver Loren van Themaat E, Panstruga R.** 2012. Transcriptome analysis of enriched *Golovinomyces orontii* haustoria by deep 454 pyrosequencing. Fungal Genetics and Biology **49**, 470–482.

**Wykoff D, Rizvi AH, Raser JM, Margolin B, O’Shea EK.** 2007. Positive feedback regulates switching of phosphate transporters in *S. cerevisiae*. Molecular Cell **27**, 1005–1013.

**Xia Y, Clarkson JM, Charnley KA.** 2001. Acid phosphatases of *Metarhizium anisopliae* during infection of the tobacco hornworm *Manduca sexta*. Archives of Microbiology **176**, 427–434.

**Zanni R, Galvez-Llompart M, Garcia-Pereira I, Galvez J, García-Domenech R.** 2018. Molecular topology and QSAR multi-target analysis to boost the in silico research for fungicides in agricultura chemistry. Molecular Diversity doi:10.1007/s11030-018-9879-3.

**Zarivi O, Cesare P, Ragnelli AM, Aimola P, Leonardi M, Bonfigli A, Colafarina S, Poma AM, Miranda M, Pacioni G.** 2015. Validation of reference genes for quantitative real-time PCR in Périgord black truffle (*Tuber melanosporum*) developmental stages. Phytochemistry **116**, 78–86.

**Zhang Y.** 2008. I-TASSER server for protein 3D structure prediction. BMC bioinformatics **9**, 40.

**Zhang Z, Henderson C, Perfect E, Carver T, Thomas B, Skamnioti P,**

**Gurr S.** 2005. Of genes and genomes, needles and haystacks: *Blumeria graminis*. *Molecular Plant Pathology* **6**, 561–575.

# CHAPTER V

## **Contribution of a secreted haustorial lytic polysaccharide monooxygenase of *Podosphaera xanthii* to the manipulation of chitin-triggered immunity of its host**



## ABSTRACT

*Podosphaera xanthii* is an obligate biotrophic powdery mildew fungus and the main causal agent of cucurbit powdery mildew disease. The lifestyle of this fungus is determined by the development of a specialized structure of parasitism inside the plant cells called haustorium, which is responsible for the acquisition of nutrients from the host and the release of effectors. One of the effector functions is the modulation of host immunity, for example, by the suppression of the activation of PAMP (pathogen-associated molecular pattern)-triggered immunity (PTI). Chitin is a major component of the fungal cell wall and a well-known fungal PAMP. As obligate biotrophs, powdery mildew fungi have had to evolve mechanisms to overcome haustorial chitin recognition by host plants; however, to date, these mechanisms remain unknown. In this work, we have analyzed one of the haustorium-specific effector candidates previously identified in the haustorial transcriptome of *P. xanthii*, with a putative predicted function as AA11 lytic polysaccharide monoxygenase (LPMO) of chitin, to determine its role in fungal development. Experiments with the recombinant protein validated its chitin-binding ability as well as its LPMO activity, breaking chitin into small oligomers. Furthermore, the silencing of the corresponding coding gene (*PxSHLPMO1*) resulted in a strong production of reactive oxygen species and in a strong reduction of fungal growth. This phenotype was rescued by the co-silencing of this gene and the plant *CERK1* gene, the main chitin receptor. Finally, BLAST searches showed that similar proteins are widely distributed in many fungal pathogens. Altogether, our results indicate that we are facing a new core effector of fungal pathogens involved in suppression of chitin-triggered immunity.





## INTRODUCTION

Powdery mildew fungi are the causal agents of the diseases with the same name, one of the most frequently plant diseases encountered around the world. Powdery mildew diseases are caused by different Ascomycota fungi from the *Erysiphales* order, among which is *Podosphaera xanthii*, the main causal agent of cucurbits powdery mildew, a disease that causes important yields losses in cucurbit crops (del Pino *et al.*, 2002; Fernández-Ortuño *et al.*, 2006; Pérez-García *et al.*, 2009; Bellón-Gómez *et al.*, 2015). Like all powdery mildew fungi, *P. xanthii* is dependent on plant living cells to complete its asexual life cycle (Vogel and Somerville, 2002; Weßling *et al.*, 2012; Martínez-Cruz *et al.*, 2014). In this cycle, the conidia transported by the wind are deposited onto the leaf of a susceptible host plant. Subsequently, their adhesion, germination and penetration are necessary steps for disease establishment (Spanu *et al.*, 2010). After penetration, the fungus forms a specialized structure of parasitism inside the epidermal plant cells, called haustorium, responsible for factor exchange with the plant such as the acquisition of nutrients (Both *et al.*, 2005; Bindschedler *et al.*, 2009; Micali *et al.*, 2011; Martínez-Cruz *et al.*, 2014). However, to complete this cycle, the pathogen needs to avoid the action of plant defense elements, such as enzymes (van den Burg *et al.*, 2007; Delaunoy *et al.*, 2014) and receptors, which recognize several pathogen-associated molecular patterns (PAMPs) (Tanaka *et al.*, 2010; De Jonge *et al.*, 2011), triggering the so-called PAMP triggered immunity (PTI) (Pieterse *et al.*, 2009). For this reason, fungal pathogens have had to evolve and adapt to their hosts by developing several strategies for overcoming plant defense responses. In this way, they count with effectors, small proteins acquired during the co-evolution

between plant pathogenic fungi and their hosts (Pieterse *et al.*, 2009) that present, among other functions, the ability to prevent the recognition of PAMPs by plant receptors (Jones and Dangl, 2006; Sánchez-Vallet *et al.*, 2013; Lo Presti *et al.*, 2015).

A primary component of fungal cell wall and a well-known PAMP is chitin (Pieterse *et al.*, 2009; Jonge *et al.*, 2010; Kombrink and Thomma, 2013; Tanaka *et al.*, 2013), a long-chain polymer of 1,4- $\beta$ -N-acetylglucosamine, a derivative of glucose (Young *et al.*, 2005; Wan *et al.*, 2008; Jonge *et al.*, 2010; Liu *et al.*, 2012a). Chitin provides structural rigidity to the fungal cell wall and also acts as the first line of defense of pathogenic fungi against plant secreted enzymes such as chitinases (Wan *et al.*, 2008; Kombrink and Thomma, 2013). As a consequence of the enzymatic activity of plant chitinases, chitin oligomers are released from the fungal cell wall that can be recognized by plant receptors such as CERK1, a transmembrane LysM-containing receptor with an intracellular kinase domain, promoting the chitin-specific signaling (Miya *et al.*, 2007; Sánchez-Vallet *et al.*, 2013; Cao *et al.*, 2014). This signaling produces the activation of several plant defense mechanisms, including the accumulation of reactive oxygen species (ROS) and the accumulation of cell wall deposits such as lignin and callose that produce a cell wall reinforcement (Kaku *et al.*, 2006; van den Burg *et al.*, 2007; Mentlak *et al.*, 2012; Doehlemann and Hemetsberger, 2013).

To counter chitin-triggered immunity, several effectors have been described in phytopathogenic fungi with roles in avoiding the recognition of chitin oligomers by plant receptors. One of those is Avr4, a *Cladosporium fulvum* apoplastic effector, which protects the chitin from the fungal cell wall from the action of plant chitinases released during the infection (van den Burg *et al.*,

2007; Bolton *et al.*, 2008). Other effectors are Ecp6 and Slp1, secreted proteins from *C. fulvum* and *Magnaporthe oryzae*, respectively. These proteins sequester the free chitin oligomers released as a consequence of the activity of plant chitinases, thus avoiding their recognition by the host. Other mechanism involved in suppression of chitin-triggered immunity is chitin deacetylase (CDA), a widely conserved enzyme that catalyzes the hydrolysis of acetamido groups of N-acetylglucosamine in chitin, promoting the conversion to chitosan, a glucosamine polymer and the deacetylated chitin derivative, which shows a considerable lower power of elicitation than chitin (Mochizuki *et al.*, 2011; Sánchez-Vallet *et al.*, 2013; Xi *et al.*, 2014).

The suppression of PAMP-triggered immunity in powdery mildew fungi is a poorly investigated aspect despite the fact that their nature as obligate biotrophs implies that the suppression of activation of host responses should be a key point in their physiology. In a previous study, the secretion of a family of chitinase-like effectors and a truncated version of chitin deacetylase with chitin-binding activity in *P. xanthii* hyphae have been described, which are all involved in manipulation of chitin-triggered immunity (Martínez-Cruz, 2016). With this regard, in the haustorial transcriptome of *P. xanthii*, a predicted lytic polysaccharide monooxygenase (LPMO) with a putative chitin-binding domain, was found among the top 50 expressed genes in the haustorium and was the most expressed gene among those codifying haustorium-specific secreted proteins (see chapter III). The LPMOs are a class of recently characterized enzymes able to oxidize different recalcitrant polysaccharides, among which are chitin (Vaaje-Kolstad *et al.*, 2010; Hemsworth *et al.*, 2015). Chitin LPMOs act on the crystalline chitin surface, introducing chain breaks and generating oxidized chain ends (Vaaje-Kolstad *et al.*, 2010). These enzymes are part of a pool of enzymes that different organisms secrete to obtain energy from dead

biomass (Hemsworth *et al.*, 2014). However, to date, they have not been reported in plant pathogenic or biotrophic fungi. Considering the putative role of this protein in chitin modification, as well as its high and exclusive expression in haustorium, in this work we have analyzed the role of this putative LPMO in powdery mildew pathogenesis. Our results suggest that the role of this effector could be the breakage of the chitin oligomers released during the development of haustoria or by the action of plant endo-chitinases in smaller oligomers, avoiding the perception of chitin by the host plant.

## MATERIAL AND METHODS

### *Plant, fungi and bacteria*

Disinfected cotyledons of zucchini (*Cucurbita pepo* L.) cv. Negro Belleza (Semillas Fitó, Barcelona, Spain) maintained in 8 cm Petri dishes with Bertrand medium at 24 °C under a 16 h light/8 h dark cycle (Álvarez and Torés, 1997), were used to culture *P. xanthii* isolate 2086. Melon plants (*Cucumis melo* L.) cv. Rochet (Semillas Fitó, Barcelona, Spain), were used to perform gene silencing experiments and were cultivated in a growth chamber under the same conditions as zucchini cotyledons. For agro-infiltration of melon cotyledons, *Agrobacterium tumefaciens* C58C1 was used and grown at 28 °C in LB medium with rifampicin (50 µg·mL<sup>-1</sup>) and spectinomycin (100 µg·mL<sup>-1</sup>) when required. For the construction and propagation of gene silencing vectors, *Eschericia coli* DH5α was used and grown at 37 °C in LB medium with ampicillin (100 µg·mL<sup>-1</sup>), spectinomycin (100 µg·mL<sup>-1</sup>) or kanamycin (50 µg·mL<sup>-1</sup>) when required. For

protein expression, *E. coli* strain B121-CodonPlus-RIL was used and grown at 37 °C in LB medium with kanamycin (50 µg·mL<sup>-1</sup>).

### *Sequence analysis and protein modelling*

The unigene PHEC27213 was selected from the *P. xanthii* secretome previously predicted (see chapter III). This unigene was the most expressed gene that codes for a haustorium-specific secreted protein (see chapter III). Although PHEC27213 was annotated without function, it showed a protein 3D-model with high analogy to an *Aspergillus oryzae* lytic polysaccharide monoxygenase (4MAH). To analyze the signal peptide and select the mature protein, SignalP 4.1 server (Petersen et al., 2011) was used. I-TASSER server (Zhang, 2008) was used to perform the 3D model of PHEC27213 and MotifScan (Pagni et al., 2007) was used to predict the putative motifs in the mature protein. To investigate the presence of putative orthologues in the genomes of other fungi, BLASTp analysis was used.

### *DNA and RNA isolation and cDNA synthesis*

To isolate DNA and RNA from *P. xanthii*-infected zucchini cotyledons, the cotyledons were frozen in liquid nitrogen and grounded in a mortar with pestle. Genomic DNA was extracted using the Epicentre MasterPure™ Yeast DNA Purification Kit (Epicentre, Madison, WI, USA) and total RNA using the TRI Reagent (Sigma-Aldrich, Saint Louis, USA) following the manufacturer's instructions. Total RNA was quantified using NanoDrop 2000 spectrophotometer (Thermo Fisher Scientific, Waltham, USA) and the cDNA synthesis was performed using random primers (Thermo Fisher Scientific) and

Superscript III Reverse Transcriptase (Thermo Fisher Scientific) according to manufacturer's recommendations.

### *Construction of protein expression and gene silencing vectors*

The plasmids used in this work are listed in Table 5.1 and showed in Figure 5.1. For the *in vitro* expression of PHEC27213 protein, the complete ORF sequence, without the nucleotides corresponding to the signal peptide and codon STOP, was amplified using the specific primers listed in Table 5.2, which contained the NdeI and XhoI restriction sites. Subsequently, *PHEC27213* amplicon was digested with fast digest restriction enzymes (Thermo Fisher Scientific) and cloned into pET30b plasmid using T4 ligase (Thermo Fisher Scientific), according to manufacturer's recommendations. The pET30b plasmid presents a 6×His-tag at both the N-terminus and the C-terminus of protein, but with the NdeI and XhoI combined digestion, only the 6×His-tag at C-terminus was conserved. The resulting expression vector pPHEC27213-EXPR was propagated and maintained in *E. coli* DH5α and verified by PCR amplification, digestion and sequencing. Finally, for the expression of the protein, pPHEC27213-EXPR was introduced into *E. coli* strain B121-CodonPlus-RIL by electroporation.

For the silencing of *PHEC27213* gene, the vector pB7GWIWG2(II) (Karimi *et al.*, 2002) and the Gateway cloning technology (Invitrogen) were used essentially as previously described by Martínez-Cruz *et al.*, (2018a). Specific primers with attB1 or attB2 tails (Table 5.2) were used to amplify a fragment of 315 bp of *PHEC27213* from the cDNA previously obtained (see above). The resulting plasmid pPHEC27213-RNAi was checked by PCR and sequencing. For gene silencing experiments, the plasmid pCmMlo1-RNAi (Martínez-Cruz

*et al.*, 2018a), containing a fragment of 412 bp from melon *CmMlo1* gene (Table 5.1), was used as a positive control, and the plasmid pGWB2 (Nakagawa *et al.*, 2007) was used as a negative control (empty vector). In addition, for silencing of *CERK1* chitin receptor from melon, the plasmid pCERK1-RNAi, containing a fragment of 614 bp from melon *CERK1* gene, was used (Martínez-Cruz, 2016). All these plasmids were propagated and maintained into *E. coli* strain DH5 $\alpha$ . For the gene silencing experiments, these plasmids were introduced into *A. tumefaciens* C58C1 by electroporation.

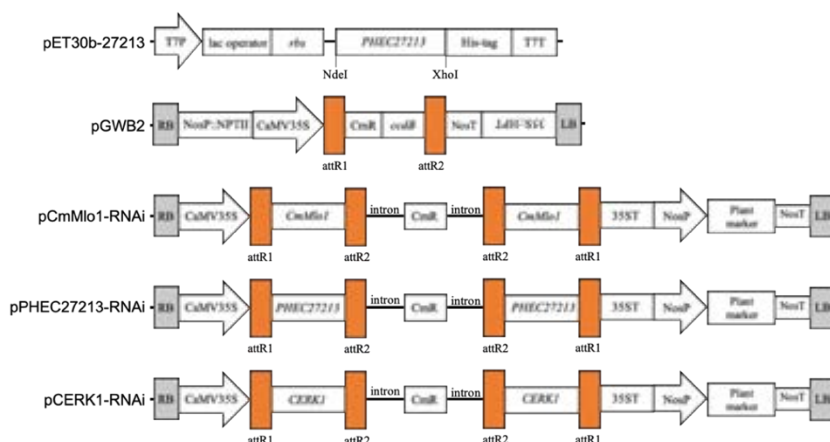


**Figure 5.1.** Schematic representation of vectors used for protein expression and gene silencing experiments. Arrows indicate the promoters and the flipped names of pGWB2 vector indicate that the gene is located in complementary strand. Abbreviations are: T7P, T7 promoter from bacteriophage T7; lac operator, operator from lac operon; rbs, ribosome binding site; His-tag, 6 $\times$ His tag for protein purification; T7T, T7 terminator from bacteriophage T7; LB, left border of T-DNA; RB, right border of T-DNA; NosP::NPTII, kanamycin resistance marker; CaMV35S, Cauliflower mosaic virus 35S promoter; attR1 and attR2, recombination sites for LR reaction; CmR, chloramphenicol resistance marker; *ccdB*, lethal gene for negative selection in bacteria; NosP, nopaline synthase promoter; NosT, nopaline synthase terminator; 35S::HPT, hygromycin B resistance marker; 35ST, 35S terminator; Plant marker, glufosinate ammonium resistance marker.



**Table 5.1.** Plasmids used in this study.

Plasmid <sup>a</sup>	Characteristics <sup>b</sup>	Reference
pGWB2	Empty vector. Negative control for gene silencing experiments.	Nakagawa <i>et al.</i> , 2007
pCmMlo1-RNAi	Positive control for gene silencing experiments. Silencing vector containing a RNA hairpin with a 412 bp fragment of melon <i>CmMlo1</i> gene.	Martínez-Cruz <i>et al.</i> , 2018
pCERK1-RNAi	Silencing vector containing a RNA hairpin with a 614 pb fragment of melon <i>CERK1</i> gene	Martínez-Cruz (2016)
pPHEC27213-RNAi	Silencing vector containing a RNA hairpin with a 360 bp fragment of <i>PHEC27213</i> .	This study
pPHEC27213-EXPR	Expression vector carrying the complete ORF of <i>PHEC27213</i> without SP and codon stop.	This study

<sup>a</sup>RNAi, RNA interference.

<sup>b</sup>SP, secretion signal peptide.

### *Protein expression and purification*

For *in vitro* production of PHEC27213 protein, *E. coli* strain B121-CodonPlus-RIL harboring the pPHEC27213-EXPR expression vector was used. For this purpose, *E. coli* cells were grown in LB medium with kanamycin (50 µg/mL) at 37 °C and induced with 0.5 mM of IPTG (isopropyl-b-D-thiogalactopyranoside) when they reached an OD<sub>600nm</sub> of 0.4. Subsequently, they were incubated at 16 °C in an orbital shaker at 80 rpm. Later, *E. coli* cells were centrifuged at 8,000 g for 5 min at 4 °C and the resulting pellet was stored at -80 °C overnight in order to increase the yield of protein extraction. The purification of soluble PHEC27213 protein, which included a 6×His-tag at the C-terminus, was carried out using Protino<sup>®</sup> Ni-TED 2000 Packed Columns (Macherey-Nagel GmbH & Co. KG, Germany), according to manufacturer's indications. Then, the purified recombinant proteins were desalted using Sephadex G-25 in PD-10 Desalting Columns (GE Healthcare, Chicago, IL,

USA) and 0.1 M sodium phosphate buffer, pH 7.0. The protein purification was confirmed using Mini-PROTEAN® Stain-Free™ Precast Gels (Bio-Rad, Hercules, CA, USA) and visualized in a ChemiDoc XRS+ system (Bio-Rad). Last, the protein concentration was estimated by the Protein Concentration Calculator web-server (<https://www.aatbio.com/tools/calculate-protein-concentration>) using the absorbance value at 280 nm and the extinction coefficient and molecular weight of the protein calculated from ExPASy web-server (<https://www.expasy.org/>).

### *Chitin-binding activity*

To perform the chitin-binding assay, 250  $\mu$ L of a solution of 1% colloidal chitin was centrifuged at 13,000 g for 5 min at 4 °C. The resulting pellet was re-suspended in a solution of 250  $\mu$ L containing 1 mg/mL of the purified PHEC27213 protein or 1mg/mL of BSA protein used as a negative control, in 0.1 M of sodium phosphate buffer, pH 7.0. The mixtures were incubated at 4 °C for 1 h with gentle manual agitation every 15 min. Later, both mixtures were centrifuged at 13,000 g for 5 min at 4 °C. After centrifugation, the supernatant and pellet were separated and the protein concentration present in the supernatant was quantified as described above, as an indicator of protein unbound to colloidal chitin.

### *Lytic polysaccharide monooxygenase activity*

To validate the lytic polysaccharide monooxygenase activity predicted for PHEC27213 protein, a chitin degradation assay was performed. In this assay, 1  $\mu$ M of purified PHEC27213 was added to a reaction mixture containing 2 mg/mL of colloidal chitin and 1 mM of ascorbic acid as a reducing agent in 0.1

M sodium phosphate buffer, pH 7.0. The reaction was incubated overnight at 37 °C with shaking at 800 rpm in an Eppendorf Thermo mixer (Eppendorf Ag, Hamburg, Germany). After incubation, the samples were centrifuged at 8,000 g for 5 min at 4 °C to remove proteins and non-degraded colloidal chitin. The chitin oligomers resulting from enzymatic degradation of chitin were analyzed by matrix assisted laser desorption ionization – time of flight – mass spectrometry (MALDI-TOF-MS) using an Ultraflex MALDI-TOF/TOF instrument (Bruker Daltonics GmbH, Bremen, Germany) with a Nitrogen 337 nm laser beam as described by Vaaje-Kolstad *et al.* (2010).

#### *Agrobacterium tumefaciens mediated-host induced gene silencing (ATM-HIGS) assay*

To study the implication of *PHEC27213* in *P. xanthii* development, the ATM-HIGS assay was carried out as described by Martínez-Cruz *et al.* (2018). The silencing plasmids pPHEC27213-RNAi and CERK1-RNAi as well as the RNAi-positive control pCmMlo1-RNAi and the negative control pGWB2 (empty vector) were introduced into *A. tumefaciens* C58C1 by electroporation. Later, transformed *A. tumefaciens* were induced with 200 µM of acetosyringone and were grown in 5 mL of LB medium supplemented with rifampicin (50 µg/mL) and spectinomycin (100 µg/mL) or kanamycin (50 µg/mL) at 28°C and 200 rpm in an orbital shaker overnight. Subsequently, the different *Agrobacterium* cultures corresponding with the different gene silencing constructs were washed twice in washing buffer and 200 µM of acetosyringone. In order to induce the Vir proteins, the bacterial cells were incubated for 2 h at room temperature in the same washing buffer without agitation. Then, the *Agrobacterium* cells were centrifuged for 10 min at 4,000 rpm and 28 °C,

resuspendend in MES buffer and their OD<sub>600nm</sub> were adjusted to 0.5-1.0 in MES buffer. Last, a 1-mL syringe without the needle was used to perform the agro-infiltrations into the abaxial surface of melon cotyledons with the different cell suspensions. For co-silencing experiments, equal volumes of the *Agrobacterium* cell suspensions carrying the pPHEC27213-RNAi and CERK1-RNAi silencing constructs were mixed before agro-infiltration. The agro-infiltrated cotyledons were maintained in a growth chamber under a 16 h light/8 h dark cycle at 24 °C for 24 h until the inoculation with a fresh *P. xanthii* conidial suspension ( $1 \times 10^5$  conidia/mL) by pulverization. Then, the cotyledons were maintained under the same conditions until analysis.

#### *RT-qPCR and qPCR*

The analysis of the expression of *PHEC27213* and the molecular estimation of *P. xanthii* biomass, were carried out by RT-qPCR and qPCR, respectively. These primers (Table 5.2) were designed using Primer3 software (Koressaar and Remm, 2007; Thornton and Basu, 2011). For gene expression analysis, total RNA was extracted, and used to synthesize cDNA as described above. To perform the RT-qPCR reactions, SsoFast EvaGreen Supermix (Bio-Rad) and a CFX384 Touch Real-Time PCR detection system (Bio-Rad) were used according to manufacturer's indications. The *P. xanthii* elongation factor-1 gene (MK249653) was used as a normalization reference gene (Zarivi *et al.*, 2015). For the molecular estimation of fungal biomass, total DNA was isolated from agro-infiltrated and infected melon cotyledons as described above. For this purpose, the *P. xanthii*  $\beta$ -tubulin gene (KC333362) and the *C. melo* actin gene (XM\_008462689.2) were quantified and the *P. xanthii*/*C. melo* genomic DNA ratio was calculated as previously described by Vela-Corcía *et al.* (2016). The

qPCR reactions were carried out in a CFX384 Touch Real-Time PCR detection system (Bio-Rad) using SsoFast EvaGreen Supermix (Bio-Rad) according to the manufacturer's indications. The RT-qPCR and qPCR conditions were: step of enzyme activation at 95 °C for 30 s, followed by 40 cycles at 95 °C for 5 s and 65 °C for 5 s. The amplification data were processed by CFX Manager Software (Bio-Rad) and the amplicon sizes were confirmed by visualization on 2% agarose gels.

**Table 5.2.** Primers used in this study.

Primer name	Sequence <sup>a,b</sup>
Plasmid construction	
27213si-F	5'- <u>AAAAAGCAGGCTCTGCGATGTATTCGCGGAGAAC</u> -3'
7213si-R	5'- AGAAAGCTGGGTGCTCGGTCCAACCGCAACAAC -3'
NdeI-27213exp-F	5'- <u>CATATG</u> CACTTTAATATTCAGTATCC -3'
XhoI-27213exp nonSTOP-R	5'- <u>CTCGAG</u> AAAGTGTCCCAATAACAAT -3'
attb1	5'-GGGGACAAGTTTGTACAAAAAAGCAGGCT-3'
attb2	5'-GGGGACCACTTTGTACAAGAAAGCTGGGT-3'
Gene expression analysis	
27213q-F	5'-AGTGTGCACCAATTCCACTG-3'
27213q-R	5'- TCCCATAACAATTGCACCAA -3'
Molecular estimation of fungal growth	
Tubg-F	5'-TTGTAGGAATCACATCCCTTCTC-3'
Tubg-R	5'-TTCTTCCGGTTGCATGGGTGGTTC-3'
Acting-F	5'-GGCTGGATTTGCCGGTGATGATGC-3'
Acting-R	5'-GGAAGGAGGAAATCAGTGTGAACC-3'

<sup>a</sup> Underlined sequences correspond to the attb1 or attb2 primer adapter.

<sup>b</sup> Italic and underlined sequences indicate the NdeI and XhoI restriction sites.

### *Haustorial count and visualization of fungal development and reactive oxygen species*

For the quantification of the number of haustoria after gene silencing, the visualization of fungal development and to analyze the activation of plant responses such as the accumulation of hydrogen peroxide, the 3,3'-diaminobenzidine (DAB) method (Thordal-Christensen *et al.*, 1997) was

performed as proposed by Martínez-Cruz *et al.* (2018). Briefly, discs of 1 cm diameter were taken from agro-infiltrated and *P. xanthii* infected cotyledons and were incubated in 1 mg/mL of DAB, pH 3.8, overnight in the dark at room temperature. After incubation, the discs were decolorized in boiling ethanol and observed by light microscopy using an Eclipse E800 microscope (Nikon). In these preparations, the haustoria are visualized as black spots, whereas the hyphae are brown stained. In the same preparations, epidermal cells with brown-red precipitates are reactive cells showing H<sub>2</sub>O<sub>2</sub> accumulation.

### *Statistical analysis*

When required, the statistical analysis of data was carried out by IBM SPSS v20 software (SPSS, Chicago, IL, USA) using Fisher's least significant difference test (LSD).

## **RESULTS**

### *PHEC27213 shows analogy with a lytic polysaccharide monoxygenase and presents a putative chitin-binding domain*

From Full-LenghterNext annotation of the exclusive haustorial secretome, the amino acid sequence of PHEC27213 protein was taken. The protein was modelled by I-TASSER server using the mature protein without the signal peptide. The resulting model of PHEC27213 showed high analogy with a lytic polysaccharide monoxygenase from *Aspergillus oryzae* (4MAH) (Figure 5.2A). On the other hand, the MotifScan software predicted a small putative chitin-binding domain (chitin binding domain 3) from amino acids 115 to 128

(Figure 5.2B). The presence of this putative chitin-binding domain and the specific secretion of this protein by the haustorium suggest that PHEC27213 could interact with chitin from the cell wall of the *P. xanthii* haustorium.

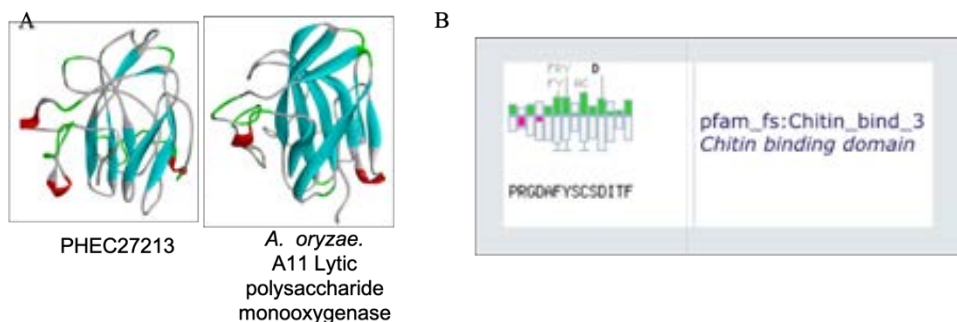


**Figure 5.2.** Main features predicted for PHEC27213 protein. A) Comparison of PHEC27213 protein model retrieved from I-TASSER server and its structural analogues from *A. oryzae*. B) The putative chitin-binding domain of PHEC27213 protein predicted by MotifScan.

### *PHEC27213 shows chitin-binding activity*

To validate the putative function of PHEC27213, this protein was expressed *in vitro* as a 6×His tag fusion in the *E. coli* strain BL21-CodonPlus-RIL (Figure 5.3). PHEC27213 was predominantly found in the soluble fraction, obtained after the purification by immobilization to nickel affinity column, with a yield of 1.34 mg/mL of soluble protein (Figure 5.3, lysate). The affinity of PHEC27213 protein for chitin and, hence, the validation of putative chitin binding domain, was studied by a chitin-binding assay using colloidal chitin (Figure 5.4). Most of the PHEC27213 was retained in the pellet in presence of colloidal chitin, whereas soluble PHEC27213 protein was hardly visualized in the supernatant (Figure 5.4A). In contrast with the bovine serum albumin (BSA) protein, which was fully recovered from the supernatant after contact with

colloidal chitin, the concentration of PHEC27213 protein recovered in the supernatant was 0.20 mg/mL (Figure 5.4B). That is, only a 20 % of total soluble protein was present in the supernatant, indicating the high affinity of this protein for chitin.

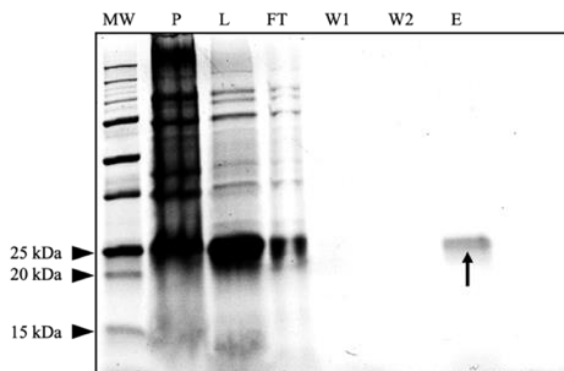


**Figure 5.3.** *In vitro* expression and purification of PHEC27213 protein. This protein was expressed in *E. coli* strain B121-CodonPlus-RIL and purified using the Protino<sup>®</sup> Ni-TED 2000 Packed Columns (Macherey-Nagel GmbH & Co). The image shows the different steps of protein purification visualized using Mini-PROTEAN<sup>®</sup> Stain-Free<sup>™</sup> Precast Gels (Bio-Rad) in a ChemiDoc XRS+ system (BioRad). The arrow indicates the band corresponding to the soluble purified protein. Lanes are: Mw, Precision Plus Protein<sup>™</sup> Unstained Standard (Bio-Rad); P, pellet sample; L, supernatant sample after cell lysis; FT, discarded flow-through after protein binding to column; W1, first washing sample; W2, second washing sample; E, eluted soluble protein.

### *PHEC27213 breaks colloidal chitin in small oligomers*

The putative predicted function of PHEC27213 was also studied in terms of chitin degradation. For this purpose, the protein was incubated overnight with colloidal chitin and ascorbic acid as reducing agent and the presence of free chitin oligomers was analyzed by MALDI-TOF. As shown in Figure 5.5, in



presence of PHEC27213 small size oligomers were detected, predominantly with a degree of polymerization (DP) of 5 (Figure 5.5A), whereas in the reaction without PHEC27213 it was not possible to see small size chitin oligomers and, due to the low solubility of chitin oligosaccharides, longer oligosaccharides were never observed (Figure 5.5B). This result revealed the role of PHEC27213 in the breakage of chitin and, hence, it was renamed PxSHLPMO1 (*P. xanthii* secreted haustorial lytic polysaccharide monoxygenase 1).

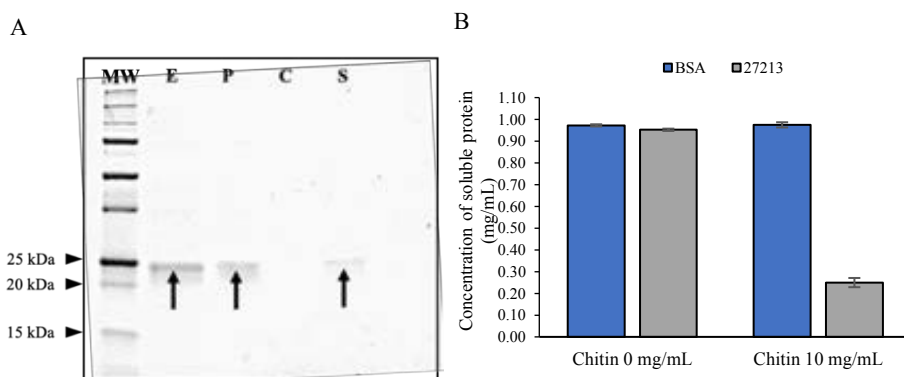


**Figure 5.4.** Chitin-binding analysis of PHEC27213. A) Polyacrylamide gel electrophoresis of PHEC27213 affinity against chitin after incubation with 10 mg/mL of colloidal chitin during 1 h. Lanes are: MW Precision Plus Protein™ Unstained Standard (Bio-Rad); E, soluble PHEC27213 adjusted to 1 mg/mL from final elution step after protein expression; P, presence of PHEC27213 protein in the pellet after incubation with colloidal chitin; C, colloidal chitin; S, presence of PHEC27213 protein in the supernatant after incubation with colloidal chitin. Arrows indicate the bands corresponding to PHEC27213 protein. B) The graph represents the amount of free PHEC27213 protein in the supernatants after incubation with (10 mg/mL) or without colloidal chitin. BSA protein was used as a negative control. Bars indicate the standard errors.

### *Silencing of PxSHLPMO1 gene alters P. xanthii development*

The high expression of *PxSHLPMO1*, which was the thirteenth most expressed gene in haustoria and the most expressed gene among the genes coding for haustorium-specific secreted proteins (see chapter III), suggested an important role in *P. xanthii* biology. For this reason the *Agrobacterium tumefaciens*-mediated host-induced gene silencing (ATM-HIGS) assay was used to validate the role of *PxSHLPMO1*.

As a previous step to HIGS assays, qRT-PCR experiments were performed to analyze the expression pattern of *PxSHLPMO1* during the first stages of infection (Figure 5.6A) and to quantify its transcripts level during gene silencing experiments (Figure 5.6B). In this way, it was possible to see how *PxSHLPMO1* was expressed in two waves, with a huge expression at 24 h followed by a decrease at 48 h and a subsequent increase at 72 h that, however, did not reach the expression levels at 24 h (Figure 5.6A). On the other hand, the transcript levels of this gene decreased around 50% during the gene silencing experiment (Figure 5.6B). After ATM-HIGS assay, the fungal growth was analyzed by means of haustorial counting using the DAB-method. After silencing of *PxSHLMO1*, the number of *P. xanthii* haustoria decreased during the first stages of the interaction, being this decrease even more evident at 72 h after inoculation, when the number of haustoria was even lower than the number of haustoria of RNAi positive control (*CmMlo1* gene) (Figure 5.7). The number of haustoria per square millimeter in agro-infiltrated melon cotyledons inoculated with *P. xanthii* was counted and graphically represented as an indicator of *P. xanthii* biomass (Figure 5.8). In this way, it was possible to see how the haustoria number showed a decrease of around three times compared to the empty vector (negative control).

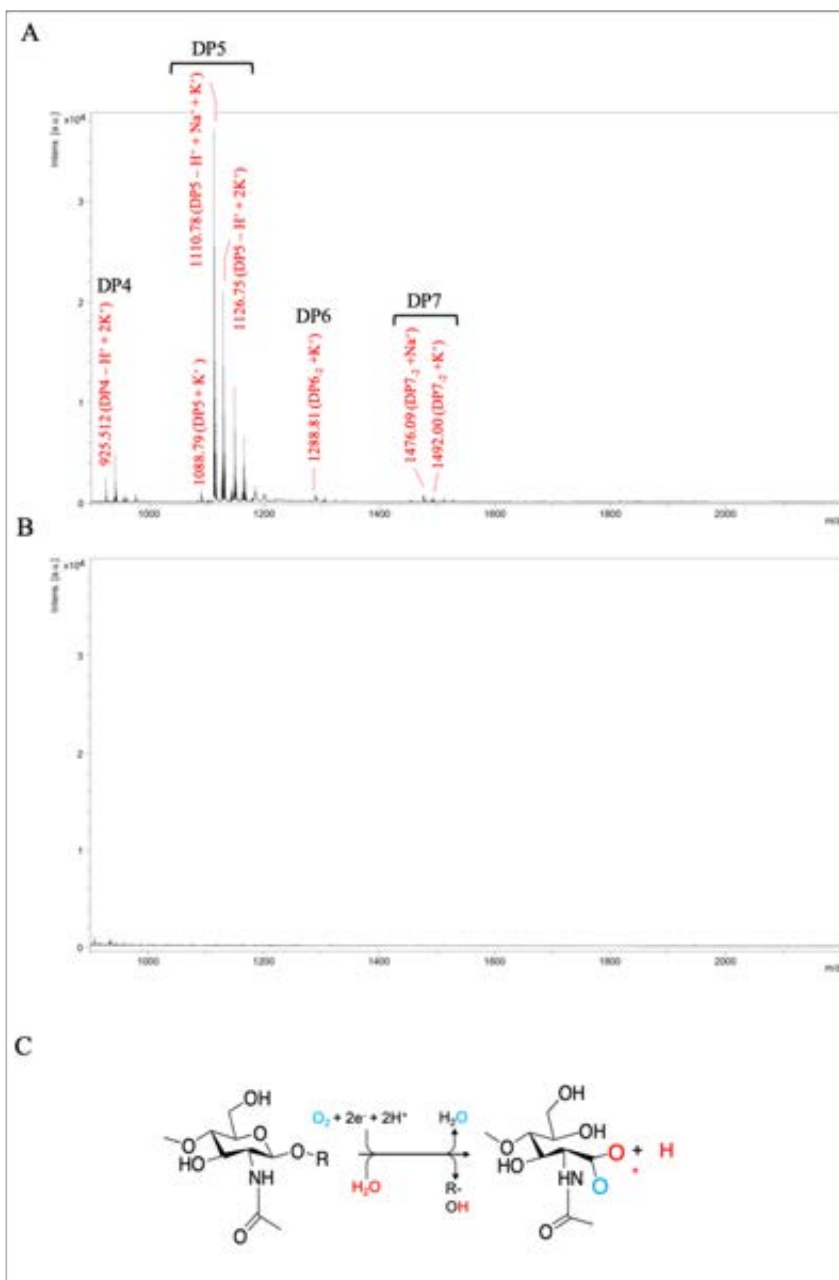


**Figure 5.5.** Lytic polysaccharide monoxygenase activity of PHEC27213 analyzed by MALDI-TOF. A) Assay with 2 mg/mL of colloidal chitin incubated in 0.1M of sodium phosphate buffer pH 7.0 with 1mM of ascorbic acid at 37 °C in presence PHEC27213. The peaks corresponding to the adducts of oxidized hexameric products coming from colloidal chitin were annotated according to Vaaje-Kolstad *et al.*, (2010) and Hemsworth *et al.*, (2014):  $DP_n$  = aldonic acid,  $DP_{n-2}$  = oxidation from R-OH to R=O. B) Same assay but in absence of PHEC27213. C) Schematic representation of the enzymatic reaction attributed to PHEC27213. In the final oxidized product, the blue oxygen comes from molecular oxygen and the red oxygen comes from water.

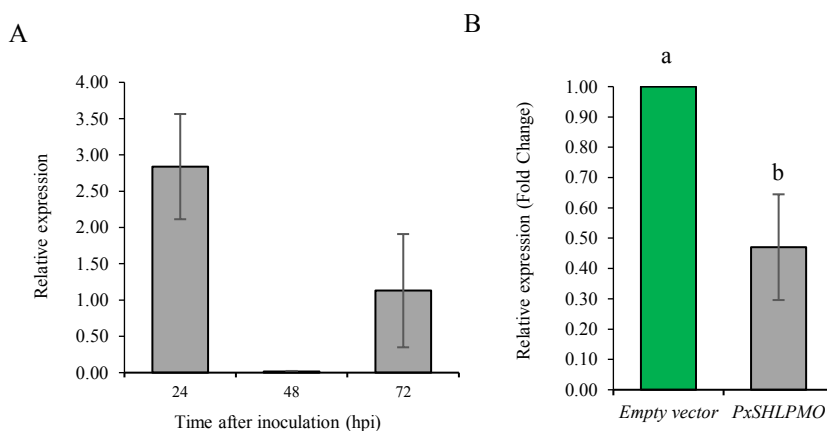


**Figure 5.6.** Expression analyses of *PxSHLPMO1* by qRT-PCR. A) Expression pattern of *PxSHLPMO1* during the first stages of infection. Total RNA was isolated from zucchini cotyledons taken at 24, 48 and 72 h after inoculation with *P. xanthii*. Transcript abundance was represented as the relative expression against *P. xanthii* elongation factor 1 gene *PxEF1* (MK249653) transcription. B) Analysis of ATM-HIGS efficacy for *PxSHLPMO1* gene. Total RNA was isolated from agro-infiltrated melon cotyledons taken at 24 h after inoculation with *P. xanthii*. The fold change indicates the change in gene expression levels after normalization to the expression of *PxEF1* (MK249653). Bars show the standard error of three technical replicates from three different experiments. Bars with different letter indicates expression significantly different at  $P=0.05$  according to Fisher's least significant difference test (LSD).

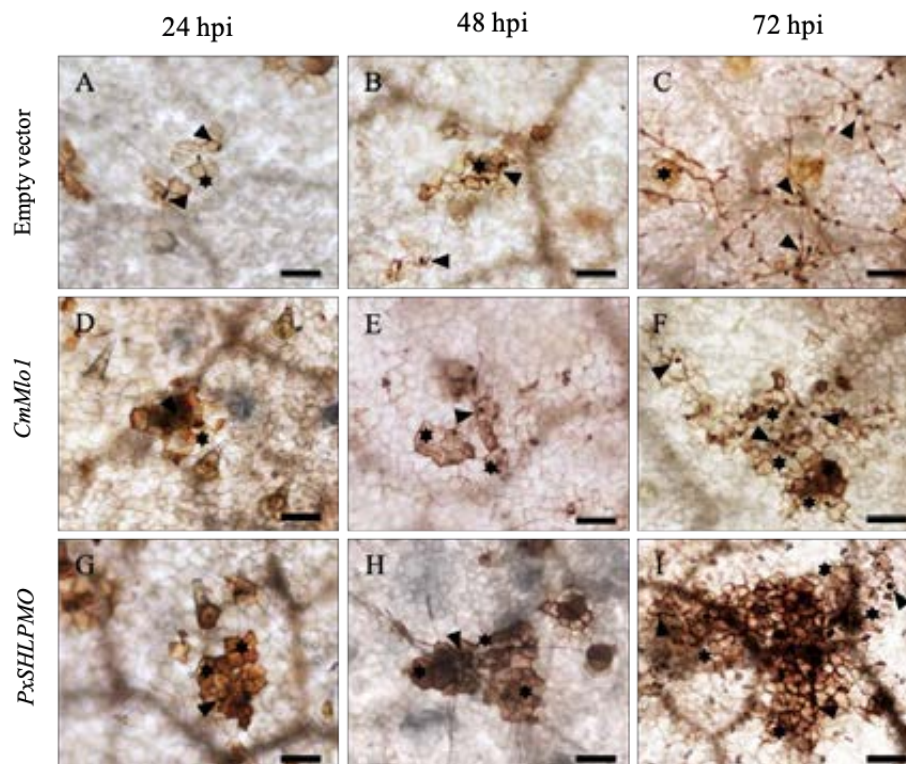


**Figure 5.7.** Time lapse of the effect of silencing of *PxSHLPMO1* on *P. xanthii* development. Gene silencing was carried out by ATM-HIGS according to Materials and Methods. Cotyledon discs were processed by the DAB-uptake method at different time points after pathogen inoculation. Empty vector was used as a negative control and silencing of melon *CmMlo1* gene was used as an RNAi positive control. Pictures were taken 24, 48 and 72 h after pathogen inoculation. Arrowheads indicate penetration points corresponding to haustoria and asterisks indicate reactive cells with accumulation of hydrogen peroxide. Bars = 100  $\mu$ m.

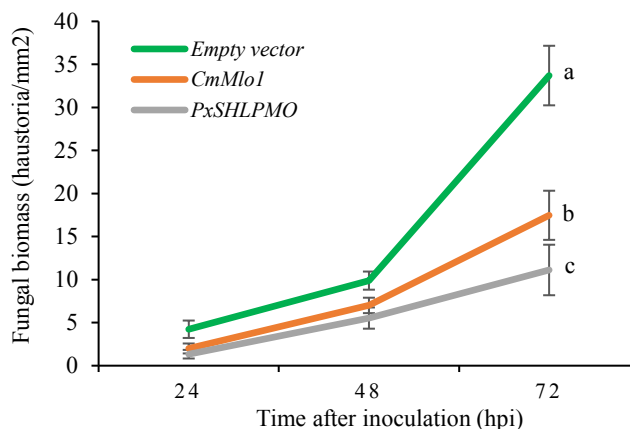


**Figure 5.8.** Effect of silencing of *PxSHLPMO1* on *P. xanthii* growth by means of haustorial counting. The haustorial counts were carried out on melon discs stained by DAB method after gene silencing using the ATM-HIGS system. The empty vector used for RNAi silencing was used as a negative control, whereas the RNAi silencing of the melon *CmMlo1* gene was used as a positive control for RNA interference. The number of haustoria per square millimeter of agro-infiltrated tissue was used as an estimation of fungal biomass. Values show the mean of 30 samples from three independent experiments. Bars indicate the standard error. The same letters indicate values that are not significantly different at  $P=0.05$  according to Fisher's least significant difference test (LSD).

Furthermore, a molecular approach was also used to estimate the fungal biomass (Figure 5.9). For this purpose, genomic DNA was isolated from agro-infiltrated melon cotyledons 72 h after inoculation with *P. xanthii* and used to quantify the *P. xanthii* tubulin/ *C. melo* actin ratio by qPCR. The results obtained by this approach were similar to those obtained by haustorial counts, showing a considerably reduction of *P. xanthii* biomass after *PxSHLPMO1* silencing compared to empty vector.

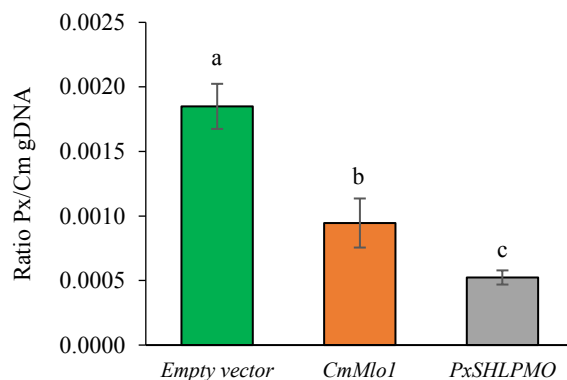


**Figure 5.9.** Molecular estimation of *P. xanthii* growth after silencing of *PxSHLPMO1*. The ATM-HIGS was used for gene silencing. The empty vector was used as a negative control and the RNAi silencing of the *CmMlo1* gene from melon was used as a positive control for RNAi-induced resistance. Agro-infiltrated melon cotyledons 72 h after inoculation of *P. xanthii* were used for isolation of genomic DNA. Genomic DNA ratio of *P. xanthii* to melon cotyledon (Px/Cm gDNA) was expressed as an indicator of molecular fungal biomass after amplification of *P. xanthii*  $\beta$ -tubulin and *C. melo* actin genes (Table 5.3). Values of bars indicate the mean  $\pm$  standard error of three technical replicates from three different DNA samples. Different letters indicate significant differences between values at  $P=0.05$  according to Fisher's least significant difference test (LSD).

The fungal biomass at 72 h after infection corresponding to haustorial counts (Figure 5.8) and the molecular estimation by qPCR (Figure 5.9) were used to calculate the percentages of reduction of *P. xanthii* growth produced by silencing of *PxSHLPMO1* gene (Table 5.3). The reductions of fungal growth obtained by both approaches were very similar although slightly higher in the case of the molecular approach.

**Table 5.3.** Effect of silencing of *PxSHLPMO1* on fungal development.

Fungal growth	Microscopic estimation		Molecular estimation	
	Number of haustoria <sup>b</sup>	Reduction (%) <sup>c</sup>	<i>P. xanthii</i> / <i>C. melo</i> <sup>d</sup>	Reduction (%) <sup>c</sup>
Empty vector (negative control)	33.71 ± 3.46 a	-	0.0018 ± 0.00017 a	-
<i>CmMlo1</i> (positive control)	17.47 ± 2.85 b	48.18	0.00089 ± 0.00019 b	50.56
<i>PxSHLPMO1</i>	11.12 ± 2.93 c	67.01	0.000523 ± 5.488E-05 c	70.94

<sup>a</sup> Fungal growth data were recorded 72 h after inoculation of *P. xanthii*.

<sup>b</sup> Data show the mean number of haustoria per square millimeter from 30 samples from three different experiments ± standard error. Values with different letter indicate significantly differences at P=0.05 according to Fisher's least significant difference test (LSD).

<sup>c</sup> Percentage of fungal growth reduction compared to empty vector negative control.

<sup>d</sup> Data indicate the mean ± standard error of the ratio *P. xanthii* β-tubulin / *C. melo* actin genes of three samples with three technical replicates from three different cotyledons.

### *Silencing of PxSHLPMO1 gene induces the release of reactive oxygen species by plant cells*

The same DAB-treated discs used for haustorial counts was also used to study the activation of plant defense responses by counting the number of melon epidermal cells with accumulation of hydrogen peroxide (H<sub>2</sub>O<sub>2</sub>). This accumulation was observed under a light microscope as brown-red precipitates (Figure 5.7, asterisks) on melon cotyledons agro-infiltrated with the *PxSHLPMO1* silencing construct at 24, 48 and 72 h after inoculation of *P. xanthii*. The quantification of reactive cells can be seen in Figure 5.10. The silencing of *PxSHLPMO1* triggered the plant defense mechanisms, causing an important accumulation of hydrogen peroxide on epidermal cells that was



higher than the caused by *CmMlo1* gene silencing used as positive control for RNAi-induced resistance. This strong response turned the tissue into a dark-brown color that even caused difficulties for quantification of haustoria (Figure 5.7I)

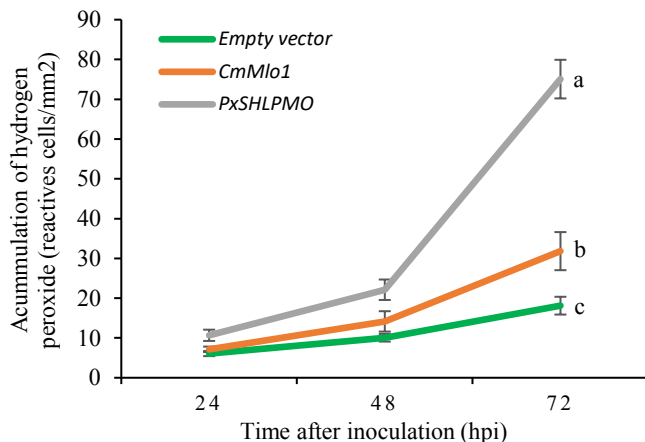


**Figure 5.10.** Time course analysis of the accumulation of hydrogen peroxide in melon cotyledons in response to inoculation with *P. xanthii* after silencing of *PxSHLPMO1*. The silencing of *PxSHLPMO1* was performed by ATM-HIGS, using the same empty vector as a negative control and the silencing of melon *CmMlo1* gene as a positive control for RNAi-induced resistance. Discs were taken at different time points and processed for the DAB-uptake method. The reactive epidermal cells were identified as containing brown-red precipitates (Figure 5.6, asterisks). Values indicate the mean  $\pm$  standard error of three different experiments with a total of 30 samples. Values with different letter are significantly different at  $P=0.05$  according to Fisher's least significant difference test (LSD).

### *Silencing of PxSHLPMO1 activates chitin-triggered immunity*

The chitin degradation action of *PxSHLPMO1* as well as the considerably reduction of *P. xanthii* growth and the activation of plant defense responses when the corresponding coding gene was silenced, suggested that *PxSHLPMO1*

could be interfering with the process of chitin recognition by the host plant. To test this hypothesis, the melon chitin receptor gene *CmCERK1*, which participates in the recognition of chitin oligomers and the activation of chitin-triggered immunity, was co-silenced together with *PxSHLPMO1* gene using the ATM-HIGS system. As in previous experiments, we first checked the efficacy of ATM-HIGS to reduce the expression of the target genes. As shown in Figure 5.11, a decrease of transcripts levels of around 50% in both genes was observed, as occurred in *PxSHLPMO1* single gene silencing.

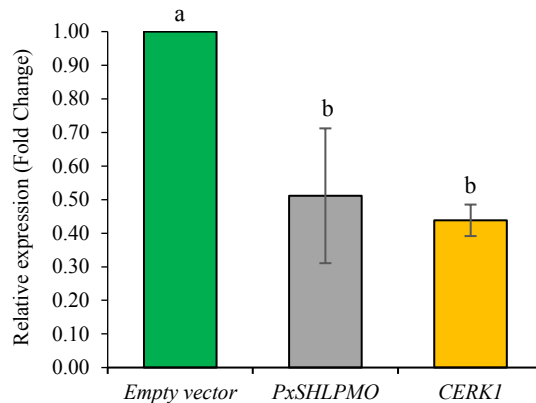


**Figure 5.11.** Analysis of ATM-HIGS efficacy on expression of *PxSHLPMO1* and *CmCERK1* genes during co-silencing experiments. Total RNA was isolated from agro-infiltrated melon cotyledons 24 h after inoculation with *P. xanthii* and expression levels was examined by qRT-PCR. The change in gene expression levels was represented as a fold change between silencing construct and empty vector sample pairs after normalization to the expression of *PxEF1* (MK249653). Bars show the standard error of three technical replicates from three different experiments. Different letters indicate expression values significantly different at  $P=0.05$  according to Fisher's least significant difference test (LSD).

The co-silencing of *PxSHLPMO1* and *CmCERK1* genes returned to the original phenotype, that is, a normal growth of *P. xanthii* as well as a low level of reactive cells compared to single *PxSHLPMO1* silencing (Figure 5.12).

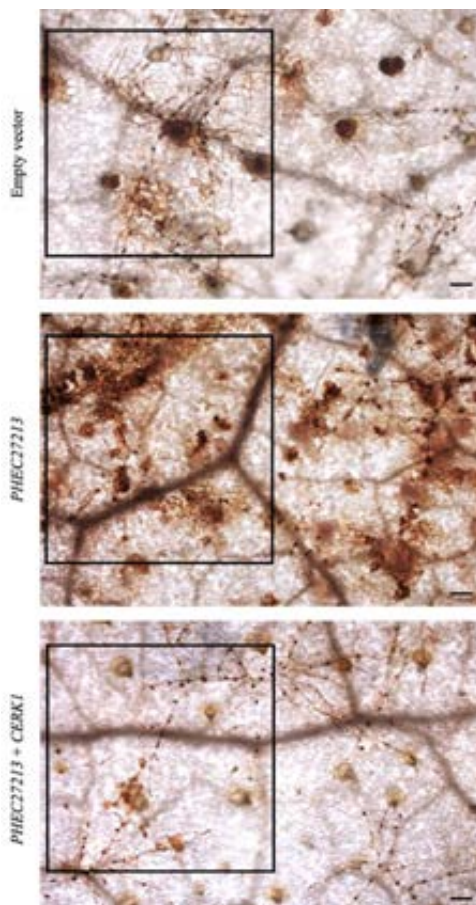


**Figure 5.12.** Effect of co-silencing of *PxSHLPMO1* and *CmCERK1* on *P. xanthii* development. Gene silencing was carried out by ATM-HIGS according to Materials and Methods. Cotyledon discs were processed by the DAB-uptake method. Empty vector was used as a negative control and silencing of melon *CmMlo1* gene was used as a positive control for RNAi-induced resistance. Pictures were taken 72 h after pathogen inoculation. Black squares indicate 1 mm<sup>2</sup> of cotyledon surface. Bars = 100 μm.

In this experiment, fungal growth was estimated by the quantification of haustorial number (Figure 5.13) as well as by a molecular estimation (Figure 5.14). The results supported the phenotypes observed by light microscopy. In both, haustorial count and molecular estimation, the *P. xanthii* development after co-silencing of *PxSHLPMO1* and *CmCERK1* genes was virtually indistinguishable from negative control and, accordingly, significantly different from the single silencing of *PxSHLPMO1* (Table 5.4).

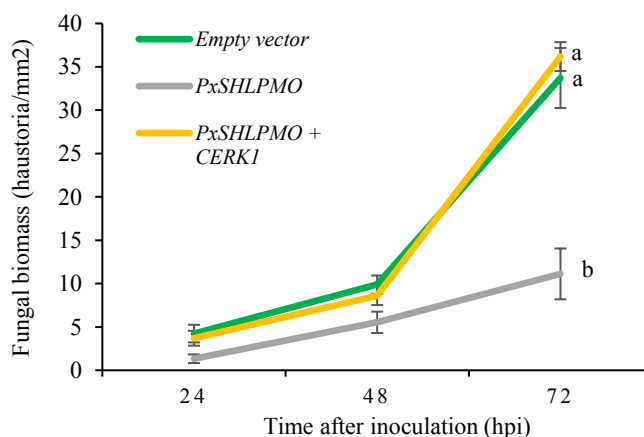


**Figure 5.13.** Effect of co-silencing of *PxSHLPMO1* and *CmCERK1* on *P. xanthii* development by means of haustorial counting. The haustorial counts were carried out on melon discs previously agro-infiltrated with the silencing constructs, inoculated with *P. xanthii* and stained by the DAB-uptake method. The empty vector was used as a negative control. The biomass was estimated as the number of haustoria per square millimeter of agro-infiltrated melon tissue. Values show the mean of 30 samples from three different experiments and the bars indicate the standard error. Values with different letter are significantly different at  $P=0.05$  according to Fisher's least significant difference test (LSD).

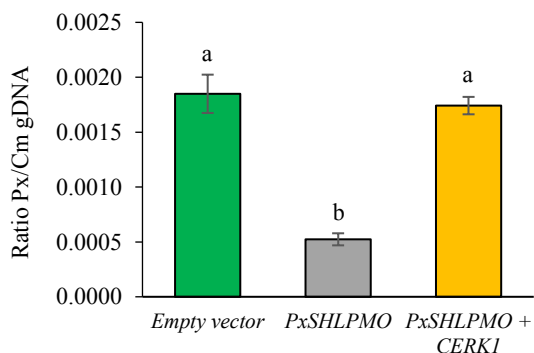


**Figure 5.14.** Molecular estimation of *P. xanthii* growth after co-silencing of *PxSHLPMO1* and *CmCERK1*. The ATM-HIGS system was used for the co-silencing of both genes. The empty vector used for RNAi was employed as a negative control. DNA was isolated from agro-infiltrated melon cotyledons 72 h after *P. xanthii* inoculation. The ratio of *P. xanthii* to melon cotyledon genomic DNA (Px/Cm gDNA) was used as an estimation of fungal biomass and was calculated by amplification of *P. xanthii*  $\beta$ -tubulin and *C. melo* actin genes by qPCR using the primers listed in Table 5.3. Bars indicate the mean  $\pm$  standard error of three technical replicates from three independent DNA samples. Different letter indicate values significantly different at  $P=0.05$  according to Fisher's least significant difference test (LSD).

In the case of the epidermal cells with accumulation of hydrogen peroxide, the co-silencing of both genes returned to the values obtained by the agro-infiltration of the empty vector (Figure 5.15), which indicated that plant responses were not activated in such circumstances.

**Table 5.4.** Effect of co-silencing of *PxSHLPMO1* and *CmCERK1* genes on *P. xanthii* development.

Silenced gene	Microscopical estimation <sup>a</sup>		Molecular estimation <sup>a</sup>	
	Number of haustoria <sup>b</sup>	Reduction (%) <sup>c</sup>	<i>P. xanthii</i> / <i>C. melo</i> <sup>d</sup>	Reduction (%) <sup>c</sup>
Empty vector	33.71 ± 3.46 a	-	0.0018 ± 0.00017 a	-
<i>PxSHLPMO1</i>	11.12 ± 2.93 c	67.01	0.000523 ± 5.488E-05 b	70.94
<i>PxSHLPMO1</i> + <i>CmCERK1</i>	36.18 ± 1.67 a	7.33	0,0017 ± 7.930E-5 a	5.56

<sup>a</sup> Fungal growth data were recorded 72 h after inoculation of *P. xanthii*.

<sup>b</sup> Data show the mean number of haustoria per square millimeter from 30 samples from three different experiments ± standard error. Values with different letter indicate significantly differences at P=0.05 according to Fisher's least significant difference test (LSD).

<sup>c</sup> Percentage of fungal growth reduction referred to values obtained with empty vector (negative control).

<sup>d</sup> Data indicate the mean ± standard error of the ratio *P. xanthii* β-tubulin/*C. melo* actin genes of three samples with three technical replicates from three different cotyledons.

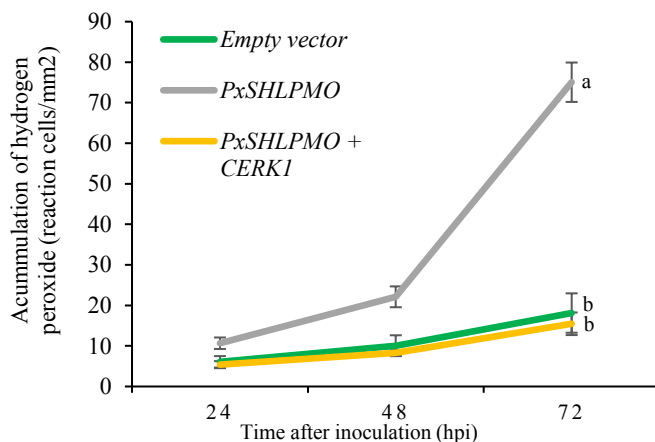


**Figure 5.15.** Analysis of hydrogen peroxide accumulation in epidermal cells of melon cotyledons in response to *P. xanthii* after co-silencing of *PxSHLPMO1* and *CmCERK1*. The ATM-HIGS system was used for silencing and the empty vector used for RNAi was employed as a negative control. The epidermal cells with accumulation of hydrogen peroxide were stained by the DAB-uptake method and identified as containing brown-red precipitates (asterisks in Figure 5.6). Data indicate the mean of 30 different samples from three experiments. Bars represent  $\pm$  standard error. Values with the same letter are not significantly different at  $P=0.05$  according to Fisher's least significant difference test (LSD).

In summary, the silencing of *PxHSLPMO1* caused the activation of a plant defense response which arrested the *P. xanthii* growth, whereas the co-silencing of *PxSHLPMO1* and melon *CmCERK1* restored the *P. xanthii* growth and caused the suppression of activation of plant responses. This results indicated that *PxSHLPMO1* was involved in the suppression of a defense signaling pathway governing by the *CERK1* receptor. Moreover, its ability to bind chitin and to break down chitin oligomers clearly indicated that *PxSHLPMO1* was a protein involved in the manipulation of chitin-triggered immunity.

*PxSHLPMO1* orthologues are widely distributed in many pathogenic ascomycete fungi

The presence of *PxSHLPMO1* orthologues was studied by BLASTp analysis using the deduced amino acid sequence of *PxSHLPMO1* as a query sequence. As shown in Table 5.5, orthologous genes are widely present in the genomes of many pathogenic fungi, mostly in animal/human pathogens, but also in plant and insect pathogens. Furthermore this gene is also present in endophytic/endomycorrhizal fungi. The presence of *PxSHLPMO1* orthologues in saprophytic fungi is very limited in comparison with its wide presence in pathogenic and endophytic/endomycorrhizal fungi.

**Table 5.5.** Fungal species assessed for the presence of *PxSHLPMO1* orthologues.

Species	Pathogenicity	Identity (%)	Accession no.
<b>Leotiomycetes</b>			
<i>Rhynchosporium commune</i>	Plant pathogen	60	CZT02273.1
<i>Rhynchosporium secalis</i>	Plant pathogen	60	CZT53033.1
<i>Rhynchosporium agropyri</i>	Plant pathogen	61	CZT08592.1
<i>Cadophora</i> sp.	Plant pathogen	61	PVH76518.1
<i>Phialophora americana</i>	Animal/human pathogen	52	KIW70575.1
<i>Phialophora hyalina</i>	Endophytic/endomycorrhizal	55	RDL36398.1
<i>Hyaloscypha finlandica</i>	Endophytic/endomycorrhizal	52	<a href="#">ACPI9527.1</a>
<i>Hyaloscypha variabilis</i>	Endophytic/endomycorrhizal	59	<a href="#">PMD37570.1</a>
<i>Coleophoma crateriformis</i>	Endophytic/endomycorrhizal	54	RDW78501.1
<i>Coleophoma cylindrospora</i>	Animal/human pathogen	60	RDW84639.1
<i>Duddingtonia flagrans</i>	Entomopathogen	53	<a href="#">RVD84252.1</a>
<i>Dactylellina haptotyla</i>	Entomopathogen	48	EPS41873.1
<i>Glarea lozoyensis</i>	Saprophytic	54	XP_008087835.1
<i>Pezoloma ericae</i>	endophytic/endomycorrhizal	53	PMD21535.1
<i>Meliniomyces bicolor</i>	Endophytic/endomycorrhizal	52	XP_024729819.1
<b>Dothiodesmycetes</b>			
<i>Pseudogymnoascus</i> sp.	Animal/human pathogen	47	KFY19308.1
<i>Cladophialophora yegresii</i>	Animal/human pathogen	52	XP_007754892.1
<i>Cladophialophora carrioni</i>	Animal/human pathogen	53	OCT50285.1
<i>Cladophialophora bantiana</i>	Animal/human pathogen	54	XP_016616728.1
<i>Cladophialophora psammophila</i>	Animal/human pathogen	54	XP_007747041.1
<i>Cladophialophora immunda</i>	Animal/human pathogen	46	XP_016253641.1



<i>Hortaea werneckii</i>	Animal/human pathogen	49	OTA23506.1
<b>Eurotiomycetes</b>			
<i>Chaetothryales sp.</i>	Animal/human pathogen	50	<a href="#">RMZ91855.1</a>
<i>Rhinoctadiella mackenziei</i>	Animal/human pathogen	54	XP_013274494.1
<i>Arthrotrichys oligospora</i>	Entomopathogen	52	XP_011117840.1
<i>Exophiala aquamarina</i>	Animal/human pathogen	54	XP_013256137.1
<i>Exophiala dermatitidis</i>	Animal/human pathogen	50	XP_009158214.1
<i>Exophiala xenobiotica</i>	Animal/human pathogen	53	XP_013315436.1
<i>Fonsecaea erecta</i>	Animal/human pathogen	53	XP_013315436.1
<i>Fonsecaea multimorphosa</i>	Animal/human pathogen	54	XP_016636211.1
<i>Fonsecaea pedrosoi</i>	Animal/human pathogen	52	XP_013285390.1
<b>Sodariomycetes</b>			
<i>Ophiostoma piceae</i>	Plant pathogen	47	EPE09813.1
<i>Sporothrix insectorum</i>	Entomopathogen	52	OAA55257.1

## DISCUSSION

As an obligate biotroph, *P. xanthii* requires living cells to complete its asexual life cycle, which ultimately implies the suppression of activation of plant defense mechanisms. The mechanisms by which *P. xanthii* avoids the recognition by the host, remain largely unknown. For this purpose, *P. xanthii*, among other abilities, has to hide its PAMPs or manipulate their detection to suppress the activation of PAMP-triggered immunity. These activities are most likely carried out by the secretion of effectors. In other fungal pathogens, such as *C. fulvum* or *M. oryzae*, effectors proteins with the ability to suppress chitin-triggered immunity have been described (van den Burg *et al.*, 2007; Bolton *et al.*, 2008; Jonge *et al.*, 2010; Sánchez-Vallet *et al.*, 2013; Xi *et al.*, 2014). In the case of *P. xanthii*, although some proteins related with chitin modification have been recently described in hyphal cells (Martínez-Cruz, 2016), to date no mechanisms specific of the haustorium have been described with the ability to avoid the recognition of chitin of this fungal structure by the epidermal plant

cells. The ability of haustorium to avoid its recognition by the plant is mandatory, because it is the fungal structure that maintains the most intimate relationship with the host cells and the main and probably the unique structure involved in nutrient uptake (Both *et al.*, 2005; Bindschedler *et al.*, 2009; Micali *et al.*, 2011; Martínez-Cruz *et al.*, 2014). Moreover, the fact that the chitin is a major component of haustorial cell wall (Micali *et al.*, 2011), suggests the importance of hiding this polymer to avoid the activation of plant defense mechanisms. In this work, the haustorial transcriptome of *P. xanthii* has allowed us to identify an effector candidate, PHEC27213, with a putative predicted function as a lytic polysaccharide monooxygenase of chitin. This protein, which presented typical effector features such as unknown annotated function, small size and a wave-like expression pattern (Pedersen *et al.*, 2012; Hacquard, 2014), was the most expressed haustorium-specific secreted protein (see chapter III), suggesting a key role of PHEC27213 for haustorial physiology. For all this, in this work we have performed a molecular characterization of PHEC27213 in order to elucidate its putative function as a chitin-hiding related protein.

The bioinformatic predicted function of PHEC27213 showed a high structural analogy with a AA11 lytic polysaccharide monooxygenase (LPMO) from *A. oryzae*. To date LPMOs have been classified in four families according to their auxiliary activity (AA) in the Cazy database (Levasseur *et al.*, 2013; Lombard *et al.*, 2014). The AA9 family members cleave cellulose and hemicellulose (Quinlan *et al.*, 2011; Phillips *et al.*, 2011; Agger *et al.*, 2014; Vu *et al.*, 2014a; Bennati-Granier *et al.*, 2015; Frommhagen *et al.*, 2015) whereas the AA11 and AA13 families target chitin and starch, respectively (Hemsworth *et al.*, 2014; Vu *et al.*, 2014b; Lo Leggio *et al.*, 2015). For its part, the AA10 LPMOs cleave both, cellulose and chitin (Vaaje-Kolstad *et al.*, 2010; Forsberg *et al.*, 2014). In addition, the AA10 LPMOs family is the unique family that

have been described in bacteria, virus and eukaryotic organisms, whereas the AA11 and AA13 families are present exclusively in fungi. Usually LPMOs enzymes have been described as single domain enzymes, however, some of these enzymes also contain carbohydrate-binding modules (CBMs) that could help to clarify their function according to substrate preferences (Horn *et al.*, 2012), as it occurs with the protein *ScLPMO10c*, a LPMO from *Streptomyces coelicolor* that cleaves cellulose and contain a cellulose-binding domain, CBM2, (Forsberg *et al.*, 2014). In this way, the presence of the chitin binding domain 3, corresponding to CBM5 according to UniProt and Cazy databases, supported the putative function of PHEC27213 as an AA11 LPMO, that is, a LPMO protein that could cleave chitin. On the other hand, the chitin-binding assay demonstrated the chitin-binding activity of PHEC27213 and the enzymatic assay showed a specific cleavage pattern for chitin. Therefore, PHEC27213 was renamed as PxSHLPMO1 for *P. xanthii* secreted haustorial LPMO1, a new LPMO of the AA11 LPMO family, family that, to date, had been only described in *A. oryzae* (Hemsworth *et al.*, 2014).

The MALDI-TOF analysis of the enzymatic reaction products after the incubation of colloidal chitin with PxSHLPMO1, showed that the product masses were consistent with a primary chain cleavage by C1 oxidation, yielding predominantly aldonic acid oligosaccharides as previously described for AA10 LPMO (Vaaje-Kolstad *et al.*, 2010). Nevertheless, in the lytic activity of AA11 LPMO, it was also significant the presence of unmodified oligosaccharides and species with -2 Da of mass (Hemsworth *et al.*, 2014), which could be representing unopened lactones (LI *et al.*, 2012). In the case of PxSHLPMO1, those species with -2 Da were a minority, being only present in the practically imperceptible peaks corresponding to DP6 and DP7. Therefore, the cleavage mechanism of PxSHLPMO1 seems to be more similar to AA10 than AA11

LPMO. However, in the case of AA10, the aldonic acid oligosaccharides presented, especially, even-numbered degrees of polymerization (DP4, DP6, DP8...) (Vaaje-Kolstad *et al.*, 2010), whereas in the case of PxSHLPMO1 the product masses showed, predominantly, a degree of polymerization of 5. This cleavage pattern is different to the previously described for LPMOs of chitin. Nonetheless, the recent discovery of LPMO activity (Vaaje-Kolstad *et al.*, 2010), its novel identification in insects (Sabbadin *et al.*, 2018) and the fact that, to date, they have not been described in pathogenic organisms, together with the wide distribution of *PxSHLPMO1* orthologues without functional annotation in the genomes of many fungal pathogens, suggest that *PxSHLPMO1* could be a novel AA11 LPMO of chitin specifically involved in pathogenic processes.

To validate this hypothesis, the silencing of *PxSHLPMO1* was carried out by the ATM-HIGS method (Martínez-Cruz *et al.*, 2018b), showing a notable reduction of *P. xanthii* growth, even higher than the reduction caused by silencing of *CmMlo1* gene, the positive control typically used in ATM-HIGS experiments with *P. xanthii* (Martínez-Cruz *et al.*, 2018a). Moreover, the accumulation of oxygen reactive species (ROS) by the plant was also higher than after the silencing of *CmMlo1* gene. This exacerbated release of ROS by the plant when *PxSHLPMO1* was silenced suggests a role of *PxSHLPMO1* linked to the suppression of the activation of plant defense responses. For this reason, the *CmCERK1* gene from melon was co-silenced together to *PxSHLPMO1* gene. *CERK1* gene encodes a transmembrane kinase receptor indispensable for perception of chitin oligomers by the plant, since the absence of CERK1 causes the loss of the ability to respond to oligosaccharide elicitors, suppressing the production of ROS, the activation of MAP kinases as well as the expression of defense related genes (Miya *et al.*, 2007; Gimenez-Ibanez *et al.*, 2009; Lee *et al.*, 2013; Petutschnig *et al.*, 2014). The silencing of both genes,

caused the reversion to wild type phenotype, that is, a normal growth of *P. xanthii* and a suppression of ROS production, concluding that CERK1 was involved in the PTI response mediated by chitin when *PxSHLPMO1* was silenced. Therefore, we conclude that the mechanism of action of *PxSHLPMO1* is to suppress the activation of plant immunity by avoiding the recognition of haustorial chitin by plant cells. This fact could be related with the dimerization of CERK1 induced by chito-oligosaccharides. It has been described that chitin octamers induce the CERK1 dimerization and, hence, activate the plant defense mechanisms mediated by chitin, whereas shorter oligomers do not promote the CERK1 dimerization and do not activate the subsequent signaling response (Liu *et al.*, 2012b). *PxSHLPMO1* activity cleaves the chitin, fundamentally, in chito-oligosaccharides with DP5, which cannot induce the dimerization of CERK1.

With all this information, we propose a model to explain the role of *PxSHLPMO1* in the *P. xanthii*-melon interaction (Figure 5.16). The protein, localized in the extrahaustorial matrix after secretion, should act on large chitin fragments probably released by plant chitinases or fungal chitinases during haustorial growth, to break them into small oligomers, thus avoiding chitin recognition by CERK1 and, hence, suppressing the activation of chitin-triggered immunity. In this model, we also propose that CERK1 should be located in the extrahaustorial membrane, as it has been also described for other plant receptors responsible for pathogen recognition such as RPW8.2, which enhances hydrogen peroxide accumulation and callosic encasement of the haustorial complex (Wang *et al.*, 2009; Kim *et al.*, 2014), although further experiments are necessary for its confirmation. The expression pattern of *PxSHLPMO1*, with a maximum expression overlapping with the maximum of formation of primary appressoria (Pérez-García *et al.*, 2001) and, hence, with the haustorial development, suggests that this protein could be acting by cleaving large chitin

fragments released by fungal chitinases, which were localized in haustorial transcriptome (chapter III), during the haustorial growth. In addition, the fact that plant endo-chitinases were found over-expressed in the melon RNA-seq during the first stages of the infection (chapter II), also suggests the possibility that PxSHLPMO1 could be also acting on chitin fragments released by the enzymatic activity of plant endo-chitinases. To date, no mechanisms have been described to evade or to suppress PTI in powdery mildew haustoria. Micali *et al.*, (2011) did not find chitosan or any other modification in the haustorial chitin and they suggested the presence of “unknown mechanisms” to allow the suppression of chitin-triggered immunity. For all this, it is tempting to think that PxSHLPMO1 could be one of the main mechanisms of the haustorium to avoid the activation of PTI induced by chitin.

Finally, the wide conservation of this enzyme among pathogenic ascomycetes and, in lesser extent, in endophytic and endomycorrhizal fungi, suggests that we are facing a novel LPMO of chitin with a different cleavage pattern and specifically related with the suppression of chitin recognition by the host. Our findings reinforce the idea that the evolution of molecular strategies to disarm the activation of chitin-activated immunity is mandatory for the successful colonization of plant environments by fungi.

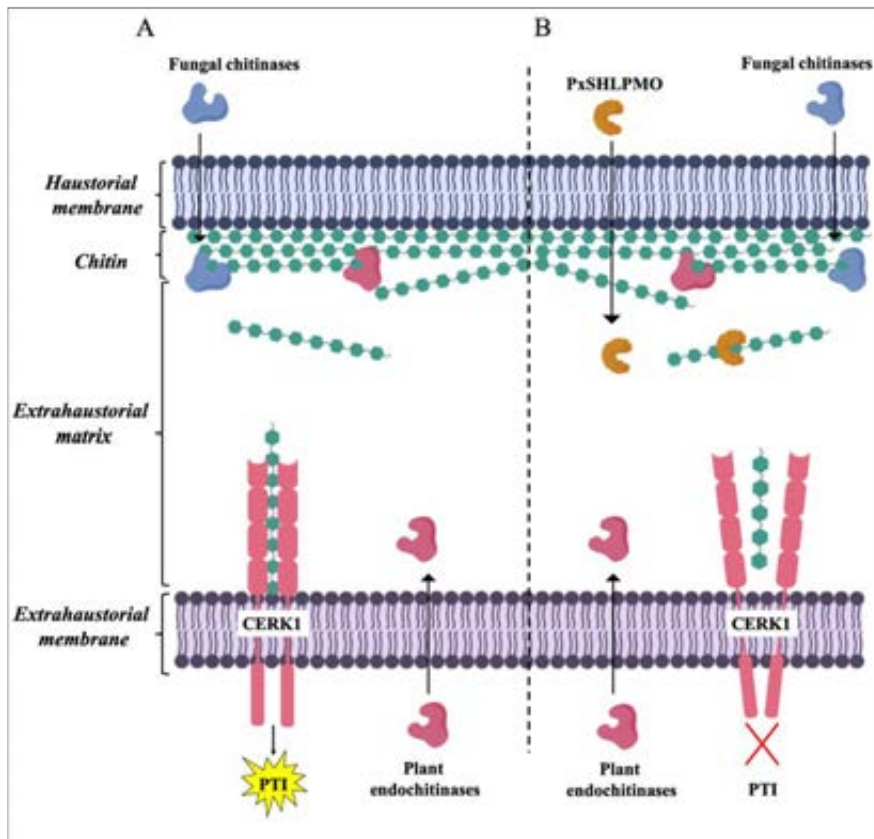


**Figure 5.16.** Schematic representation of the role proposed for PxSHLPMO1. A) Without the action of PxSHLPMO1, the fungal chitinases during the haustorial growth and/or the activity of plant secreted endo-chitinases release chitin fragments with a high number of oligomers that are recognized by CERK1 receptor, activating PTI (chitin-triggered immunity). B) When PxSHLPMO1 is released to the extrahaustorial matrix, this protein may act by cleaving the chitin fragments into oligomers with a predominant degree of polymerization of 5 (DP5) that cannot induce the CERK1 dimerization, thus suppressing the activation of PTI.

---

## REFERENCES

**Agger JW, Isaksen T, Varnai A, Vidal-Melgosa S, Willats WGT, Ludwig R, Horn SJ, Eijssink VGH, Westereng B.** 2014. Discovery of LPMO activity on hemicelluloses shows the importance of oxidative processes in plant cell wall degradation. *Proceedings of the National Academy of Sciences* **111**, 6287–6292.

**Álvarez B, Torés JA.** 1997. Cultivo in vitro de *Sphaerotheca fuliginea* (Schlecht. ex Fr.), efecto de diferentes fuentes de carbono sobre su desarrollo. *Boletín de sanidad vegetal. Plagas* **23**, 283–288.

**Bellón-Gómez D, Vela-Corcía D, Pérez-García A, Torés JA.** 2015. Sensitivity of *Podosphaera xanthii* populations to anti-powdery-mildew fungicides in Spain. *Pest Management Science* **71**, 1407–1413.

**Bennati-Granier C, Garajova S, Champion C, et al.** 2015. Substrate specificity and regioselectivity of fungal AA9 lytic polysaccharide monoxygenases secreted by *Podospira anserina*. *Biotechnology for Biofuels* **8**, 90.

**Bindschedler L V., Burgis TA, Mills DJS, Ho JTC, Cramer R, Spanu PD.** 2009. In planta proteomics and proteogenomics of the biotrophic barley fungal pathogen *Blumeria graminis* f. sp. hordei. *Molecular & Cellular Proteomics* **8**, 2368–2381.

**Bolton MD, Van Esse HP, Vossen JH, et al.** 2008. The novel *Cladosporium fulvum* lysin motif effector Ecp6 is a virulence factor with orthologues in other fungal species. *Molecular Microbiology* **69**, 119–136.

**Both M, Csukai M, Stumpf MPH, Spanu PD.** 2005. Gene expression profiles of *Blumeria graminis* indicate dynamic changes to primary metabolism



during development of an obligate biotrophic pathogen. *The Plant Cell* **17**, 2107–2122.

**van den Burg HA, Harrison SJ, Joosten MHAJ, Vervoort J, de Wit PJGM.** 2007. *Cladosporium fulvum* Avr4 protects fungal cell walls against hydrolysis by plant chitinases accumulating during infection. *Molecular Plant-Microbe Interactions* **19**, 1420–1430.

**Cao Y, Liang Y, Tanaka K, Nguyen CT, Jedrzejczak RP, Joachimiak A, Stacey G.** 2014. The kinase LYK5 is a major chitin receptor in *Arabidopsis* and forms a chitin-induced complex with related kinase CERK1. *eLife* **3**, e03766.

**Delaunais B, Jeandet P, Clément C, Baillieux F, Dorey S, Cordelier S.** 2014. Uncovering plant-pathogen crosstalk through apoplastic proteomic studies. *Frontiers in Plant Science* **5**, 249.

**Doehlemann G, Hemetsberger C.** 2013. Apoplastic immunity and its suppression by filamentous plant pathogens. *New Phytologist* **198**, 1001–1016.

**Fernández-Ortuño D, Pérez-García A, López-Ruiz F, Romero D, De Vicente A, Torés JA.** 2006. Occurrence and distribution of resistance to QoI fungicides in populations of *Podosphaera fusca* in south central Spain. *European Journal of Plant Pathology* **115**, 215–222.

**Forsberg Z, Mackenzie AK, Sorlie M, Rohr AK, Helland R, Arvai AS, Vaaje-Kolstad G, Eijsink VGH.** 2014. Structural and functional characterization of a conserved pair of bacterial cellulose-oxidizing lytic polysaccharide monoxygenases. *Proceedings of the National Academy of Sciences* **111**, 8446–8451.

**Frommhagen M, Sforza S, Westphal AH, Visser J, Hinz SWA, Koetsier MJ, Van Berkel WJH, Gruppen H, Kabel MA.** 2015. Discovery of the combined oxidative cleavage of plant xylan and cellulose by a new fungal polysaccharide monoxygenase. *Biotechnology for Biofuels* **8**, 101.

**Gimenez-Ibanez S, Hann DR, Ntoukakis V, Petutschnig E, Lipka V, Rathjen JP.** 2009. AvrPtoB targets the LysM receptor kinase CERK1 to promote bacterial virulence on plants. *Current Biology* **19**, 423–429.

**Hacquard S.** 2014. The genomics of powdery mildew fungi: Past achievements, present status and future prospects. *Advances in Botanical Research* **70**, 109-142

**Hemsworth GR, Henrissat B, Davies GJ, Walton PH.** 2014. Discovery of a new family of lytic polysaccharide mono-oxygenases. *Nature Chemical Biology* **10**, 122–126.

**Hemsworth GR, Johnston EM, Davies GJ, Walton PH.** 2015. Lytic polysaccharide monooxygenases in biomass conversion. *Trends in Biotechnology* **33**, 747–761.

**Horn SJ, Vaaje-kolstad G, Westereng B, Eijsink VG.** 2012. Novel enzymes for the degradation of cellulose. *Biotechnology for Biofuels* **5**, 45.

**Jones JD, Dangl JL.** 2006. The plant immune system. *Nature* **444**, 323–329.

**De Jonge R, Bolton MD, Thomma BPHJ.** 2011. How filamentous pathogens co-opt plants: The ins and outs of fungal effectors. *Current Opinion in Plant Biology* **14**, 400–406.

**Jonge R De, Esse HP Van, Kombrink A, Shinya T, Desaki Y, Bours R, Krol S Van Der, Shibuya N, Joosten MHAJ, Thomma BPHJ.** 2010. Conserved fungal LysM Effector Ecp6 prevents chitin-triggered immunity in plants. *Science* **329**, 953–955.

**Kaku H, Nishizawa Y, Ishii-Minami N, Akimoto-Tomiya C, Dohmae N, Takio K, Minami E, Shibuya N.** 2006. Plant cells recognize chitin fragments for defense signaling through a plasma membrane receptor. *Proceedings of the National Academy of Sciences* **103**, 11086–11091.

**Karimi M, Inzé D, Depicker A.** 2002. GATEWAY™ vectors for

*Agrobacterium*-mediated plant transformation. Trends in Plant Science **7**, 193–195.

**Kim H, O’Connell R, Maekawa-Yoshikawa M, Uemura T, Neumann U, Schulze-Lefert P.** 2014. The powdery mildew resistance protein RPW8.2 is carried on VAMP721/722 vesicles to the extrahaustorial membrane of haustorial complexes. Plant Journal **79**, 835–847.

**Kombrink A, Thomma BPHJ.** 2013. LysM effectors secreted proteins supporting fungal life. PLoS Pathog **9**, e1003769.

**Koressaar T, Remm M.** 2007. Enhancements and modifications of primer design program Primer3. Bioinformatics **23**, 1289–1291.

**Lee W-S, Rudd JJ, Hammond-Kosack KE, Kanyuka K.** 2013. *Mycosphaerella graminicola* LysM effectormMediated stealth pathogenesis subverts recognition through both CERK1 and CEBiP homologues in wheat . Molecular Plant-Microbe Interactions **27**, 236–243.

**Lo Leggio L, Simmons TJ, Poulsen JCN, et al.** 2015. Structure and boosting activity of a starch-degrading lytic polysaccharide monooxygenase. Nature Communications **6**, 5961.

**Levasseur A, Drula E, Lombard V, Coutinho PM, Henrissat B.** 2013. Expansion of the enzymatic repertoire of the CAZy database to integrate auxiliary redox enzymes. Biotechnology for Biofuels **6**, 41.

**LI X, Beeson WT, Phillips CM, Marletta MA, Cate JH.** 2012. Structural basis for substrate targeting and catalysis by fungal polysaccharide monooxygenases. Structure **20**, 1051–1061.

**Liu B, Li J-F, Ao Y, et al.** 2012a. Lysin Motif-Containing Proteins LYP4 and LYP6 Play dual roles in peptidoglycan and chitin perception in rice innate immunity. The Plant Cell **24**, 3406–3419.

**Liu T, Liu Z, Song C, et al.** 2012b. Chitin-induced dimerization activates a

plant immune receptor. *Science* **336**, 1160–1164.

**Lombard V, Golaconda Ramulu H, Drula E, Coutinho PM, Henrissat B.** 2014. The carbohydrate-active enzymes database (CAZy) in 2013. *Nucleic Acids Research* **42**, D490–D495.

**Martínez-Cruz J, Romero D, Dávila JC, Pérez-García A.** 2014. The *Podospaera xanthii* haustorium, the fungal Trojan horse of cucurbit-powdery mildew interactions. *Fungal genetics and biology* **71**, 21–31.

**Martínez-Cruz,** 2016. Análisis morfológico y funcional de la interacción *Podospaera xanthii*- cucurbitáceas. PhD thesis, University of Malaga, Malaga, Spain.

**Martínez-Cruz J, Romero D, de la Torre FN, Fernández-Ortuño D, Torés JA, de Vicente A, Pérez-García A.** 2018a. The functional characterization of *Podospaera xanthii* candidate effector genes reveals novel target functions for fungal pathogenicity. *Molecular Plant-Microbe Interactions* **31**, 914-931.

**Martínez-Cruz J, Romero D, De Vicente A, Pérez-García A.** 2018b. Transformation by growth onto agro-infiltrated tissues (TGAT), a simple and efficient alternative for transient transformation of the cucurbit powdery mildew pathogen *Podospaera xanthii*. *Molecular Plant Pathology* **19**, 2502–2515.

**Mentlak TA, Kombrink A, Shinya T, et al.** 2012. effector-mediated suppression of chitin-triggered immunity by *Magnaporthe oryzae* is necessary for rice blast disease. *The Plant Cell* **24**, 322–335.

**Micali CO, Neumann U, Grunewald D, Panstruga R, O'Connell R.** 2011. Biogenesis of a specialized plant-fungal interface during host cell internalization of *Golovinomyces orontii* haustoria. *Cellular Microbiology* **13**, 210–226.

**Miya A, Albert P, Shinya T, Desaki Y, Ichimura K, Shirasu K, Narusaka**

**Y, Kawakami N, Kaku H, Shibuya N.** 2007. CERK1, a LysM receptor kinase, is essential for chitin elicitor signaling in *Arabidopsis*. Proceedings of the National Academy of Sciences **104**, 19613–19618.

**Mochizuki S, Saitoh K ichiro, Minami E, Nishizawa Y.** 2011. Localization of probe-accessible chitin and characterization of genes encoding chitin-binding domains during rice-*Magnaporthe oryzae* interactions. Journal of General Plant Pathology **77**, 163–173.

**Nakagawa T, Kurose T, Hino T, Tanaka K, Kawamukai M, Niwa Y, Toyooka K, Matsuoka K, Jinbo T, Kimura T.** 2007. Development of series of gateway binary vectors, pGWBs, for realizing efficient construction of fusion genes for plant transformation. Journal of bioscience and bioengineering **104**, 34–41.

**Pagni M, Ioannidis V, Cerutti L, Zahn-Zabal M, Jongeneel CV, Hau J, Martín O, Kuznetsov D, Falquet L.** 2007. MyHits: Improvements to an interactive resource for analyzing protein sequences. Nucleic Acids Research **35**, W433–W437.

**Pedersen C, van Themaat EVL, McGuffin LJ, et al.** 2012. Structure and evolution of barley powdery mildew effector candidates. BMC Genomics **13**, 694.

**Pérez-García A, Olalla L, Rivera E, Del Pino D, Cánovas I, De Vicente A, Torés JA.** 2001. Development of *Sphaerotheca fusca* on susceptible, resistant, and temperature-sensitive resistant melon cultivars. Mycological Research **105**, 1216–1222.

**Pérez-García A, Romero D, Fernández-Ortuño D, López-Ruiz F, De Vicente A, Torés JA.** 2009. The powdery mildew fungus *Podosphaera fusca* (synonym *Podosphaera xanthii*), a constant threat to cucurbits. Molecular plant pathology **10**, 153–160.

**Petersen TN, Brunak S, von Heijne G, Nielsen H.** 2011. SignalP 4.0: discriminating signal peptides from transmembrane regions. *Nature Methods* **8**, 785.

**Petutschnig EK, Stolze M, Lipka U, et al.** 2014. A novel *Arabidopsis* CHITIN ELICITOR RECEPTOR KINASE 1 (CERK1) mutant with enhanced pathogen-induced cell death and altered receptor processing. *New Phytologist* **204**, 955–967.

**Phillips CM, Beeson WT, Cate JH, Marletta MA.** 2011. Cellobiose dehydrogenase and a copper-dependent polysaccharide monooxygenase potentiate cellulose degradation by *Neurospora crassa*. *ACS chemical biology* **6**, 1399–1406.

**Pieterse CMJ, Leon-Reyes A, Van Der Ent S, Van Wees SCM.** 2009. Networking by small-molecule hormones in plant immunity. *Nature Chemical Biology* **5**, 308–316.

**del Pino D, Olalla L, Pérez-García A, Rivera ME, García S, Moreno R, de Vicente A, Torés JA.** 2002. Occurrence of races and pathotypes of cucurbit powdery mildew in southeastern Spain. *Phytoparasitica* **30**, 459–466.

**Lo Presti L, Lanver D, Schweizer G, Tanaka S, Liang L, Tollot M, Zuccaro A, Reissmann S, Kahmann R.** 2015. Fungal effectors and plant susceptibility. *Annual Review of Plant Biology* **66**, 513–545.

**Quinlan RJ, Sweeney MD, Lo Leggio L, et al.** 2011. Insights into the oxidative degradation of cellulose by a copper metalloenzyme that exploits biomass components. *Proceedings of the National Academy of Sciences* **108**, 15079–15084.

**Sabbadin F, Hemsworth GR, Ciano L, et al.** 2018. An ancient family of lytic polysaccharide monooxygenases with roles in arthropod development and biomass digestion. *Nature Communications* **9**, 756.

**Sánchez-Vallet A, Saleem-Batcha R, Kombrink A, Hansen G, Valkenburg D-J, Thomma BP, Mesters JR.** 2013. Fungal effector Ecp6 outcompetes host immune receptor for chitin binding through intrachain LysM dimerization. *eLife* **2**, e00790.

**Spanu PD, Abbott JC, Amselem J, et al.** 2010. Genome expansion and gene loss in powdery mildew fungi reveal tradeoffs in extreme parasitism. *Science* **330**, 1543–1546.

**Tanaka S, Ichikawa A, Yamada K, Tsuji G, Nishiuchi T, Mori M, Koga H, Nishizawa Y, O'Connell R, Kubo Y.** 2010. HvCEBiP, a gene homologous to rice chitin receptor CEBiP, contributes to basal resistance of barley to *Magnaporthe oryzae*. *BMC Plant Biology* **10**, 288.

**Tanaka K, Nguyen CT, Liang Y, Cao Y, Stacey G, Tanaka K, Nguyen CT, Liang Y, Cao Y, Stacey G.** 2013. Role of LysM receptors in chitin-triggered plant innate immunity Role of LysM receptors in chitin-triggered plant innate immunity. *Plant Signaling & Behavior* **8**, e22598.

**Thordal-Christensen H, Zhang Z, Wei Y, Collinge DB.** 1997. Subcellular localization of H<sub>2</sub>O<sub>2</sub> in plants. H<sub>2</sub>O<sub>2</sub> accumulation in papillae and hypersensitive response during the barley-powdery mildew interaction. *Plant Journal* **11**, 1187–1194.

**Thornton B, Basu C.** 2011. Real-time PCR (qPCR) primer design using free online software. *Biochemistry and Molecular Biology Education* **39**, 145–154.

**Vaaje-Kolstad G, Westereng B, Horn SJ, Liu Z, Zhai H, Sørli M, Eijsink VGH.** 2010. An oxidative enzyme boosting the enzymatic conversion of recalcitrant polysaccharides. *Science* **330**, 219–222.

**Vela-Corcía D, Bautista R, De Vicente A, Spanu PD, Pérez-García A.** 2016. *De novo* analysis of the epiphytic transcriptome of the cucurbit powdery

mildew fungus *Podosphaera xanthii* and identification of candidate secreted effector proteins. PLoS ONE **11**, e0163379.

**Vogel J, Somerville S.** 2002. Isolation and characterization of powdery mildew-resistant *Arabidopsis* mutants. Proceedings of the National Academy of Sciences **97**, 1897–1902.

**Vu V V, Beeson WT, Phillips CM, Cate JHD, Marletta MA.** 2014a. Determinants of regioselective hydroxylation in the fungal polysaccharide monooxygenases. Journal of the American Chemical Society **136**, 562–565.

**Vu V V., Beeson WT, Span EA, Farquhar ER, Marletta MA.** 2014b. A family of starch-active polysaccharide monooxygenases. Proceedings of the National Academy of Sciences **111**, 13822–13827.

**Wan J, Zhang X, Stacey G.** 2008. Chitin signaling and plant disease resistance. Molecular Plant Pathology **6**, 831–833.

**Wang W, Wen Y, Berkey R, Xiao S.** 2009. Specific Targeting of the Arabidopsis Resistance Protein RPW8.2 to the Interfacial Membrane Encasing the Fungal Haustorium Renders Broad-Spectrum Resistance to Powdery Mildew. the Plant Cell Online **21**, 2898–2913.

**Weßling R, Schmidt SM, Micali CO, Knaust F, Reinhardt R, Neumann U, Ver Loren van Themaat E, Panstruga R.** 2012. Transcriptome analysis of enriched *Golovinomyces orontii* haustoria by deep 454 pyrosequencing. Fungal Genetics and Biology **49**, 470–482.

**Xi Y, Pan PL, Ye YX, Yu B, Zhang CX.** 2014. Chitin deacetylase family genes in the brown planthopper, *Nilaparvata lugens* (Hemiptera: Delphacidae). Insect Molecular Biology **23**, 695–705.

**Young VL, Simpson RM, Ward VK.** 2005. Characterization of an exochitinase from *Epiphyas postvittana nucleopolyhedrovirus* (family *Baculoviridae*). Journal of General Virology **86**, 3253–3261.



**Zarivi O, Cesare P, Ragnelli AM, Aimola P, Leonardi M, Bonfigli A, Colafarina S, Poma AM, Miranda M, Pacioni G.** 2015. Validation of reference genes for quantitative real-time PCR in Périgord black truffle (*Tuber melanosporum*) developmental stages. *Phytochemistry* **116**, 78–86.

**Zhang Y.** 2008. I-TASSER server for protein 3D structure prediction. *BMC bioinformatics* **9**, 40.

# CHAPTER VI

## General Discussion



Powdery mildew diseases are widely distributed throughout the world and affect a multitude of crops of enormous economic importance, such as cereals, grapevine, vegetables and ornamentals (Ridout *et al.*, 2006; Braun and Cook, 2012; Takamatsu, 2013; Seifi *et al.*, 2014), inflicting significant losses in the crop yield. Despite their economic and agronomic importance, molecular tools and genomic resources for the fungi that cause these diseases are scarce. With the advent of the “omics” technologies and the development of specific tools such as HIGS, an increase of interest for the powdery mildew fungi has been observed in the last years. However, to date, most of the molecular studies have been focused on the “model” powdery mildew fungus *B. graminis* f. sp. *hordei*, the causal agent of barley powdery mildew.

In the particular case of the cucurbit powdery mildew *P. xanthii*, the information currently available is very little in comparison with other powdery mildews and ridiculous compared to other plant fungal pathogens. As previously indicated, the management of cucurbit powdery mildew is highly dependent on chemicals and that is the reason why high levels of resistance to main fungicides have been frequently reported in *P. xanthii* populations (Fernández-Ortuño *et al.*, 2006; Bellón-Gómez *et al.*, 2015), making the management of the disease very difficult. All this shows the need to obtain new information about the molecular mechanisms that govern the *P. xanthii* – cucurbits interaction that could be useful in developing novel disease control tools such as resistant cultivars or phytosanitary products to successfully face this disease. Therefore, the present Ph.D. thesis was planned to obtain new information from the interaction *P. xanthii* – cucurbits, focusing on obtaining molecular data from the compatible interaction, separating the study of what happens in the plants infected by *P. xanthii* from the study of the haustorium and its role in the pathogenesis.

## TRANSCRIPTOMIC APPROACHES TO UNRAVEL THE PLANT-PATHOGEN MOLECULAR DIALOGUE

From our point of view, the first step in the development of new and appropriate programs for the control of cucurbit powdery mildew is to understand the molecular dialogue between the pathogen and its host. For that reason, we have focused on deciphering both parts of dialogue mainly by transcriptomic studies that allow us to know those expression changes occurred in melon plants as a consequence of *P. xanthii* infection, as well as to identify those *P. xanthii* genes potentially related with the pathogenesis. Although the transcriptomic analyses performed have allowed us to identify two major dysregulated processes in melon plants infected with *P. xanthii* (see chapter II) as well as to identify several transcripts coding for secreted proteins highly expressed in the *P. xanthii* haustorium (see chapter III), these findings are just the tip of the iceberg due to the multiple possibilities of the new transcriptomic and bioinformatic approaches to decipher more in detail the molecular aspects of this interaction.

The development of the *de novo* haustorial transcriptome of *P. xanthii* and its comparison with the previously performed epiphytic transcriptome (Vela-Corcía *et al.*, 2016), not only have allowed us to identify haustorium-specific genes, but also to develop a new general transcriptome by combining both epiphytic and haustorial transcriptomes, although the sequencing techniques used were different. This analysis has been possible thanks to the development of new bioinformatic software such as TransFlow (Seoane *et al.*, 2018), which is able to assembly raw reads with different origin and size. RNA-seq analysis is an effective approach to elucidate the primary changes in gene expression,

providing a precise measurement of transcript levels and allowing researchers to detect transcripts with low abundance (’t Hoen *et al.*, 2008; Marguerat and Bähler, 2010). In this way, it has been possible to detect the few number of fungal transcripts present in RNA-seq analysis of melon leaves infected with *P. xanthii* during the first stages of the infection, when the amount of fungal biomass is practically negligible compared to the plant biomass, which will allow the development of new approaches such as dual RNA-seq, using the general transcriptome of *P. xanthii* as a reference transcriptome for the mapping process of fungal reads.

To date, transcriptomic studies have been limited to analyse changes in gene expression in the infected host or in the pathogen, however, for a more comprehensive understanding of the interactions that occurred during host-pathogen relationships, it is necessary to know the changes in gene expression that are associated in the host and in the pathogen. This can be currently done by the so-called dual RNA-seq analysis (Westermann *et al.*, 2012, 2017). Dual RNA-seq analysis is an unbiased simultaneous transcriptomic study to elucidate the infectious process (Enguita *et al.*, 2016), which has been used in several infection models including plant diseases (Alkan *et al.*, 2015; Meyer *et al.*, 2016; Westermann *et al.*, 2016; Nuss *et al.*, 2017). For example, the dual RNA-seq study of *Eucalyptus nitens* – *Phytophthora cinnamomi* compatible interaction has allowed to identify several virulence factors as well as potentially manipulated hosts targets and modulated host defence-related mechanisms (Meyer *et al.*, 2016). However, dual RNA-seq not only allows a better understanding of the simultaneous changes in gene expression, but also allows the identification of non-coding RNA both in the host and in the pathogen, revealing those ncRNAs associated with virulence and pathogenesis, that are not detectable with other approaches (Westermann *et al.*, 2016, 2017). This fact

is of vital importance to understand plant-powdery mildew interactions, taking into account the importance of ncRNAs in other powdery mildew infection models (Xin *et al.*, 2010, 2011; Kusch *et al.*, 2018) and specially the putative importance of ncRNAs in the physiology of the *P. xanthii* haustorium (see chapter III).

The adaption of host and pathogen gene expression is mediated by complex gene regulatory networks (GRN). Consequently, an improvement of molecular interaction predictions is necessary to promote our understanding about molecular interplay between both organisms (Schulze *et al.*, 2016). In this way, the practicability and applicability of dual RNA-seq analysis in the field of biological interactions prediction stands out (Dix *et al.*, 2016; Schulze *et al.*, 2016). The gene regulatory networks (GRN) prediction can be carried out through network inference (NI) approaches, using gene expression data from dual RNA-seq analysis (Figure 6.1). The input material to develop a network inference is a matrix of gene expression containing the changes in expression values of genes from host and pathogen during infection (Schulze *et al.*, 2016). Although the result of a network inference can be different depending on the approach, the correlation network (Figure 6.2) is one of the fastest and simplest methods to predict gene regulatory networks (GRN). In this case, the interaction prediction is based in the pairwise correlation between each pair of genes. Always that a correlation value between the expression of two genes is above a user defined cut-off, an interaction is predicted (Schulze *et al.*, 2016). In this manner it has been possible to detect several putative base interactions in the *Zea mays/Aspergillus flavus* pathosystem such as the co-regulation of AflS, a key *A. flavus* regulator of aflatoxin cluster, with several ROS producing genes from *Z. mays*, suggesting a monitoring of host ROS levels by fungal AflS (Musungu *et al.*, 2016).

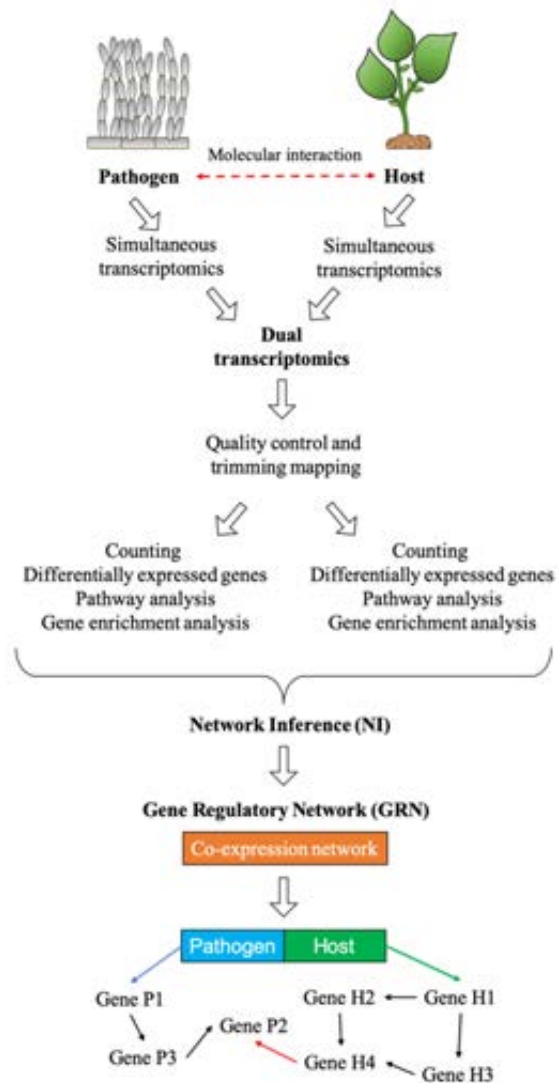


**Figure 6.1.** Schematic representation of a gene regulatory network (GRN) prediction carried out by network inference (NI) using transcriptomic data from simultaneous RNA-seq analyses. The putative molecular interactions of intra-specie (black bar) and inter-species (red bar) can be predicted by, among other system biology approaches, by a co-expression network. Adapted from Schulze *et al.*, (2016).



Although correlation does not always mean causality, this gene regulatory network and other system biology approaches based in transcriptomic data, such as Bayesian network (Schulze *et al.*, 2016), provides a valuable information in order to predict cross-species interactions (Dix *et al.*, 2016), avoiding other techniques substantially longer, tedious and complex such as a massive yeast two hybrid screening (Weßling *et al.*, 2014). The wide applications of high-throughput transcriptomic analyses are helping us to a better understanding of the molecular mechanism underlying pathogenesis and the molecular response of the host cells against the infection. Regarding the *P. xanthii* – melon interaction, dual RNA-seq analysis will be particularly useful to identify, for example, fungal effector candidates or ncRNAs potentially involved in dysregulation of primary metabolism and secondary metabolism and their host targets. Thus, if protein-protein associations are found, protein-protein interactions should be investigated further. After proper analyses, these findings may lead to the discovery of susceptibility genes (*S*) and, ultimately, to the development of resistant cultivars by molecular breeding or gene editing.

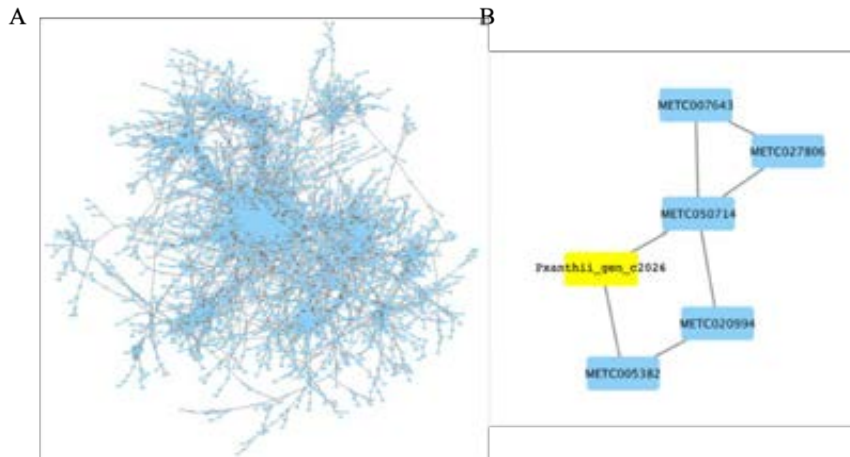


**Figure 6.2.** Example of interspecific *C. melo* and *P. xanthii* correlation network performed from simultaneous transcriptomic analysis using Pearson correlation analysis and visualized using Cytoscape software. The network contains edges (lines that imply linkage) and nodes (*C. melo* or *P. xanthii* genes). A) Global correlation network. B) Isolate subnetwork found within the global network. Blue nodes indicate *C. melo* genes and the yellow node indicates a *P. xanthii* gene.

## THE HAUSTORIUM IS NOT ANOTHER FUNGAL CELL

The importance of haustoria for rust and powdery mildew fungi has been widely described, fundamentally as a structure for feeding and factor exchange with the host (Szabo and Bushnell, 2001; Voegelé *et al.*, 2002; Voegelé and Mendgen, 2003, 2011; Oliva *et al.*, 2010; Martínez-Cruz *et al.*, 2014, 2018a). Although in this work we have deepened into this structure, deciphering several biological processes and secreted proteins specific to haustorium (see chapter III), many molecular mechanisms that underlies its function remain largely unknown, mainly due to the low quality of extracted RNA from isolate haustoria

(see chapter III). Identification of such processes could provide valuable information in the fight against powdery mildew diseases. The accomplishment of a better quality haustorial transcriptome could help us to get this goal. For that purpose, a new haustorial isolation method with a shorter required time and/or appropriate fixation method that preserve the RNA in tissue samples should be performed in order to obtain RNA preparations of better quality. In this way, the on ice fixation using Farmer's solution provides good quality of RNA from samples obtained by laser capture microdissection (Kerk *et al.*, 2003). Moreover, the combination of this fixation technique together with the laser capture microdissection have been successfully used in the transcriptomic analysis of isolated uredinia formed by the *Melampsora larici-populina* and *Pakopsora pachyrizi* rust fungi (Tremblay *et al.*, 2009; Hacquard *et al.*, 2010). In the other hand, the development of the *P. xanthii* genome could help to identify those haustorial transcripts that due to the degradation of RNA were not assembled, thus contributing to obtain additional and valuable information from the already obtained haustorial sequences.

The haustorium is not only present in fungal pathogens such as rust or powdery mildew fungi, it is also present in parasitic plants (Yoshida *et al.*, 2016). Although the structure of the plant parasitic haustorium and its connection with the host are quite different from fungal haustorium, its function is very similar, being involved in suppression of host immunity, probably by the release of effectors (Saucet and Shirasu, 2016), and in the transfer of nutrients (Honaas *et al.*, 2013; Yoshida *et al.*, 2016). The proximity of functions between both plant and fungal haustoria suggests that other important features described in parasitic plant haustoria could also be present in fungal haustoria. In this way, it is worthwhile to note the transfer of genetic material via the haustorium in parasitic plants (Yoshida *et al.*, 2016).

The plant parasitic haustorium not only acquires nutrients and water from the host, but also is able to obtain proteins, different metabolites, mRNAs and even viruses (Kim *et al.*, 2014; Kim and Westwood, 2015). It has been described that a huge amount of mRNAs are bidirectionally transferred between the parasitic plant *Cuscuta* spp. and their hosts (Roney *et al.*, 2006; Kim *et al.*, 2014; Thieme *et al.*, 2015). In the case of the interaction between *Cuscuta pentagona* and *Arabidopsis*, about 1% of mRNAs are acquired by *Cuscuta* from *Arabidopsis* and approximately 0.6% is transferred in the other sense, that is, from *Cuscuta* to *Arabidopsis*. These mRNAs cover the 45% of total *Cuscuta* expressed unigenes and the 24% of total *Arabidopsis* expressed unigenes (Kim *et al.*, 2014). Although features related to mRNA mobility have not been described (Thieme *et al.*, 2015) and the biological role of this bi-directional flow remains unsolved, it is tempting to speculate that it could be related with the maintenance of parasitism, the manipulation of the host plant or the acquisition of host physiological components (Yoshida *et al.*, 2016), since they seem to have some kind of transference selectivity (Leblanc *et al.*, 2013), being the abundant presence of a given transcript in the haustorium one of the factors related to the selective mobility (Kim *et al.*, 2014). In this work, we have described the haustorium as a structure with a high transcription rate and, hence, it could be directly related with this bi-directional transport and, perhaps, with some kind of genetic manipulation different to previously described by the small RNAs in other plant-powdery mildew interactions (Piccinelli *et al.*, 2005; Xin *et al.*, 2010, 2011; Kusch *et al.*, 2018). This fact is supported by the detection of translational products coming from parasitic plants mobile mRNAs in the hosts, suggesting that mRNAs may be transferred and translated to develop their biological functions in their destination (Těšitel *et al.*, 2015).

Therefore, will the powdery mildew haustorium be able to obtain not only nutrients from the plant cells? The data from parasitic plant haustoria, together the huge rate of haustorial transcription and the high amount of non-coding RNAs present in the haustorium of *P. xanthii* and described in this work (see chapter III), as well as the acquisition of RNAi by the haustorium in HIGS assays (Nowara *et al.*, 2010; Martínez-Cruz *et al.*, 2018a) and the co-localization of Rab5 protein from *P. xanthii* and VirD2 protein from *A. tumefaciens* into small haustorial vesicles during TGAT transformation (Martínez-Cruz *et al.*, 2018b), make tempting to speculate that fungal haustoria could have a bulk flow of genetic material similar to plant parasitic haustoria. Although more information is necessary to decipher this putative function, it could suppose a key point to increase our knowledge about powdery mildew diseases and help us to develop new control strategies. With this regard, we have to mention that during the process of assembly and annotation of haustorial transcriptomes, plant reads are filtered out. It would be interesting to examine the raw reads of the *P. xanthii* haustorial transcriptome and search for plant transcripts. The identification of plant transcripts in the haustorial transcriptome would be additional evidence to explain the features of powdery mildew fungi as obligate biotrophs and host-specific parasites.

## **HAUSTORIUM-SPECIFIC SECRETED PROTEINS: UNTAPPED TARGETS FOR RATIONAL FUNGICIDE DESIGN**

Since ancient times different strategies have been developed for plant disease management (Awasthi, 2015). Currently, such strategies include cultural

practices, the use of resistant cultivars, the application of fungicides and the use of biological control agents, among others. However, the repeated applications of fungicides remain as the main control tool against powdery mildew diseases (McGrath, 2010). The fungicides currently used against powdery mildews include contact fungicides, such as Sulphur, a multisite fungicide, and the systemic fungicides, the most popular among growers, which affect a specific physiological function in the fungal cell (Fraaije *et al.*, 2007). Among the latter are, for example, the Q<sub>o</sub> inhibitors that targets the cytochrome *bcl* complex of the respiratory chain essential for fungal respiration and ATP biosynthesis (Fernández-Ortuño *et al.*, 2008), the DMI fungicides that inhibit the biosynthesis of ergosterol, the major membrane lipid in fungi (Steffens *et al.*, 1996) or the benzimidazole fungicides that interfere with the microtubule assembly, targeting the  $\beta$ -tubulin subunit of fungal tubulin (Ishii, 2004). However, powdery mildew fungi have shown a great ability to develop resistance to the chemical compounds used for their control (McGrath, 2001; López-Ruiz *et al.*, 2010; Bellon-Gómez *et al.*, 2015; Kunova *et al.*, 2016), due, among other factors, to the large number of asexual spores that they are able to produce and the genome plasticity, presenting a huge amount of transposable elements that promotes gene duplication, mutation and specialization (Bergthorsson *et al.*, 2007; Hahn, 2009; Spanu *et al.*, 2010; Levasseur and Pontarotti, 2011; Pedersen *et al.*, 2012; Hacquard, 2014). All this makes the development of effective control tools for powdery mildew fungi a difficult barrier to overcome.

In the past, the identification of new chemical compounds for plant disease management has been carried out mainly by massive screening of thousands of compounds in conjunction with serendipity. By this approach, only about 1 out of 10,000 molecules screened was selected after different stages of development

(Schwinn and Geissbühler, 1986). In addition to the low efficiency of this approach, we must add the decreasing rate of new active ingredients around the world as a consequence of fungicide resistance or environmental toxicity issues (Worthing and Walker, 1983). This situation calls for different and potentially more efficient alternative approaches for fungicide design such as the termed rational synthesis approach, which was defined by Geissbühler *et al.* (1983) as “the intellectual and experimental exploration of working hypotheses generated from biological information on specific target systems”, that is, designing new fungicides with a particular target in mind (Lucas, 1998). For this purpose is necessary, as stated above, a comprehensive knowledge of molecular mechanisms underlying the pathogenesis of the target organism. In this work, we have deepened into the physiological functions of the main pathogenesis-related fungal structure of powdery mildews, the haustorium (Oliva *et al.*, 2010), focusing on the panel of secreted proteins of *P. xanthii* haustorium and describing the role implication of some of these proteins for fungal development and pathogenesis (see chapter IV and chapter V). Due to the lack of new fungicides and the need of development of novel chemistry, in this work we aimed to investigate the potential of haustorium-specific secreted proteins as untapped targets for the rational design of fungicides. The first step in this process is the identification of biological targets that could be essential for fungal pathogenicity as could be the haustorium-specific secreted proteins without annotated function. The next steps include the prediction of protein function and its experimental validation as well as the verification of gene importance by gene silencing. Last, the search for known inhibitors, the subsequent screening of analogues molecules and their refinement to increase fungicide efficacy, would result in the identification of novel potential fungicide compounds (Figure 6.3).

This approach would include the different levels mentioned by Schwinn and Geissbühler (1986) for the rational design of fungicides: i) Molecular level: molecular information about the target, by mutating the coding gene or silencing its expression and performing models that reflect binding sites of the target enzyme; ii) Biochemical level: Biochemical information by testing systems that reflect the activity of the target enzyme; iii) Morphological level: Morphological information by microscopic and macroscopic observation of whole organism development after the lack of enzyme function.

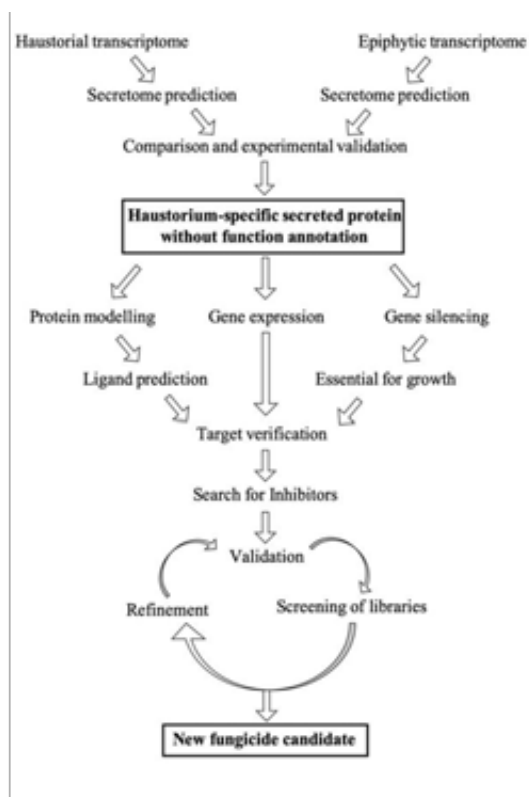


**Figure 6.3.** Schematic representation of the process of target discovery and rational fungicide design based on the use of haustorium-specific secreted proteins without annotated function.



However, this approach is not free of problems, for example, the difficulties in haustorial isolation (Godfrey *et al.*, 2010; Weßling *et al.*, 2012) to obtain haustoria preparations free of contaminants. In any case, the development of bioinformatic tools helps us to accomplish this approach. In this way, software such as Secretool, PECAS and DeepLoc (Cortázar *et al.*, 2014; Cortazar *et al.*, 2015; Almagro Armenteros *et al.*, 2017) allowed an accurate prediction of the secreted proteins, whereas software such as I-TASSER, Phyre2, CATH/Gene3D and MotifScan allowed us to define molecular 3D models and to predict motif and ligands with a high reliability (Pagni *et al.*, 2007; Zhang, 2008; Kelly *et al.*, 2015; Lam *et al.*, 2016). However, the main problem we face with this approach is the recalcitrant difficulty of the genetic manipulation of obligate biotrophs, which has been solved thanks to previous works developed in our laboratory. These works have included gene silencing and transient transformation systems in both cases using *A. tumefaciens* (Martínez-Cruz *et al.*, 2018a; 2018b), which have been especially useful for functional characterization of effector candidates, thus, representing the cornerstone of this rational approach. In the case of enzymatic targets, once enzyme inhibitors have been identified and using the structure-activity relationships of this primary data, cheminformatics approaches such as molecular topology (Zanni *et al.*, 2018) can be used to screen hundreds of thousands of compounds from virtual libraries to identify more potent inhibitors, which, after experimental validation, will be the candidates to consider as novel fungicides.

The molecular advances about the *P. xanthii*-cucurbits interaction obtained in this Ph.D. thesis have allowed us to identify two potential targets for this rational process of fungicide design, which are related with two different biological processes and are fully necessary for the development of *P. xanthii*: i) two acid phosphatases involved in the acquisition of phosphorus (see chapter

IV) and ii) a lytic polysaccharide monooxygenase with a role in the manipulation of plant chitin-triggered immunity (see chapter V). For the first target, enzyme inhibitors have been already found that, when applied to plants, suppress fungal growth. This is the first premise for novel fungicide design by molecular topology. We hope that this knowledge will allow us to discover novel chemistry that can be used to control phytopathogenic fungi by targeting phosphorous metabolism.

## REFERENCES

**Alkan N, Friedlander G, Ment D, Prusky D, Fluhr R.** 2015. Simultaneous transcriptome analysis of *Colletotrichum gloeosporioides* and tomato fruit pathosystem reveals novel fungal pathogenicity and fruit defense strategies. *New Phytologist* **205**, 801–815.

**Almagro Armenteros JJ, Sønderby CK, Sønderby SK, Nielsen H, Winther O.** 2017. DeepLoc: prediction of protein subcellular localization using deep learning. *Bioinformatics* **33**, 3387–3395.

**Awasthi LP.** 2015. In: *Recent advances in the diagnosis and management of plant diseases*. Springer. New Delhi.

**Bellón-Gómez D, Vela-Corcía D, Pérez-García A, Torés JA.** 2015. Sensitivity of *Podosphaera xanthii* populations to anti-powdery-mildew fungicides in Spain. *Pest Management Science* **71**, 1407–1413.

**Bergthorsson U, Andersson DI, Roth JR.** 2007. Ohno's dilemma: Evolution of new genes under continuous selection. *Proceedings of the National Academy of Sciences* **104**, 17004–17009.

**Braun U and Cook RT.** 2018. In: *Taxonomic manual of the Erysiphales (powdery mildew)*. Utrecht: CBS-KNAW Fungal Biodiversity Centr. pp. 707

**Cortázar AR, Aransay AM, Alfaro M, Oguiza JA, Lavín JL.** 2014. SECRETOOL: Integrated secretome analysis tool for fungi. *Amino Acids* **46**, 471–473.

**Cortazar AR, Oguiza JA, Aransay AM, Lavín JL.** 2015. PECAS: Prokaryotic and eukaryotic classical analysis of secretome. *Amino Acids* **47**, 2659–2663.

**Dix A, Vlais S, Guthke R, Linde J.** 2016. Use of systems biology to

decipher host–pathogen interaction networks and predict biomarkers. *Clinical Microbiology and Infection* **22**, 600–606.

**Enguita F, Costa M, Fusco-Almeida A, Mendes-Giannini M, Leitão A.** 2016. Transcriptomic crosstalk between fungal invasive pathogens and their host cells: Opportunities and challenges for next-generation sequencing methods. *Journal of Fungi* **2**, 7.

**Fernández-Ortuño D, Pérez-García A, López-Ruiz F, Romero D, de Vicente A, Torés JA.** 2006. Occurrence and distribution of resistance to QoI fungicides in populations of *Podosphaera fusca* in south central Spain. *European Journal of Plant Pathology* **115**, 215–222.

**Fernández-Ortuño D, Torés JA, De Vicente A, Pérez-García A.** 2008. Mechanisms of resistance to QoI fungicides in phytopathogenic fungi. *International Microbiology* **11**, 1–9.

**Fraaije BA, Cools HJ, Kim SH, Motteram J, Clark WS, Lucas JA.** 2007. A novel substitution I381V in the sterol 14 $\alpha$ -demethylase (CYP51) of *Mycosphaerella graminicola* is differentially selected by azole fungicides. *Molecular Plant Pathology* **8**, 245–254.

**Geissbüler H, Müller U, Patchlatko P, Andwaespe HR.** 1983. Biorational design of chemicals. In: *Chemistry and world food supplies: the new frontiers*. Chemrawn 11, pp. 643-656. Oxford, New York: Pergamon Press

**Godfrey D, Böhlenius H, Pedersen C, Zhang Z, Emmersen J, Thordal-Christensen H.** 2010. Powdery mildew fungal effector candidates share N-terminal Y/F/WxC-motif. *BMC Genomics* **11**.

**Hacquard S, Delaruelle C, Legué V, Tisserant E, Kohler A, Frey P, Martin F, Duplessis S.** 2010. Laser capture microdissection of uredinia formed by *Melampsora larici-populina* revealed a transcriptional switch between biotrophy and sporulation. *Molecular plant-microbe interactions* **23**, 1275–

1286.

**Hacquard S.** 2014. The genomics of powdery mildew fungi: Past achievements, present status and future prospects. *Advances in Botanical Research* **70**, 109-142

**Hahn MW.** 2009. Distinguishing among evolutionary models for the maintenance of gene duplicates. *Journal of Heredity* **100**, 605–617.

**'t Hoen PAC, Ariyurek Y, Thygesen HH, Vreugdenhil E, Vossen RHAM, de Menezes RX, Boer JM, van Ommen GJB, den Dunnen JT.** 2008. Deep sequencing-based expression analysis shows major advances in robustness, resolution and inter-lab portability over five microarray platforms. *Nucleic Acids Research* **36**, e141

**Honaas LA, Wafula EK, Yang Z, et al.** 2013. Functional genomics of a generalist parasitic plant: Laser microdissection of host-parasite interface reveals host-specific patterns of parasite gene expression. *BMC Plant Biology* **13**, 9.

**Ishii H.** 2004. Studies on fungicide resistance in phytopathogenic fungi. *Journal of General Plant Pathology* **70**, 379–381.

**Kelly LA, Mezulis S, Yates C, Wass M, Sternberg M.** 2015. The Phyre2 web portal for protein modelling, prediction, and analysis. *Nature Protocols* **10**, 845–858.

**Kerk NM, Ceserani T, Tausta SL, Sussex IM, Nelson TM.** 2003. Laser capture microdissection of cells from plant tissues. *Plant physiology* **132**, 27–35.

**Kim G, LeBlanc M, Wafula EK, DePamphilis CW, Westwood JH.** 2014. Genomic-scale exchange of mRNA between a parasitic plant its hosts. *Science* **345**, 808–811.

**Kim G, Westwood JH.** 2015. Macromolecule exchange in *Cuscuta*-host

plant interactions. *Current Opinion in Plant Biology* **26**, 20–25.

**Kusch S, Frantzeskakis L, Thieron H, Panstruga R.** 2018. Small RNAs from cereal powdery mildew pathogens may target host plant genes. *Fungal Biology* **122**, 1050–1063.

**Lam SD, Dawson NL, Das S, Sillitoe I, Ashford P, Lee D, Lehtinen S, Orengo CA, Lees JG.** 2016. Gene3D: Expanding the utility of domain assignments. *Nucleic Acids Research* **44**, D404–D409.

**Leblanc M, Kim G, Patel B, Stromberg V, Westwood J.** 2013. Quantification of tomato and *Arabidopsis* mobile RNAs trafficking into the parasitic plant *Cuscuta pentagona*. *New Phytologist* **200**, 1225–1233.

**Levasseur A, Pontarotti P.** 2011. The role of duplications in the evolution of genomes highlights the need for evolutionary-based approaches in comparative genomics. *Biology Direct* **6**, 11.

**Marguerat S, Bähler J.** 2010. RNA-seq: From technology to biology. *Cellular and Molecular Life Sciences* **67**, 569–579.

**Martínez-Cruz J, Romero D, Dávila JC, Pérez-García A.** 2014. The *Podosphaera xanthii* haustorium, the fungal Trojan horse of cucurbit-powdery mildew interactions. *Fungal genetics and biology* **71**, 21–31.

**Martínez-Cruz J, Romero D, de la Torre FN, Fernández-Ortuño D, Torés JA, de Vicente A, Pérez-García A.** 2018a. The functional characterization of *Podosphaera xanthii* candidate effector genes reveals novel target functions for fungal pathogenicity. *Molecular Plant-Microbe Interactions* **31**, 914–931.

**Martínez-Cruz J, Romero D, De Vicente A, Pérez-García A.** 2018b. Transformation by growth onto agro-infiltrated tissues (TGAT), a simple and efficient alternative for transient transformation of the cucurbit powdery mildew pathogen *Podosphaera xanthii*. *Molecular Plant Pathology* **19**, 2502–2515.

**McGrath T.** 2010. Fungicide Resistance in Cucurbit Powdery Mildew Fungi. *Plant Disease* **85**, 236–245.

**Meyer FE, Shuey LS, Naidoo S, Mamni T, Berger DK, Myburg AA, van den Berg N, Naidoo S.** 2016. Dual RNA-Sequencing of *Eucalyptus nitens* during *Phytophthora cinnamomi* challenge reveals pathogen and host factors influencing compatibility. *Frontiers in Plant Science* **7**, 1–15.

**Musungu BM, Bhatnagar D, Brown RL, Payne GA, OBrian G, Fakhoury AM, Geisler M.** 2016. A network approach of gene co-expression in the *Zea mays/Aspergillus flavus* pathosystem to map host/pathogen interaction pathways. *Frontiers in Genetics* **7**, 206.

**Nowara D, Gay A, Lacomme C, Shaw J, Ridout C, Douchkov D, Hensel G, Kumlehn J, Schweizer P.** 2010. HIGS: Host-induced gene silencing in the obligate biotrophic fungal pathogen *Blumeria graminis*. *The Plant Cell* **22**, 3130–3141.

**Nuss AM, Beckstette M, Pimenova M, Schmöhl C, Opitz W, Pisano F, Heroven AK, Dersch P.** 2017. Tissue dual RNA-seq allows fast discovery of infection-specific functions and riboregulators shaping host–pathogen transcriptomes. *Proceedings of the National Academy of Sciences* **114**, E791–E800.

**Oliva R, Win J, Raffaele S, et al.** 2010. Recent developments in effector biology of filamentous plant pathogens. *Cellular Microbiology* **12**, 705–715.

**Pagni M, Ioannidis V, Cerutti L, Zahn-Zabal M, Jongeneel CV, Hau J, Martin O, Kuznetsov D, Falquet L.** 2007. MyHits: Improvements to an interactive resource for analyzing protein sequences. *Nucleic Acids Research* **35**, W433–W437.

**Pedersen C, van Themaat EVL, McGuffin LJ, et al.** 2012. Structure and evolution of barley powdery mildew effector candidates. *BMC Genomics* **13**,

694.

**Ridout CJ, Skamnioti P, Porritt O, Sacristan S, Jones JDG, Brwon KM.** 2006. Multiple avirulence paralogues in cereal powdery mildew fungi may contribute to parasite fitness and defeat of plant resistance. *The Plant Cell* **18**, 2402–2414.

**Roney JK, Khatibi PA, Westwood JH.** 2006. Cross-species translocation of mRNA from host plants into the parasitic plant dodder. *Plant Physiology* **143**, 1037–1043.

**Saucet SB, Shirasu K.** 2016. Molecular parasitic plant–host interactions. *PLOS Pathogens* **12**, e1005978.

**Schulze S, Schleicher J, Guthke R, Linde J.** 2016. How to predict molecular interactions between species? *Frontiers in Microbiology* **7**, 1–13.

**Schwinn F, Geissbühler H.** 1986. Towards a more rational approach to fungicide design. *Crop protection* **5**, 33–40.

**Seifi A, Gao D, Zheng Z, Pavan S, Faino L, Visser RGF, Wolters AMA, Bai Y.** 2014. Genetics and molecular mechanisms of resistance to powdery mildews in tomato (*Solanum lycopersicum*) and its wild relatives. *European Journal of Plant Pathology* **138**, 641–665.

**Seoane P, Espigares M, Carmona R, et al.** 2018. TransFlow: A modular framework for assembling and assessing accurate de novo transcriptomes in non-model organisms. *BMC Bioinformatics* **19**, 416.

**Spanu PD, Abbott JC, Amselem J, et al.** 2010. Genome expansion and gene loss in powdery mildew fungi reveal tradeoffs in extreme parasitism. *Science* **330**, 1543–1546.

**Steffens JJ, Pell EJ, Tien M.** 1996. Mechanisms of fungicide resistance in phytopathogenic fungi. *Current Opinion in Biotechnology* **7**, 348–355.

**Szabo LJ, Bushnell WR.** 2001. Hidden robbers: The role of fungal



haustoria in parasitism of plants. Proceedings of the National Academy of Sciences **98**, 7654–7655.

**Takamatsu S.** 2013. Molecular phylogeny reveals phenotypic evolution of powdery mildews (Erysiphales, Ascomycota). Journal of General Plant Pathology **79**, 218–226.

**Těšitel J, Těšitelová T, Fisher JP, Lepš J, Cameron DD.** 2015. Integrating ecology and physiology of root-hemiparasitic interaction: Interactive effects of abiotic resources shape the interplay between parasitism and autotrophy. New Phytologist **205**, 350–360.

**Thieme CJ, Rojas-Triana M, Stecyk E, et al.** 2015. Endogenous *Arabidopsis* messenger RNAs transported to distant tissues. Nature Plants **1**, doi:10.1038/NPLANTS.2015.25.

**Tremblay A, Li S, Scheffler BE, Matthews BF.** 2009. Laser capture microdissection and expressed sequence tag analysis of uredinia formed by *Phakopsora pachyrhizi*, the causal agent of Asian soybean rust. Physiological and Molecular Plant Pathology **73**, 163–174.

**Vela-Corcía D, Bautista R, De Vicente A, Spanu PD, Pérez-García A.** 2016. *De novo* analysis of the epiphytic transcriptome of the cucurbit powdery mildew fungus *Podosphaera xanthii* and identification of candidate secreted effector proteins. PLoS ONE **11**, e0163379.

**Vela-Corcía D, Romero D, De Vicente A, Pérez-García A.** 2018. Analysis of  $\beta$ -tubulin-carbendazim interaction reveals that binding site for MBC fungicides does not include residues involved in fungicide resistance. Scientific Reports **8**, 7161.

**Voegelé RT, Mendgen K.** 2003. Rust haustoria : Uptake and beyond. New Phytologist **159**, 93–100.

**Voegelé RT, Mendgen KW.** 2011. Nutrient uptake in rust fungi: How sweet

is parasitic life? *Euphytica* **179**, 41–55.

**Voegelé RT, Struck C, Hahn M, Mendgen K.** 2002. The role of haustoria in sugar supply during infection of broad bean by the rust fungus *Uromyces fabae*. *Proceedings of the National Academy of Sciences* **98**, 8133–8138.

**Weßling R, Epple P, Altmann S, et al.** 2014. Convergent targeting of a common host protein-network by pathogen effectors from three kingdoms of life. *Cell Host and Microbe* **16**, 364–375.

**Weßling R, Schmidt SM, Micali CO, Knaust F, Reinhardt R, Neumann U, Ver Loren van Themaat E, Panstruga R.** 2012. Transcriptome analysis of enriched *Golovinomyces orontii* haustoria by deep 454 pyrosequencing. *Fungal Genetics and Biology* **49**, 470–482.

**Westermann AJ, Barquist L, Vogel J.** 2017. Resolving host–pathogen interactions by dual RNA-seq. *PLoS Pathogens* **13**, 1–19.

**Westermann AJ, Förstner KU, Amman F, Barquist L, Chao Y, Schulte LN, Müller L, Reinhardt R, Stadler PF, Vogel J.** 2016. Dual RNA-seq unveils noncoding RNA functions in host-pathogen interactions. *Nature* **529**, 496–501.

**Westermann AJ, Gorski SA, Vogel J.** 2012. Dual RNA-seq of pathogen and host. *Nature Reviews Microbiology* **10**, 618–630.

**Worthing C, Andwalker S.** 1983. *The pesticide manual*, 7<sup>th</sup> edition. Croydon: British Crop Protection Council

**Xin M, Wang Y, Yao Y, et al.** 2010. Diverse set of microRNAs are responsive to powdery mildew infection and heat stress in wheat (*Triticum aestivum* L.). *BMC Plant Biology*, 123.

**Xin M, Wang Y, Yao Y, Song N, Hu Z, Qin D, Xie C, Peng H, Ni Z, Sun Q.** 2011. Identification and characterization of wheat long non-protein coding RNAs responsive to powdery mildew infection and heat stress by using

microarray analysis and SBS sequencing. *BMC Plant Biology* **11**, 61.

**Yoshida S, Cui S, Ichihashi Y, Shirasu K.** 2016. The haustorium, a specialized invasive organ in parasitic plants. *Annual Review of Plant Biology* **67**, 643–667.

**Zanni R, Galvez-Llompert M, Garcia-Pereira I, Galvez J, García-Domenech R.** 2018. Molecular topology and QSAR multi-target analysis to boost the in silico research for fungicides in agricultura chemistry. *Molecular Diversity* doi:10.1007/s11030-018-9879-3.

**Zhang Y.** 2008. I-TASSER server for protein 3D structure prediction. *BMC bioinformatics* **9**, 40.

# Conclusions



The main conclusions derived from this work have been the following:

- 1- The *P. xanthii* infection of melon plants causes extensive reprogramming of primary metabolism-related genes, probably as a consequence of the struggle for acquisition/limitation of nutrients.
  
- 2- The repression of key secondary metabolism-related genes of the host during the *P. xanthii*–melon compatible interaction seems to be one of the main strategies of the fungal pathogen to carry out a successful infective process.
  
- 3- Flow cytometry has been shown as a useful tool for the isolation of haustoria virtually free of visible contaminants and, therefore, to perform specific studies on haustorial cells. However, isolation of high quality RNA from these cells is a pending issue.
  
- 4- The development of the haustorial transcriptome *P. xanthii* and its comparison with the epiphytic transcriptome has allowed us to obtain new insights about the role of the haustorium in the biotrophy and the pathogenesis of powdery mildew fungi.

- 5- The acquisition of phosphorus in *P. xanthii* seems to be carried out mainly via haustoria through the activity of two acid phosphatases highly expressed and specifically secreted by this structure.
  
- 6- Results included in this work show that phosphorous uptake plays a key role in plant-fungus interaction and identify phosphorous metabolism as a potential target for the development of new fungicides.
  
- 7- The expression of a haustorium-specific secreted lytic polysaccharide monoxygenase during the development of the haustorium is essential to suppress the activation of chitin-triggered immunity by the host.
  
- 8- Our findings reinforce the idea that the development of molecular strategies to disarm the activation of chitin-triggered immunity is mandatory for the successful colonization of plant environments by fungi.

# Conclusiones





---

Las principales conclusiones derivadas de este trabajo han sido las siguientes:

1. La infección por *P. xanthii* de plantas de melón provoca una extensa reprogramación de genes relacionados con el metabolismo primario, probablemente como consecuencia de la lucha por la adquisición/limitación de nutrientes.
2. La represión de genes clave relacionados con el metabolismo secundario de la planta durante la interacción compatible *P. xanthii*-melón parece ser una de las principales estrategias del patógeno para llevar a cabo con éxito la infección.
3. La citometría de flujo se ha mostrado como una herramienta útil para el aislamiento de haustorios virtualmente libres de contaminantes visibles y, por lo tanto, para realizar estudios específicos en células haustoriales. Sin embargo, el aislamiento de RNA de alta calidad de estas células es un problema pendiente.
4. El desarrollo del transcriptoma haustorial de *P. xanthii* y su comparación con el transcriptoma epifítico nos ha permitido obtener nuevos conocimientos sobre el papel del haustorio en la biotrofia y la patogenia de los oídios.

5. La adquisición de fósforo en *P. xanthii* parece llevarse a cabo principalmente a través del haustorio y mediante la actividad de dos fosfatasa ácidas altamente expresadas y secretadas específicamente por esta estructura.
  
6. Los resultados incluidos en este trabajo muestran que la captación de fósforo juega un papel clave en la interacción planta-hongo e identifica el metabolismo del fósforo como una diana potencial para el desarrollo de nuevos fungicidas.
  
7. La expresión de una monooxigenasa lítica de polisacáridos secretada y específica del haustorio durante el desarrollo del mismo es esencial para suprimir la activación de la inmunidad activada por quitina por parte del huésped.
  
8. Nuestros hallazgos refuerzan la idea de que, para la colonización exitosa de las plantas por los hongos, es obligatorio el desarrollo de estrategias moleculares que desarmen la activación de la inmunidad disparada por quitina.

# Appendix I



## RESEARCH

## Open Access



# TransFlow: a modular framework for assembling and assessing accurate de novo transcriptomes in non-model organisms

Pedro Seoane<sup>1†</sup>, Marina Espigares<sup>1†</sup>, Rosario Carmona<sup>2</sup>, Álvaro Polonio<sup>3</sup>, Julia Quintana<sup>4</sup>, Enrico Cretazzo<sup>5</sup>, Josefina Bota<sup>6</sup>, Alejandro Pérez-García<sup>3</sup>, Juan de Dios Alché<sup>2</sup>, Luis Gómez<sup>7,8</sup> and M. Gonzalo Claros<sup>1\*</sup>

From 5th International Work-Conference on Bioinformatics and Biomedical Engineering Granada, Spain. 26-28 April 2017

## Abstract

**Background:** The advances in high-throughput sequencing technologies are allowing more and more de novo assembling of transcriptomes from many new organisms. Some degree of automation and evaluation is required to warrant reproducibility, repetitivity and the selection of the best possible transcriptome. Workflows and pipelines are becoming an absolute requirement for such a purpose, but the issue of assembling evaluation for de novo transcriptomes in organisms lacking a sequenced genome remains unsolved. An automated, reproducible and flexible framework called TransFlow to accomplish this task is described.

**Results:** TransFlow with its five independent modules was designed to build different workflows depending on the nature of the original reads. This architecture enables different combinations of Illumina and Roche/454 sequencing data, and can be extended to other sequencing platforms. Its capabilities are illustrated with the selection of reliable plant reference transcriptomes and the assembling six transcriptomes (three case studies for grapevine leaves, olive tree pollen, and chestnut stem, and other three for haustorium, epiphytic structures and their combination for the phytopathogenic fungus *Podospaera xanthii*). Arabidopsis and poplar transcriptomes revealed to be the best references. A common result regarding de novo assemblies is that Illumina paired-end reads of 100 nt in length assembled with OASES can provide reliable transcriptomes, while the contribution of longer reads is noticeable only when they complement a set of short, single-reads.

**Conclusions:** TransFlow can handle up to 181 different assembling strategies. Evaluation based on principal component analyses allows its self-adaptation to different sets of reads to provide a suitable transcriptome for each combination of reads and assemblers. As a result, each case study has its own behaviour, prioritises evaluation parameters, and gives an objective and automated way for detecting the best transcriptome within a pool of them. Sequencing data type and quantity (preferably several hundred millions of  $2 \times 100$  nt or longer), assemblers (OASES for Illumina, MIRA4 and EULER-SR reconciled with CAP3 for Roche/454) and strategy (preferably scaffolding with OASES, and probably merging with Roche/454 when available) arise as the most impacting factors.

**Keywords:** Transcriptome, Assembling, Workflow, pipeline, PCA, Non-model organism

\*Correspondence: [claros@uma.es](mailto:claros@uma.es)

<sup>†</sup>Pedro Seoane and Marina Espigares contributed equally to this work.

<sup>1</sup>Departamento de Biología Molecular y Bioquímica, Universidad de Málaga, Campus de Teatinos s/n, 29071 Málaga, Spain

Full list of author information is available at the end of the article



© The Author(s). 2018 **Open Access** This article is distributed under the terms of the Creative Commons Attribution 4.0 International License (<http://creativecommons.org/licenses/by/4.0/>), which permits unrestricted use, distribution, and reproduction in any medium, provided you give appropriate credit to the original author(s) and the source, provide a link to the Creative Commons license, and indicate if changes were made. The Creative Commons Public Domain Dedication waiver (<http://creativecommons.org/publicdomain/zero/1.0/>) applies to the data made available in this article, unless otherwise stated.